

General Disclaimer

One or more of the Following Statements may affect this Document

- This document has been reproduced from the best copy furnished by the organizational source. It is being released in the interest of making available as much information as possible.
- This document may contain data, which exceeds the sheet parameters. It was furnished in this condition by the organizational source and is the best copy available.
- This document may contain tone-on-tone or color graphs, charts and/or pictures, which have been reproduced in black and white.
- This document is paginated as submitted by the original source.
- Portions of this document are not fully legible due to the historical nature of some of the material. However, it is the best reproduction available from the original submission.

LOCKHEED MISSILES & SPACE COMPANY
HUNTSVILLE RESEARCH & ENGINEERING CENTER
HUNTSVILLE RESEARCH PARK
4800 BRADFORD BLVD., HUNTSVILLE, ALABAMA

PREDICTION OF SMOOTHED
SUNSPOT NUMBER USING
DYNAMIC RELATIONS
BETWEEN THE SUN
AND PLANETS


April 1969

Contract NAS8-21445

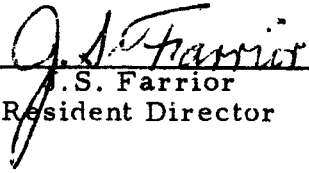
by

R. S. Pimm
T. Bjorn

Prepared for George C. Marshall Space Flight Center
Huntsville, Alabama



T. R. Beal, Manager
Dynamics & Guidance Dept.



J. S. Farrior
Resident Director

PRECEDING PAGE BLANK NOT FILMED.

FOREWORD

This document represents the final report on Contract NAS8-21445, "Study of Mathematical Analysis and Prediction of Solar Activity." The work was performed by personnel in the Dynamics & Guidance Department of Lockheed's Huntsville Research & Engineering Center, and Lockheed's Electronics Sciences Laboratory, Palo Alto, California. Work began on 24 June 1968 and was completed on 24 March 1969.

ACKNOWLEDGEMENT

For assistance received during this study, the authors extend grateful appreciation to: NASA/MSFC personnel for their direction of this study, and in particular the technical coordinator, C.L. Hasseltine; Dr. D.F. Specht of Lockheed/Palo Alto who developed the regression procedures used in the study and provided extensive technical leadership throughout the course of the effort; and J.H. Butler of Lockheed/Huntsville who made valuable contributions in the planning and execution of the study, particularly in the area of possible techniques for the solution of complex problems related to solar forecasting.

PRECEDING PAGE BLANK NOT FILMED.

SUMMARY

The objective of this study was to develop a technique for the prediction of solar activity, making use of the results of previous scientific investigations which had indicated a relation between solar activity and planet interactions. The nature of the interaction between planets and sun which might be influential in causing sunspots is not known. Twenty-one parameters, or "predictors," were developed, each of which describes some aspect of the dynamics in the sun-planets system. Each of these predictors may be determined from a knowledge of the planets' positions and velocities.

The twenty-one predictors were preprocessed for a subsequent multiple, nonlinear regression analysis. The preprocessing included a $\text{Sin}X/X$ filtering, determination of the cross-correlation and shift for each parameter, and normalization of each parameter. The cross-correlation determination and shifting were computed for two configurations of sunspot numbers, the usual 11-year cycle and the 22-year cycle, where polarity of spot groups is used to determine the algebraic sign of sunspot number.

The next step was a regression analysis to determine the nonlinear relationship between each predictor and sunspot number, individually. The NONLIN algorithm was used for this purpose. These nonlinear relationships were then combined iteratively by the ITLIN program to produce the estimate of sunspot number. The entire procedure was performed for both the 11-year and 22-year cycle configurations.

Future estimates of the 22-year sunspot cycle were made for various combinations of the predictors. The results, while not accurate enough for use at this time, indicate that the basic procedure is feasible. Several areas in which further investigation would be beneficial are discussed.

PRECEDING PAGE BLANK NOT FILMED.

CONTENTS

Section		Page
	FOREWORD	iii
	ACKNOWLEDGEMENT	iii
	SUMMARY	v
1	INTRODUCTION	1-1
2	CALCULATION OF PREDICTORS	2-1
3	DATA BASE USED FOR SUNSPOT NUMBER ESTIMATION	3-1
	3.1 General	3-1
	3.2 Data Preprocessing and Data Setup Prior to Estimation of Sunspot Number	3-3
	3.3 Normalizing Predictor Parameters	3-10
4	NONLIN-ITLIN: The Technique Used to Estimate Sunspot Number	4-1
	4.1 NONLIN	4-1
	4.2 ITLIN	4-6
	4.3 Schematic of Entire Estimation Process	4-7
5	RESULTS OF SUNSPOT NUMBER ESTIMATION EXPERIMENTS	5-1
	5.1 Phase I Experiment: Evaluation of the NONLIN-ITLIN Technique	5-1
	5.2 Predicting Sunspot Number	5-4
6	CONCLUSIONS	6-1
7	RECOMMENDATIONS	7-1
8	REFERENCES	8-1

CONTENTS (Continued)

Section	Page
APPENDIXES	
A: SinX/X Filter Coefficients for Three Filter Configurations	A-1
B: NONLIN Coefficients	B-1
C: ITLIN Coefficients	C-1
D: Components of Vector Predictors	D-1

Section 1
INTRODUCTION

Many investigations have considered the possibility of planetary influence on the formation of sunspots. As early as 1923, Ellsworth Huntington (Ref. 1) noted three hypotheses concerning ways in which other bodies may affect the Sun's atmosphere: the meteoric, the gravitational and the electrical. He concluded that even though the exact nature of the influence was not known, that the number of eminent scientists who have in one way or another advocated a planetary hypothesis is so large that their work cannot be overlooked.

More recently, Paul Jose (Ref. 2) discussed the relationship between solar activity and the motion of the Sun relative to the center of gravity of the solar system. He computed various functions that would be descriptive of dynamic relations between the planets and the Sun, and concluded that certain dynamic forces exerted on the Sun by the motions of the planets were the cause of solar activity.

Other work may be cited which provides definite indication of planetary influences on solar activity. Wood and Wood (Ref. 3) conducted a systematic analysis of the velocity, acceleration and rate of change of acceleration (jerk) of the Sun's motion about the center of mass of the solar system. They concluded that the influence of the inner planets on the fluctuation of the acceleration of the Sun in inertial space is as important as that of the outer planets; and that the short-time acceleration and jerk patterns are repetitive with a clear 11.08-year period. Nilo Arriaga (Ref. 4), after analyzing the trajectory of the Sun about the center of gravity of the solar system, drew the following conclusion: "A future hypothesis of the solar activity would rest, therefore, on the following assumptions: (1) the planetary system produces a tidal effect on the surface of the Sun; (2) during the minima, there is a resonance between the tidal wave and the rotation of the Sun; (3) the time necessary for the occurrence of a resonance is a period of 11.5 years; (4) the rupture of this resonance

is the cause of solar activity." Further examples of work, which indicate a relation between planet motions and solar activity, are provided by Bigg (Ref. 5), Suda (Ref. 6), Nemeth (Ref. 7), Gold (Ref. 8), Takahashi (Ref. 9), Schuster (Ref. 10) and Dewey (Ref. 11).

The purpose of this study was to use any known relationships between the planets and the Sun to predict sunspot number at least one cycle into the future. The approach was slanted more toward an engineering perspective than a scientific technique. The ultimate goal was not the physical explanation of solar activity, but the development of an improved method of long-range forecasting. Therefore, the effort was concentrated toward identifying, computing and using parameters that might be descriptive of some interaction between the Sun and planets. Once these parameters were identified and values computed for the recorded history of sunspot number (1749 to present), they were inserted into a nonlinear, multiple regression program to determine the statistical combination which resulted in the best prediction of sunspot number.

Two points should be emphasized concerning the procedure: (1) the goal was improvement of long-range forecasting, rather than short-term forecasting. Thus, the data were analyzed for general trends over a period of months rather than characteristics which appeared daily or weekly. Filtering and smoothing the data were employed to enhance these trends; and (2) it was not a necessary prerequisite of any parameter being considered for use in the analysis that there be an exhaustive theory on the manner in which it affected solar activity. Parameters must have met two requirements before being included: (1) there must be some reason to expect a correlation with solar activity; and (2) the parameter must be predictable itself. It was felt that ample evidence of correlation had been demonstrated for parameters associated with the dynamic interactions between the planets and Sun. These parameters also can be computed with reasonable accuracy for any time in the future. It would be of no use whatsoever (from the standpoint of this analysis) to have a quantity perfectly correlated with sunspot number if it cannot be predicted itself.

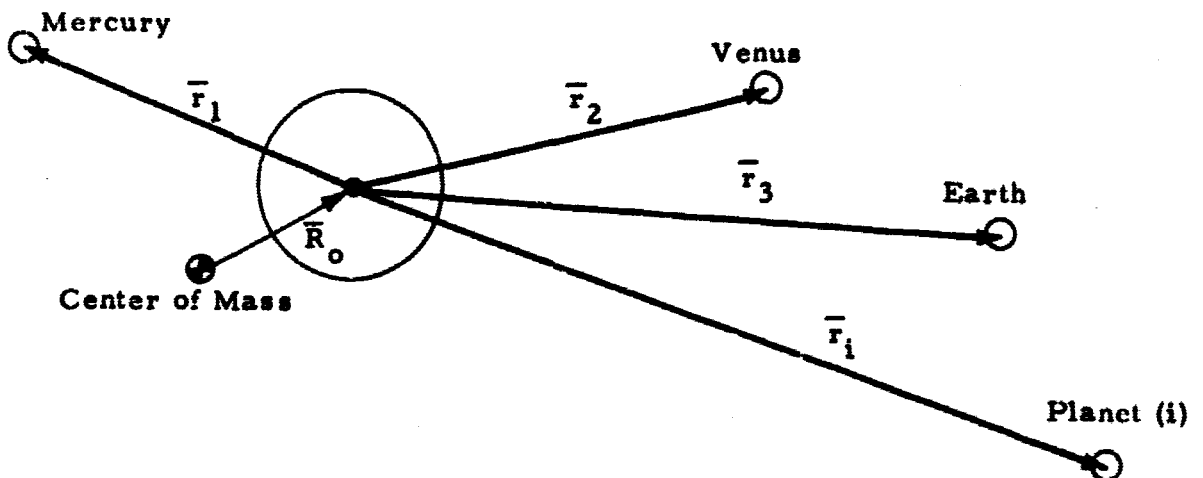
The remainder of this report presents a technique for prediction of sunspot numbers based upon a multiple nonlinear regression between 21 "predictors" and the smoothed Wolf number. A detailed discussion of the parameters to be used as predictors is given first, followed by an explanation of the manner in which they were combined to produce a prediction. Finally, the results are summarized and recommendations given concerning further studies that show promise of improving the technique.

Section 2
CALCULATION OF PREDICTORS

The following discussion presents in detail the method by which each predictor was calculated. Each one depends ultimately upon a knowledge of the position and velocity of the nine planets. In the development it is assumed that the Sun and planets constitute a closed system. Figures 2-1 through 2-10 compare each predictor with the monthly average sunspot number from 1749 to 1964.

Parameter 1: Distance of the Sun from the Center of Mass of the Solar System, R_0 (Fig. 2-1)

The heliocentric ecliptic position vector, \bar{r}_i , of each planet is known ($i = 1, 9$) as are the masses of each planet, m_i , and the mass of the Sun, m_s . The system thus appears as shown below, with \bar{R}_0 to be determined.



The total mass of the system is M ;

$$M = m_s + \sum_{i=1}^9 m_i$$

The position of the center of mass (cm) with respect to the center of the Sun ($-\bar{R}_o$) is

$$M \bar{r}_{cm} = \sum_{i=1}^9 m_i \bar{r}_i$$

$$\bar{r}_{cm} = \frac{1}{M} \sum_{i=1}^9 m_i \bar{r}_i$$

Thus, the position of the Sun with respect to the center of mass is

$$\bar{R}_o = -\bar{r}_{cm} = -\frac{1}{M} \sum_{i=1}^9 m_i \bar{r}_i$$

where each component of \bar{R}_o (in the ecliptic system) is

$$x_o = -\frac{1}{M} \sum_{i=1}^9 m_i X_i$$

$$y_o = -\frac{1}{M} \sum_{i=1}^9 m_i Y_i$$

$$z_o = -\frac{1}{M} \sum_{i=1}^9 m_i Z_i$$

The distance, R_o is then given by

$$R_o = |\bar{R}_o| = \sqrt{X_o^2 + Y_o^2 + Z_o^2}$$

Parameter 2: Velocity of the Sun with Respect to the Center of Mass of the Solar System, V_o (Figure 2-1)

Once the position vector of the Sun with respect to the cm is known, it is a simple differentiation to obtain velocity:

$$\bar{V}_o = \frac{d(\bar{R}_o)}{dt}$$

$$\bar{V}_o = \dot{x}_o \bar{i} + \dot{y}_o \bar{j} + \dot{z}_o \bar{k}$$

where

$$\dot{x}_o = -\frac{1}{M} \frac{d}{dt} \left(\sum_1^9 m_i x_i \right)$$

$$\dot{x}_o = -\frac{1}{M} \sum_1^9 m_i \dot{x}_i$$

and

$$\dot{y}_o = -\frac{1}{M} \sum_1^9 m_i \dot{y}_i$$

$$\dot{z}_o = -\frac{1}{M} \sum_1^9 m_i \dot{z}_i$$

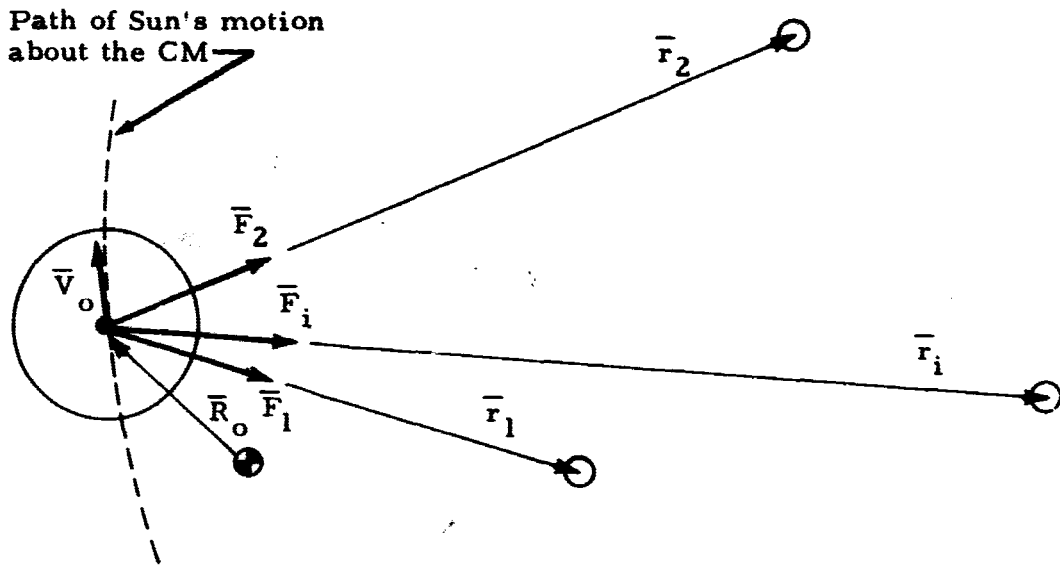
The velocities of each planet ($\dot{x}_i, \dot{y}_i, \dot{z}_i$) are known from a planet ephemeris subroutine (Ref. 12). The resultant velocity is then

$$V_o = |\bar{V}_o| = \sqrt{\dot{x}_o^2 + \dot{y}_o^2 + \dot{z}_o^2}$$

Parameter 3: Acceleration of the Sun with Respect to the Center of Mass, A_o (Figure 2-2)

Acceleration is most conveniently calculated by using Newton's second law and summing the forces acting on the Sun. It is assumed in the analysis

that the only forces present are the gravitational attractions on the Sun by each planet. The force diagram would appear as shown below.



Summing Forces:

$$m_s \vec{a}_o = \sum_1^9 \vec{F}_i = m_s \ddot{\vec{R}}_o$$

$$m_s \vec{a}_o = \sum_1^9 \frac{G m_s m_i \vec{r}_i}{r_i^3}$$

gives the resultant total acceleration

$$\vec{a}_o = G \sum_1^9 \frac{m_i \vec{r}_i}{r_i^3}$$

The ecliptic components are:

$$\ddot{x}_o = G \sum_1^9 \frac{m_i x_i}{r_i^3}$$

$$\ddot{y}_o = G \sum_1^9 \frac{m_i y_i}{r_i^3}$$

$$\ddot{z}_o = G \sum_1^9 \frac{m_i z_i}{r_i^3}$$

Thus, acceleration may be computed from a knowledge of position only:

$$A_o = |\bar{a}_o| = \sqrt{\ddot{x}_o^2 + \ddot{y}_o^2 + \ddot{z}_o^2}$$

Parameter 4: Angular Momentum of the Sun about the Center of Mass, H_o
(Figure 2-2)

By definition, the angular momentum of an object about a given point is

$$\bar{H} = m \bar{r} \times \bar{V} .$$

For the Sun's motion about the center of mass, this equation becomes

$$\bar{H}_o = m_s \bar{R}_o \times \bar{V}_o$$

$$H_x = m_s (y_o \dot{z}_o - z_o \dot{y}_o)$$

$$H_y = m_s (z_o \dot{x}_o - x_o \dot{z}_o)$$

$$H_z = m_s (x_o \dot{y}_o - y_o \dot{x}_o)$$

The magnitude of this vector is then

$$H_o = |\bar{H}_o| = \sqrt{H_x^2 + H_y^2 + H_z^2} .$$

Parameter 5: Radius of Curvature of the Sun's Path, Zeta (Figure 2-3)

The distance to the center of curvature for any curve is given by

$$\rho = \frac{v^3}{|\dot{\mathbf{r}} \times \ddot{\mathbf{r}}|}$$

For the Sun's motion, this equation becomes

$$\text{Zeta} = \frac{v_o^3}{|\dot{\mathbf{v}}_o \times \ddot{\mathbf{a}}_o|}$$

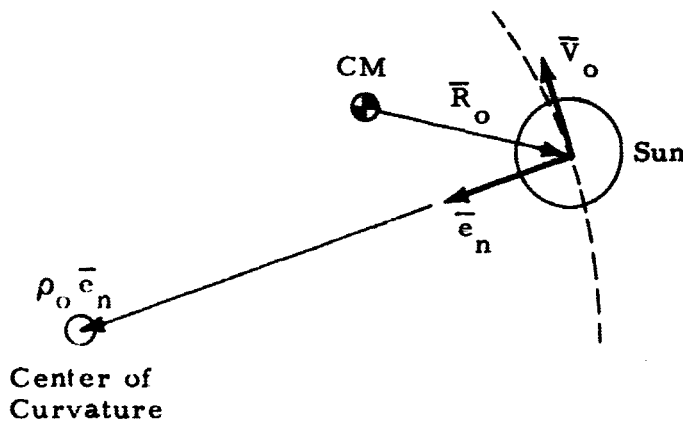
Evaluating the denominator,

$$\dot{\mathbf{v}}_o \times \ddot{\mathbf{a}}_o = (\dot{y}_o \ddot{z}_o - \dot{z}_o \ddot{y}_o) \bar{\mathbf{i}} + (\dot{z}_o \ddot{x}_o - \dot{x}_o \ddot{z}_o) \bar{\mathbf{j}} + (\dot{x}_o \ddot{y}_o - \dot{y}_o \ddot{x}_o) \bar{\mathbf{k}}$$

$$\dot{\mathbf{v}}_o \times \ddot{\mathbf{a}}_o = k_x \bar{\mathbf{i}} + k_y \bar{\mathbf{j}} + k_z \bar{\mathbf{k}}$$

$$|\dot{\mathbf{v}}_o \times \ddot{\mathbf{a}}_o| = \sqrt{k_x^2 + k_y^2 + k_z^2}$$

which is the magnitude of the vector from the Sun to the center of curvature. The direction of the vector, which will be required later, is normal to the Sun's path. A representation of this vector is shown below ($\bar{\mathbf{e}}_n$).



Parameter 6: Rate of Change of Angular Momentum about the Center of Mass, L_o (Figure 2-3)

The angular momentum, from above, is given by

$$\bar{H}_o = m_s \bar{R}_o \times \bar{V}_o .$$

The rate of change of \bar{H}_o is

$$\bar{L}_o = \frac{d|\bar{H}_o|}{dt} = m_s (\dot{\bar{R}}_o \times \bar{V}_o + \bar{R}_o \times \dot{\bar{V}}_o)$$

$$\bar{L}_o = m_s (\bar{R}_o \times \bar{a}_o) .$$

The components are

$$L_x = m_s (y_o \ddot{z}_o - z_o \ddot{y}_o)$$

$$L_y = m_s (z_o \ddot{x}_o - x_o \ddot{z}_o)$$

$$L_z = m_s (x_o \ddot{y}_o - y_o \ddot{x}_o) .$$

So that the magnitude is

$$L_o = |\bar{L}_o| = \sqrt{L_x^2 + L_y^2 + L_z^2} .$$

Parameter 7: Rate of Change of Acceleration (Jerk) of the Sun about the Center of Mass, J_o (Figure 2-4)

The derivative of acceleration has been named jerk (J). It is computed for the Sun's motion about the center of mass as follows:

$$\bar{J} = \frac{d \bar{a}_o}{dt}$$

$$\bar{J} = \frac{d}{dt} G \sum_1^9 \frac{m_i \bar{r}_i}{r_i^3}$$

$$\bar{J} = G \sum_1^9 \left(\frac{m_i \dot{\bar{r}}_i}{r_i^3} - 3 \frac{m_i \bar{r}_i \dot{r}_i}{r_i^4} \right)$$

Note here that $\dot{\bar{r}}_i$ is the total velocity and \dot{r}_i the radial component of velocity of each planet about the Sun:

$$J_x = G \sum_1^9 m_i \left(\frac{\dot{x}_i}{r_i^3} - 3 \dot{r}_i \frac{x_i}{r_i^4} \right)$$

$$J_y = G \sum_1^9 m_i \left(\frac{\dot{y}_i}{r_i^3} - 3 \dot{r}_i \frac{y_i}{r_i^4} \right)$$

$$J_z = G \sum_1^9 m_i \left(\frac{\dot{z}_i}{r_i^3} - 3 \dot{r}_i \frac{z_i}{r_i^4} \right)$$

Thus a knowledge of planetary position and velocity allows determination of the jerk.

$$J_o = |\bar{J}_o| = \sqrt{J_x^2 + J_y^2 + J_z^2}$$

Parameter 8: Angular Momentum of the Sun about the Center of Curvature, P
(Figure 2-4)

The angular momentum of the Sun about the center of curvature may be written as

$$\bar{P} = m_s \bar{\rho} \times \bar{V}_o$$

One of the properties of the radius of curvature, $\bar{\rho}$, is the fact that it is normal to the path of motion, and hence to the velocity vector \bar{V}_o since the velocity is tangent to the path of motion. Thus

$$\bar{P} = m_s \rho V_o \bar{e}_b$$

where \bar{e}_b is a unit vector in the binormal direction (normal to the plane of $\bar{\rho}$ and \bar{V}_o). The final expression for angular momentum is then

$$P = |\bar{P}| = m_s \rho V_o$$

Parameters 9 and 10: Rate of Change of Angular Momentum about the Center of Curvature, \dot{P} and \dot{P}' (Figure 2-5)

Parameter 9 is the rate of change of the magnitude of the angular momentum about the center of curvature, \dot{P} :

$$\dot{P} = \frac{d}{dt} |\bar{P}|$$

$$\dot{P} = \frac{d}{dt} (m_s \rho V_o)$$

$$\dot{P} = m_s (\dot{\rho} V_o + \rho \dot{V}_o)$$

Both $\dot{\rho}$ and \dot{V}_o are computed in a subsequent analysis.

Parameter 10 is the magnitude of the rate of change of angular momentum, \dot{P}' . Thus,

$$\dot{P}' = \left| \frac{d}{dt} \bar{P} \right|$$

The derivative may be evaluated as follows:

$$\bar{P} = m_s (\bar{\rho} \times \bar{V}_o)$$

$$\dot{\bar{P}} = m_s \frac{d}{dt} (\bar{\rho} \times \bar{V}_o)$$

$$\dot{\bar{P}} = m_s (\dot{\bar{\rho}} \times \bar{V}_o + \bar{\rho} \times \dot{\bar{V}}_o)$$

From a subsequent analysis for $\dot{\bar{\rho}}$ it is known that

$$\dot{\bar{\rho}} = \dot{\rho} \bar{e}_n + \rho V_o \tau \bar{e}_b - V_o \bar{e}_t$$

where τ is the torsion of curvature.

Also

$$\bar{V}_o = V_o \bar{e}_t .$$

Thus, the first vector product becomes

$$\dot{\bar{\rho}} \times \bar{V}_o = (\dot{\rho} \bar{e}_n + \rho V_o \tau \bar{e}_b - V_o \dot{e}_t) \times V_o \bar{e}_t$$

$$\dot{\bar{\rho}} \times \bar{V}_o = -\dot{\rho} V_o \bar{e}_b + \rho V_o^2 \tau \bar{e}_n$$

The second vector product may be obtained by first expressing \bar{a}_o in the $\bar{e}_n, \bar{e}_t, \bar{e}_b$ system,

$$\bar{a}_o = \frac{d\bar{V}_o}{dt}$$

$$\bar{a}_o = \frac{d}{dt} (V_o \bar{e}_t)$$

$$\bar{a}_o = \dot{V}_o \bar{e}_t + V_o \dot{\bar{e}}_t .$$

The rate of change of the magnitude of velocity \dot{V}_o is

$$\dot{V}_o = \frac{1}{V_o} (\dot{x}_o \ddot{x}_o + \dot{y}_o \ddot{y}_o + \dot{z}_o \ddot{z}_o) .$$

The derivative of \bar{e}_t is obtained by the Frenet-Serret equations,

$$\dot{\bar{e}}_t = \frac{d\bar{e}_t}{ds} \frac{ds}{dt} = V_o \frac{d\bar{e}_t}{ds}$$

$$\dot{\bar{e}}_t = \frac{V_o}{\rho} \bar{e}_n .$$

Therefore,

$$\bar{a}_o = \dot{V}_o \bar{e}_t + \frac{V_o^2}{\rho} \bar{e}_n .$$

The vector product then becomes

$$\bar{\rho}_o \times \bar{a}_o = \rho \bar{e}_n \times \left(\dot{v}_o \bar{e}_t + \frac{v_o^2}{\rho} \bar{e}_n \right)$$

$$\bar{\rho}_o \times \bar{a}_o = -\rho \dot{v}_o \bar{e}_b,$$

so that the final expression for $\dot{\bar{P}}$ is

$$\dot{\bar{P}} = m_s \left[\rho v_o^2 \tau \bar{e}_n - (\dot{\rho} v_o + \dot{v}_o \rho) \bar{e}_b \right],$$

and

$$\dot{P}' = |\dot{\bar{P}}| = m_s \left[(\rho v_o^2 \tau)^2 + (\dot{\rho} v_o + \dot{v}_o \rho)^2 \right]^{1/2}$$

Notice that \dot{P} (Parameter 9) is one component of \dot{P}' (Parameter 10).

Parameter 11: The Torsion of Curvature of the Sun's Motion, Tau (Figure 2-6)

The definition of the torsion of curvature is

$$\tau = \frac{\dot{\bar{r}} \cdot (\ddot{\bar{r}} \times \dddot{\bar{r}})}{|\dot{\bar{r}} \times \ddot{\bar{r}}|^2},$$

which for the Sun's motion takes the form

$$\tau = \frac{\bar{v}_o \cdot (\bar{a}_o \times \bar{j}_o)}{|\bar{v}_o \times \bar{a}_o|^2}$$

The denominator may be conveniently evaluated from the previous development of the radius of curvature as follows:

$$\rho = \frac{v_o^3}{|\bar{v}_o \times \bar{a}_o|}$$

$$|\bar{V}_0 \times \bar{a}_0|^2 = v_0^6 / \rho^2.$$

The triple scalar product in the numerator may be evaluated as,

$$\bar{V}_0 \cdot (\bar{a}_0 \times \bar{J}_0) = \dot{x}_0 (\dot{y}_0 \ddot{z}_0 - \ddot{z}_0 \dot{y}_0) + \dot{y}_0 (\dot{z}_0 \ddot{x}_0 - \ddot{x}_0 \dot{z}_0) + \dot{z}_0 (\dot{x}_0 \ddot{y}_0 - \ddot{y}_0 \dot{x}_0).$$

Thus, the final expression for torsion is

$$\tau = \frac{\rho^2}{v_0^6} \left[\dot{x}_0 (\dot{y}_0 \ddot{z}_0 - \ddot{z}_0 \dot{y}_0) + \dot{y}_0 (\dot{z}_0 \ddot{x}_0 - \ddot{x}_0 \dot{z}_0) + \dot{z}_0 (\dot{x}_0 \ddot{y}_0 - \ddot{y}_0 \dot{x}_0) \right].$$

where the first, second, and third derivatives are the components of velocity, acceleration, and jerk previously computed.

Parameter 12: Rate of Change of the Radius of Curvature, ROD (Figure 2-6)

The radius of curvature may be written as

$$\bar{\rho} = \rho \bar{e}_n,$$

where \bar{e}_n is a unit vector normal to the path of motion. The rate of change of $\bar{\rho}$ is then

$$\dot{\bar{\rho}} = \frac{d}{dt} (\rho \bar{e}_n)$$

$$\dot{\bar{\rho}} = \dot{\rho} \bar{e}_n + \rho \dot{\bar{e}}_n.$$

To evaluate $\dot{\rho}$:

$$\rho = v_0^3 (k_x^2 + k_y^2 + k_z^2)^{-1/2}$$

$$\dot{\rho} = 3 v_0^2 \dot{v}_0 (k_x^2 + k_y^2 + k_z^2)^{-1/2}$$

$$- \frac{1}{2} v_0^3 (k_x^2 + k_y^2 + k_z^2)^{-3/2} \left[2 k_x \frac{d k_x}{dt} + 2 k_y \frac{d k_y}{dt} + 2 k_z \frac{d k_z}{dt} \right]$$

$$k_x = \dot{y}_0 \ddot{z}_0 - \dot{z}_0 \ddot{y}_0$$

$$\frac{dk_x}{dt} = \ddot{y}_0 \ddot{z}_0 + \dot{y}_0 \dddot{z}_0 - \ddot{z}_0 \ddot{y}_0 - \dot{z}_0 \dddot{y}_0$$

$$\frac{dk_x}{dt} = \dot{y}_0 \dddot{z}_0 - \dot{z}_0 \dddot{y}_0$$

Similarly

$$\frac{dk_y}{dt} = \dot{z}_0 \dddot{x}_0 - \dot{x}_0 \dddot{z}_0$$

$$\frac{dk_z}{dt} = \dot{x}_0 \dddot{y}_0 - \dot{y}_0 \dddot{x}_0$$

where \ddot{x}_0 , \ddot{y}_0 and \ddot{z}_0 are the components of jerk. The derivative $\frac{dV_0}{dt}$ is the rate of change of the magnitude of the velocity vector, and may be denoted by

$$\ddot{S} = \frac{dV_0}{dt}$$

$$\ddot{S} = \frac{d}{dt} (\dot{x}_0^2 + \dot{y}_0^2 + \dot{z}_0^2)^{1/2}$$

$$\ddot{S} = \frac{1}{V_0} (\dot{x}_0 \ddot{x}_0 + \dot{y}_0 \ddot{y}_0 + \dot{z}_0 \ddot{z}_0)$$

Thus $\dot{\rho}$ becomes

$$\dot{\rho} = \frac{3V_0(\bar{V}_0 \cdot \bar{a}_0)}{|\bar{V}_0 \times \bar{a}_0|} - \frac{V_0^3(\bar{V}_0 \times \bar{J}_0) \cdot (\bar{V}_0 \times \bar{a}_0)}{|\bar{V}_0 \times \bar{a}_0|^3}$$

where

$$\bar{V}_0 \times \bar{a}_0 = (\dot{y}_0 \ddot{z}_0 - \dot{z}_0 \ddot{y}_0)\bar{i} + (\dot{z}_0 \ddot{x}_0 - \dot{x}_0 \ddot{z}_0)\bar{j} + (\dot{x}_0 \ddot{y}_0 - \dot{y}_0 \ddot{x}_0)\bar{k}$$

$$\bar{V}_0 \times \bar{J}_0 = (\dot{y}_0 \dddot{z}_0 - \dot{z}_0 \dddot{y}_0)\bar{i} + (\dot{z}_0 \dddot{x}_0 - \dot{x}_0 \dddot{z}_0)\bar{j} + (\dot{x}_0 \dddot{y}_0 - \dot{y}_0 \dddot{x}_0)\bar{k}$$

and $\ddot{x}_o, \ddot{y}_o, \ddot{z}_o$ are components of jerk.

To evaluate $\dot{\bar{e}}_n$, the Frenet-Serret formulas are utilized:

$$\dot{\bar{e}}_n = \frac{d(\bar{e}_n)}{dS} \frac{dS}{dt}$$

$$\frac{d\bar{e}_n}{dS} = \tau \bar{e}_b - \kappa \bar{e}_t,$$

where

τ = torsion of curvature

\bar{e}_b = unit vector in the binormal direction

κ = curvature = $1/\rho$

\bar{e}_t = unit vector in the tangential direction

$$\tau = \frac{\bar{V}_o \cdot (\bar{a}_o \times \bar{J}_o)}{|\bar{V}_o \times \bar{a}_o|^2}.$$

The derivative of \bar{e}_n becomes

$$\dot{\bar{e}}_n = V_o \tau \bar{e}_b - V_o \kappa \bar{e}_t.$$

Thus,

$$\begin{aligned} \dot{\bar{\rho}} = & \left\{ \frac{3 V_o (\bar{V}_o \cdot \bar{a}_o)}{|\bar{V}_o \times \bar{a}_o|} - \frac{V_o^3 (\bar{V}_o \times \bar{J}_o) \cdot (\bar{V}_o \times \bar{a}_o)}{|\bar{V}_o \times \bar{a}_o|^3} \right\} \bar{e}_n \\ & + \rho \frac{\bar{V}_o \cdot (\bar{a}_o \times \bar{J}_o)}{|\bar{V}_o \times \bar{a}_o|^2} \bar{e}_b - V_o \bar{e}_t. \end{aligned}$$

And taking the absolute value,

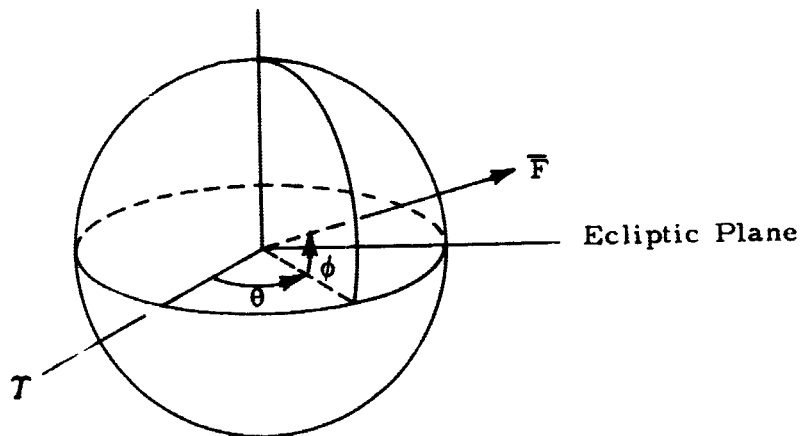
$$\text{ROD} = |\dot{\rho}| = \left\{ \left[\frac{3 v_o (\bar{v}_o \cdot \bar{a}_o)}{|\bar{v}_o \times \bar{a}_o|} - \frac{v_o^3 (\bar{v}_o \times \bar{J}_o) \cdot (\bar{v}_o \times \bar{a}_o)}{|\bar{v}_o \times \bar{a}_o|^3} \right]^2 + \left[\frac{\rho \bar{v}_o \cdot (\bar{a}_o \times \bar{J}_o) v_o}{|\bar{v}_o \times \bar{a}_o|^2} + v_o^2 \right]^2 \right\}^{1/2}$$

Parameters 13 and 14: Ecliptic Force Component Rate, HF and HF' (Figure 2-7)

This parameter is one suggested by Dr. R. M. Head of NASA's Electronics Research Center, Cambridge, Massachusetts. It is defined as follows:

$$\text{HF} = F \cos \phi \theta ,$$

where F is the magnitude of the resultant force acting on the Sun due to the gravitational attractions of the planets. The angles θ and ϕ are ecliptic longitude and latitude of the force vector as shown below.



The force magnitude can be obtained from Newton's Second Law:

$$\bar{F} = m_s \bar{a}_o$$

$$\bar{F} = m_s (\ddot{x}_o \bar{i} + \ddot{y}_o \bar{j} + \ddot{z}_o \bar{k})$$

$$\bar{F} = F_x \bar{i} + F_y \bar{j} + F_z \bar{k}$$

$$F = |\bar{F}| = (F_x^2 + F_y^2 + F_z^2)^{1/2}$$

The angles may be evaluated as follows:

$$\cos \phi = + \sqrt{\frac{F_x^2 + F_y^2}{F^2}} \quad -90^\circ \leq \phi \leq 90^\circ$$

$$\tan \theta = \frac{F_y}{F_x}$$

Taking the derivative

$$\sec^2 \theta \dot{\theta} = \frac{F_x \dot{F}_y - F_y \dot{F}_x}{F_x^2}$$

$$\dot{\theta} = \frac{F_x \dot{F}_y - F_y \dot{F}_x}{F_x^2} \cos^2 \theta$$

But the cosine of θ is

$$\cos \theta = \frac{F_x}{\sqrt{F_x^2 + F_y^2}}$$

$$\cos^2 \theta = \frac{F_x^2}{F_x^2 + F_y^2}$$

so that

$$\dot{\theta} = \frac{F_x \dot{F}_y - F_y \dot{F}_x}{F_x^2} \frac{F_x^2}{F_x^2 + F_y^2}$$

$$\dot{\theta} = \frac{F_x \dot{F}_y - F_y \dot{F}_x}{F_x^2 + F_y^2}$$

The derivatives of the components of force may be evaluated in terms of the jerk vector:

$$\frac{d\bar{F}}{dt} = \frac{d}{dt} (m_s \ddot{x}_o \bar{i} + m_s \ddot{y}_o \bar{j} + m_s \ddot{z}_o \bar{k})$$

$$\dot{\bar{F}} = m_s \dddot{x}_o \bar{i} + m_s \dddot{y}_o \bar{j} + m_s \dddot{z}_o \bar{k},$$

so that

$$\dot{F}_x = m_s \dddot{x}_o$$

$$\dot{F}_y = m_s \dddot{y}_o$$

$$\dot{F}_z = m_s \dddot{z}_o.$$

The final expression for HF is then:

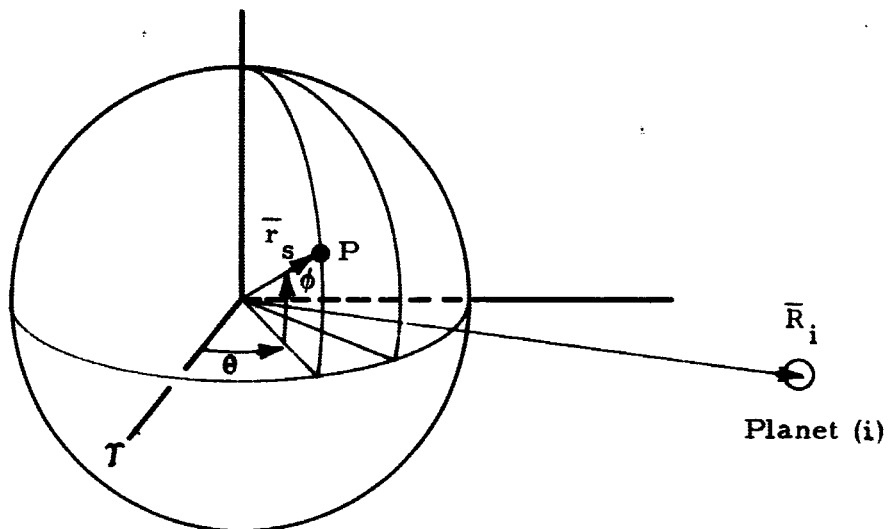
$$HF = F \left(\frac{\sqrt{F_x^2 + F_y^2}}{F} \right) \left(\frac{F_x \dot{F}_y - F_y \dot{F}_x}{F_x^2 + F_y^2} \right)$$

$$HF = \frac{F_x \dot{F}_y - F_y \dot{F}_x}{\sqrt{F_x^2 + F_y^2}}$$

The procedure for obtaining HF' is exactly the same, but a slightly different numerical technique was used. The results turned out to be nearly equivalent.

Parameters 15, 16, 17 and 21: Tide-Raising Force and Tide-Raising Potential
 (Figures 2-7, 2-8, and 2-9)

The diagram below shows an arbitrary point, P, on the surface of the Sun, and a given planet.



The gravitational potential at any point, P, on the surface of the Sun (r_s, θ, ϕ) because of the presence of a planet with mass m_i located at $\bar{R}_i (R_i, \theta_i, \phi_i)$ is

$$V = - \frac{G m_i}{\rho_i},$$

where ρ_i = the distance between point P and the planet,

$$V = - \frac{G m_i}{(R_i^2 + r_s^2 - 2 R_i r_s \cos \beta_i)^{1/2}}$$

$$V = - \frac{G m_i}{R_i} \left(1 + \frac{r_s^2}{R_i^2} - 2 \frac{r_s}{R_i} \cos \beta_i \right)^{-1/2}.$$

The angle β_i is the heliocentric angle between the \bar{r}_s and \bar{R}_i vectors. Using the binomial theorem and neglecting higher order terms, the following is obtained:

$$\begin{aligned}
 V &= -\frac{G m_i}{R_i} \left[1 - \frac{1}{2} \left(\frac{r_s^2}{R_i^2} - 2 \frac{r_s}{R_i} \cos \beta_i \right) + \frac{3}{8} \left(\frac{r_s^2}{R_i^2} - 2 \frac{r_s}{R_i} \cos \beta_i \right)^2 + \dots \right] \\
 V &= -\frac{G m_i}{R_i} \left[1 - \frac{1}{2} \frac{r_s^2}{R_i^2} + \frac{r_s}{R_i} \cos \beta_i + \frac{3}{8} \left(\frac{r_s^4}{R_i^4} - 4 \frac{r_s^3}{R_i^3} \cos \beta_i + 4 \frac{r_s^2}{R_i^2} \cos^2 \beta_i \right) \right] \\
 V &= -\frac{G m_i}{R_i} \left[1 + \frac{r_s}{R_i} \cos \beta_i + \left(\frac{r_s}{R_i} \right)^2 \left(\frac{3}{2} \cos^2 \beta_i - \frac{1}{2} \right) \right] \\
 V &= -\frac{G m_i}{R_i} - \frac{G m_i}{R_i^2} r_s \cos \beta_i - \frac{G m_i}{2 R_i^3} r_s^2 (3 \cos^2 \beta_i - 1) .
 \end{aligned}$$

Let

$$\begin{aligned}
 V_1 &= -\frac{G m_i}{R_i} \\
 V_2 &= -\frac{G m_i}{R_i^2} r_s \cos \beta_i \\
 V_3 &= -\frac{G m_i}{2 R_i^3} r_s^2 (3 \cos^2 \beta_i - 1)
 \end{aligned}$$

The first term is constant if R_i is constant. Taking the gradient of V_1 with respect to the xyz coordinates of the Sun's surface thus results in no force,

$$\nabla V_1 = -\frac{\partial}{\partial x} \left(\frac{G m_i}{R_i} \right) \bar{i} - \frac{\partial}{\partial y} \left(\frac{G m_i}{R_i} \right) \bar{j} - \frac{\partial}{\partial z} \left(\frac{G m_i}{R_i} \right) \bar{k} = 0 \dots$$

The second term gives rise to a force with uniform intensity Gm_i/R_i^2 as will be shown:

$$\bar{F}_2 = -\nabla V_2 = \frac{Gm_i}{R_i^2} \left[\frac{\partial}{\partial x} (r_s \cos\beta_i) \bar{i} + \frac{\partial}{\partial y} (r_s \cos\beta_i) \bar{j} + \frac{\partial}{\partial z} (r_s \cos\beta_i) \bar{k} \right]$$

$$\cos\beta_i = \frac{\bar{r}_s \cdot \bar{R}_i}{r_s R_i}$$

$$\cos\beta_i = \frac{xx_i + yy_i + zz_i}{r_s R_i}$$

$$r_s \cos\beta_i = \frac{xx_i + yy_i + zz_i}{R_i}$$

$$\frac{\partial(r_s \cos\beta_i)}{\partial x} = \frac{\partial}{\partial x} \left(\frac{xx_i + yy_i + zz_i}{R_i} \right)$$

$$\frac{\partial(r_s \cos\beta_i)}{\partial x} = \frac{x_i}{R_i}$$

Similarly,

$$\frac{\partial(r_s \cos\beta_i)}{\partial y} = \frac{y_i}{R_i}$$

$$\frac{\partial(r_s \cos\beta_i)}{\partial z} = \frac{z_i}{R_i}$$

Thus,

$$\bar{F}_2 = \frac{Gm_i}{R_i^2} \left[\frac{x_i}{R_i} \bar{i} + \frac{y_i}{R_i} \bar{j} + \frac{z_i}{R_i} \bar{k} \right]$$

$$\bar{F}_2 = \frac{Gm_i}{R_i^2} \frac{\bar{R}_i}{R_i}$$

so that \bar{F}_2 is a force of uniform intensity Gm_i/R_i^2 in the direction of \bar{R}_i/R_i . It is the usual expression for the force arising from the gravitational attraction of another body. When divided by the mass of the Sun and summed over all the planets it is the Parameter 3.

The remaining term V_3 constitutes the tide-raising potential,

$$V_3 = \frac{Gr_s^2}{2} \sum_1^9 \frac{m_i}{R_i^3} (3 \cos^2 \beta_i - 1),$$

where the summation is taken over all the planets. Note that the potential is a function not only of time because of the changing positions of the planets, but of the particular point chosen on the Sun's surface. Since a relation is being sought between the potential and smoothed sunspot number, which is basically a function of time, the time-variant properties of V_3 are of prime interest. A possible solution to the problem is to choose arbitrarily a point fixed in space, but located extremely close to the surface of the Sun. Once a given point is assumed, it is possible to determine the variation of V_3 with time. The potential V_3 is Parameter No. 21 (Figure 2-10).

The tide-raising force per unit mass is obtained from the gradient of V_3 .

$$\bar{F}_3 = -\nabla V_3 = \frac{Gm_i}{2R_i^3} \left[\frac{\partial}{\partial x} r_s^2 (3 \cos^2 \beta_i - 1) \bar{i} + \frac{\partial}{\partial y} r_s^2 (3 \cos^2 \beta_i - 1) \bar{j} + \frac{\partial}{\partial z} r_s^2 (3 \cos^2 \beta_i - 1) \bar{k} \right].$$

Evaluating the partial derivative with respect to x:

$$\frac{\partial}{\partial x} r_s^2 (3 \cos^2 \beta_i - 1) = 2 r_s \frac{\partial r_s}{\partial x} (3 \cos^2 \beta_i - 1) + 6 r_s^2 \cos \beta_i \frac{\partial \cos \beta_i}{\partial x}$$

$$\frac{\partial \cos \beta_i}{\partial x} = \frac{\partial}{\partial x} \left(\frac{xx_i + yy_i + zz_i}{r_s R_i} \right)$$

$$\frac{\partial \cos \beta_i}{\partial x} = \frac{x_i}{r_s R_i} - \frac{x \cos \beta_i}{r_s^2}$$

$$\begin{aligned} \frac{\partial}{\partial x} r_s^2 (3 \cos^2 \beta_i - 1) &= 2x (3 \cos^2 \beta_i - 1) + 6 r_s^2 \cos \beta_i \left(\frac{x_i}{r_s R_i} - \frac{x \cos \beta_i}{r_s^2} \right) \\ &= 6x \cos^2 \beta_i - 2x + \frac{6 r_s \cos \beta_i x_i}{R_i} - 6x \cos^2 \beta_i \\ &= 6 \frac{r_s}{R_i} \cos \beta_i x_i - 2x \end{aligned}$$

Similarly,

$$\frac{\partial}{\partial y} r_s^2 (3 \cos^2 \beta_i - 1) = 6 \frac{r_s}{R_i} \cos \beta_i y_i - 2y$$

$$\frac{\partial}{\partial z} r_s^2 (3 \cos^2 \beta_i - 1) = 6 \frac{r_s}{R_i} \cos \beta_i z_i - 2z$$

so that

$$\bar{F}_3 = \frac{Gm_i}{2R_i^3} \left[\left(6 \frac{r_s}{R_i} \cos \beta_i x_i - 2x \right) \bar{i} + \left(6 \frac{r_s}{R_i} \cos \beta_i y_i - 2y \right) \bar{j} + \left(6 \frac{r_s}{R_i} \cos \beta_i z_i - 2z \right) \bar{k} \right]$$

$$\bar{F}_3 = \frac{Gm_i}{R_i^3} \left(3 \frac{r_s}{R_i} \cos \beta_i \bar{R}_i - \bar{r}_s \right)$$

The vertical component of tidal force per unit mass at any point can be obtained as follows:

$$F'_{3r} = \bar{F}_3 \cdot \frac{\bar{r}_s}{r_s}$$

$$F'_{3r} = \frac{G m_i}{R_i^3} \left[3 \frac{r_s}{R_i} \cos \beta_i \frac{\bar{R}_i \cdot \bar{r}_s}{r_s} - \frac{\bar{r}_s \cdot \bar{r}_s}{r_s} \right]$$

$$F'_{3r} = \frac{G m_i}{R_i^3} \left[3 r_s \cos^2 \beta_i - r_s \right]$$

$$F'_{3r} = \frac{G m_i r_s}{R_i^3} (3 \cos^2 \beta_i - 1) .$$

The total vertical component of the tidal force is then

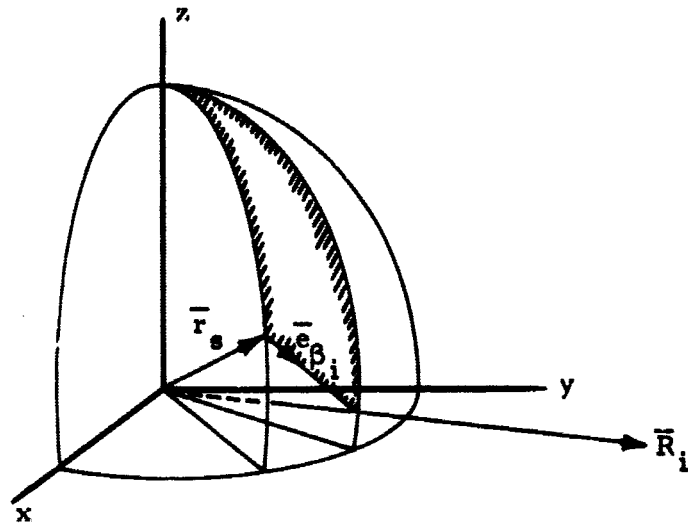
$$F_{3r} = G r_s \sum_1^9 \frac{m_i}{R_i^3} (3 \cos^2 \beta_i - 1) .$$

This expression is Parameter No. 15 (Figure 2-7).

Next the north-south and east-west positions of the horizontal tidal force must be computed. First determine the magnitude of the horizontal component,

$$F'_{3h} = \bar{F}_3 \cdot \bar{e}_{\beta_i} .$$

where \bar{e}_{β_i} is a unit vector perpendicular to \bar{r}_s (in the horizontal plane) and in the direction toward \bar{R}_i , as shown



$$F'_{3h} = \frac{G m_i}{R_i^3} \left[3 \frac{r_s}{R_i} \cos\beta_i \bar{R}_i \cdot \bar{e}_{\beta_i} - \bar{r}_s \cdot \bar{e}_{\beta_i} \right]$$

$$F'_{3h} = \frac{3 G m_i r_s}{R_i^4} \cos\beta_i \bar{R}_i \cdot \bar{e}_{\beta_i} .$$

The dot product may be evaluated by noting that the angle between \bar{R}_i and \bar{e}_{β_i} is $90 - \beta_i$. Thus,

$$\bar{R}_i \cdot \bar{e}_{\beta_i} = R_i \cos(90 - \beta_i) = R_i \sin\beta_i ,$$

so that

$$F'_{3h} = \frac{3 G m_i r_s}{R_i^3} \cos\beta_i \sin\beta_i$$

$$F'_{3h} = \frac{3}{2} G \frac{m_i r_s}{R_i^3} \sin 2\beta_i .$$

In order to sum the horizontal tidal forces due to each planet, the direction of \bar{e}_{β_i} relative to the local north-south line must be determined. This direction is facilitated by expressing \bar{r}_s and \bar{R}_i in terms of celestial longitude and latitude. The celestial longitude and latitude of the planet (λ_i and ϕ_i) are known for any time from the planet ephemeris analysis. The longitude and latitude of the point on the Sun is known once a point has been chosen. Working with the spherical triangle shown above,

$$\sin\beta_i \cos A_{z_i} = \cos(90 - \phi_i) \sin(90 - \phi_s) - \sin(90 - \phi_i) \cos(90 - \phi_s) \cos(\lambda_i - \lambda_s)$$

$$\cos A_{z_i} = \frac{1}{\sin\beta_i} \left[\sin\phi_i \cos\phi_s - \cos\phi_i \sin\phi_s \cos(\lambda_i - \lambda_s) \right]$$

The correct quadrant of A_{z_i} may be determined from the quadrant of $\lambda_i - \lambda_s$. Thus,

$$F'_{3h \text{ N-S}} = F'_{3h} \cos A_{z_i}$$

$$F'_{3h \text{ E-W}} = F'_{3h} \sin A_{z_i}$$

The total components are next obtained by a summation over all the planets,

$$F_{3h \text{ N-S}} = \sum_1^9 F'_{3h} \cos A_{z_i}$$

$$F_{3h \text{ E-W}} = \sum_1^9 F'_{3h} \sin A_{z_i}$$

The horizontal component of tidal force (Parameter 16, Fig. 2-8) is then

$$F_{3H} = \left[(F_{3h \text{ N-S}})^2 + (F_{3h \text{ E-W}})^2 \right]^{1/2}$$

The total tide-raising force at any point on the Sun (Parameter 17, Fig. 2-8) may then be computed as

$$F_3 = \left[F_{3h \text{ N-S}}^2 + F_{3h \text{ E-W}}^2 + F_{3r}^2 \right]^{1/2} .$$

Parameter 18: Planetary Couple, CUP (Figure 2-9)

According to MacCullagh's formula, the potential of a body at a distant point is

$$V = -\frac{GM}{r} - \frac{G(A+B+C-3I)}{2r^3} ,$$

where

M is the mass of the body

r is the distance from the body to the point

A, B, C are the moments of inertia about the principal axes.

The force on a distant unit mass at \bar{r} is $-\nabla V$, and from Newton's Third Law, the distant mass exerts an equal and opposite force on the body. This force results in a couple of moment $\bar{r} \times \nabla V$ about the origin, exerted by the distant unit mass. This couple is the result of the lack of spherical symmetry of the body, which expresses itself in the fact that V is not just a function of r , but involves x, y , and z in addition. Therefore, in finding the couple, all those parts of V that are simply functions of r may be ignored. The moment of inertia I about the axis to the point in question provides the only part of V that is not a function of r only;

$$I = \frac{Ax^2 + By^2 + Cz^2}{r^2} .$$

Call this part of V , V_1 .

$$V_1 = \frac{3GI}{2r^3}$$

$$V_1 = \frac{3G}{2r^5} (Ax^2 + By^2 + Cz^2) .$$

To compute the gradient,

$$\nabla V_1 = \frac{\partial V_1}{\partial x} \bar{i}' + \frac{\partial V_1}{\partial y} \bar{j}' + \frac{\partial V_1}{\partial z} \bar{k}'$$

$$\nabla V_1 = -\frac{15G}{2r^7} (Ax^2 + By^2 + Cz^2) \bar{r} + \frac{3G}{r^5} (Ax\bar{i}' + By\bar{j}' + Cz\bar{k}')$$

$$\nabla V_1 = -\frac{15GI}{2r^5} \bar{r} + \frac{3G}{r^5} (Ax\bar{i}' + By\bar{j}' + Cz\bar{k}') .$$

The precessional couple is then

$$\bar{\Gamma} = \bar{r} \times \nabla V_1$$

$$\bar{\Gamma} = \bar{r} \times \left(-\frac{15GI}{2r^5} \bar{r} \right) + \bar{r} \times \left[\frac{3G}{r^5} (Ax\bar{i}' + By\bar{j}' + Cz\bar{k}') \right]$$

$$\bar{\Gamma} = \frac{3G}{r^5} (x\bar{i}' + y\bar{j}' + z\bar{k}') \times (Ax\bar{i}' + By\bar{j}' + Cz\bar{k}')$$

$$\bar{\Gamma} = \frac{3G}{r^5} [(C-B) yz\bar{i}' + (A-C) xz\bar{j}' + (B-A) xy\bar{k}'] .$$

Assume that the Sun is symmetric about its axis of rotation. Thus,

$$A = B ,$$

and

$$\bar{\Gamma} = \frac{3G}{r^5} [(C-A) yz\bar{i}' + (A-C) xz\bar{j}']$$

$$\bar{\Gamma} = \frac{3G}{r^5} [(C-A) yz\bar{i}' - (C-A) xz\bar{j}']$$

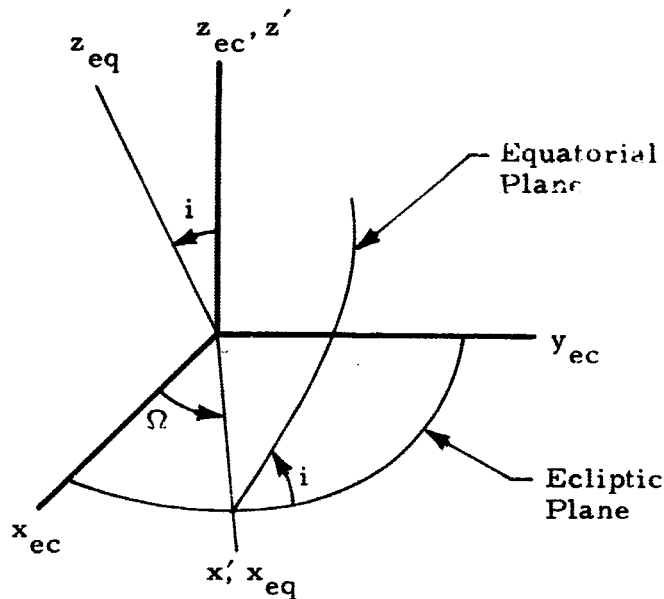
$$\bar{\Gamma} = \frac{3G(C-A)}{r^5} [yz\bar{i}' - xz\bar{j}'] .$$

The value of $(C-A)$ is not accurately known for the Sun. This inaccuracy may be removed from the analysis by normalizing the couple,

$$\bar{\Gamma}' = \frac{1}{C-A} \bar{\Gamma} = \frac{3G}{r^5} (yz \bar{i}' - xz \bar{j}') .$$

Note that this expression is the normalized precessional couple due to the reactive force of one planet and that the coordinates of this planet (x, y, z) are in the Sun-centered equatorial system. It is thus necessary to transform the known heliocentric ecliptic coordinates of the planet into the equatorial system.

Two rotations are required as shown:



From the American Ephemeris and Nautical Almanac values of i and Ω are known,

$$\begin{aligned} i &= 7^{\circ}15' \\ \Omega &= 73^{\circ}40' + 50'' \cdot 25t \\ t &= \text{time in years from 1850.} \end{aligned}$$

Thus,

$$\begin{bmatrix} x_{eq} \\ y_{eq} \\ z_{eq} \end{bmatrix} = \begin{bmatrix} \cos\Omega & \sin\Omega & 0 \\ -\sin\Omega \cos i & \cos\Omega \cos i & \sin i \\ \sin\Omega \sin i & -\cos\Omega \sin i & \cos i \end{bmatrix} \begin{bmatrix} x_{ec} \\ y_{ec} \\ z_{ec} \end{bmatrix}$$

Summation of the x and y components of each planetary couple produces,

$$\begin{aligned} \Gamma'_x &= 3G \cdot \sum_1^9 \frac{y_i z_i}{r_i^5} \\ \Gamma'_y &= -3G \cdot \sum_1^9 \frac{x_i z_i}{r_i^5} \end{aligned}$$

The magnitude of the total couple is then,

$$CUP = |\bar{\Gamma}'_o| = [\Gamma'^2_x + \Gamma'^2_y]^{1/2}$$

Parameters 19 and 20: Coriolis Acceleration, SCC and SSC (Figures 2-9 and 2-10)

Two types of coriolis accelerations have been inferred from the report by Wood (Ref. 13). Both are defined by the expression

$$\bar{a}_c = 2 \bar{\omega}_{\theta z} \times \bar{V}_{rt}$$

where $\bar{\omega}_{\theta z}$ = angular velocity of the \bar{R}_o vector.

The difference between the two lies in the manner in which \bar{V}_{rt} is computed. For the "Sun-center" coriolis, SCC

$$\bar{V}_{rt} = \frac{\bar{V}_o \cdot \bar{R}_o}{R_o} \bar{e}_r$$

which is simply the radial component of the total velocity of the Sun about the CM

$$\bar{V}_{rt} = \dot{r}_s \bar{e}_r$$

Thus,

$$SCC = 2\omega_{\theta z} \times \dot{r}_s \bar{e}_r$$

But,

$$\bar{\omega}_{\theta z} \times \bar{R}_o = V_L \bar{e}_\theta ,$$

where

\bar{e}_θ is a unit vector in the plane of motion perpendicular to \bar{R}_o .

Since $\bar{\omega}_{\theta z}$ is perpendicular to \bar{R}_o ,

$$\omega_{\theta z} R_o = V_L$$

$$\omega_{\theta z} R_o = \sqrt{V_o^2 - \dot{r}_s^2}$$

$$\omega_{\theta z} = \frac{1}{R_o} \sqrt{V_o^2 - \dot{r}_s^2} .$$

Therefore,

$$SCC = 2\omega_{\theta z} \dot{r}_s$$

$$SCC = \frac{2}{R_o} \left(\sqrt{V_o^2 - \dot{r}_s^2} \right) \dot{r}_s ,$$

or alternately

$$SCC = \frac{2 V_\theta V_r}{R_o}$$

The "Sun-surface" Coriolis acceleration SCC is obtained from

$$\bar{V}_{rt} = \dot{r}_r \bar{e}_r + \bar{\omega}_\theta \times \bar{\rho}_{ss} ,$$

where

$\bar{\omega}_{\odot}$ is the angular velocity of the Sun and

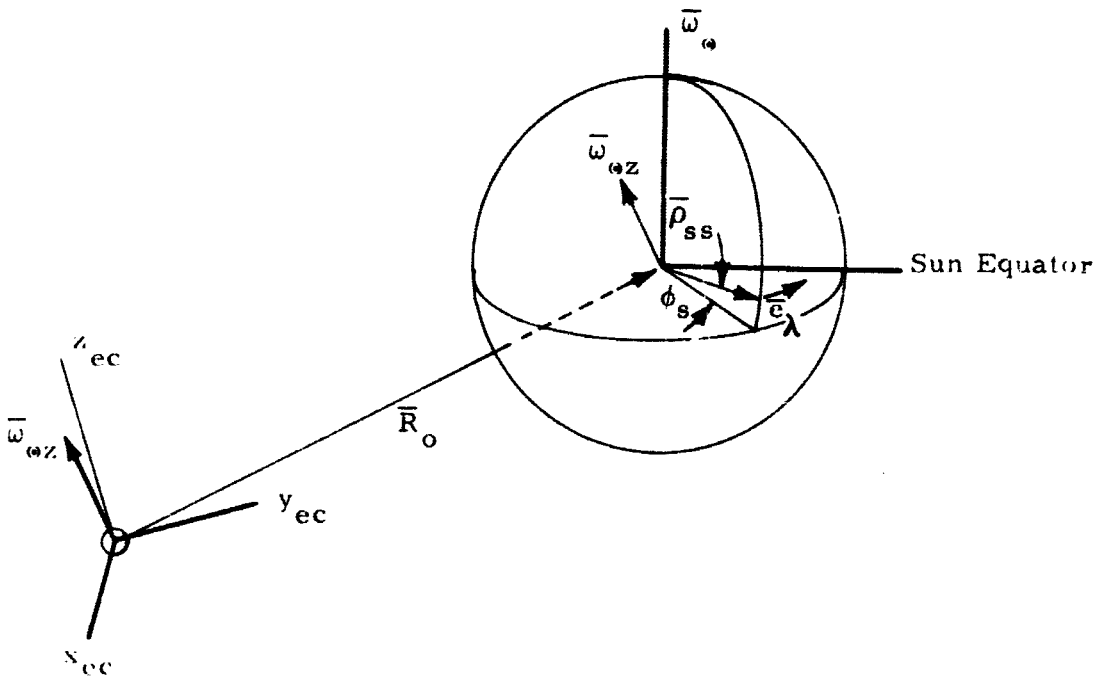
$\bar{\rho}_{SS}$ is a vector from the center of the Sun to any arbitrary point on the surface of the Sun.

The "Sun-surface" Coriolis becomes

$$SSC = 2\bar{\omega}_{\odot z} \times (\dot{r}_s \bar{e}_r + \bar{\omega}_{\odot} \times \bar{\rho}_{SS})$$

$$SSC = \bar{a}_{CC} + 2\bar{\omega}_{\odot z} \times (\bar{\omega}_{\odot} \times \bar{\rho}_{SS}) .$$

To evaluate the second term; the following illustration is helpful:



$$\bar{\omega}_{\odot} \times \bar{\rho}_{SS} = \omega_{\odot} \rho_{SS} \sin(90 - \phi) \bar{e}_{\lambda} ,$$

where \bar{e}_{λ} is a unit vector perpendicular to the meridional plane of the arbitrary point on the Sun's surface, and ϕ is the latitude, measured from the Sun's

equator, to the point. The magnitude of $\bar{\omega}_{\odot}$ will vary depending on the latitude ϕ since the Sun's rotation is not uniform;

$$\begin{aligned}\bar{\omega}_{\odot} \times \bar{\rho}_{SS} &= \omega_{\odot} \rho_{SS} \cos \phi \bar{e}_{\lambda} \\ \bar{\omega}_{\odot z} \times (\bar{\omega}_{\odot} \times \bar{\rho}_{SS}) &= \omega_{\odot z} \omega_{\odot} \rho_{SS} \cos \phi \bar{e}_b \times \bar{e}_{\lambda},\end{aligned}$$

where \bar{e}_b is a unit vector in the direction of $\bar{\omega}_{\odot z}$. The direction of \bar{e}_b will not vary much from the perpendicular to the ecliptic, since the motion of most planets is very nearly in the ecliptic. Furthermore, the plane of the Sun's equator is inclined by only $7^{\circ}15'$ to the ecliptic. For these reasons the following approximation may be made:

$$\bar{e}_b \times \bar{e}_{\lambda} \approx \sin(90 - \phi) = \cos \phi.$$

Thus,

$$\bar{\omega}_{\odot z} \times (\bar{\omega}_{\odot} \times \bar{\rho}_{SS}) \approx \omega_{\odot z} \omega_{\odot} \rho_{SS} \cos^2 \phi,$$

and

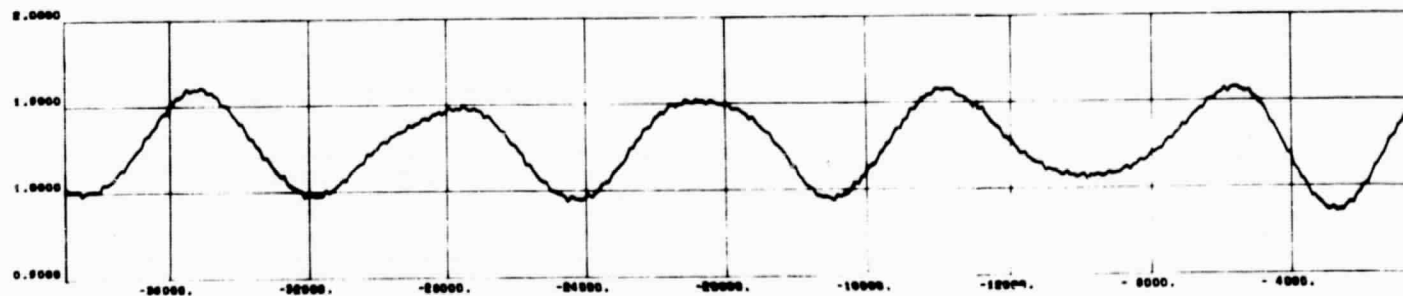
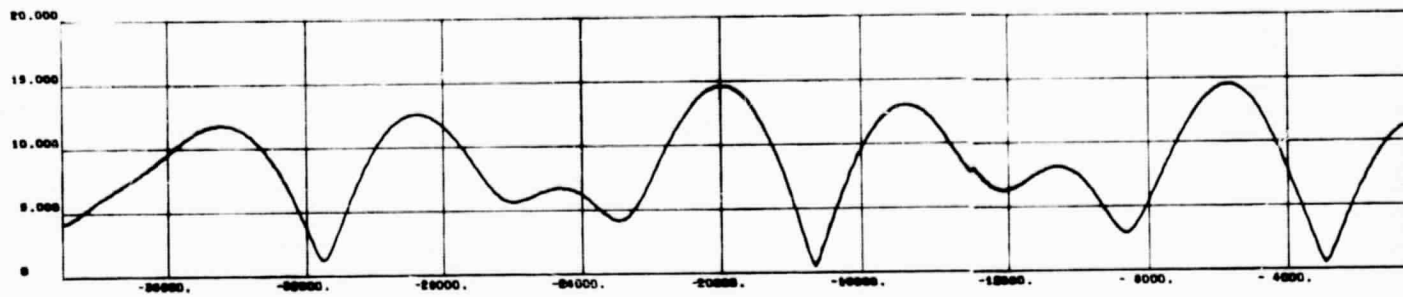
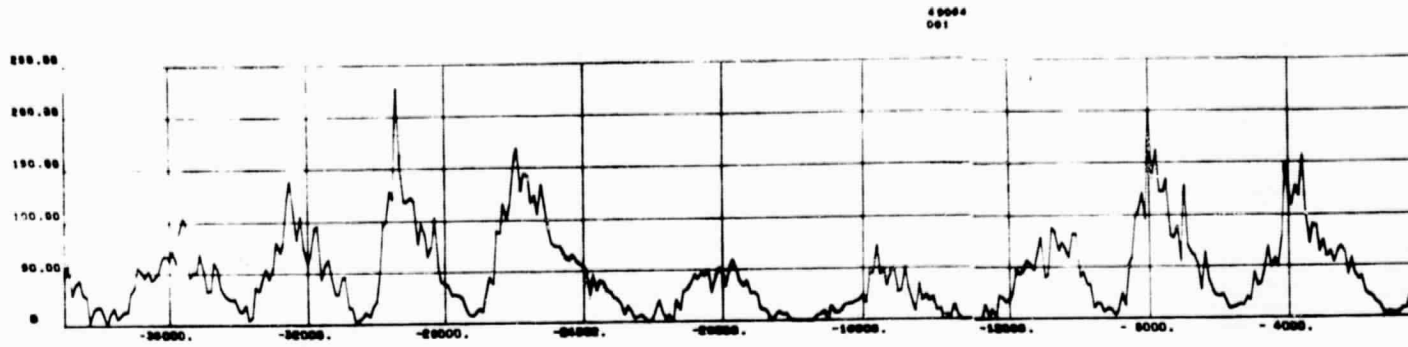
$$SSC = a_{cc} + 2\omega_{\odot z} \omega_{\odot} \rho_{SS} \cos^2 \phi.$$

For points on the Sun's equator, $\phi = 0$, and $\cos^2 \phi = 1.0$. The second term then has the form of a_{cc} with \dot{r}_s replaced by $\rho_{SS} \omega_{\odot}$. The magnitude of \dot{r}_s is small compared with the magnitude of $\rho \omega_{\odot}$. The radial distance of the Sun from the CM changes by a maximum of 2.18 solar radii over a period of years. Thus even if it were possible to change by the maximum amount in one year, the magnitude of \dot{r}_s would be 2.18 solar radii per year. On the other hand, the magnitude of $\rho \omega_{\odot}$ is approximately 90 solar radii per year. Thus, for points located reasonably close to the solar equator, a close approximation to the Sun-surface Coriolis acceleration is

$$SSC = 2 \omega_{\odot z} \omega_{\odot} \rho_{SS}$$

This concludes the description of how each predictor was computed. The next section begins a discussion of how the predictors are combined to produce a forecast. Values of smoothed sunspot number to be predicted are shown in Figs. 2-11 and 2-12. Figure 2-12 is the 22-year cycle given by a consideration of magnetic polarity.

PRECEDING PAGE BLANK NOT FILMED.



FOLDOUT FRAME

FOLDOUT FRAME /

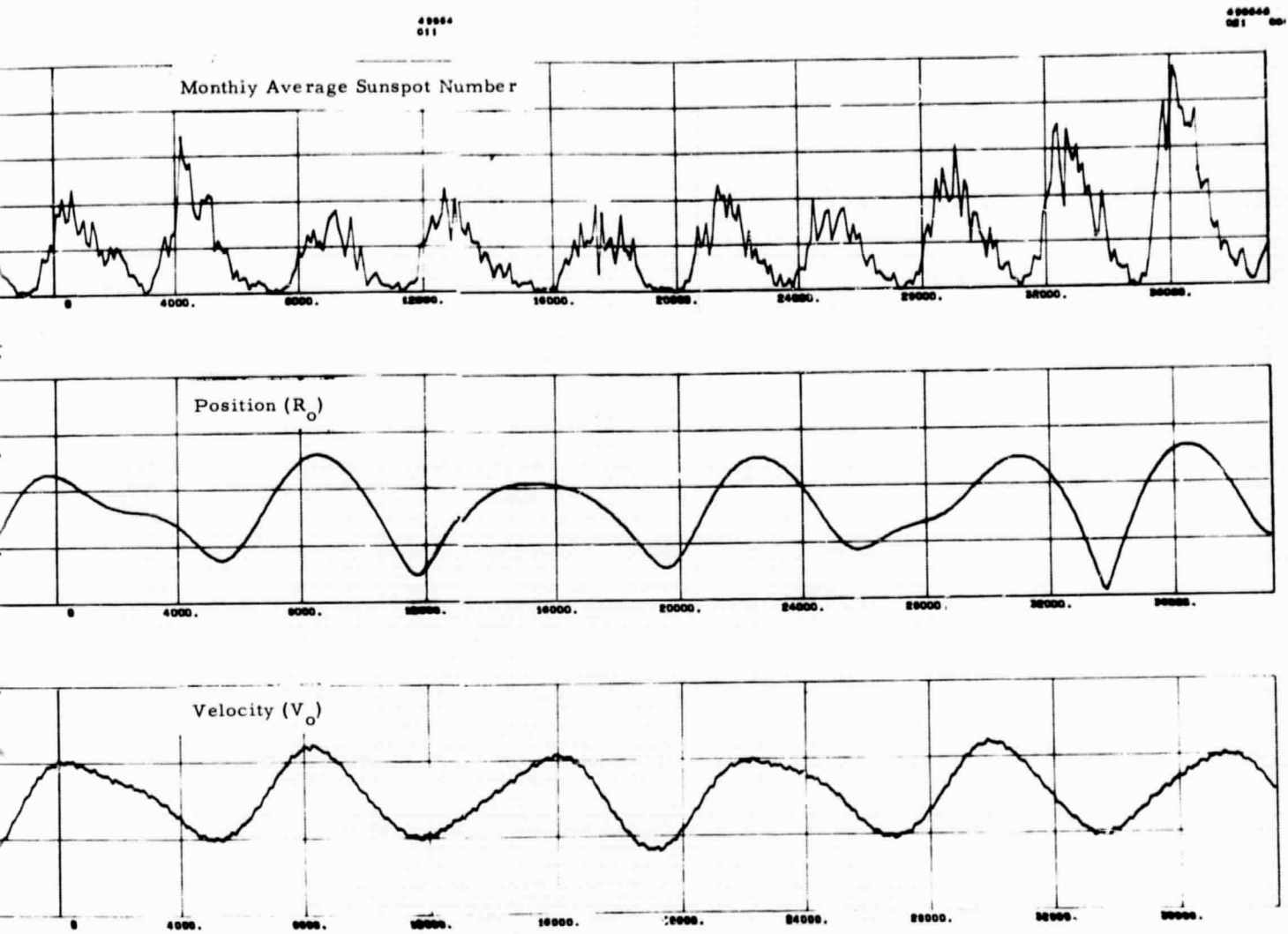
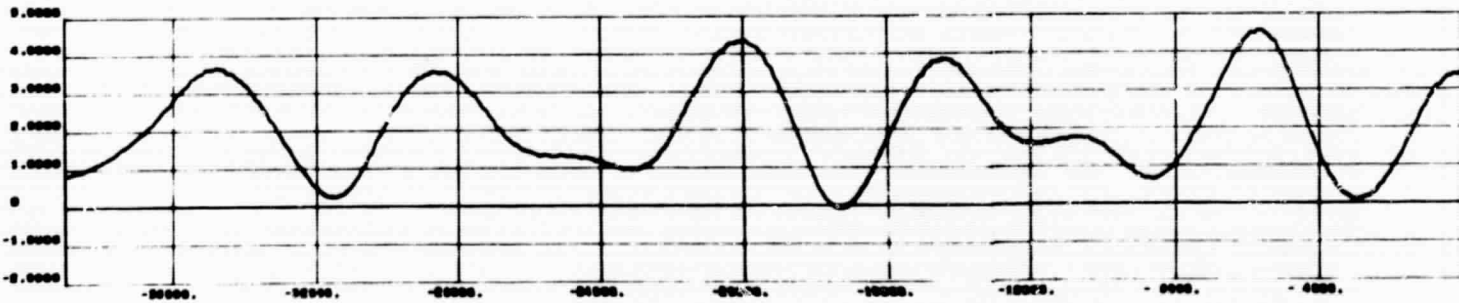
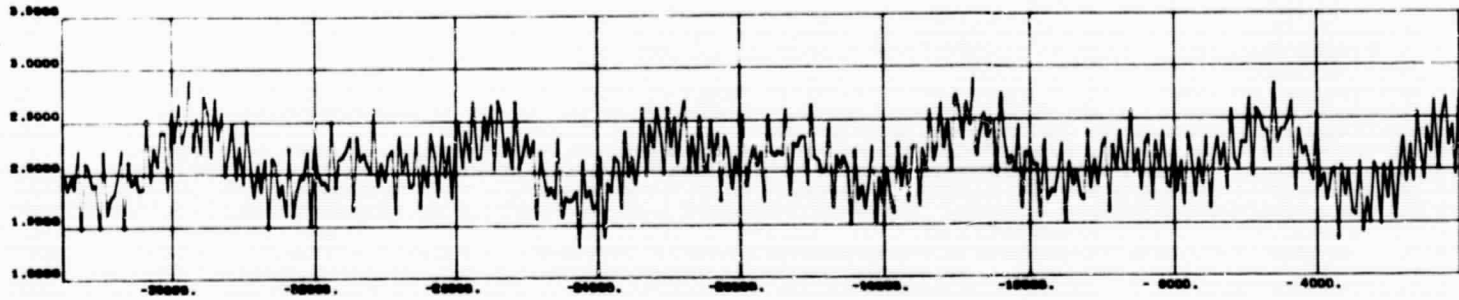
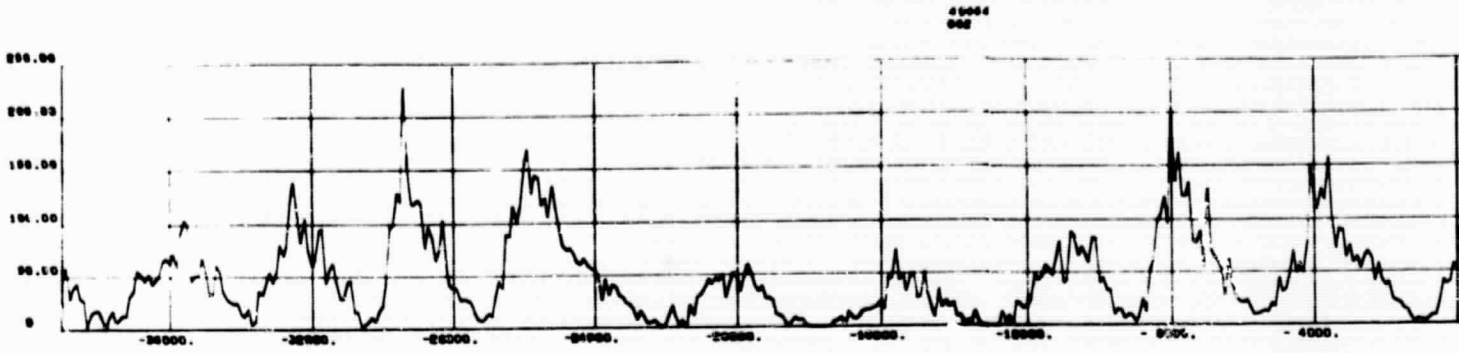


Fig. 2-1 - Position and Velocity Compared with Sunspot Number

FOLDOUT FRAME

FOLDOUT FRAME 2

PRECEDING PAGE BLANK NOT FILMED



FOGOUT FRAME /

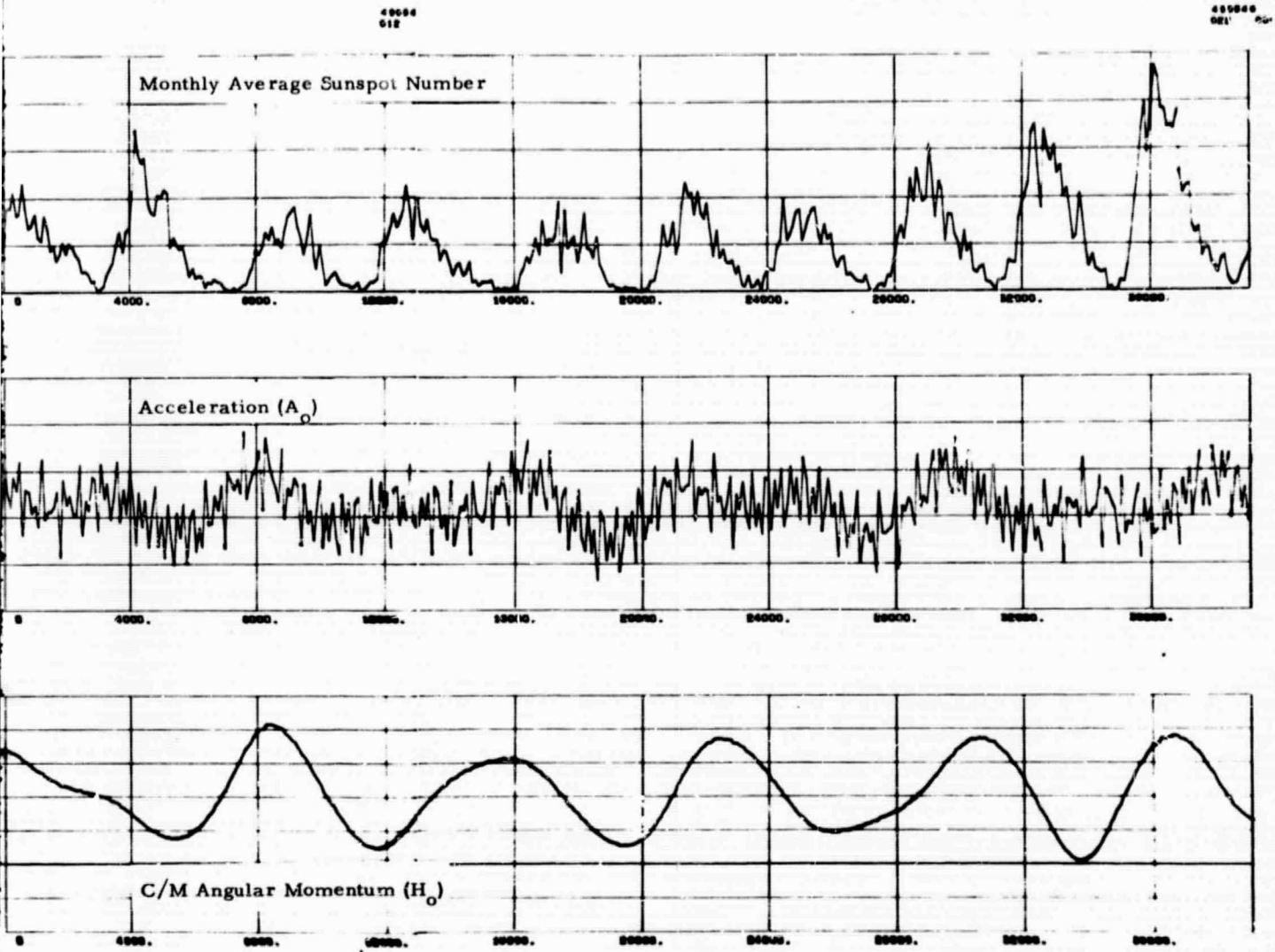
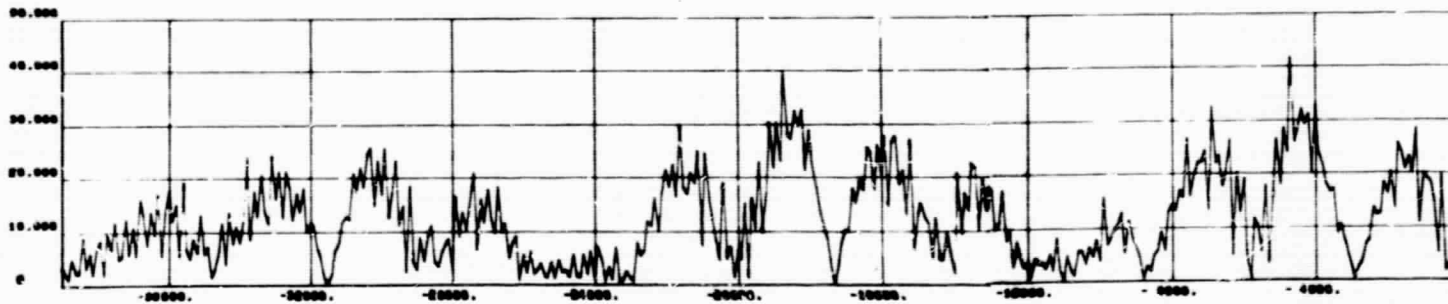
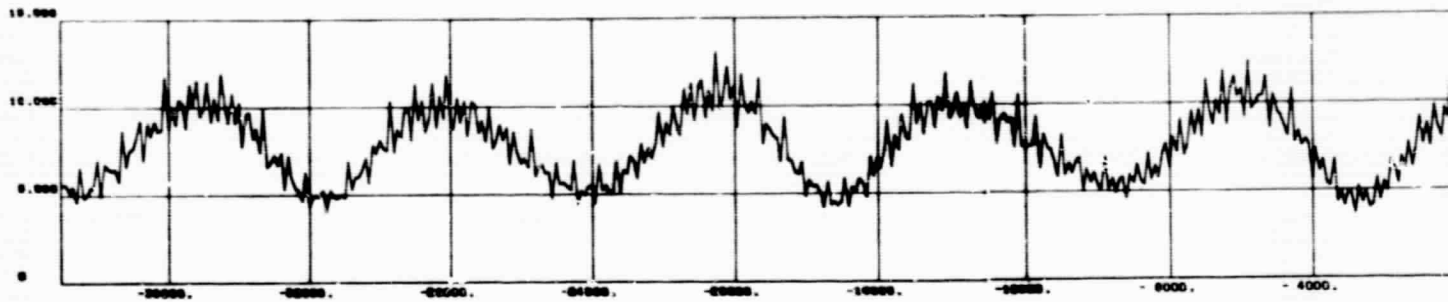
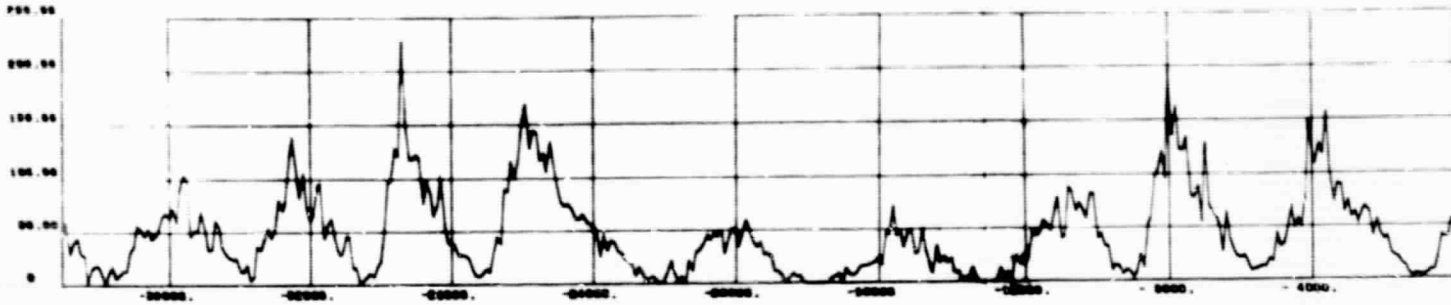


Fig. 2-2 - Acceleration and Angular Momentum Compared with Sunspot Number

PRECEDING PAGE BLANK NOT FILMED.

2004
C02



FOLDOUT FRAME /

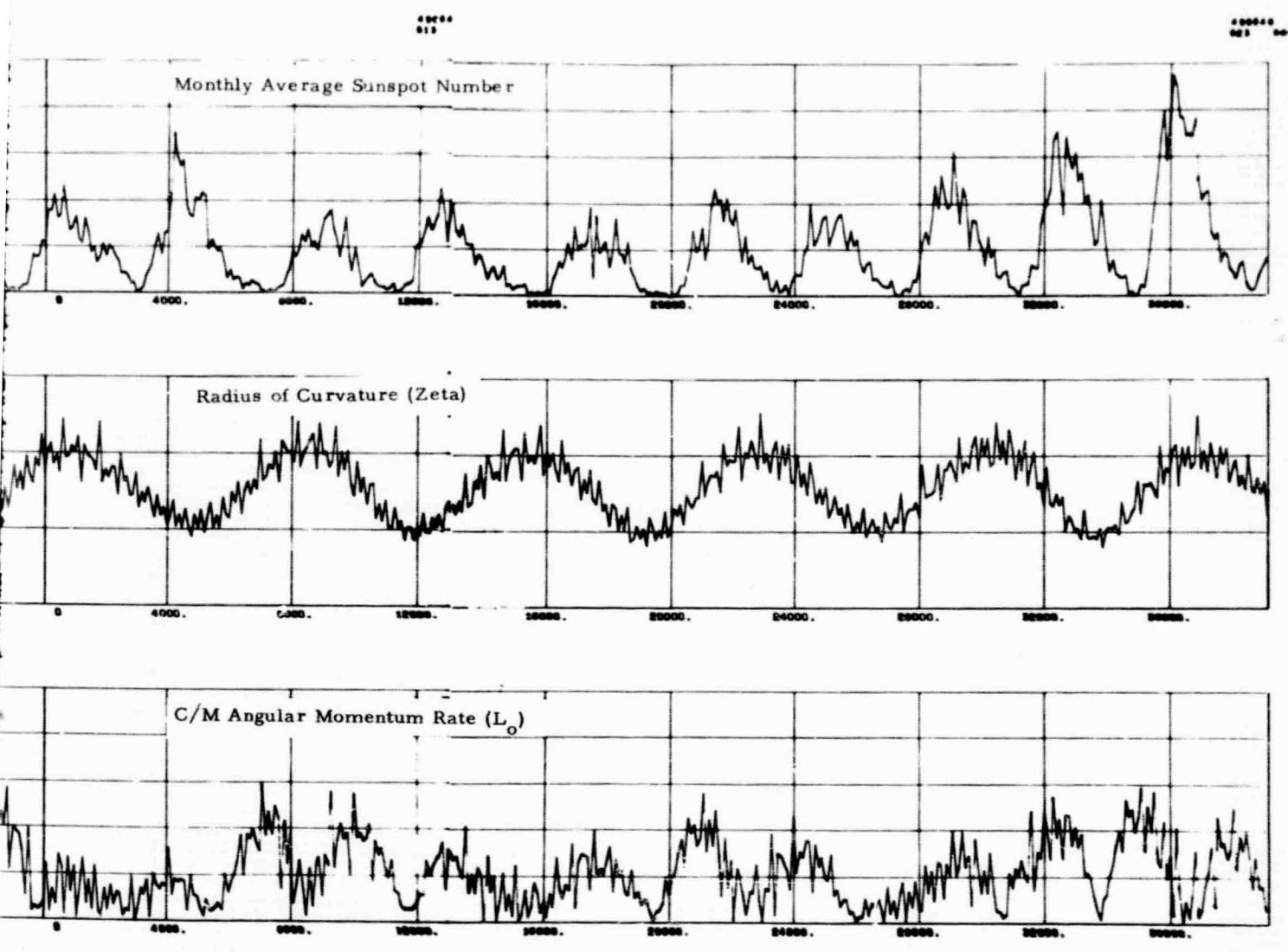
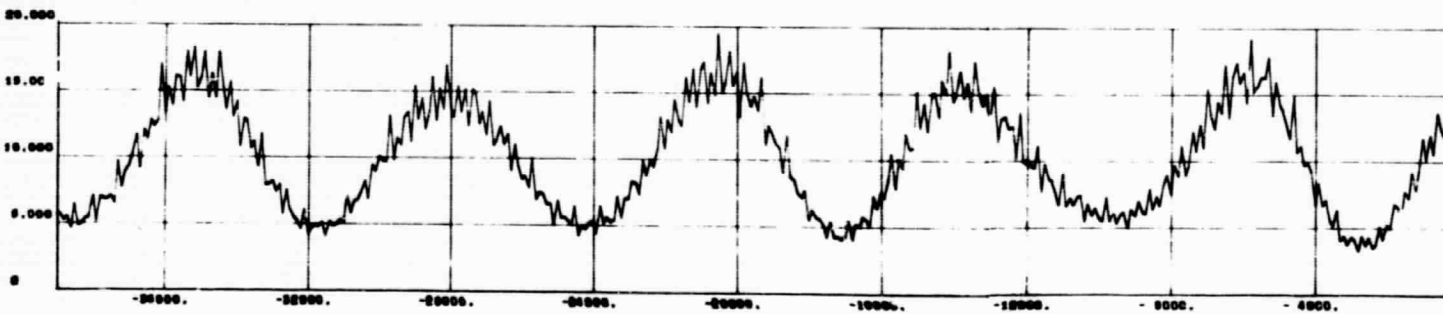
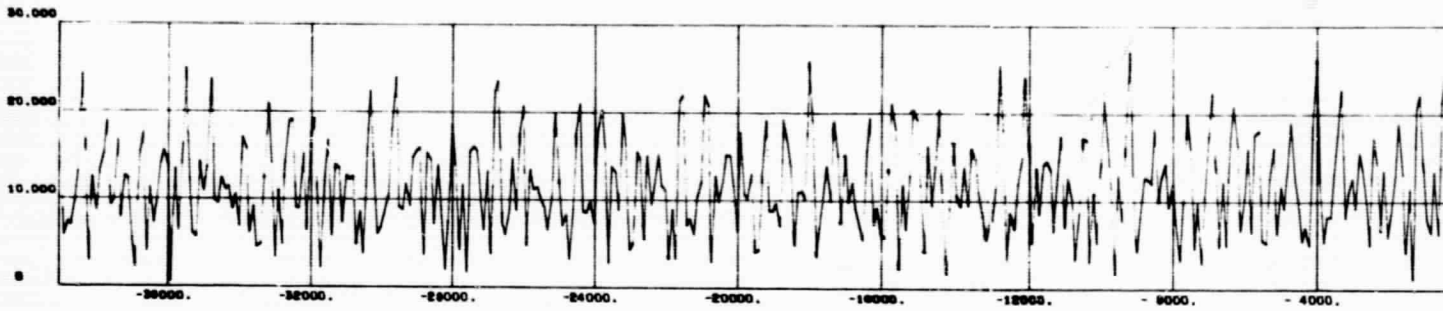
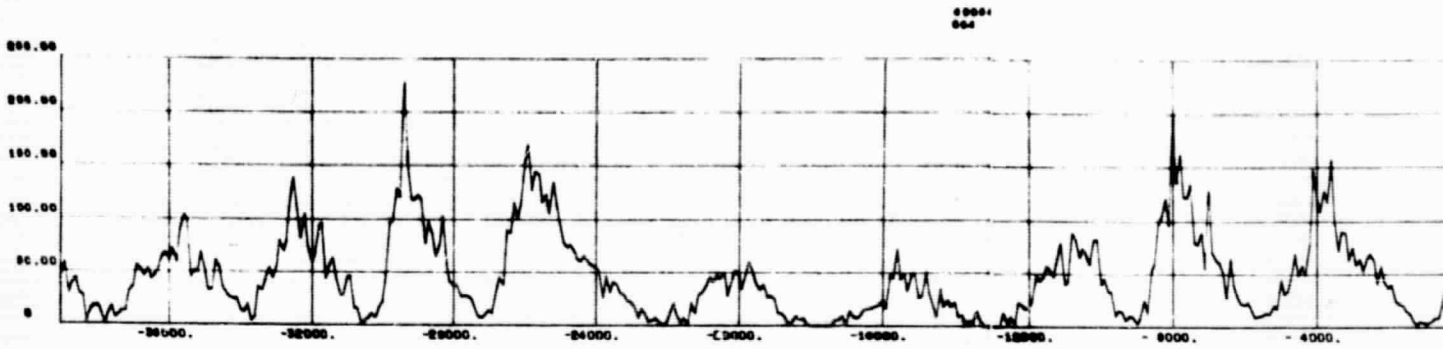


Fig. 2-3 - Radius of Curvature and Angular Momentum Rate Compared with Sunspot Number

PRECEDING PAGE BLANK NOT FILMED.

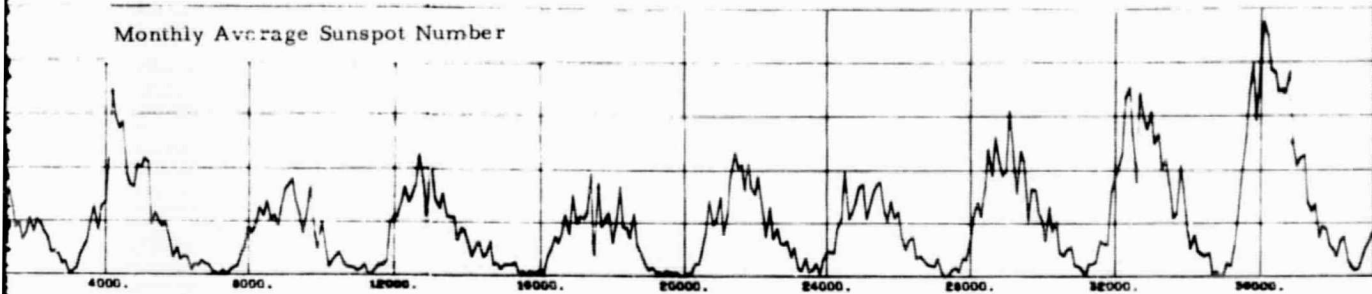


FOLDOUT FRAME /

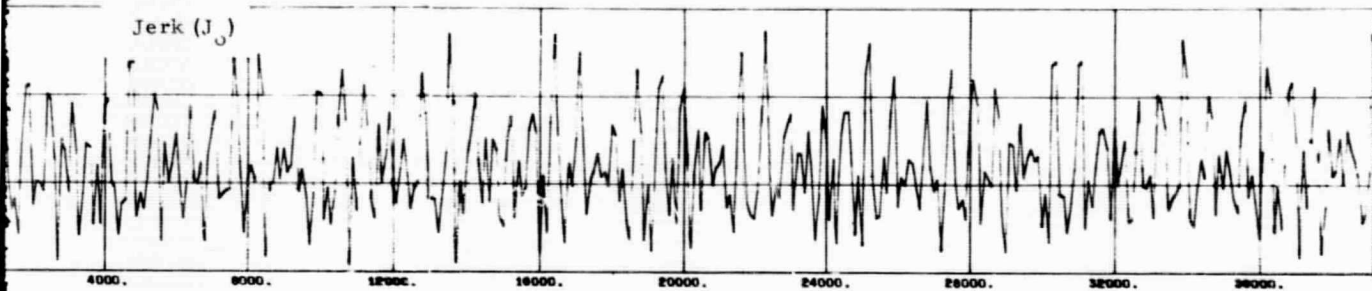
48094
G14

48094B
G24 30

Monthly Average Sunspot Number



Jerk (J_j)



Angular Momentum About the Center of Curvature (P)

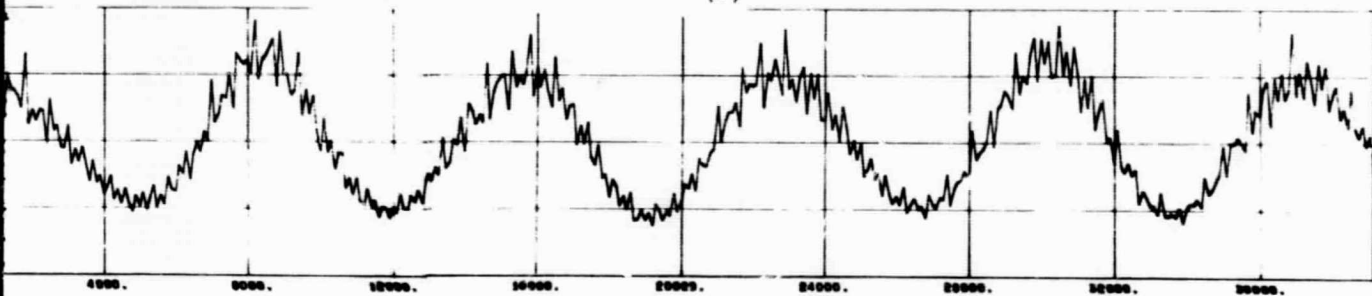
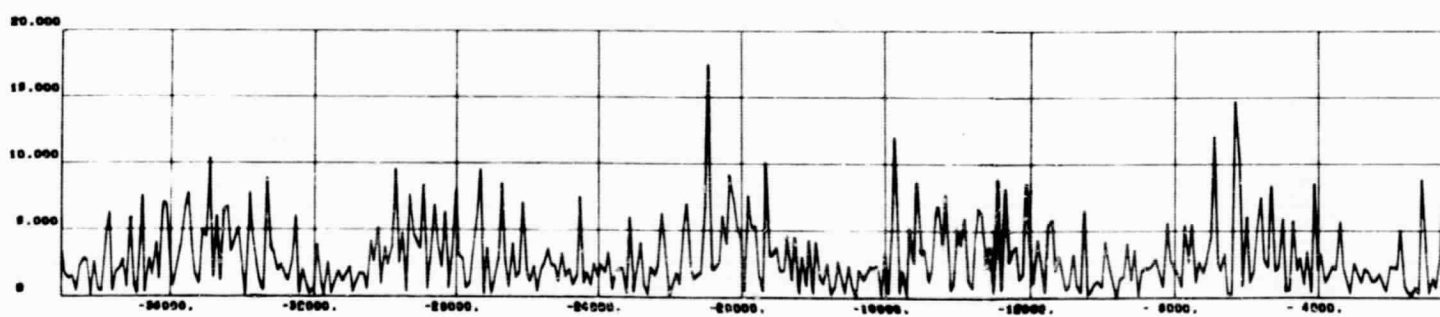
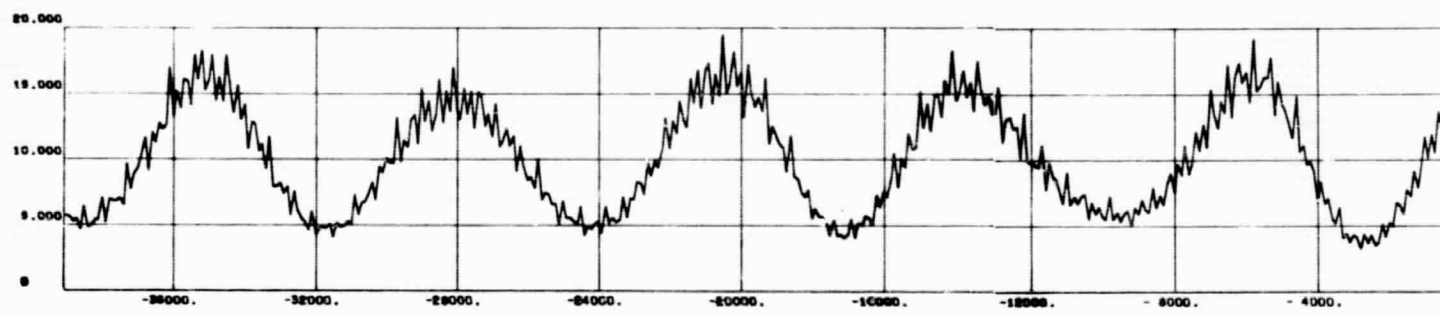
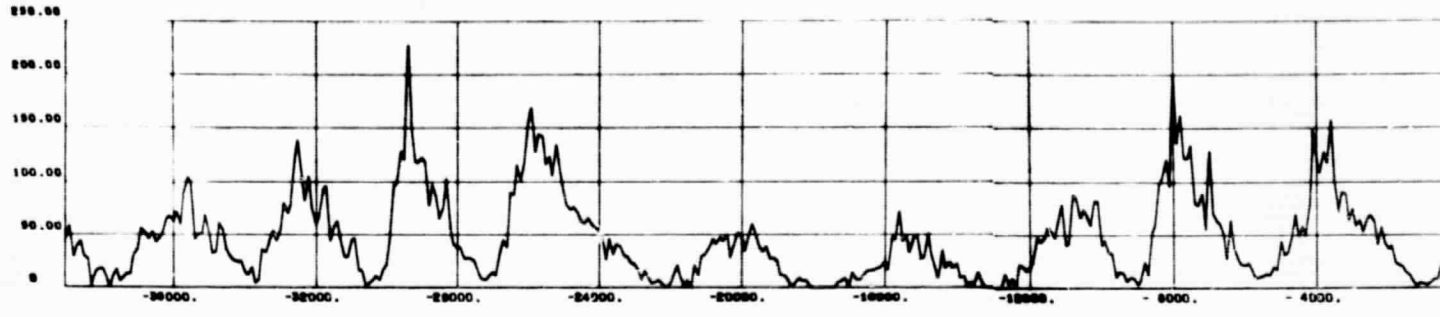


Fig. 2-4 - Jerk and C/C Angular Momentum Compared with Sunspot Number

PRECEDING PAGE BLANK NOT FILMED.

4 9094
500



FOLDED FRAME /

49084
018

49084
028 661

Monthly Average Sunspot Number

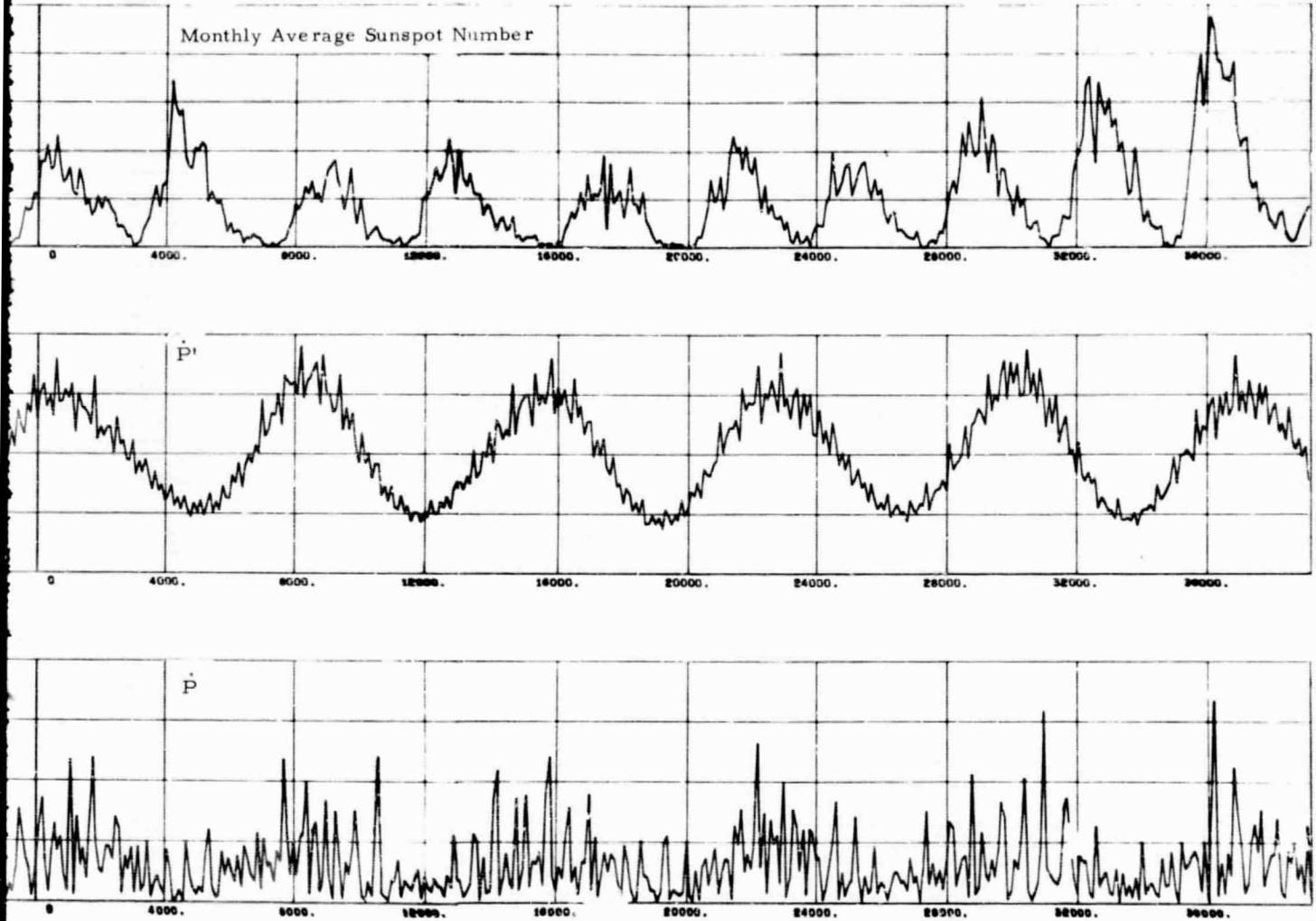
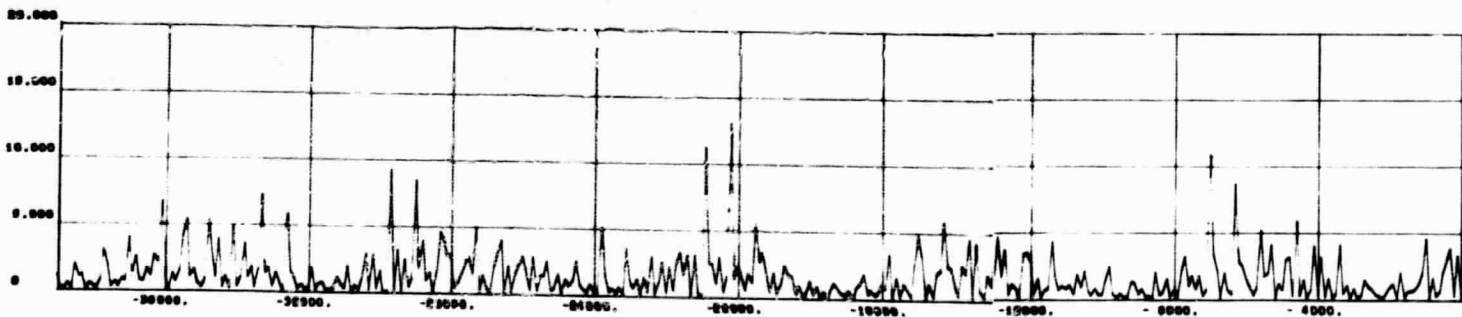
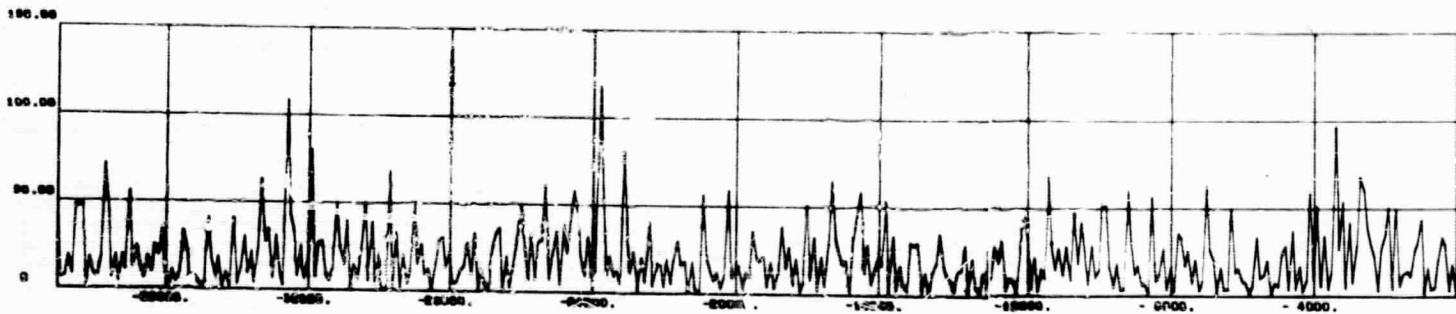
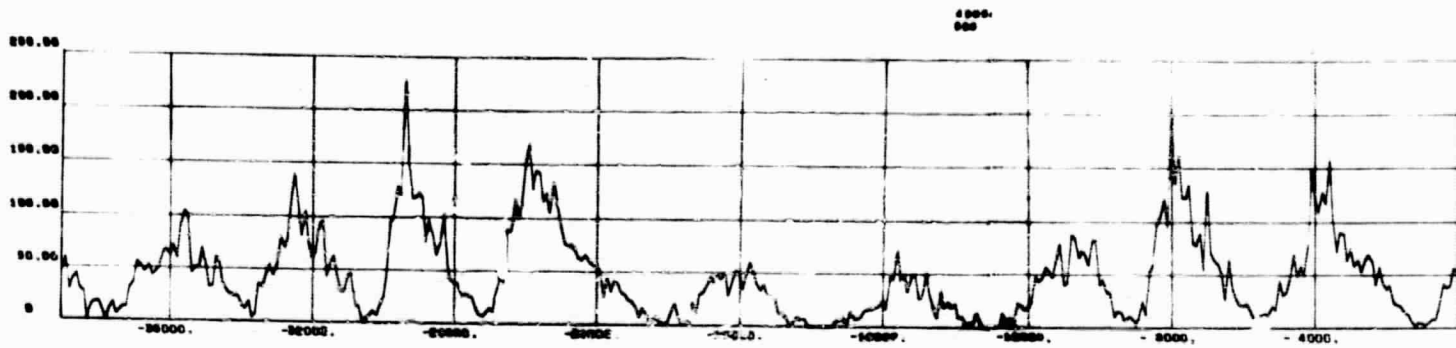


Fig. 2-5 - Rates of Change of C/C Angular Momentum Compared with Sunspot Number

PRECEDING PAGE BLANK NOT FILMED.



FOLDOUT FRAME /

40004
010

40046
020 00

Monthly Average Sunspot Number

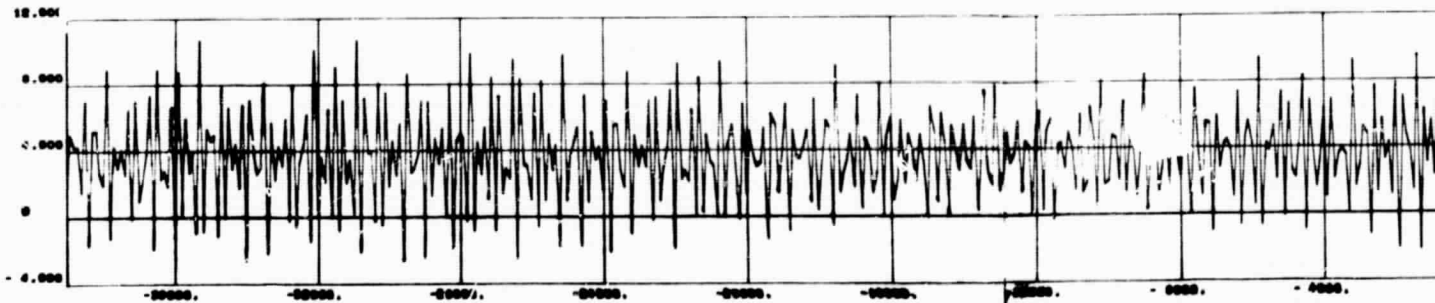
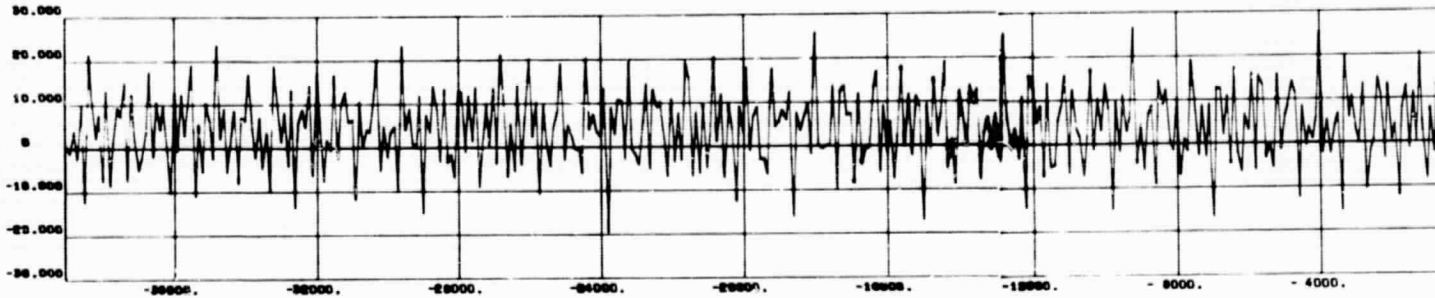
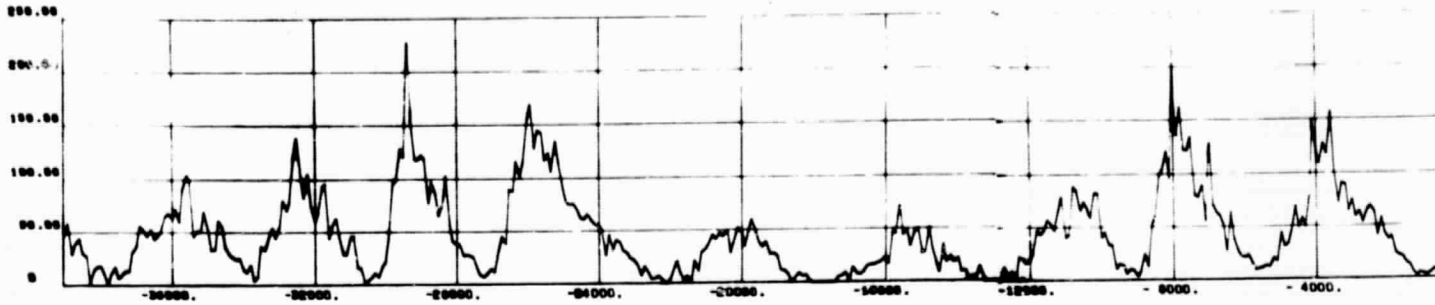
Torsion of Curvature

Rate of Change of Radius of Curvature

Fig. 2-6 - Torsion and Rate of Change of Curvature Compared with Sunspot Number

PRECEDING PAGE BLANK NOT FILMED.

4984
087

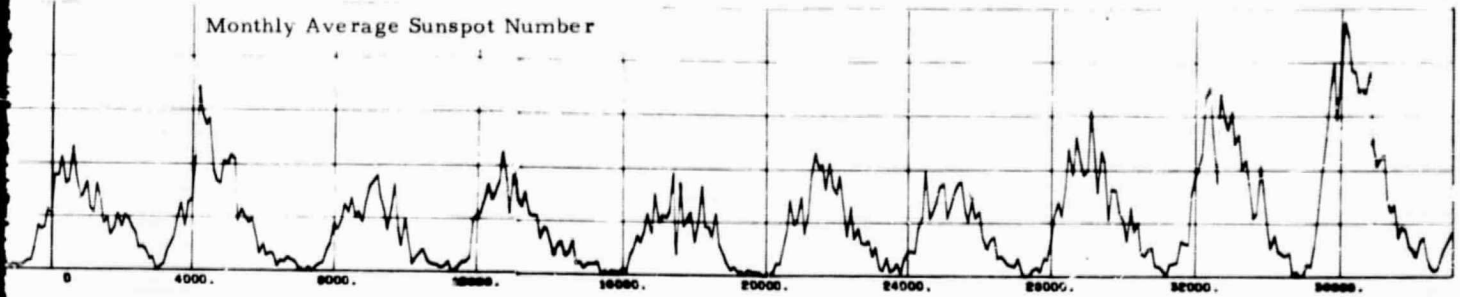


FOLDOUT FRAME

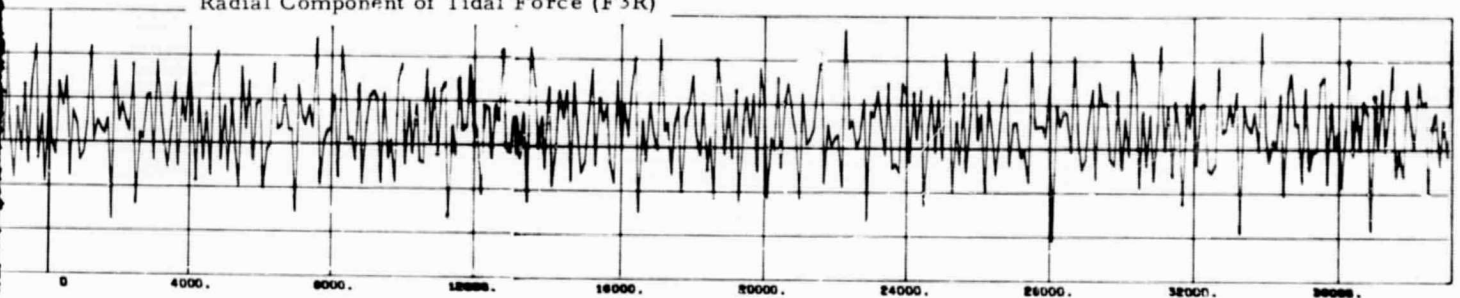
40004
017

40004
027 50

Monthly Average Sunspot Number



Radial Component of Tidal Force (F3R)



Ecliptic Force Component Rate (HF and HF')

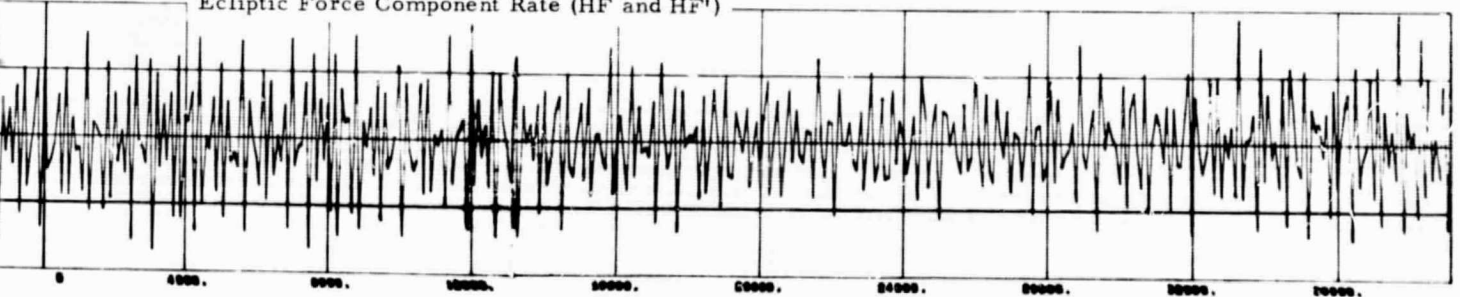
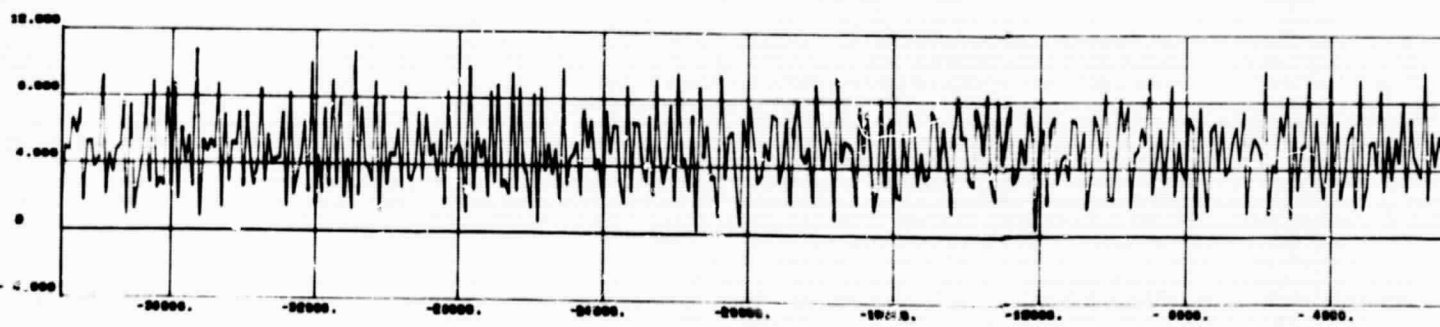
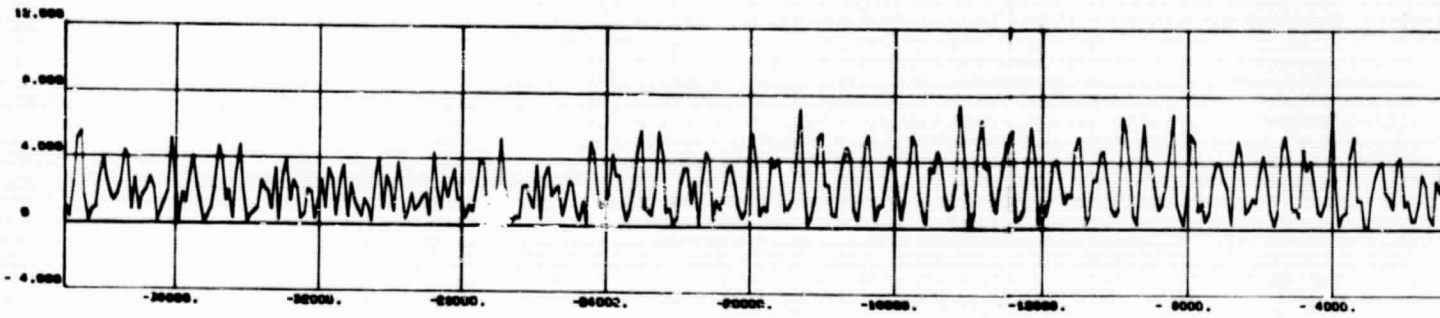
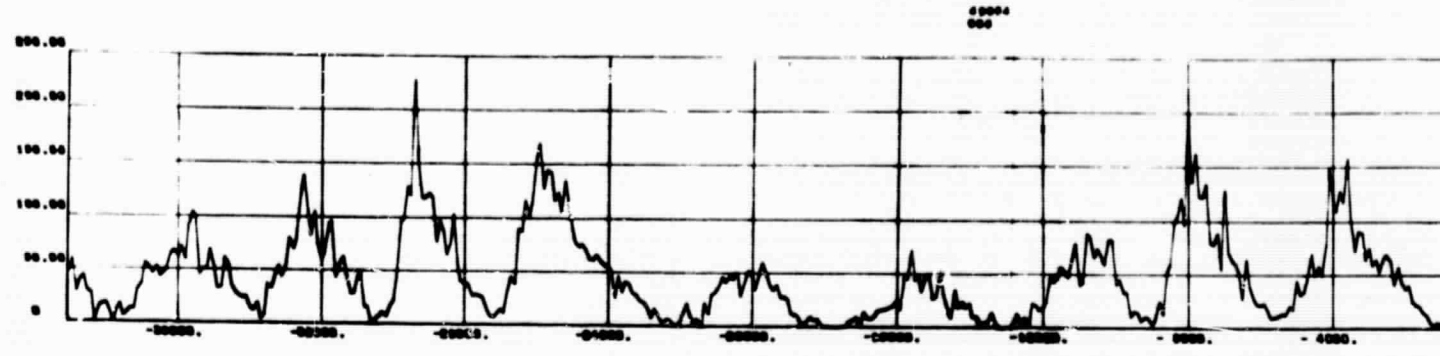


Fig. 2-7 - Radial Tidal Force and Ecliptic Force Rate Compared with Sunspot Number

PRECEDING PAGE BLANK NOT FILMED



FOLDOUT FRAME /

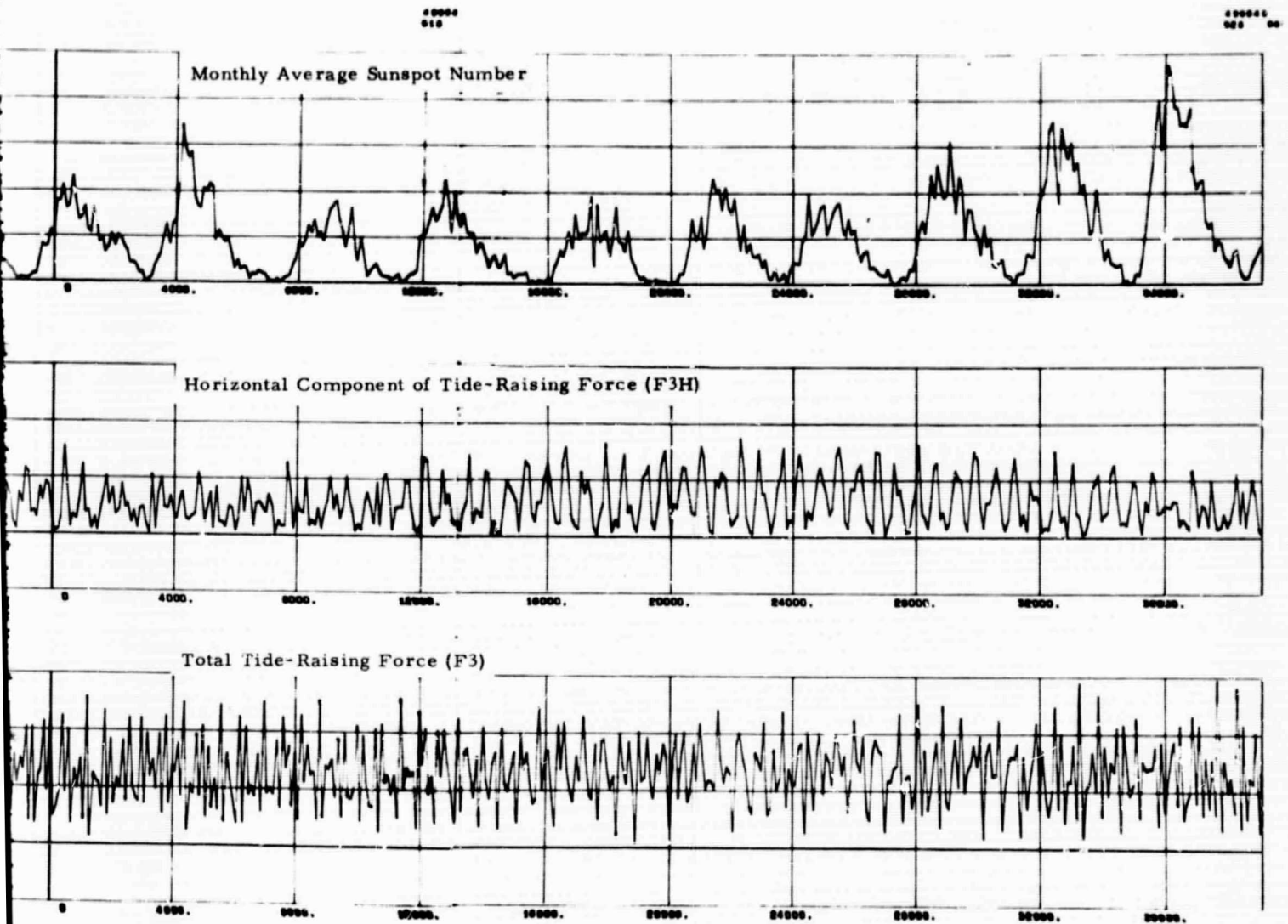
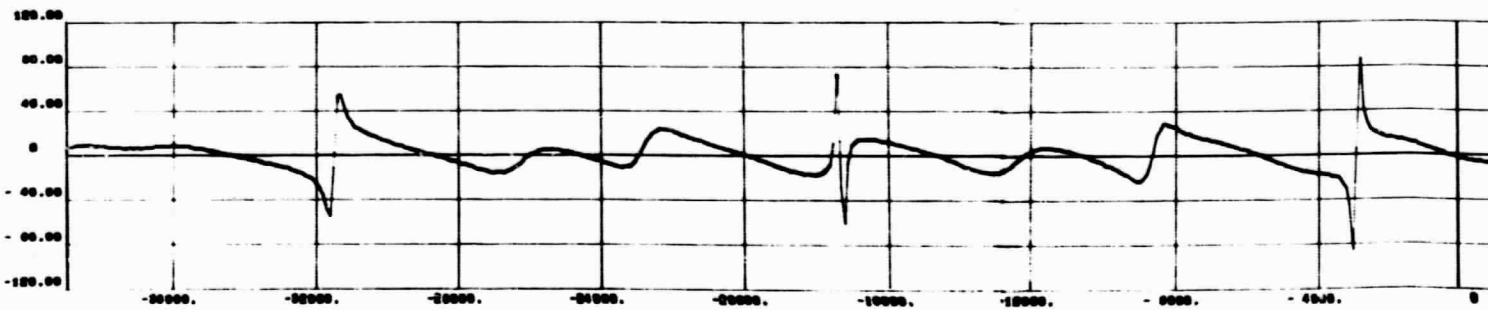
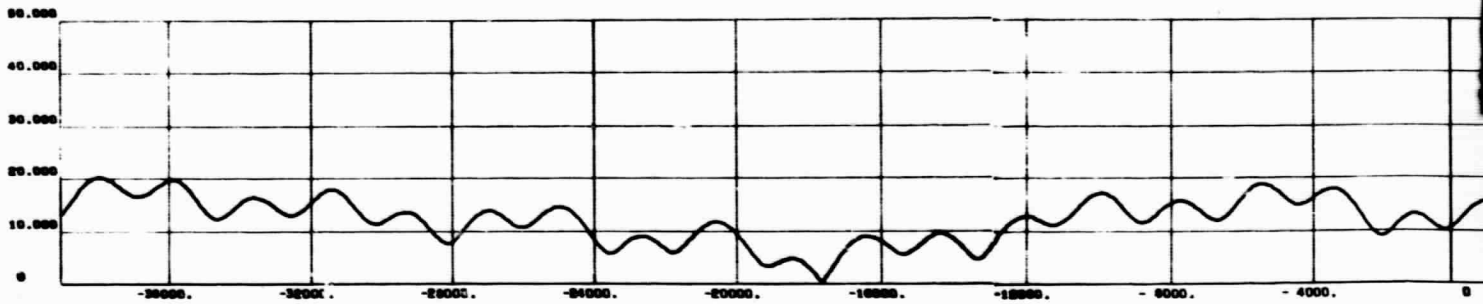
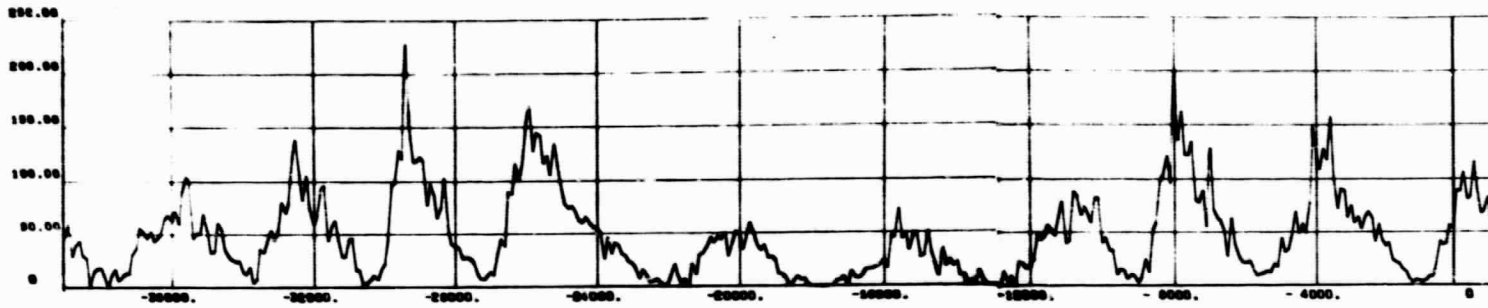


Fig. 2-8 - Horizontal and Total Tidal Forces Compared with Sunspot Number

PRECEDING PAGE BLANK NOT FILMED

40004
507



FOLDOUT FRAME /

40004
G10

40004
G09 001

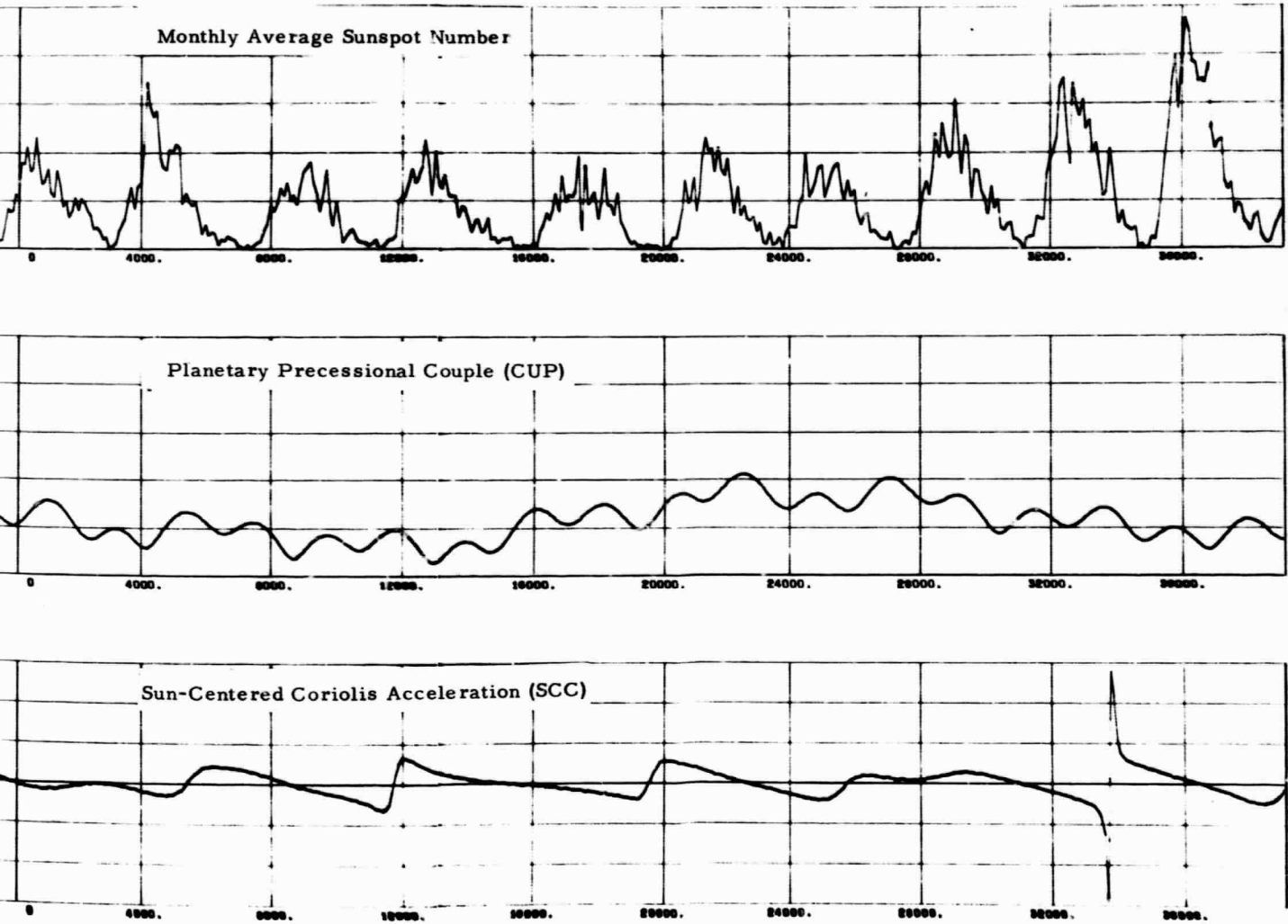
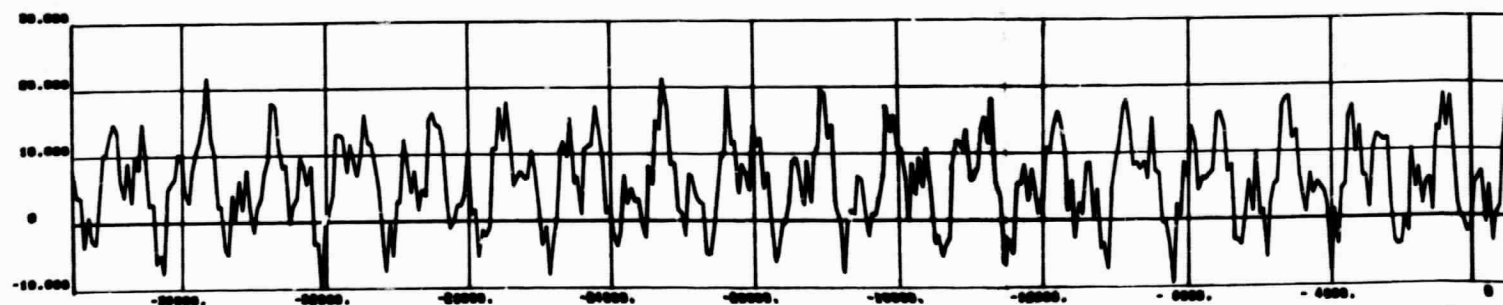
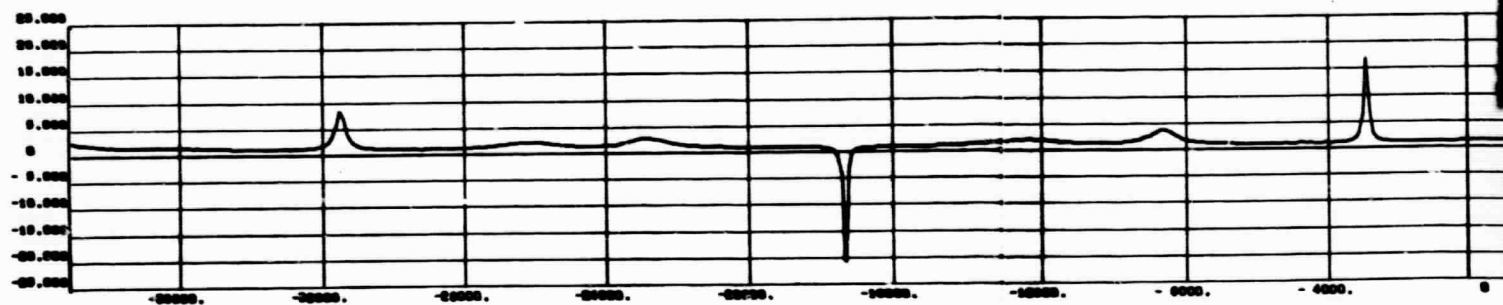
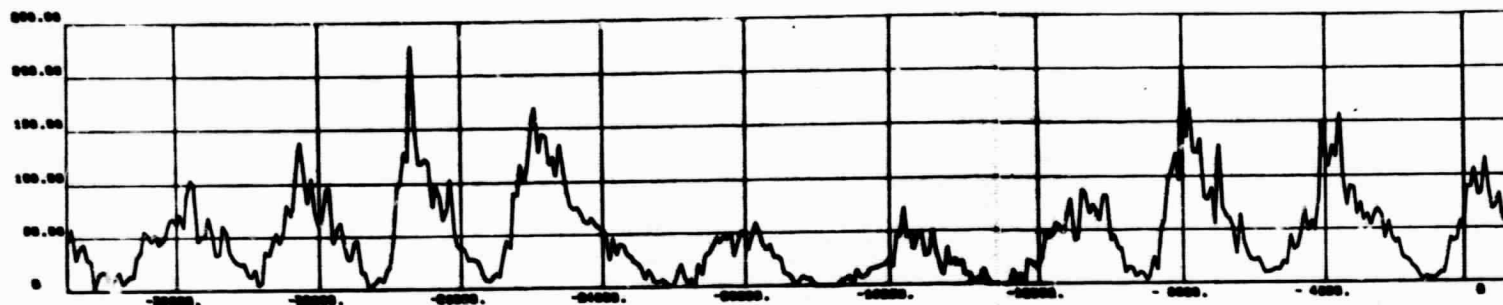


Fig. 2-9 - Planetary Couple and Sun-Centered Coriolis Compared with Sunspot Number

PRECEDING PAGE BLANK NOT FILMED.

0004
010



FOLDOUT FRAME |

40004
000

40040
000 00

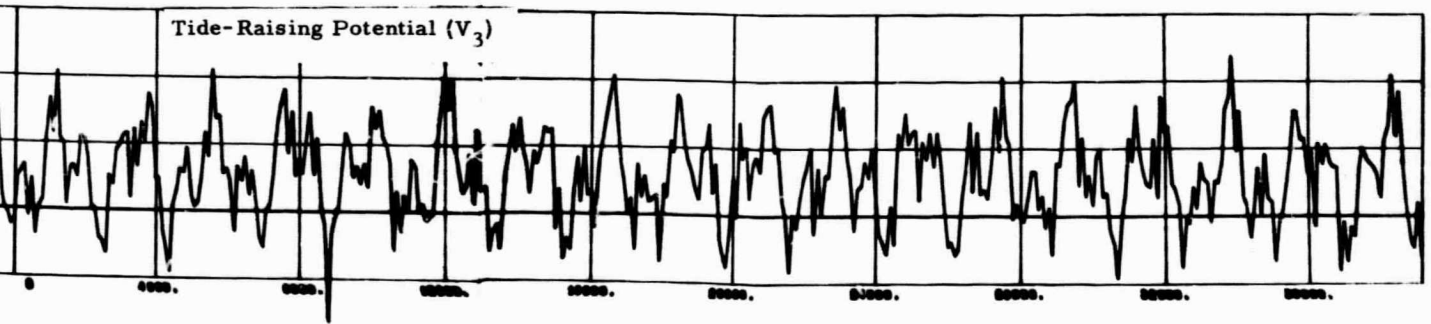
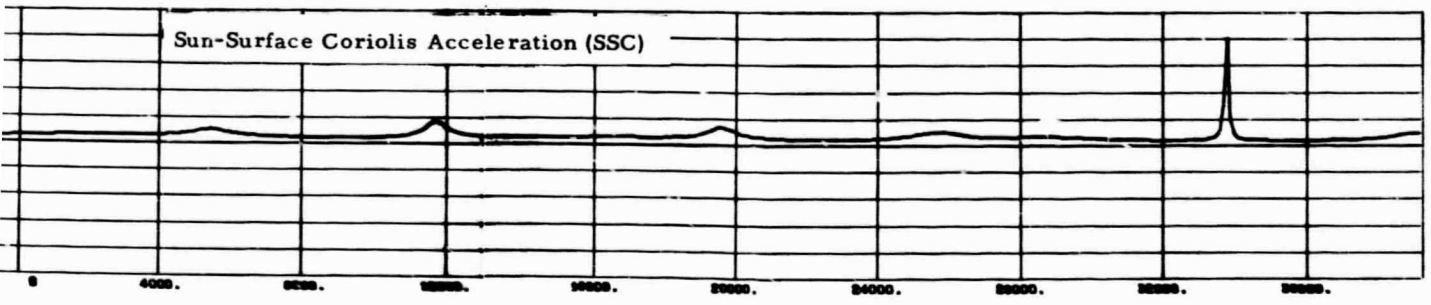
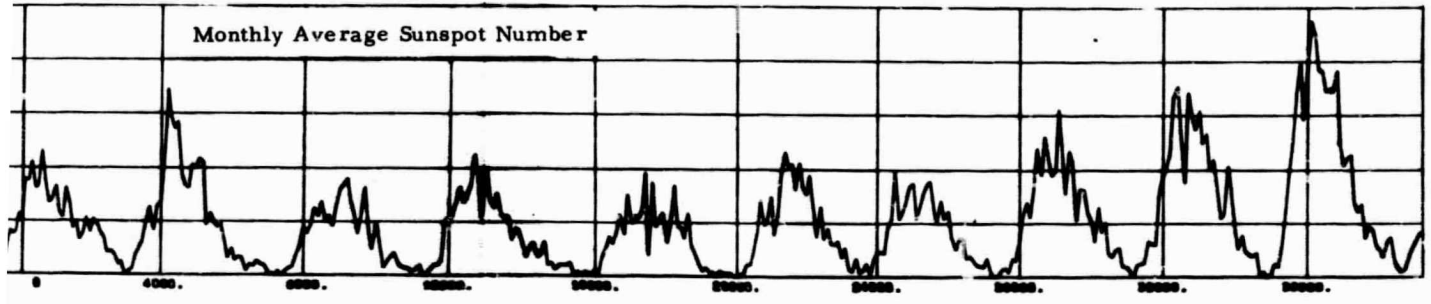
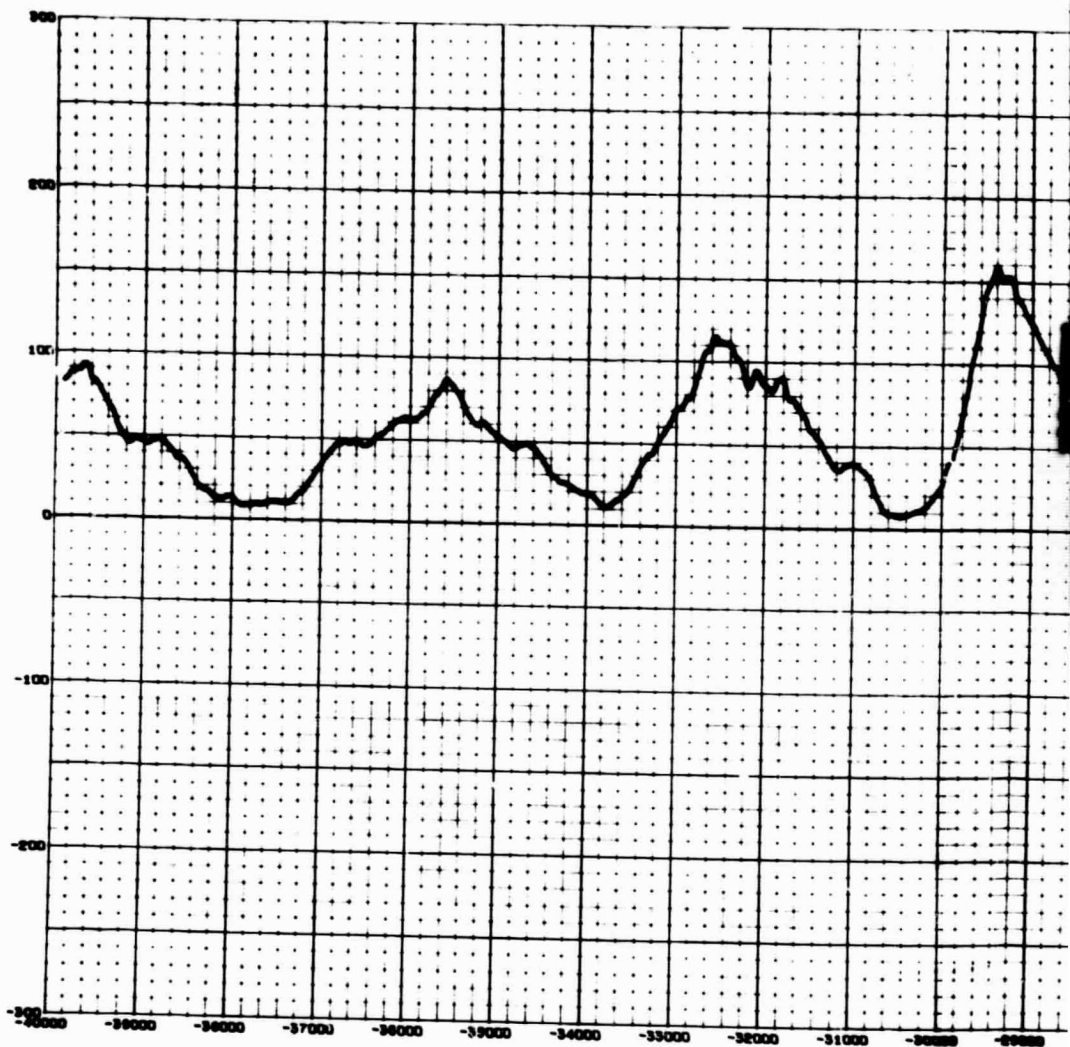


Fig. 2-10 - Sun Surface Coriolis and Tide-Raising Potential Compared with Sunspot Number

PRECEDING PAGE BLANK NOT FILMED

NU



FOLDOUT FRAME /

NUMBER SUNSPOTS VS. MODIFIED JULIAN DATE

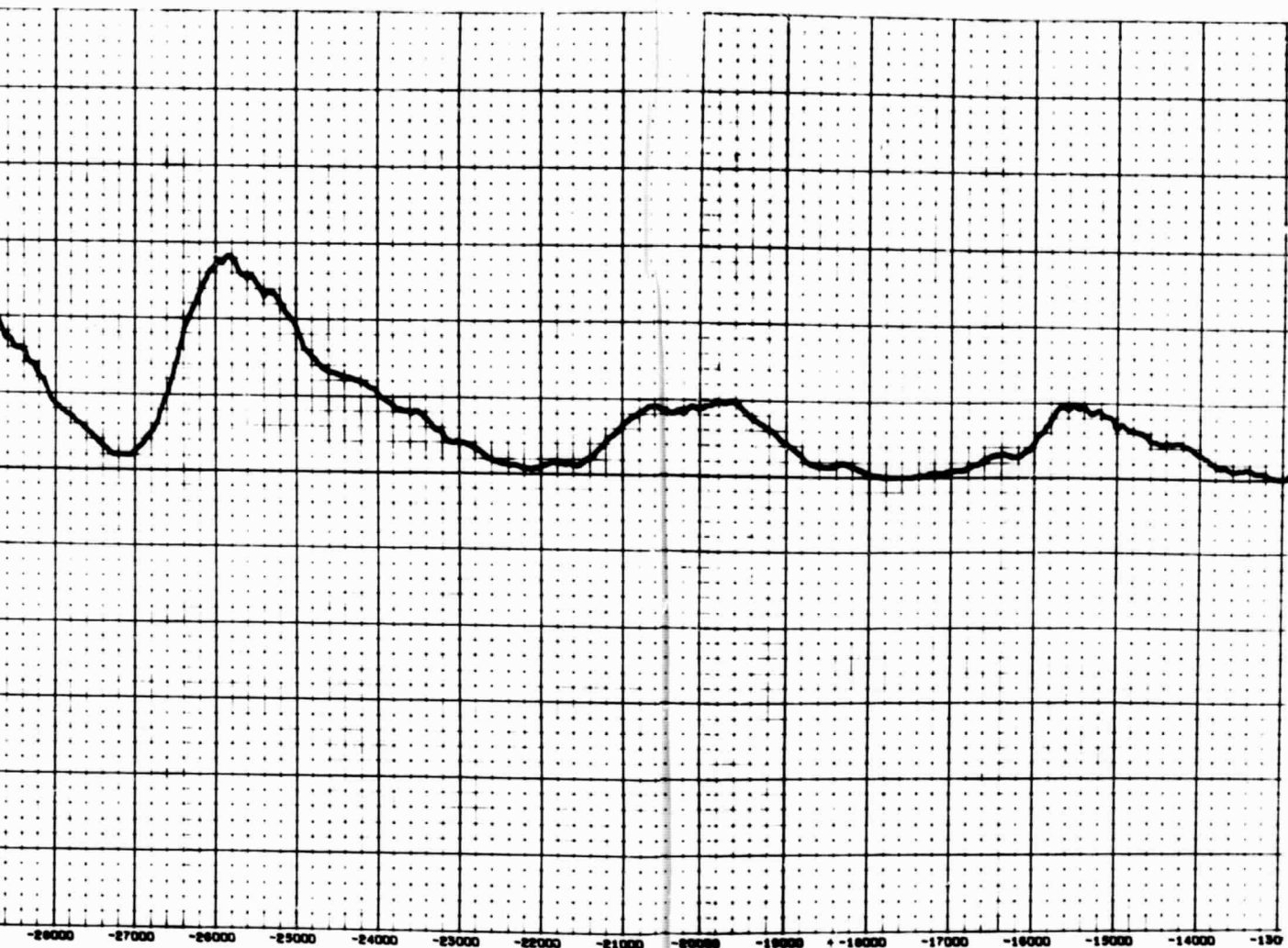
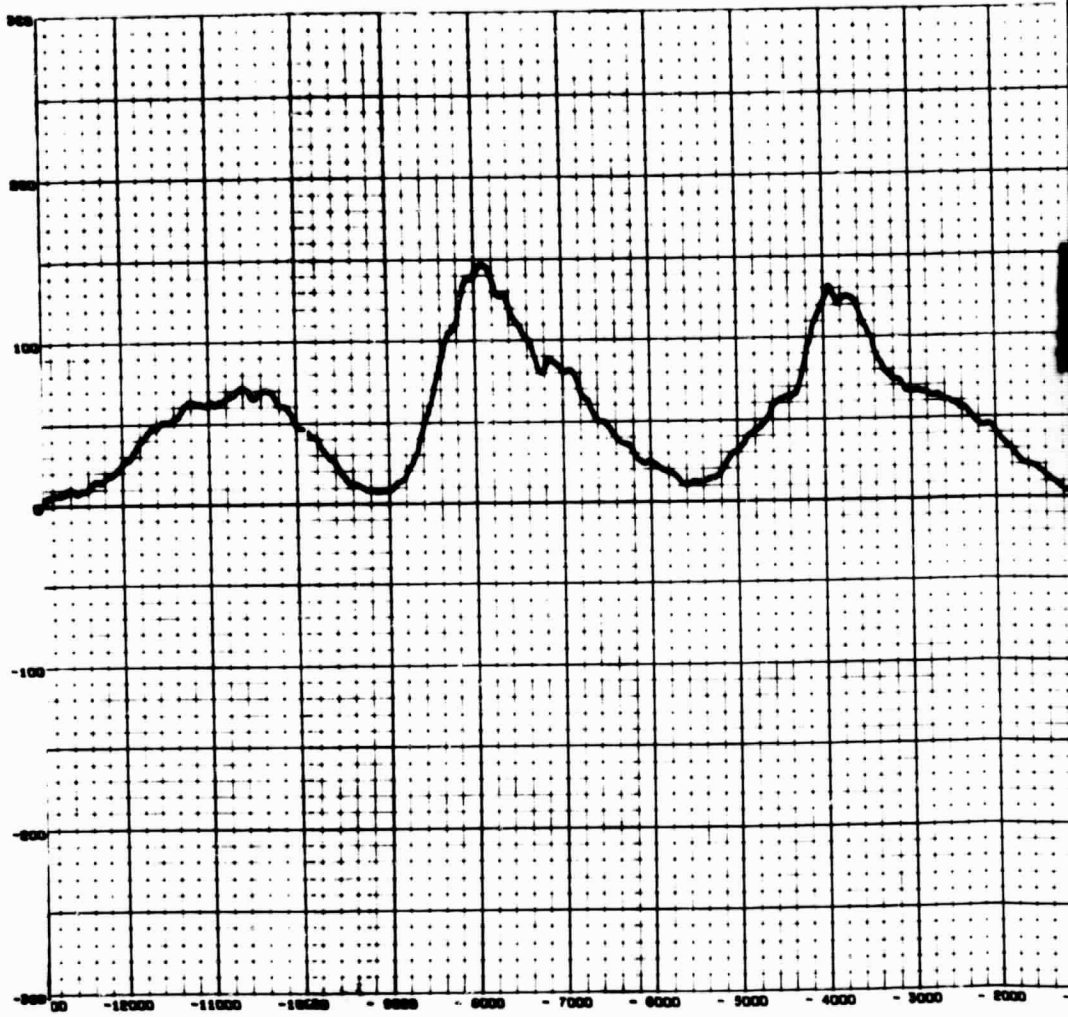


Fig. 2-11a - Time History of |SSN|

PRECEDING PAGE BLANK NOT FILMED.



FOLDOUT FRAME |

NUMBER SUNSPOTS VS. MODIFIED JULIAN DATE

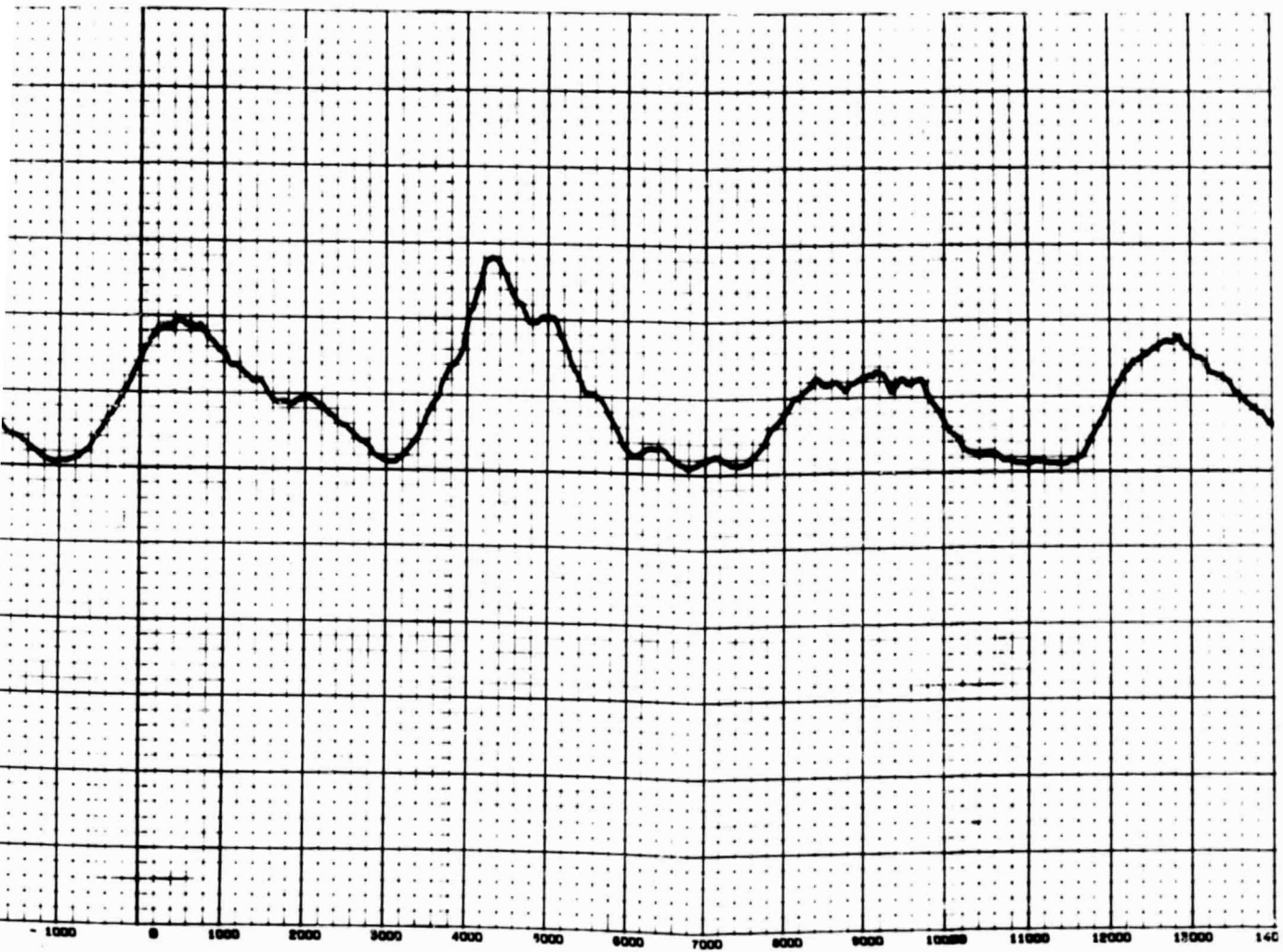
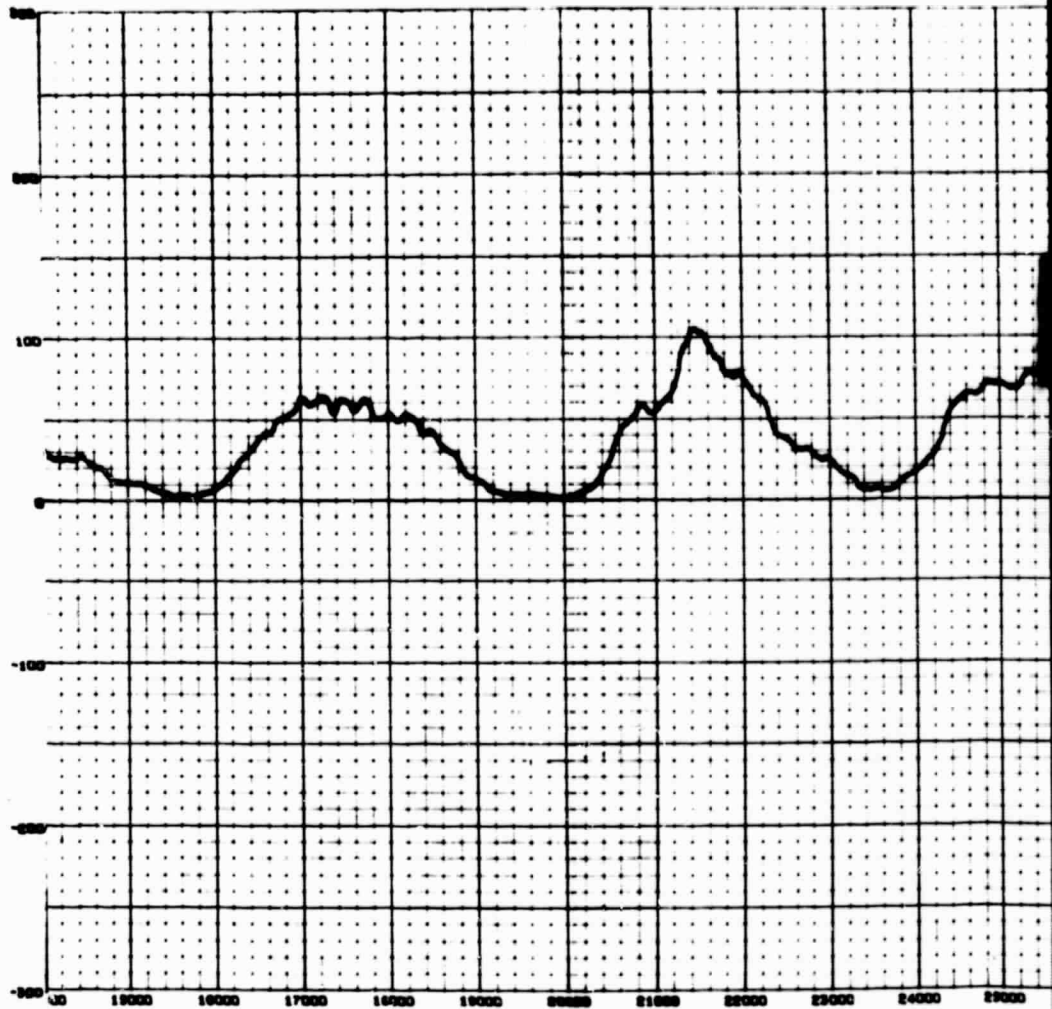


Fig. 2-11b - Time History of |SSN|

PRECEDING PAGE BLANK NOT FILMED.

NUMBER SUNSPOTS VS. MO



FOLDED FRAME /

MODIFIED JULIAN DATE

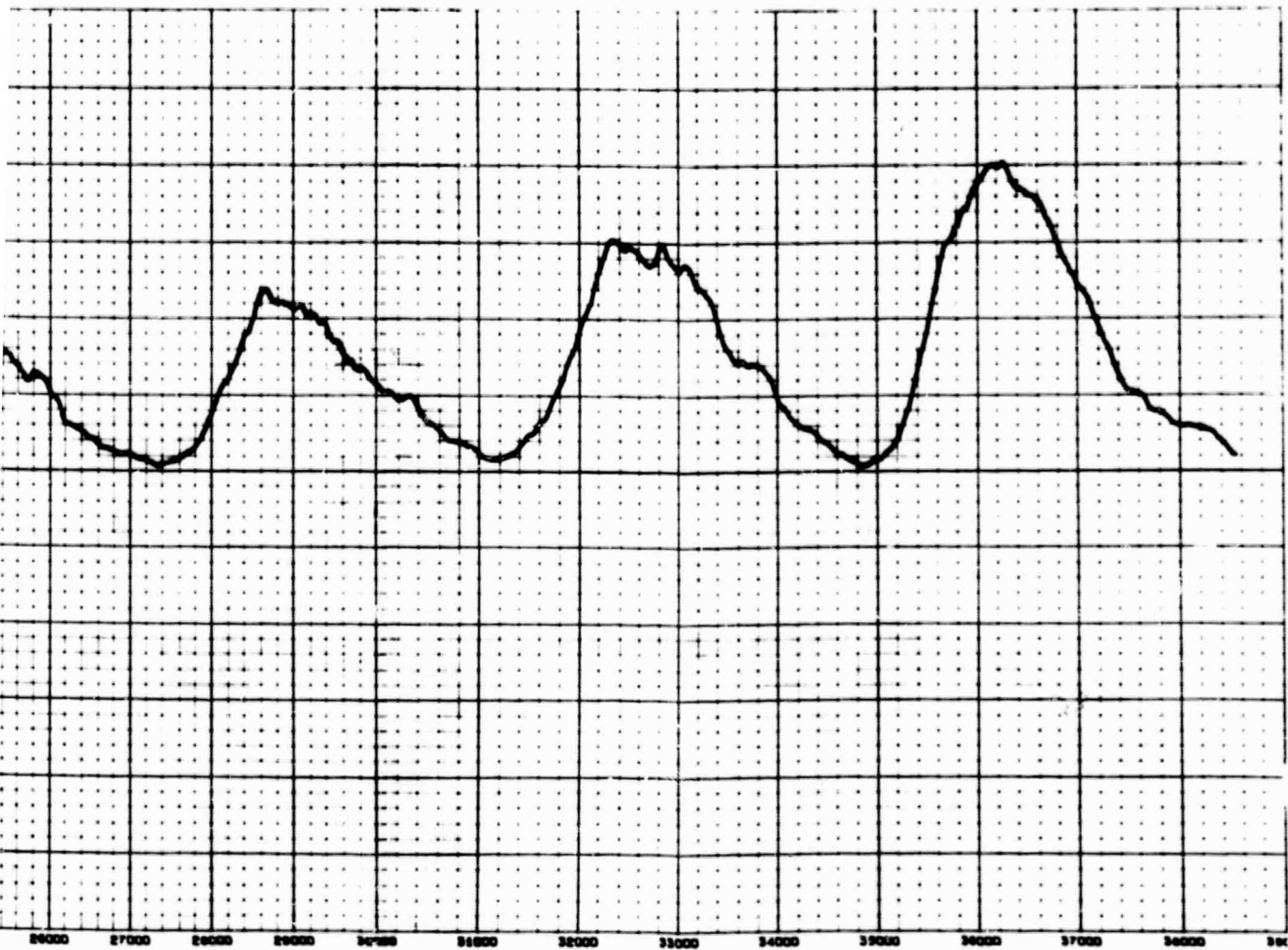
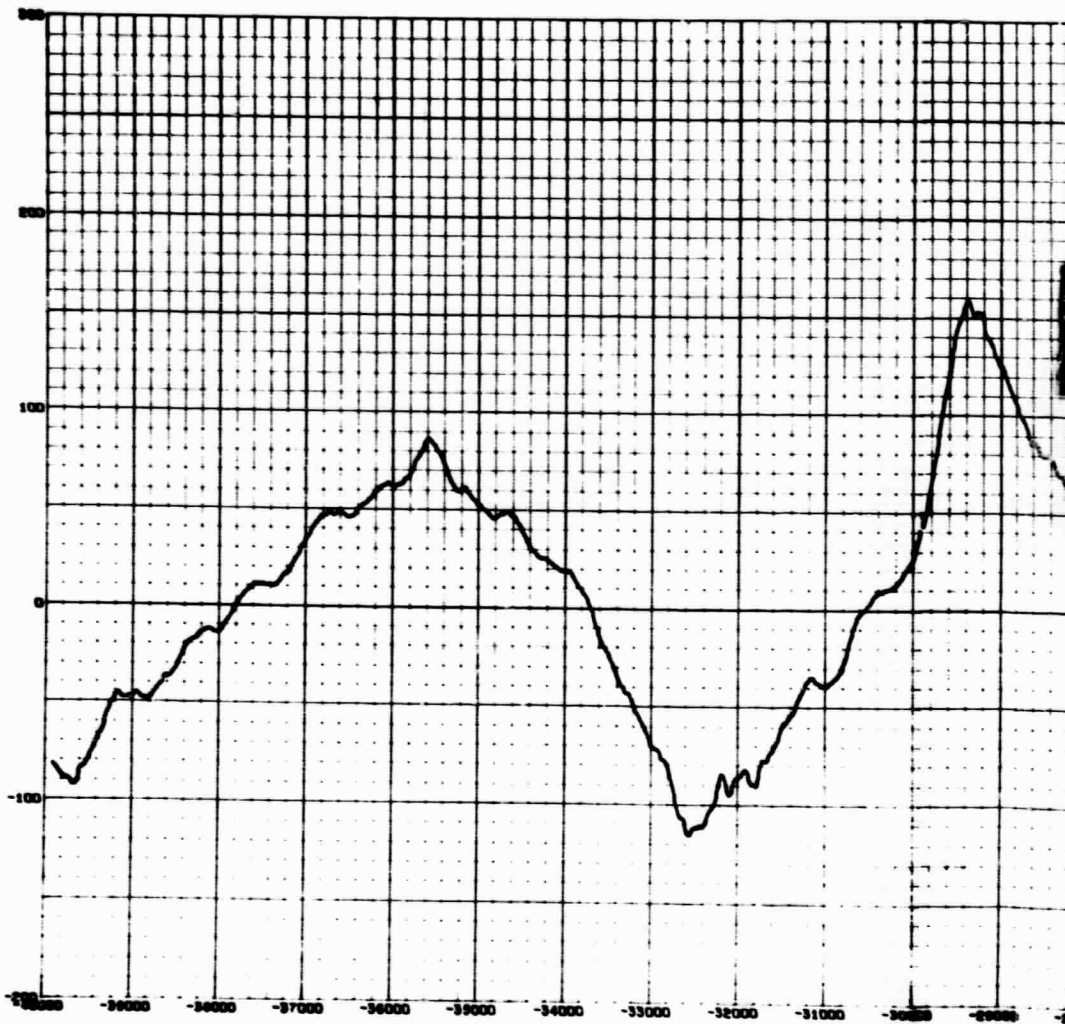


Fig. 2-11c - Time History of |SSN|



FOLDOUT FRAME 60

SSN VS. MODIFIED JULIAN DATE

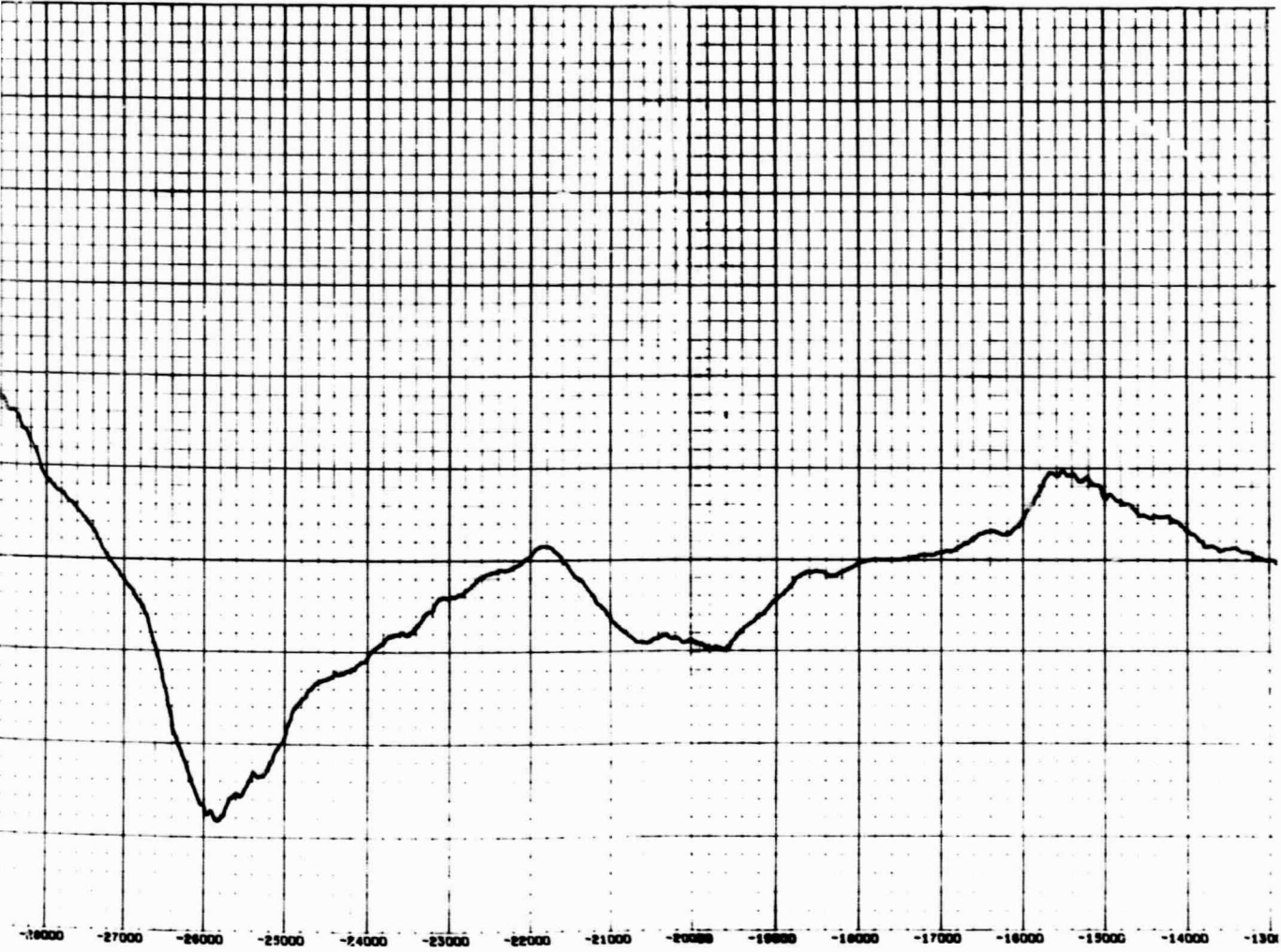
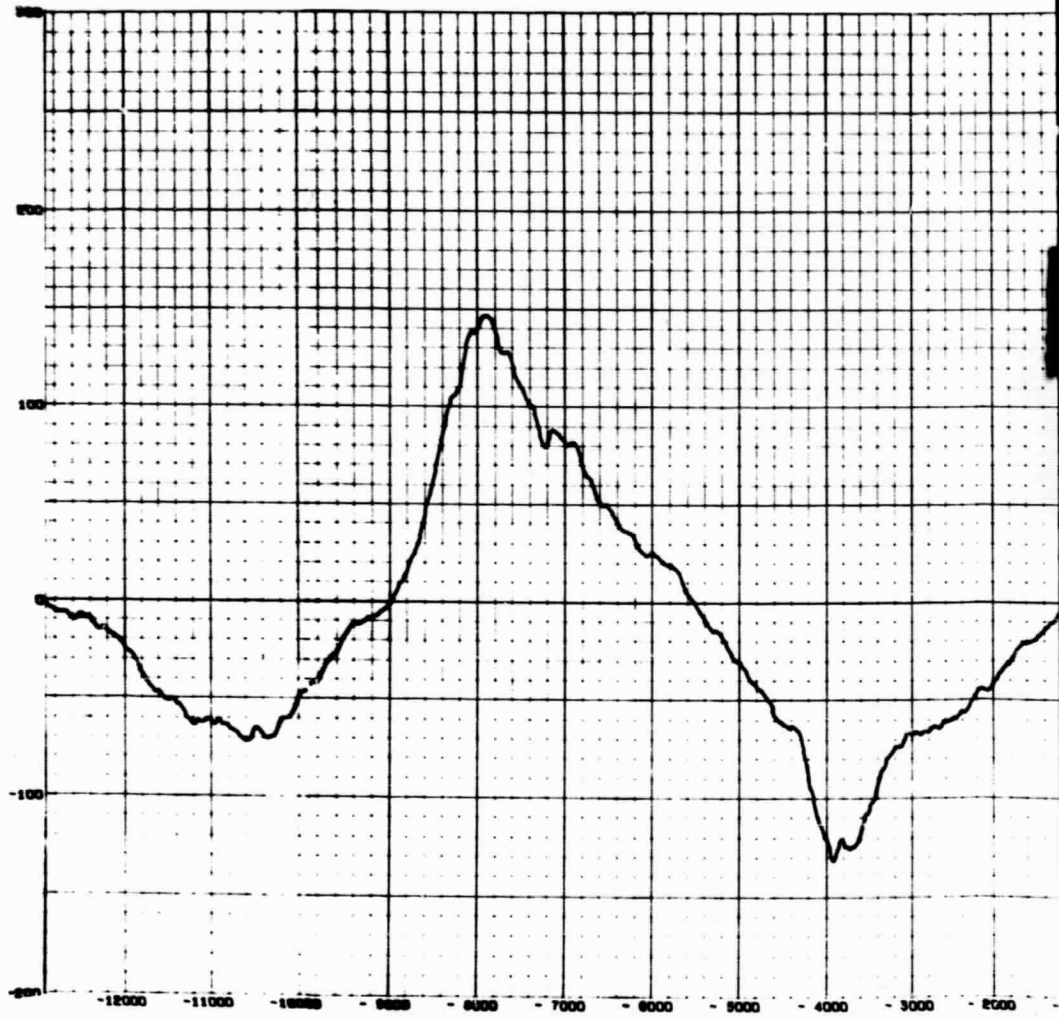
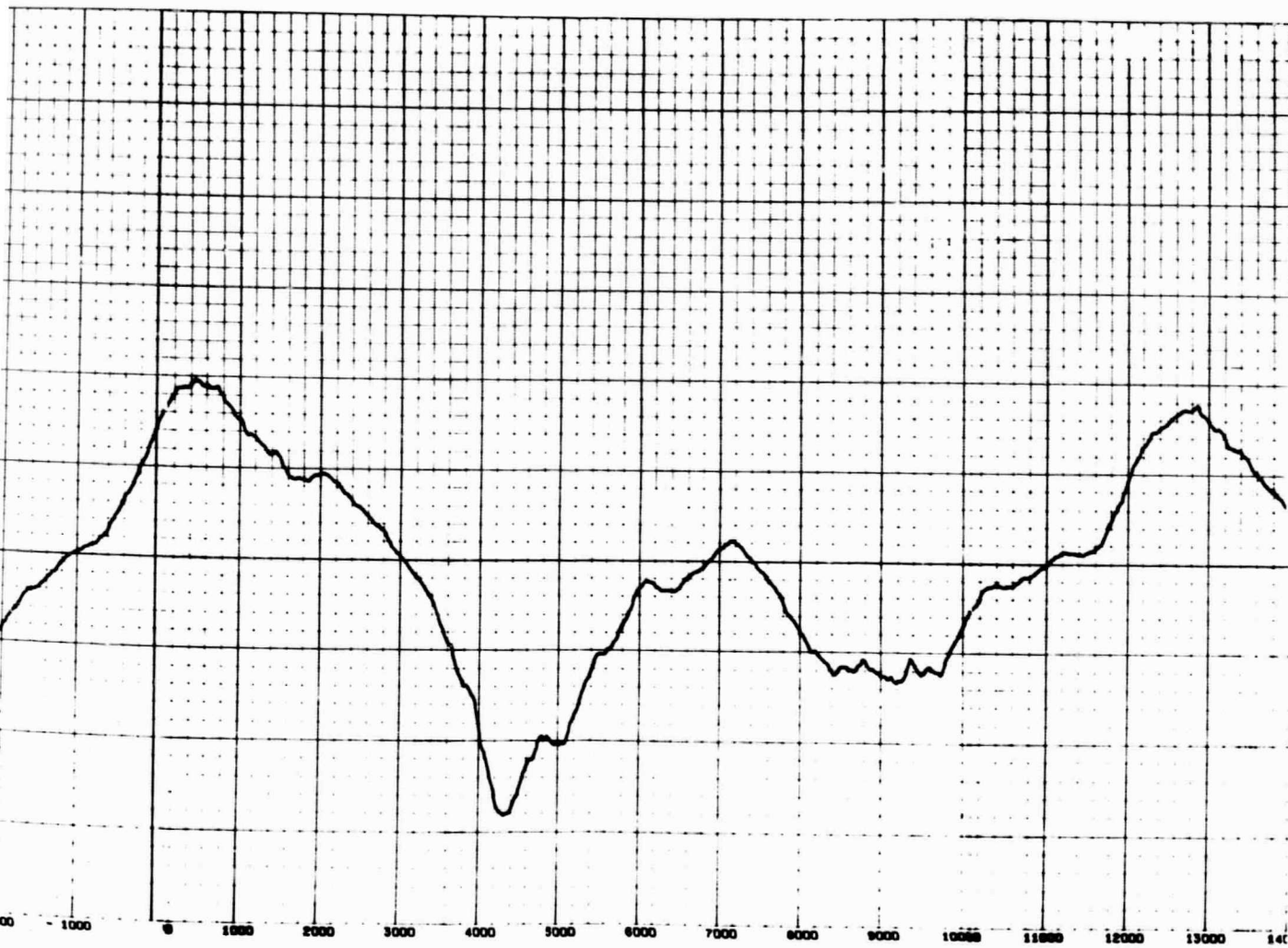


Fig. 2-12a - Time History of \pm SSN

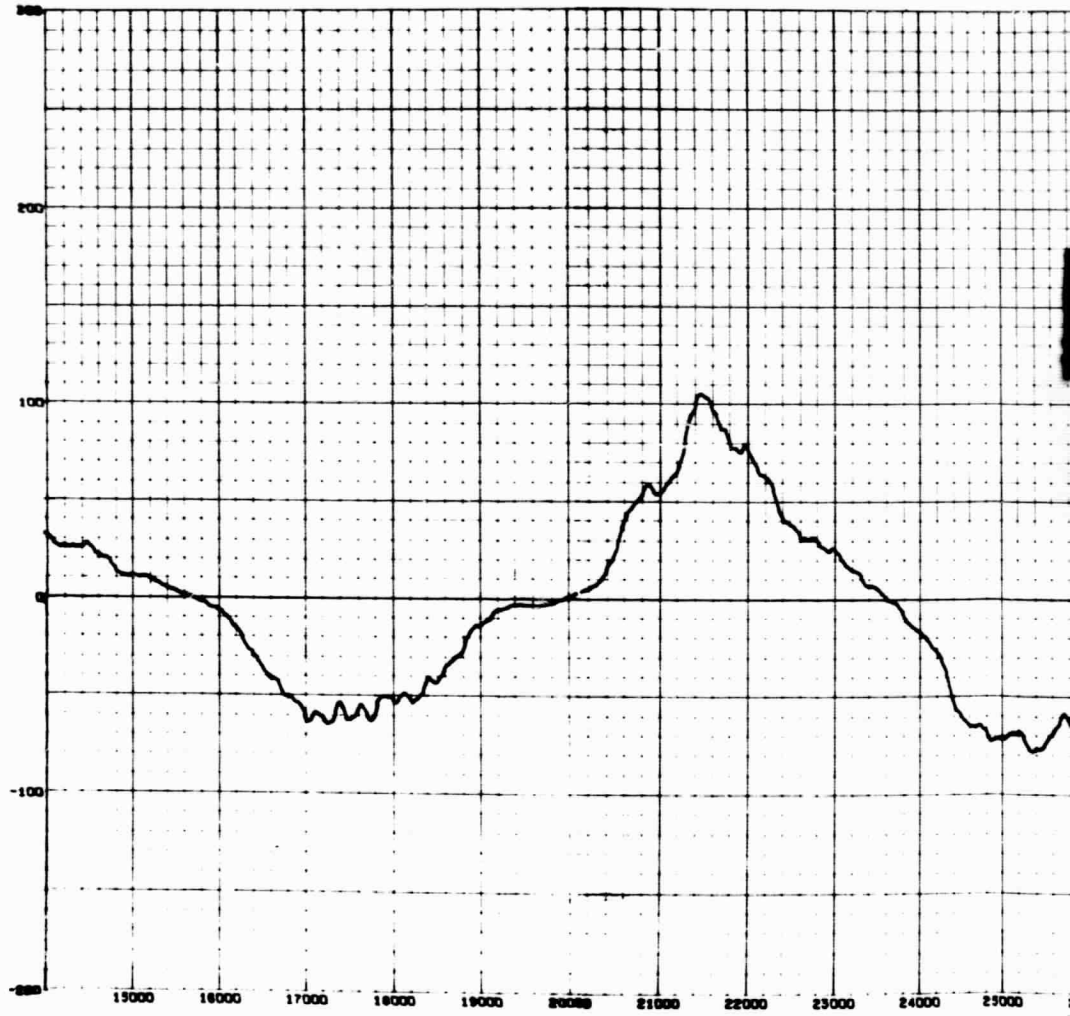


FOLDOUT FRAME 62

SSN VS. MODIFIED JULIAN DATE

Fig. 2-12b - Time History of \pm SSN

SSN VS. MODIFIED



FOLDOUT FRAME

FIED JULIAN DATE

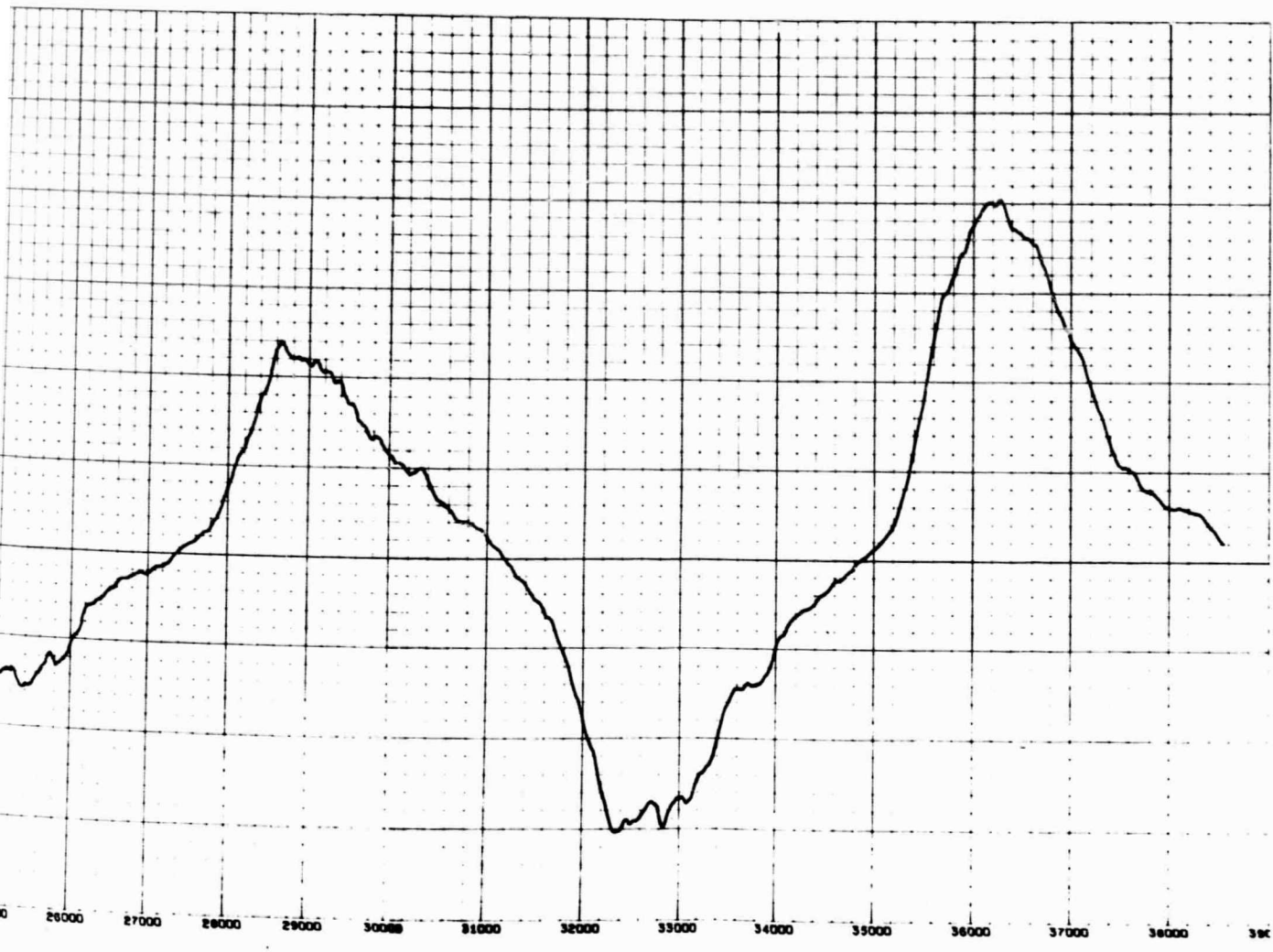


Fig. 2-12c - Time History of \pm SSN

FOLDOUT FRAME

Section 3

DATA BASE USED FOR SUNSPOT NUMBER ESTIMATION

3.1 GENERAL

The data used in the estimation of sunspot number consist of 21 parameters relating to the dynamic interaction between the planets and the Sun. The method used to derive these parameters has been described in Section 2. Figures 2-1 through 2-10 show plots of these prediction parameters as a function of modified Julian Date (MJD). Table 3-1 lists the 21 predictors corresponding to Figs. 2-1 through 2-10.

These parameters are easily computed for any time in the future or past. For the purpose of this study they were found for a range of time that began 20 years before the first recorded sunspot cycle and extended 20 years beyond the last sunspot cycle. This was done for three reasons: (1) so that data could be filtered and end effects of the filter would not affect the estimates; (2) so that a cross-correlation function between these parameters and sunspot number could be obtained using a constant sample size; and (3) so that prediction parameters would be available to predict sunspot number into the future. (The third reason is obvious; the first two reasons will be better understood after reading Section 4.) These parameters were sampled every 20 days from MJD -47400 to MJD 46020 for a total of 4672 samples. The sampling rate was chosen so the entire time history of sunspot number, SSN, could be processed by the computer at one time. At the same time it should be emphasized that this sampling rate was high enough to extract all the useful information from these parameter waveforms, insofar as the prediction of smoothed sunspot number was concerned.

74
9/15

Table 3-1
PARAMETERS USED TO ESTIMATE SUNSPOT NUMBER

Number	Abbreviation	Parameter
1	Ro	position
2	Vo	velocity
3	Ao	acceleration
4	Ho	angular momentum
5	Zeta	radius of curvature of Sun's path
6	Lo	rate of change of angular momentum
7	Jo	rate of change of acceleration
8	P	angular momentum about center of curvature of Sun's path
9	\dot{P}	rate of change of P
10	\bar{P}'	rate of change of \bar{P}
11	Tau	torsion of curvature
12	ROD	rate of change of radius of curvature
13	HF	longitudinal rate of change of horizontal force
14	HF'	HF calculated by different method
15	F3R	radial tide-raising force
16	F3H	horizontal tide-raising force
17	F3	total tide-raising force
18	CUP	planetary precessional couple
19	SCC	Sun-center Coriolis
20	SSC	Sun-surface Coriolis
21	V3	tide-raising potential

The values of sunspot number are initially monthly means with linear interpolation between these values to get a sunspot number, R_z , every 20 days. The history of R_z begins at MJD -40100 and continues to 38720 for a total of 3942 samples. These values of R_z were smoothed to produce a yearly running average

$$SSN(t_i) = \frac{1}{19} \sum_{j=-9}^{+9} R_z(t_i + j)$$

where

$$MJD -39920 \leq t_i \leq MJD 38540.$$

Due to the end effect of this smoothing operation the number of values of sunspot number SSN is reduced from 3942 to 3924. Figure 2-11 is this yearly average of sunspot number SSN as a function of Modified Julian Date. In this plot the average period of SSN is approximately 11 years. It has been suggested (Ref. 14) that the SSN be plotted as positive and negative values to indicate the change in magnetic polarity of the sunspot pairs. Figure 2-12 is a plot of $\pm SSN$ as a function of MJD, which produces a 22-year cycle. During the course of this study the correlation between each of these configurations and the 21 predictors was found (see Section 4.2).

3.2 DATA PREPROCESSING AND DATA SETUP PRIOR TO ESTIMATION OF SUNSPOT NUMBER

A number of preprocessing procedures were applied to the predictor parameters before estimates of sunspot number were made. This was done to assure that the predictor parameters are used in the most meaningful way. Preprocessing procedures include filtering, cross-correlation with sunspot numbers, and normalizing. In addition to describing these preprocessing techniques the data base setup is discussed.

3.2.1 Filtering the Predictor Parameters

Since many of the predictor parameters had high frequency content and it was not desirable to estimate a sunspot number waveform that contained high frequency components, some of the parameters were filtered. To avoid the problem of phase shift a digital filter was used based on the convolution of $\sin x/x$ with the input data. This filter was mechanized using the equations given below:

$$X'_j = H_0 \cdot X_j + \sum_{i=1}^{Narg} H_i \cdot (X_{j+i} + X_{j-i})$$

X_j = original data point

X'_j = filtered data point

$H_0 \rightarrow H_{Narg}$ = filter coefficients

$Narg + 1$ = number of filter coefficients

$$H_i = \frac{\sin(2\pi f_{co} t_i)}{H_{sum} \cdot (2\pi f_{co} t_i)}$$

t_i = $i \cdot$ sampling frequency

f_{co} = cutoff frequency in cycles/year

$$H_{sum} = 1 + \sum_{i=1}^{Narg} 2 \cdot H_i$$

$$H_0 = 1 / H_{sum}$$

$$\omega t_{Narg} \approx 4\pi$$

During the course of this study filter coefficients were derived for cutoff frequencies of one year, one-half year and one-fourth of a year. Since the sampling frequency was 20/365 there were 19, 37, and 73 coefficients, respectively, for these three filters. While these coefficients are easily derived, a

listing of them is provided in Appendix A. Table 3-2 indicates the amount of filtering each of the 21 input parameters received.

Figures 3-1 through 3-21 show plots of sample portions of the time histories of the 21 predictor parameters after filtering, and shifting the appropriate value of τ days.

3.2.2 Cross-Correlation of Predictor Parameters with Sunspot Number

The cross-correlation function between predictor parameters is defined as

$$\alpha_j(\tau) = \frac{1}{N} \sum_{i=1}^N P_j(t_i + \tau) \cdot SSN(t_i) \quad \begin{array}{l} j = 1 \text{ to } 21 \\ \tau = -T \text{ to } T \end{array}$$

where

- P_j = predictor parameter, j
- SSN = sunspot number
- N = total number of sunspot numbers in data base
- $2T$ = range over which $\alpha(\tau)$ is obtained

At any value of τ the correlation coefficient is defined as

$$\rho_j = \frac{\alpha_j(\tau) - \bar{P}_j \cdot \overline{SSN}}{\sigma_{P_j} \cdot \sigma_{SSN}}$$

where

- \bar{P}_j = expected value of P_j
- \overline{SSN} = expected value of SSN
- σ_{P_j} = standard deviation of P_j
- σ_{SSN} = standard deviation of SSN.

Table 3-2
FILTER CHARACTERISTICS APPLIED TO PREDICTOR PARAMETERS

Parameter	Cutoff Frequency (cycles/year)	No. of Coefficients
Po	No Filtering	—
Vo	1.0	19
Ao	0.50	73
Ho/10 ^{35*}	1.00	37
Zeta	0.50	73
Lo/10 ^{24*}	0.50	73
Jo	0.50	73
P	0.50	73
Ṗ	0.50	73
P'	0.50	73
Tau	0.50	73
ROD	0.50	73
HF	0.50	73
HF'	0.50	73
F3R	0.50	73
F3H	0.50	73
F3	0.50	73
CUP	No Filtering	—
SCC	No Filtering	—
SSC	No Filtering	—
V3	0.50	73

*These parameters were normalized as indicated before filtering.

The reason for obtaining these cross-correlation functions was two-fold. First, it showed what shift in τ is necessary to achieve the best correlation with SSN for each of the predictor parameters. Second, by finding the cross-correlation functions between $|SSN|$ and the predictor (11-year sunspot cycle) and also between $\pm SSN$ and the predictors (22-year sunspot cycle) it was possible to determine which configuration correlated best with the predictors. Plots of the cross-correlation function as a function of τ in days for the 21 predictors are shown in Figs. 3-22 through 3-42. Figures 3-22a, 3-23a, etc., are for cross-correlation functions using $|SSN|$ while Figs. 3-22b, 3-23b, etc., are for cross-correlation functions using $\pm SSN$. These plots are seen to be somewhat periodic with the period approaching that of SSN. In order to have values of predictor parameters available to predict SSN into the future the value of τ where maximum correlation occurs for each of the parameters was forced to be negative. As can be seen from Figs. 3-22 through 3-42 this restriction causes little or no decrease in peak correlation. It is true that correlations where τ is positive tend to be higher but the difference is small and the negative τ restriction is necessary to find SSN^{\wedge} into the future. Table 3-3 lists the maximum correlation coefficient and the value of τ where that correlation occurs for the $|SSN|$ and the $\pm SSN$ configurations. This table indicates which parameters are most strongly related to SSN and the time lag needed to obtain this relation. Using this information each of the 21 predictors are shifted to indicated amounts for use in estimating SSN.

Table 3-3 shows that the correlation coefficients for the $\pm SSN$ configuration are generally higher than for the $|SSN|$ configuration. However, for 10 of the 21 parameters the correlation coefficients for $|SSN|$ are higher than for $\pm SSN$. Thus, it is seen that about half of the predictor parameters have a stronger relationship to the 11-year cycle and the other half to the 22-year cycle. Since the correlation coefficients for $\pm SSN$ are generally higher it would seem proper to use this configuration to estimate SSN. However, since

* SSN^{\wedge} indicate estimated value of SSN.

Table 3-3

CORRELATION COEFFICIENT AND ACCOMPANYING τ VALUE FOR 21 PREDICTOR PARAMETERS CORRELATED WITH $|SSN|$ AND $\pm SSN$

Parameter	$ SSN $	Configuration	$\pm SSN$	Configuration
	ρ	τ	ρ	τ
Po	-.08955	-2500	-.5547	-2500
Vo	+.05269	-1150	-.6888	-2600
Ao	.12843	-1600	-.4356	-2700
Ho/10 ³⁵	-.04177	-2550	-.6162	-2550
Zeta	+.04646	-4700	-.7057	-2600
Lo/10 ²⁴	.20969	-1000	.0436	-1350
Jo	-.11875	-3450	-.06552	-3450
P	-.01875	- 50	-.6992	-2600
\dot{P}	-.07364	-3450	-.6584	- 700
\dot{P}'	+.05452	-4700	-.6853	-2600
Tau	-.21165	-2500	-.17938	-2800
ROD	+.09207	-4200	-.64346	-2500
HF	.17183	-1150	-.07168	-3900
HF'	-.17308	-3900	-.07242	-4200
F3R	+.12533	-1300	+.05988	-2400
F3H	-.20430	-4100	+.08249	-2100
F3	-.20978	-.4000	-.09018	-4400
CUP	+.20482	-3500	+.09527	-2100
SCC	+.12184	-1700	+.31255	- 600
SSC	+.14757	-2500	+.19143	-2400
V3	-.06276	-4100	+.05881	-2000

half of the parameters show a stronger relation to $|SSN|$ and it has been pointed out by Fox and Ezekial (Ref. 15) that accuracy of estimate and correlation coefficient both have their place and are not necessarily directly proportional*, both configurations were used to estimate sunspot number.

3.2.3 Data Base Setup and Experiment Procedure

This study had two distinct phases, or sets of experiments, each requiring a particular data base setup. In phase one the estimating technique was to be evaluated using known values of SSN and in phase two, SSN was estimated (\hat{SSN}) for the future.

As indicated in Section 3.1 there were 3924 values of SSN. In phase one the first 3200 of these data points (MJD -39920 to MJD 24060) along with the appropriate data points for each of the 21 predictors are used to find an estimated regression of SSN. A detailed explanation of the regression procedure is found in Section 4. Using the regression coefficients generated from these 3200 samples and the next (in time) 724 values of the predictor parameters, 724 values of SSN (MJD 24080 to MJD 38540) are estimated (\hat{SSN}). These values of \hat{SSN} are compared to the actual values of SSN and the error statistics are generated. The values of \hat{SSN} are also found from MJD -39920 to 24060 and the error statistics are found. By comparing the two sets of error statistics it is possible to determine the difference in error between \hat{SSN} and SSN over the range where the regression coefficients were generated and the error between \hat{SSN} and SSN when future values of the predictor parameters are used. Thus, an indication of how well the procedure extrapolates into the future is obtained.

* In studying this statement it would seem to indicate that estimates of SSN should have been made for all values of τ instead of finding the cross-correlation function. However, the cost of such an effort would have been out of the question. Therefore, a faster, more economical method of finding the shifts necessary for the strongest relationship was used, i.e., cross-correlation.

In phase two of the study the entire SSN waveform, 3924 samples along with the appropriate 3924 values of each of the predictors, are used to find an estimated regression of SSN. The coefficients generated in this way are then used in conjunction with the next 250 values of each of the predictor parameters to find \hat{SSN} into the future. The values of \hat{SSN} are from MJD 38560 to MJD 43540. Shown below is a breakdown of the two data base setups.

Regression Estimate			Future Estimation	
	No. Points	Time Period	No. Points	Time Period
Phase 1	3200	MJD -39920 to 24060 (1749 to 1925)	724	MJD 24080 to 38540 (1925 to 1964)
Phase 2	3924	MJD -39920 to 38540 (1749 to 1964)	250	MJD 38560 to 43540 (1964 to 1978)

3.3 NORMALIZING PREDICTOR PARAMETERS

To make the estimate of SSN, it is necessary to estimate a probability density function using a Taylor's series expansion. (See Section 4.1 for details.) To minimize distortion of the estimated density relative to the actual density and also to minimize the error due to the series expansion it is desirable to "sphericalize" the data in some way. A simple method of accomplishing this is to normalize each of the parameters to have unit variance. If the means and standard deviations of the predictor parameters used to establish the regression surface, i.e., the training set data, are called \bar{p}_j and S_j , respectively, then the normalized predictor parameter p'_{ji} may be expressed as

$$p'_{ji} = (p_{ji} - \bar{p}_j) / S_j$$

or

$$j = 1 \text{ to } 21$$

$$p'_{ji} = \frac{1}{S_j} \cdot p_{ji} - \bar{p}_j / S_j$$

Table 3-4 shows the actual values of $1/S_j$ and \bar{p}_j/S_j for each of the 21 parameters.

Table 3-4
 "SPHERE" COEFFICIENTS FOR THE 21 PREDICTOR PARAMETERS

Parameter	$1/S_j$	\bar{p}_j/S_j
Ro	3.09×10^{-6}	+ 2.536
Vo	4.97×10^2	+ 6.250
Ao	4.88×10^{10}	+10.29
Ho/ 10^{35}	8.79	+ 1.806
Zeta	5.13×10^{-6}	+ 3.970
Lo/ 10^{24}	1.38×10^{-2}	+ 1.539
Jo	2.96×10^{18}	+33.48
P	2.49×10^{-4}	+ 2.514
\dot{P}	1.05×10^4	- 0.02916
\dot{P}'	$9.6 \times 10^{+3}$	+ 2.794
Tau	$1.49 \times 10^{+3}$	+ 0.038
ROD	1.54×10^{-3}	+ 2.32
HF	1.099×10^{18}	+ 4.779
HF'	$2.1 \times 10^{+18}$	+ 9.32
F3R	2.1×10^{-2}	+28.47
F3H	1.6×10^{-2}	+12.94
F3	1.29×10^{-2}	+22.39
CUP	$2.45 \times 10^{+13}$	+ 2.80
SCC	$6.39 \times 10^{+9}$	+ 1.39
SSC	8.14×10^7	+ 1.28
V3	2.14×10^{-1}	+ 1.24

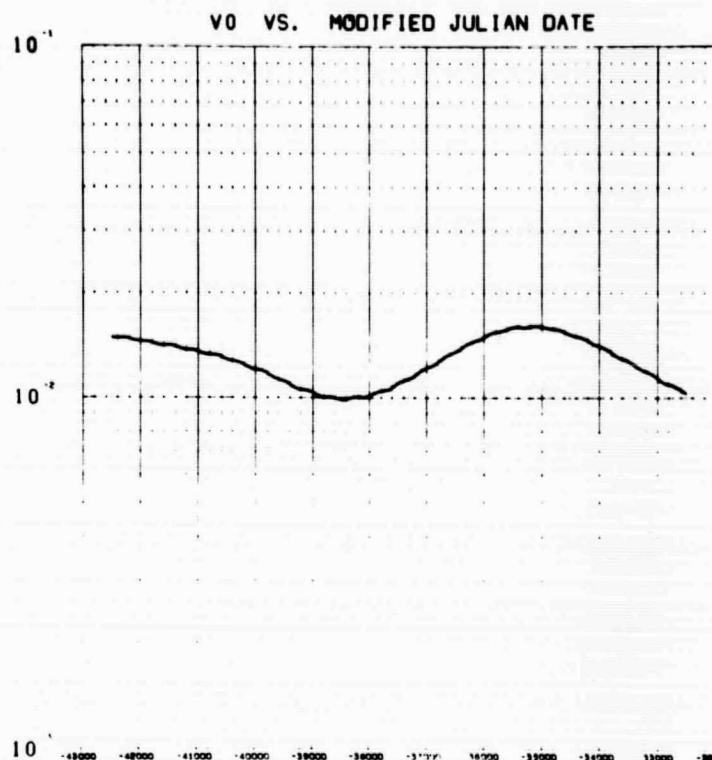
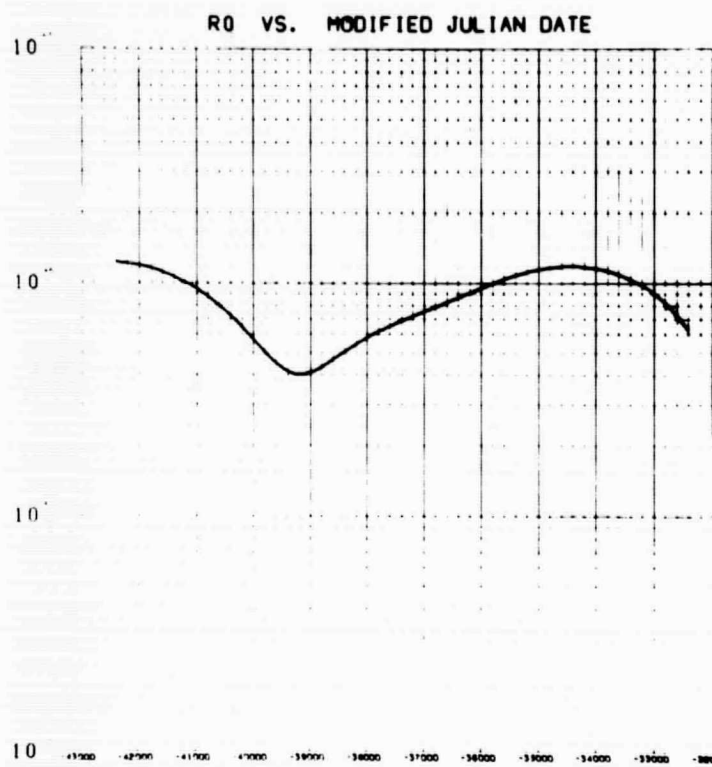


Fig. 3-1 - Time History of Filtered R0

Fig. 3-2 - Time History of Filtered V0

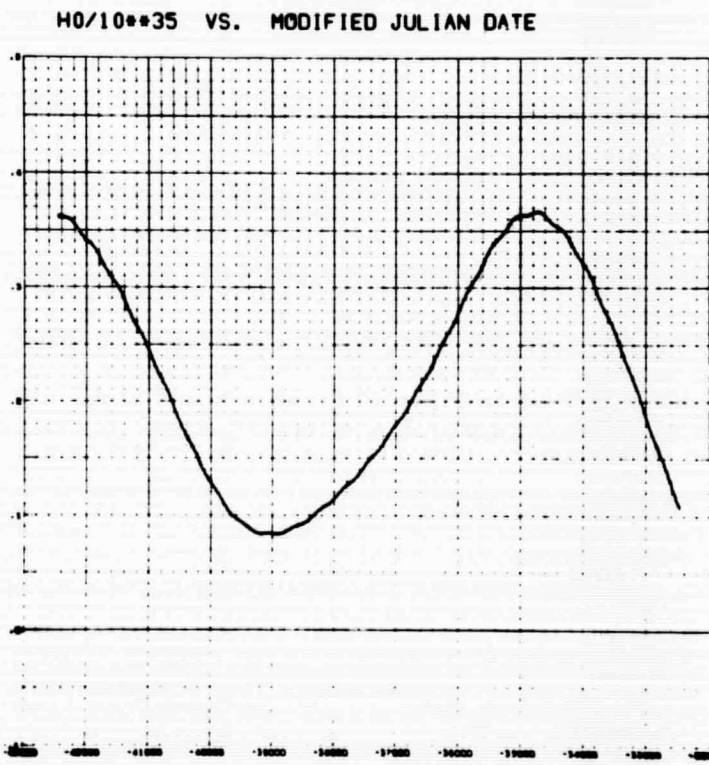
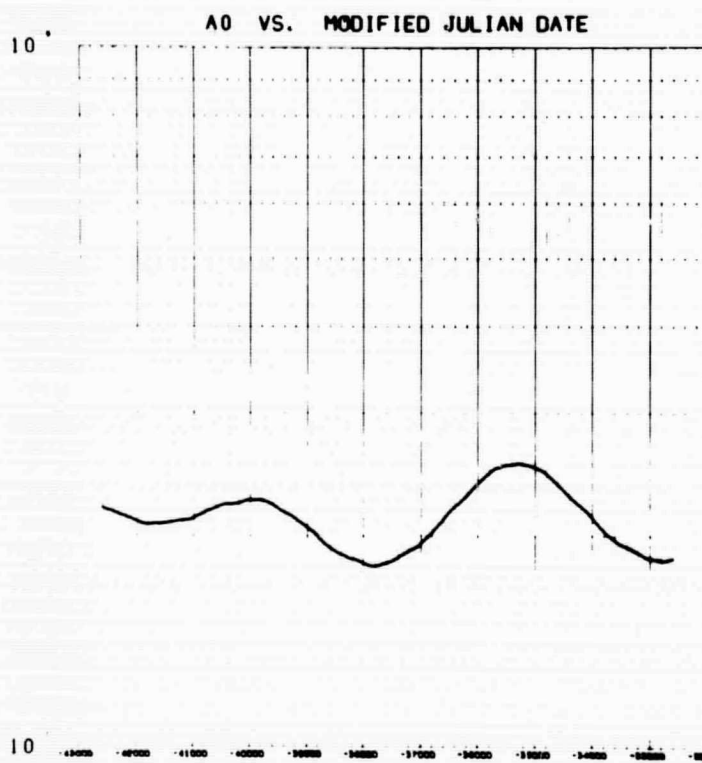


Fig. 3-3 - Time History of Filtered A0

Fig. 3-4 - Time History of Filtered H0

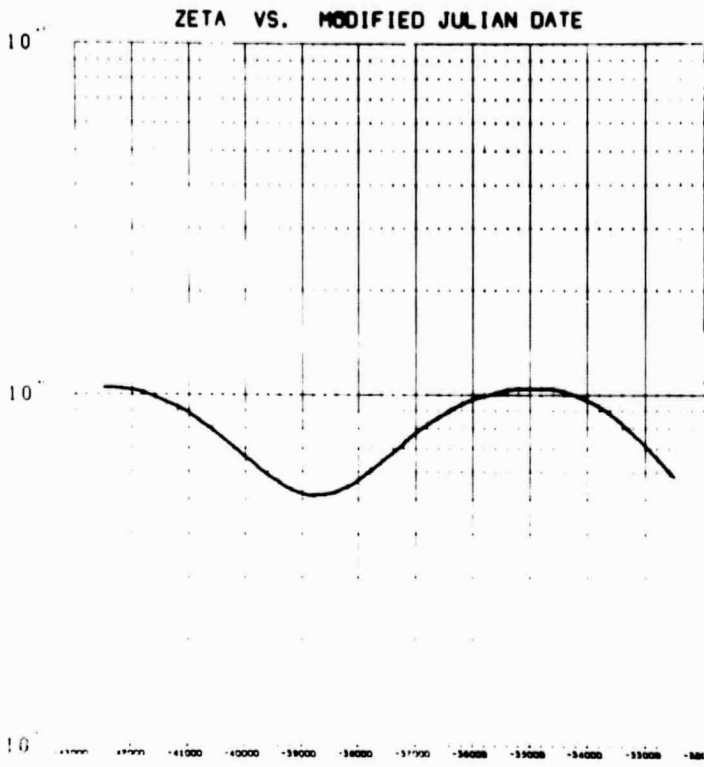


Fig. 3-5 - Time History of Filtered Zeta

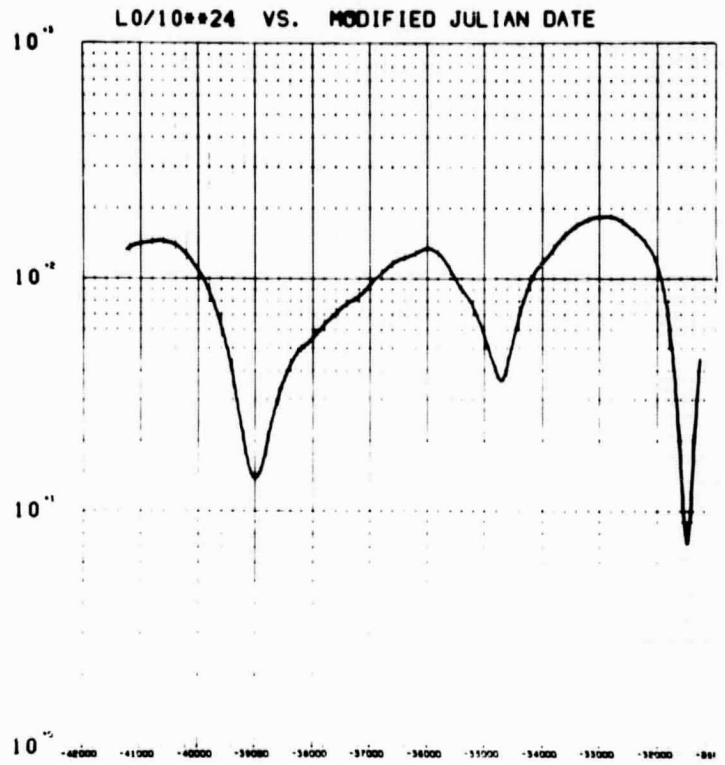


Fig. 3-6 - Time History of Filtered L0

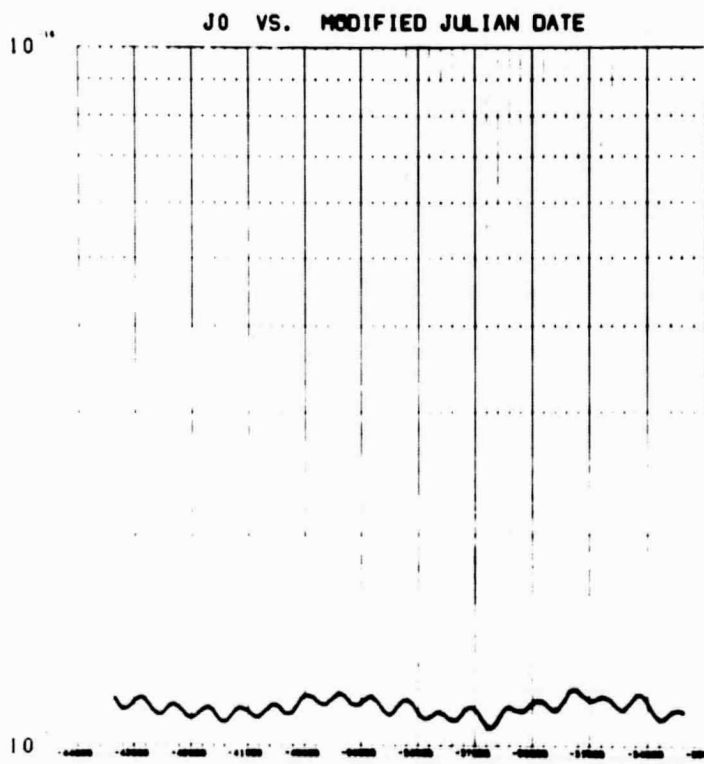


Fig. 3-7 - Time History of Filtered J0

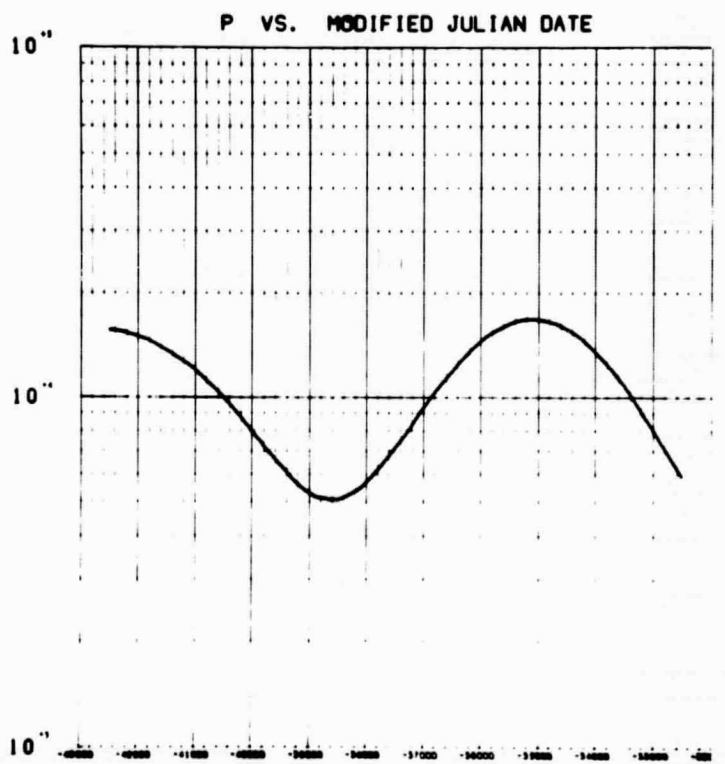


Fig. 3-8 - Time History of Filtered P

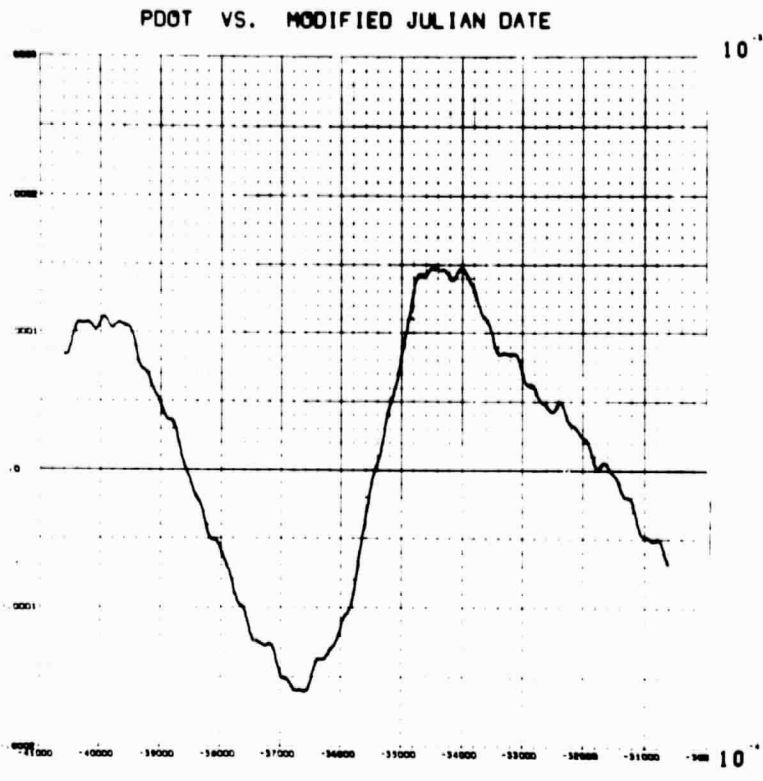


Fig. 3-7 - Time History of Filtered \dot{P}

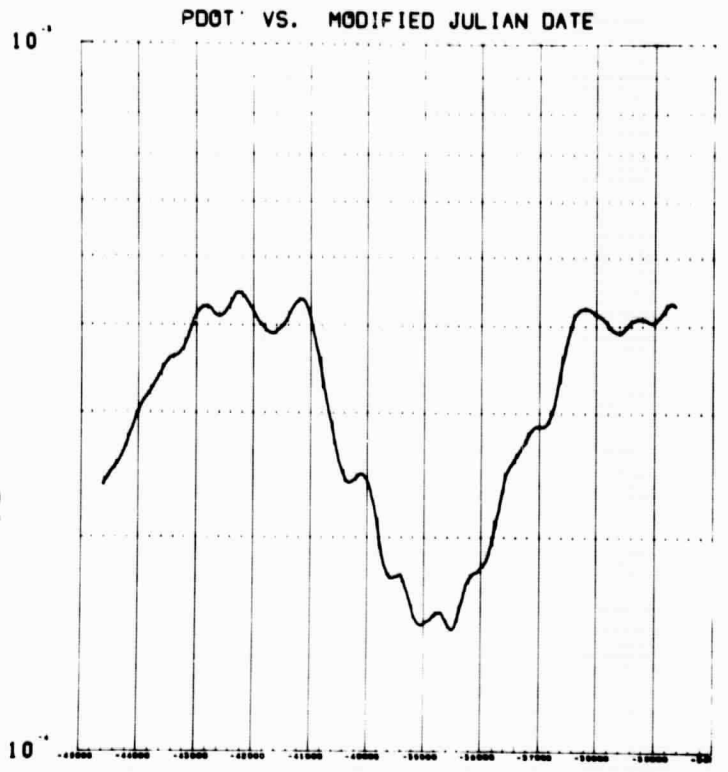


Fig. 3-10 - Time History of Filtered \dot{P}

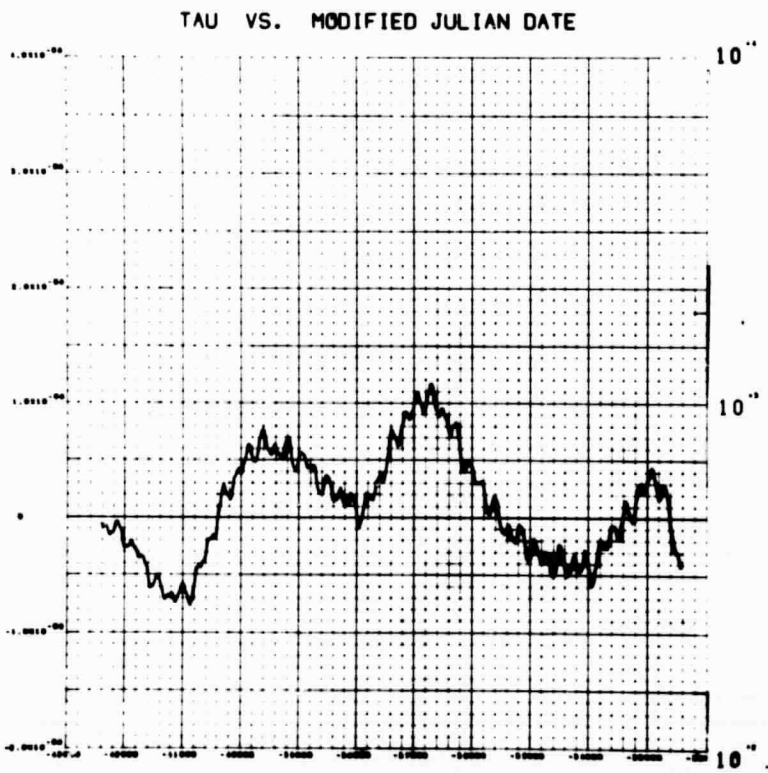


Fig. 3-11 - Time History of Filtered τ

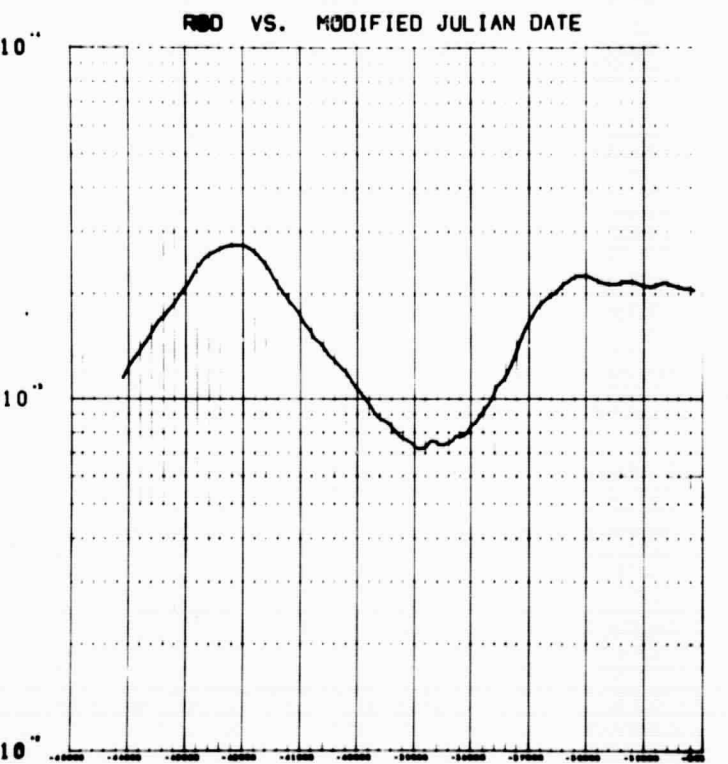


Fig. 3-12 - Time History of Filtered ROD

HF VS. MODIFIED JULIAN DATE

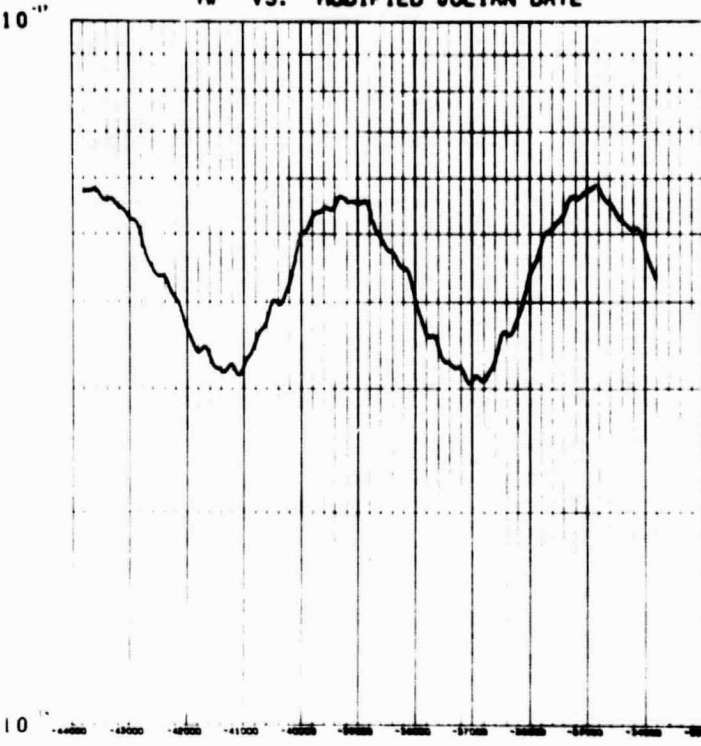


Fig. 3-13 - Time History of Filtered HF

HF' VS. MODIFIED JULIAN DATE

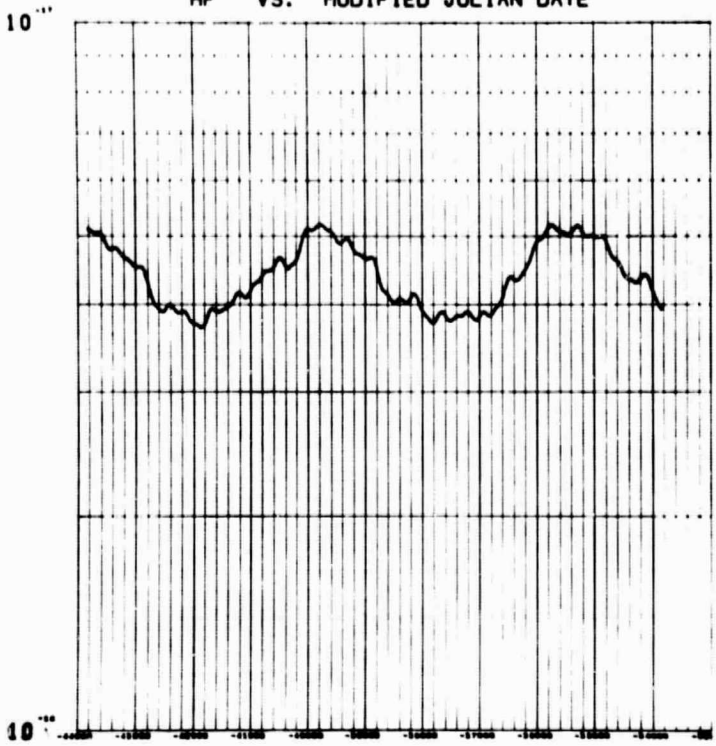


Fig. 3-14 - Time History of Filtered HF'

F3R VS. MODIFIED JULIAN DATE

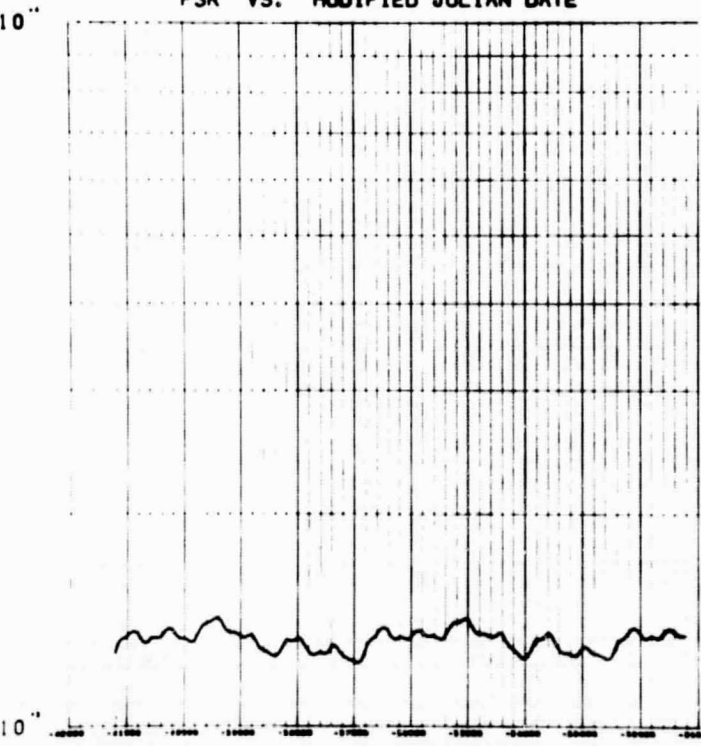


Fig. 3-15 - Time History of Filtered F3R

F3H VS. MODIFIED JULIAN DATE

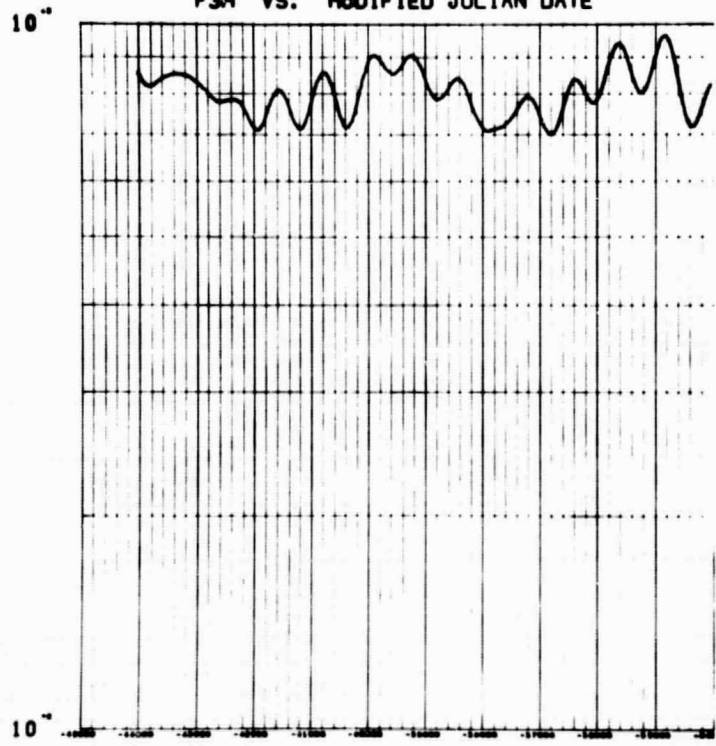


Fig. 3-16 - Time History of Filtered F3H

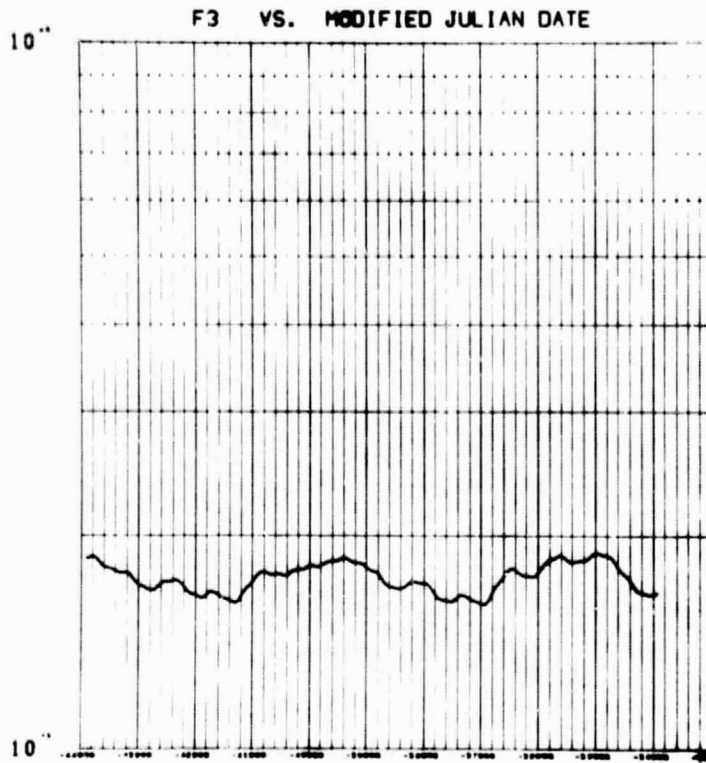


Fig. 3-17 - Time History of Filtered F3

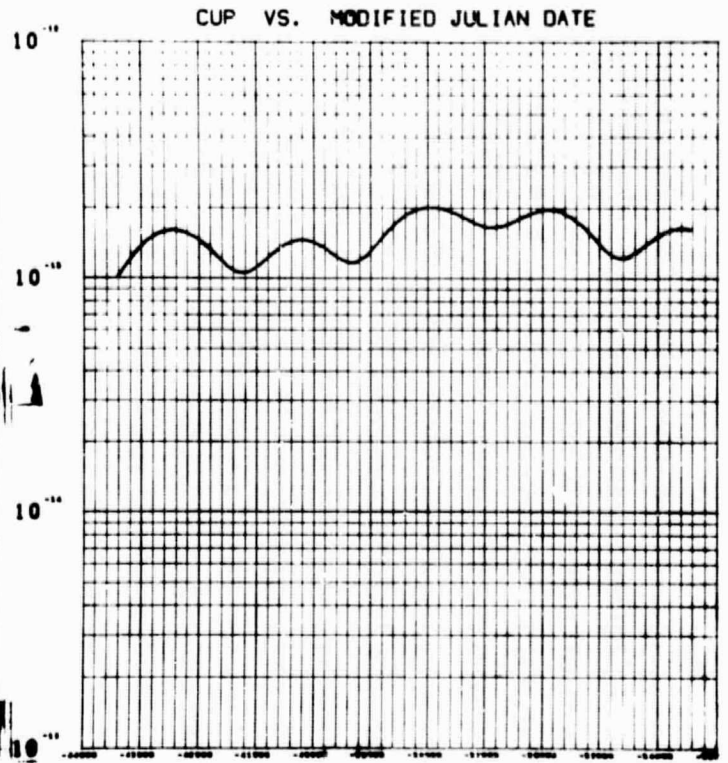


Fig. 3-18 - Time History of Filtered CUP

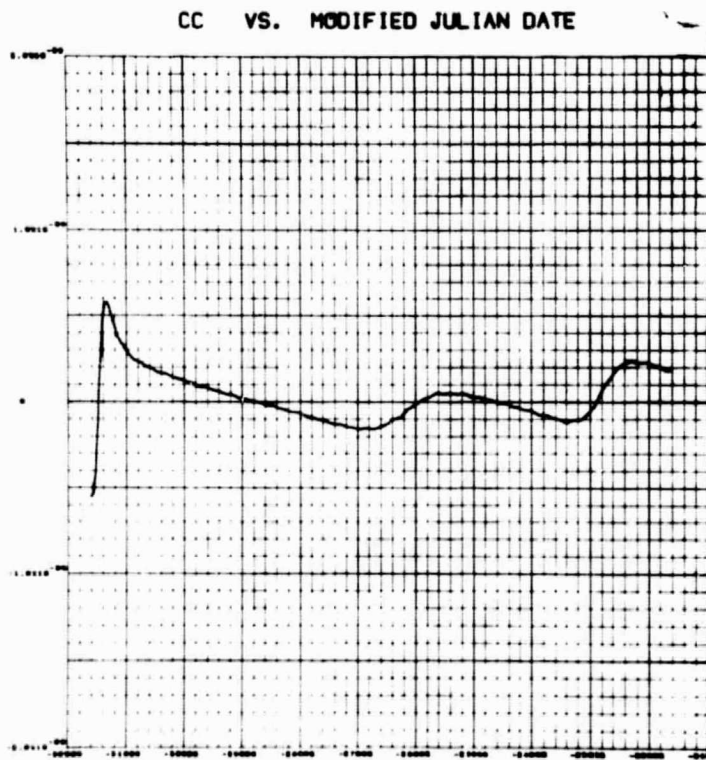


Fig. 3-19 - Time History of Filtered SCC

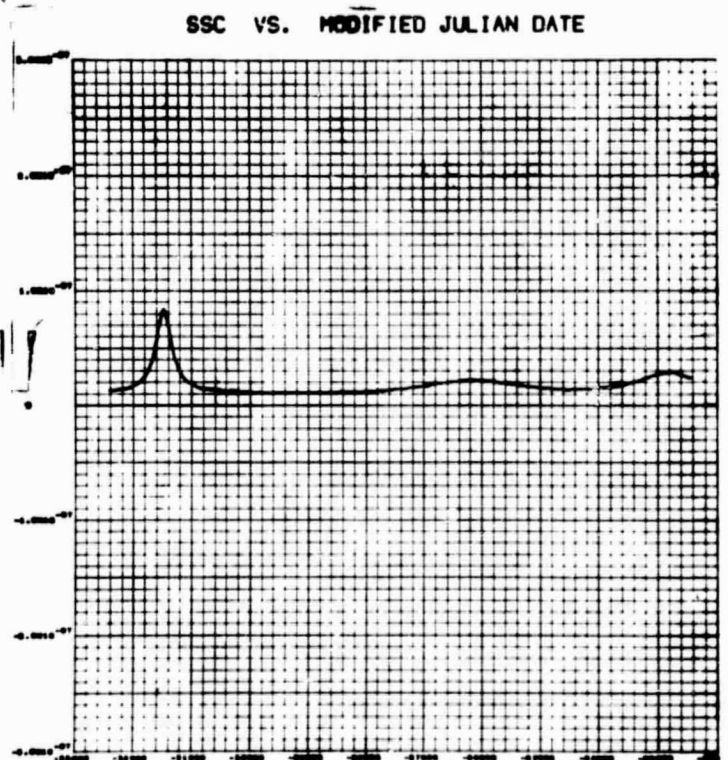


Fig. 3-20 - Time History of Filtered SSC

V3 VS. MODIFIED JULIAN DATE

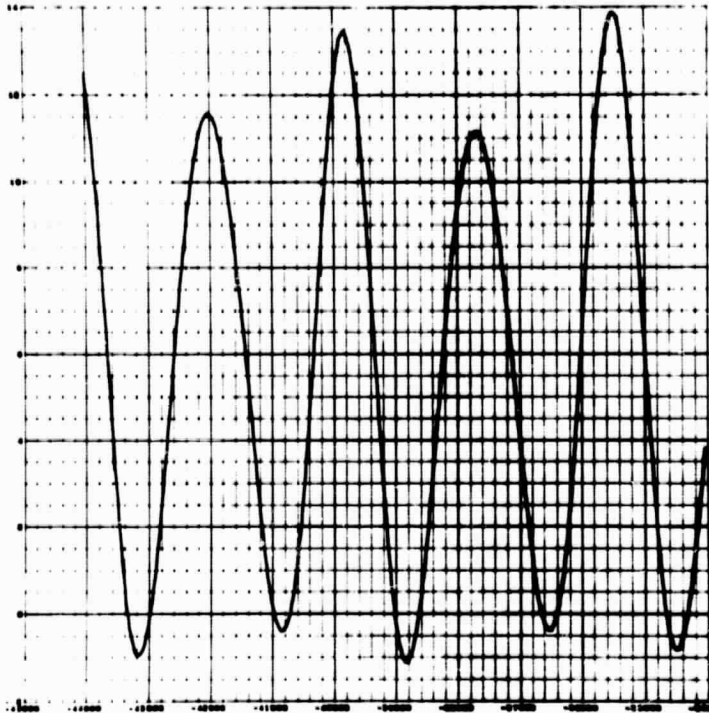
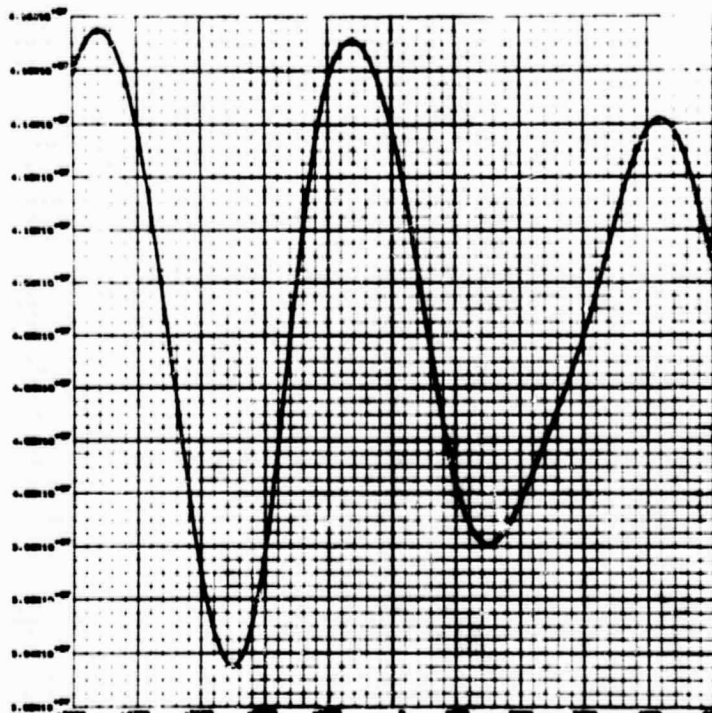


Fig. 3-21 - Time History of Filtered V3

CROSS CORRELATION FUNCTION VS. TAU



CROSS CORRELATION FUNCTION VS. TAU

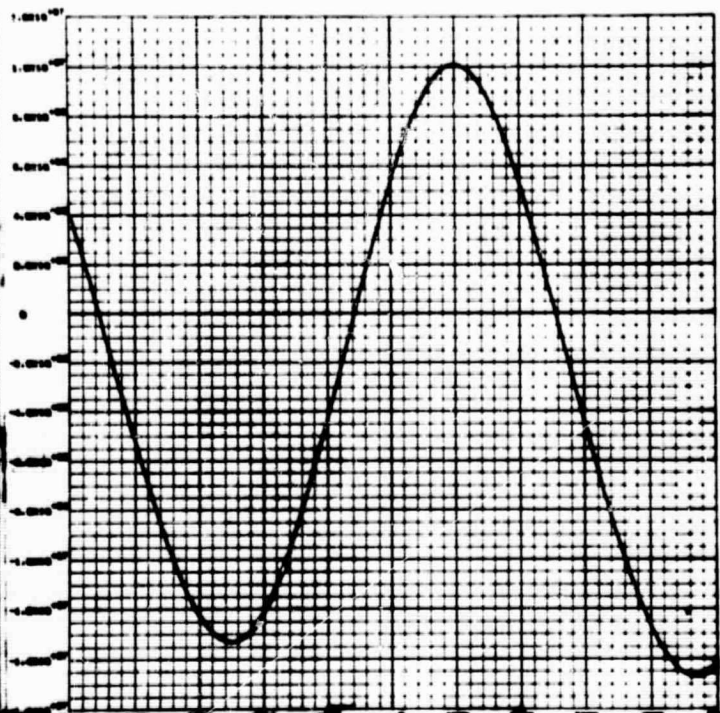
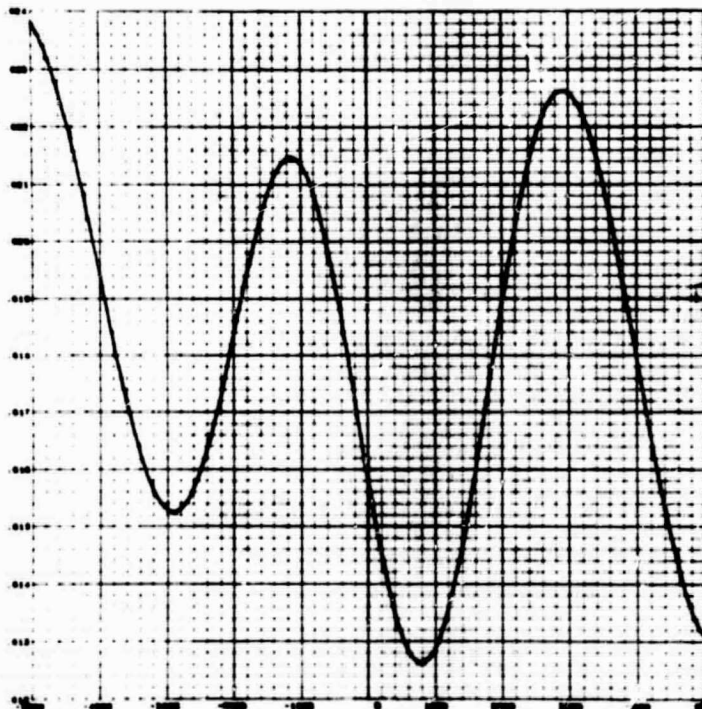


Fig. 3-22a - Cross-Correlation Functions of Ro and Sunspot Number (using |SSN|) Fig. 3-22b - Cross Correlation Functions of Ro and Sunspot Number (using +SSN)

CROSS CORRELATION FUNCTION VS. TAU



CROSS CORRELATION FUNCTION VS. TAU

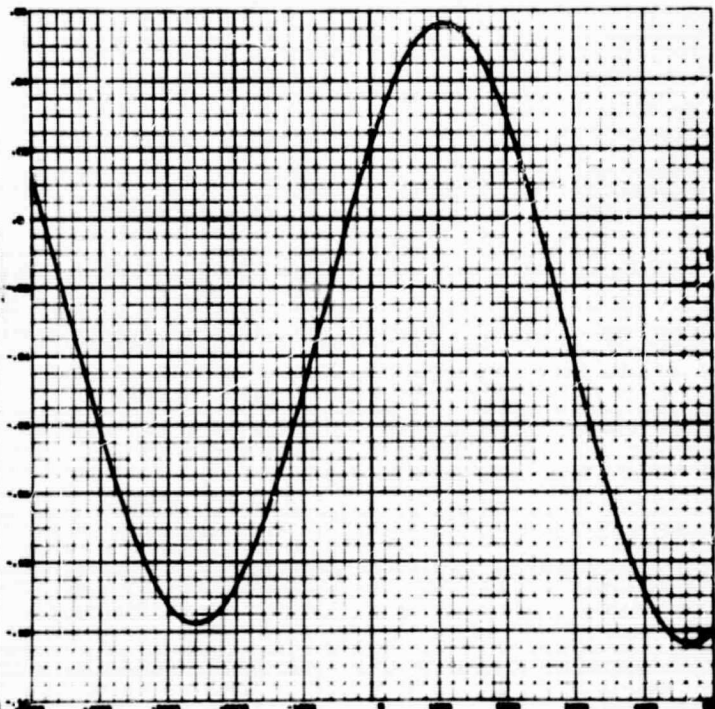
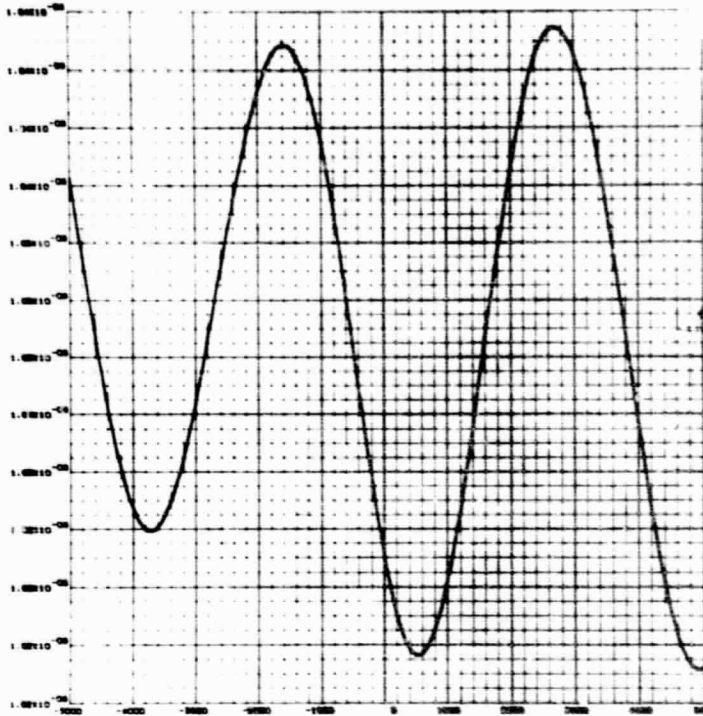


Fig. 3-24a - Cross-Correlation Functions of Vo and Sunspot Number (using |SSN|) Fig. 3-24b - Cross-Correlation Functions of Vo and Sunspot Number (using +SSN)

CROSS CORRELATION FUNCTION VS. TAU



CROSS CORRELATION FUNCTION VS. TAU

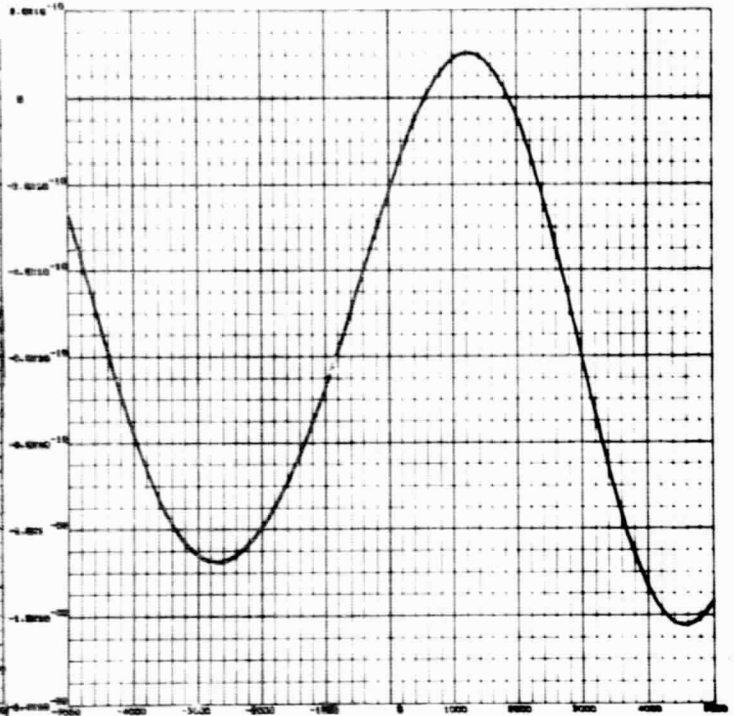
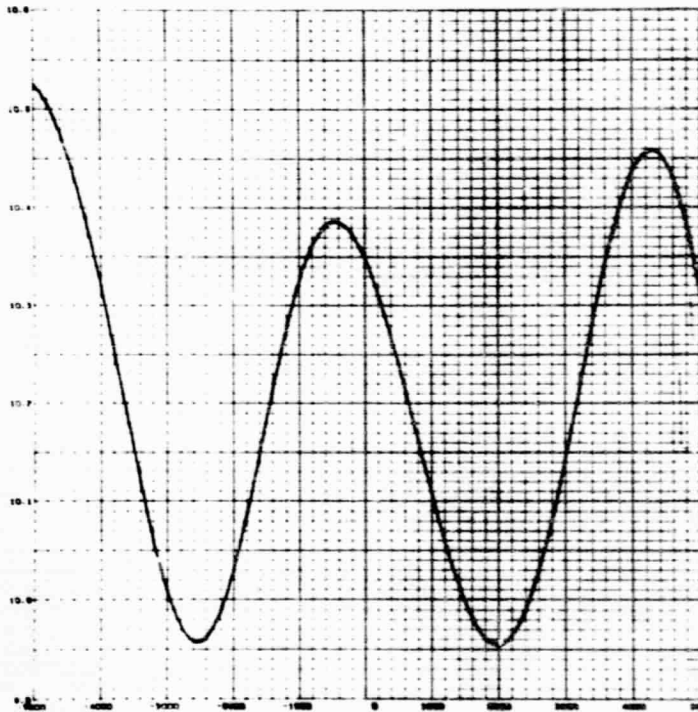


Fig. 3-24a - Cross-Correlation Functions of A0 and Sunspot Number (using |SSN|) Fig. 3-24b - Cross-Correlation Functions of A0 and Sunspot Number (using ±SSN)

CROSS CORRELATION FUNCTION VS. TAU



CROSS CORRELATION FUNCTION VS. TAU

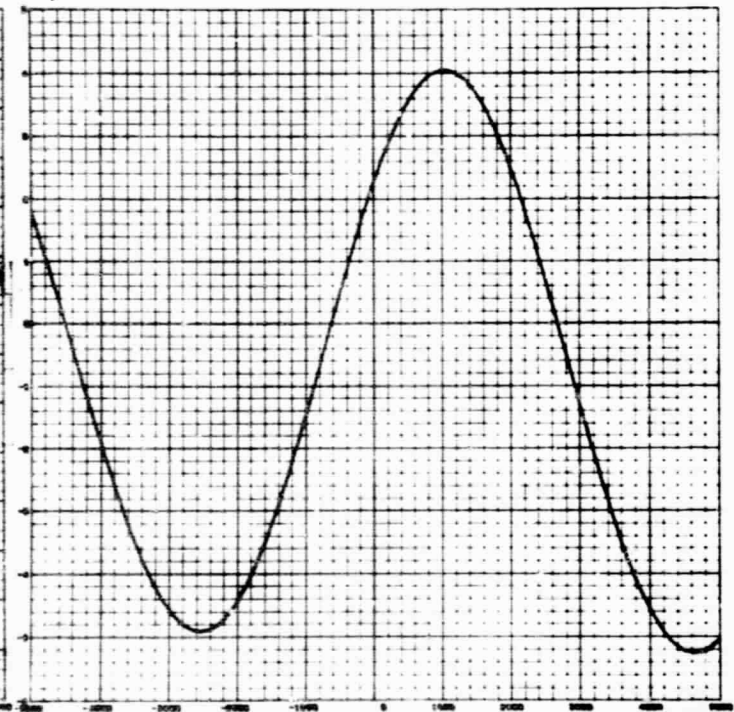
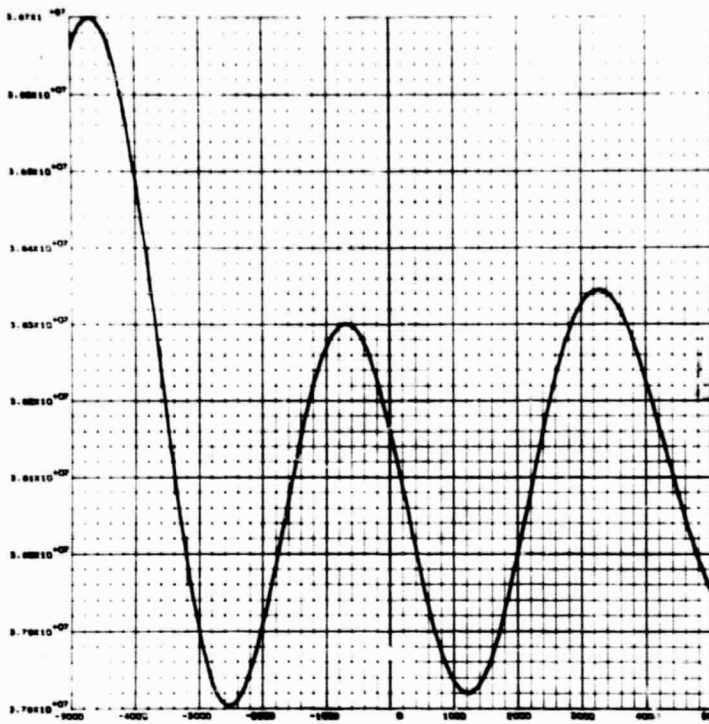


Fig. 3-25a - Cross-Correlation Functions of H0 and Sunspot Number (using |SSN|) Fig. 3-25b - Cross-Correlation Functions of H0 and Sunspot Number (using ±SSN)

CROSS CORRELATION FUNCTION VS. TAU



CROSS CORRELATION FUNCTION VS. TAU

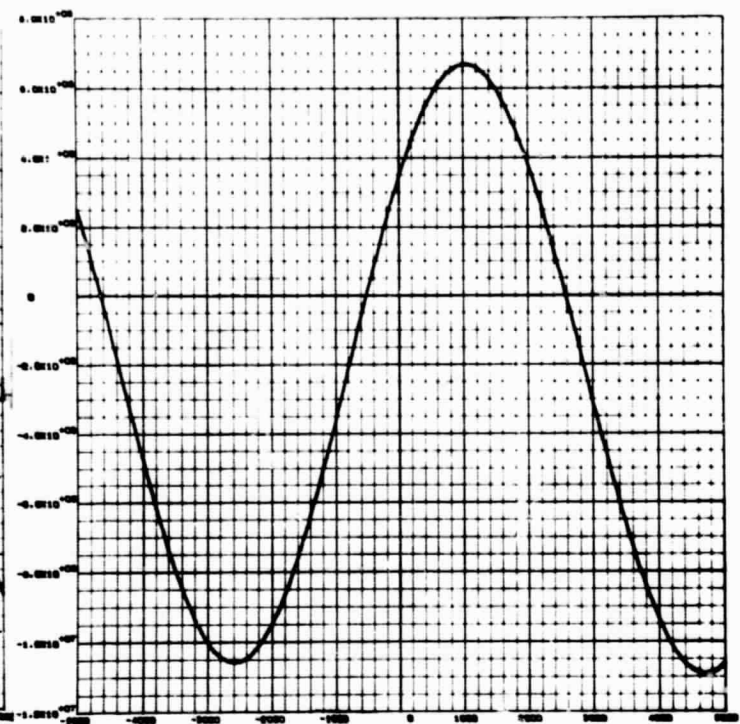
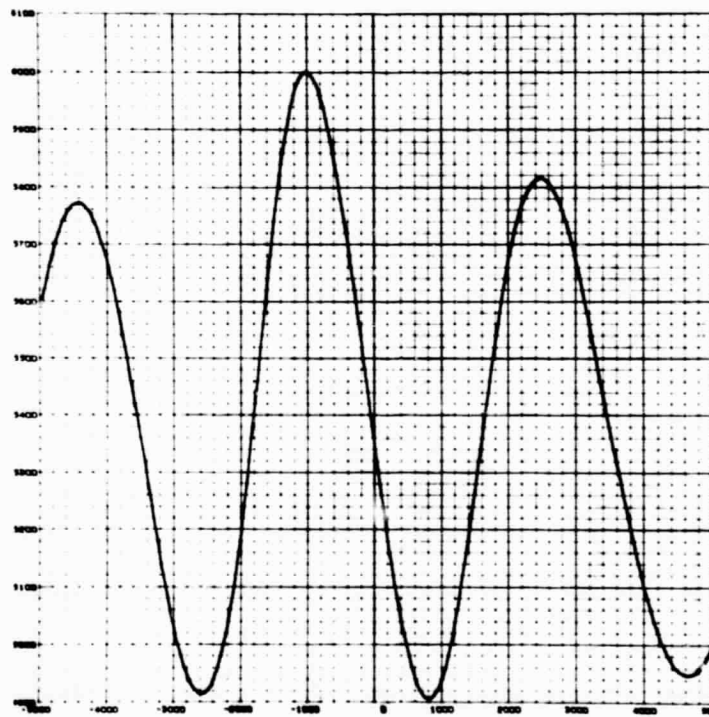


Fig. 3-26a - Cross-Correlation Functions of Zeta and Sunspot Number (using |SSN|) Fig. 3-26b - Cross-Correlation Functions of Zeta and Sunspot Number (using +SSN)

CROSS CORRELATION FUNCTION VS. TAU



CROSS CORRELATION FUNCTION VS. TAU

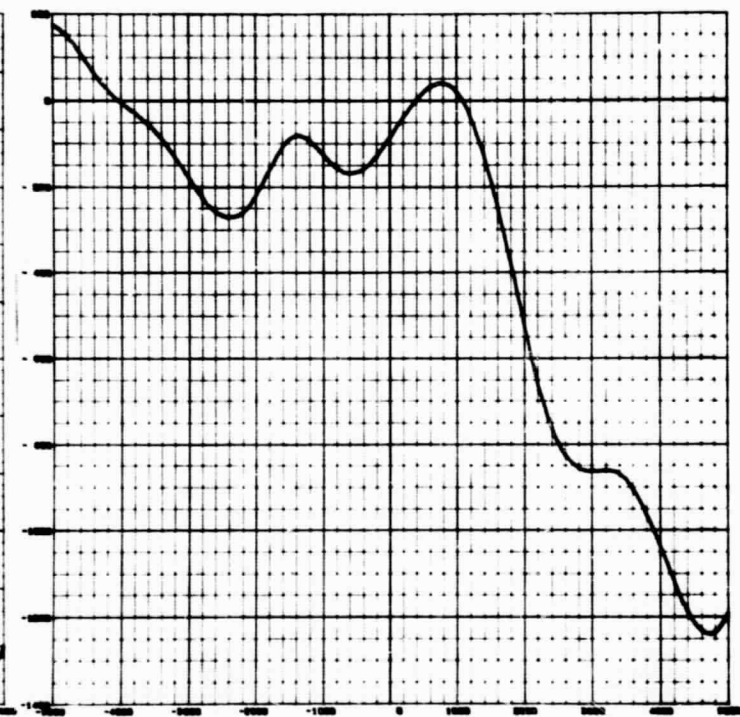
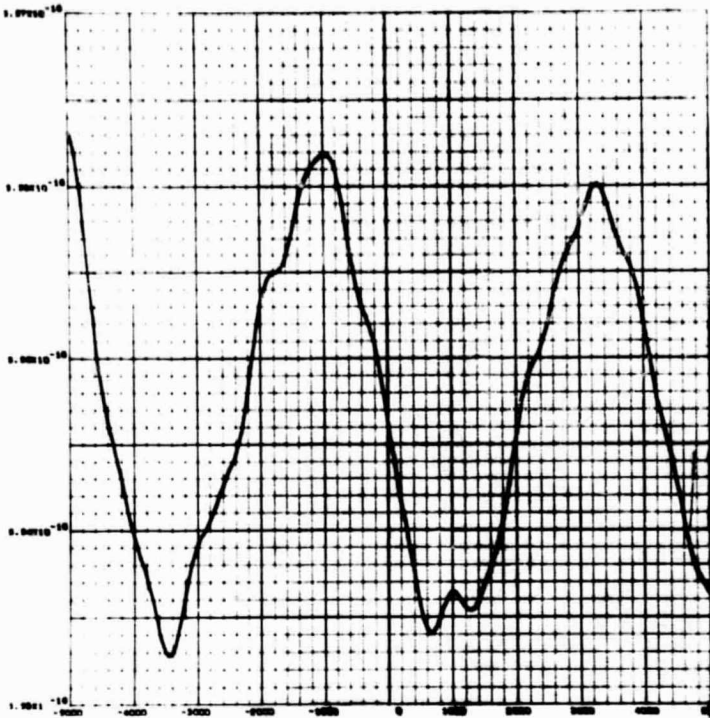


Fig. 3-27a - Cross-Correlation Functions of Lo and Sunspot Number (using |SSN|) Fig. 3-27b - Cross-Correlation Functions of Lo and Sunspot Number (using +SSN)

CROSS CORRELATION FUNCTION VS. TAU



CROSS CORRELATION FUNCTION VS. TAU

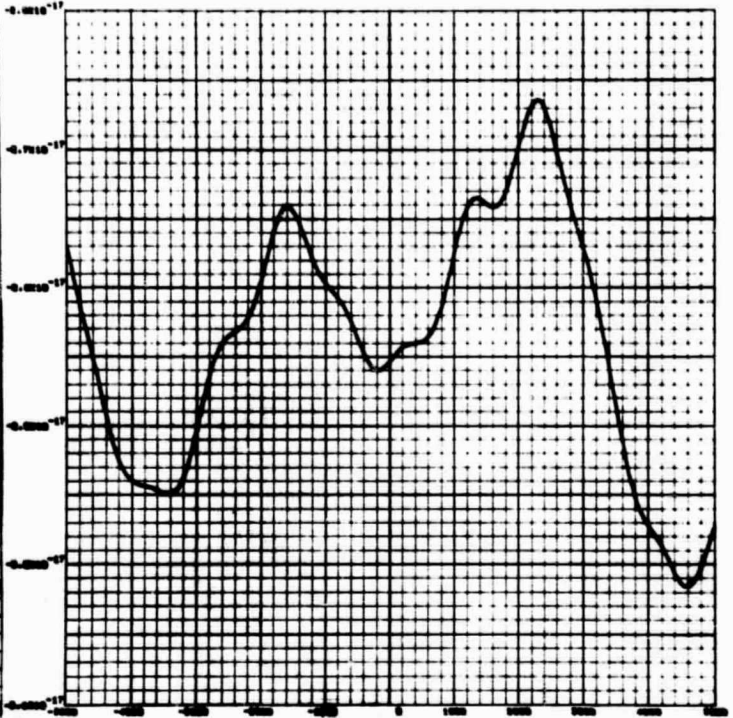
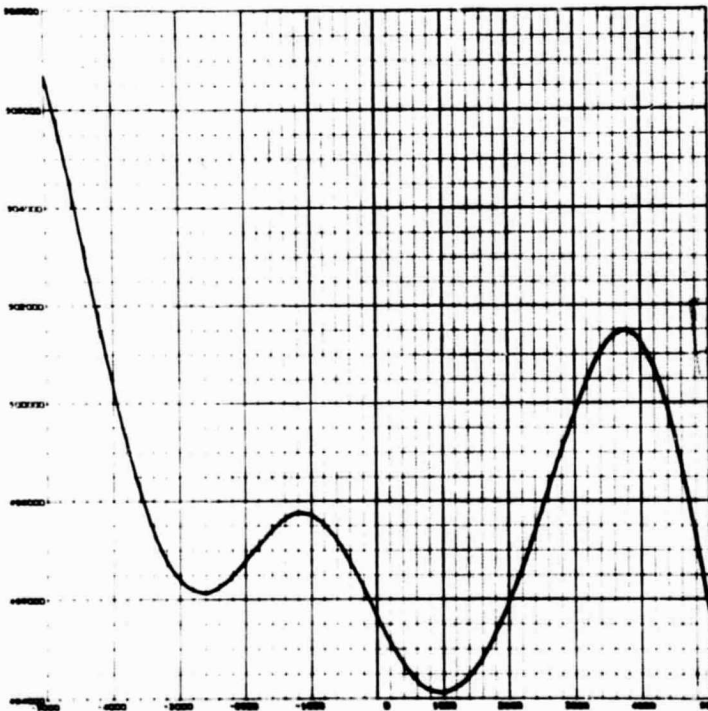


Fig. 3-28a - Cross-Correlation Functions of Jo and Sunspot Number (using |SSN|), Fig. 3-28b - Cross-Correlation Functions of Jo and Sunspot Number (using \pm SSN)

CROSS CORRELATION FUNCTION VS. TAU



CROSS CORRELATION FUNCTION VS. TAU

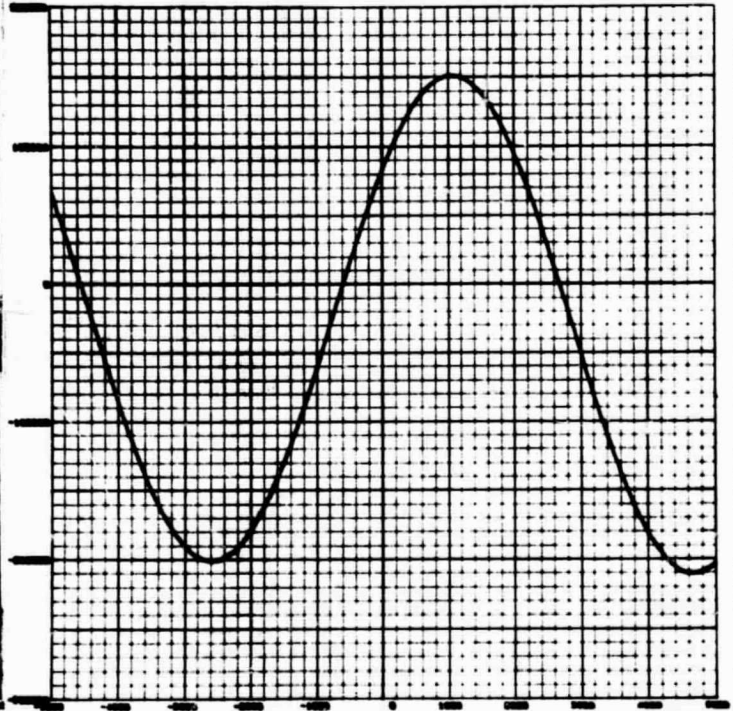


Fig. 3-29a - Cross-Correlation Functions of P and Sunspot Number (using |SSN|) Fig. 3-29b - Cross-Correlation Functions of P and Sunspot Number (using \pm SSN)

CROSS CORRELATION FUNCTION VS. TAU

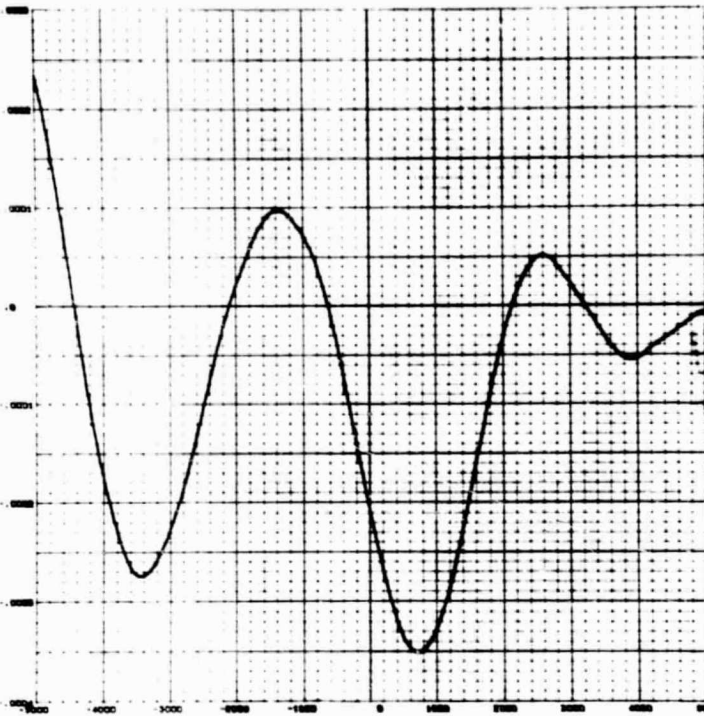


Fig. 3-30a - Cross-Correlation Functions of \dot{P} and Sunspot Number (using $|\text{SSN}|$)

CROSS CORRELATION FUNCTION VS. TAU

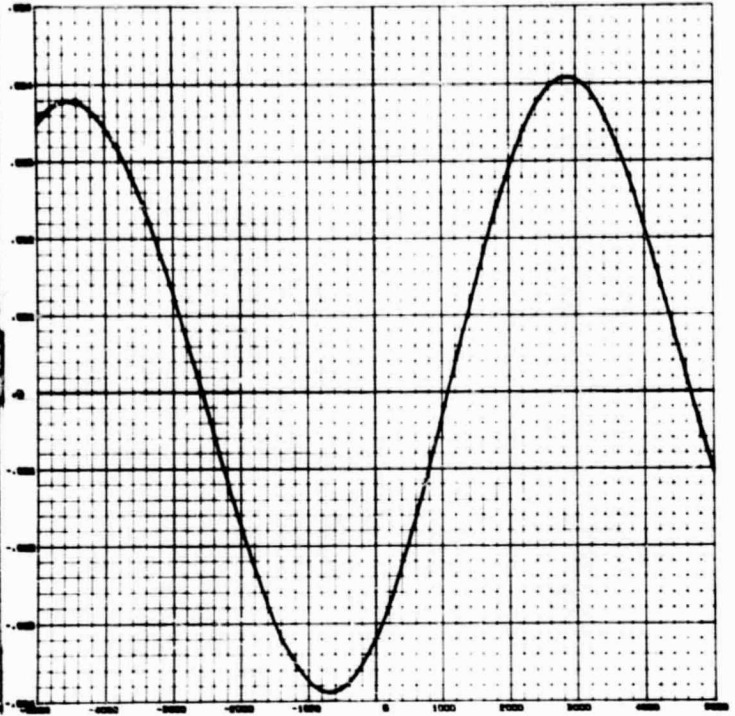


Fig. 3-30b - Cross-Correlation Functions of \dot{P} and Sunspot Number (using $+\text{SSN}$)

CROSS CORRELATION FUNCTION VS. TAU

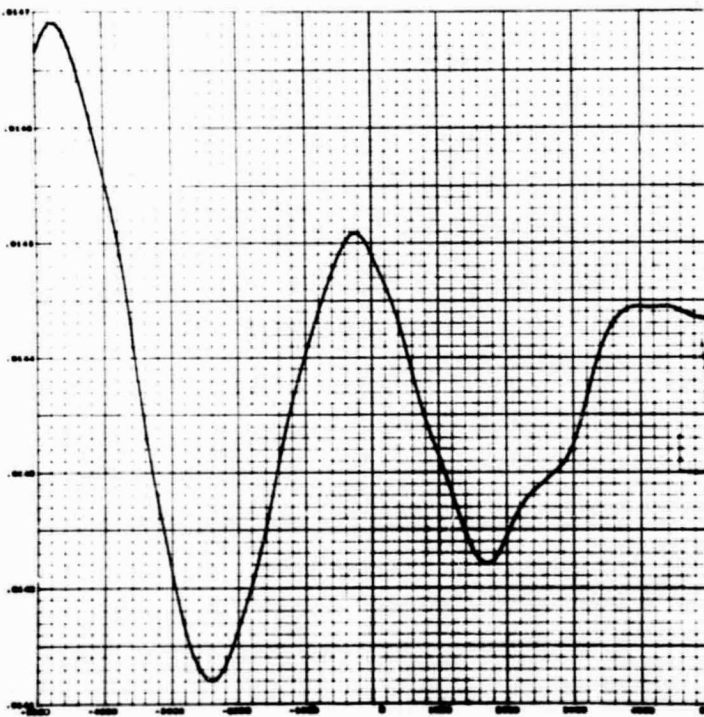


Fig. 3-31a - Cross-Correlation Functions of \dot{P} and Sunspot Number (using $|\text{SSN}|$)

CROSS CORRELATION FUNCTION VS. TAU

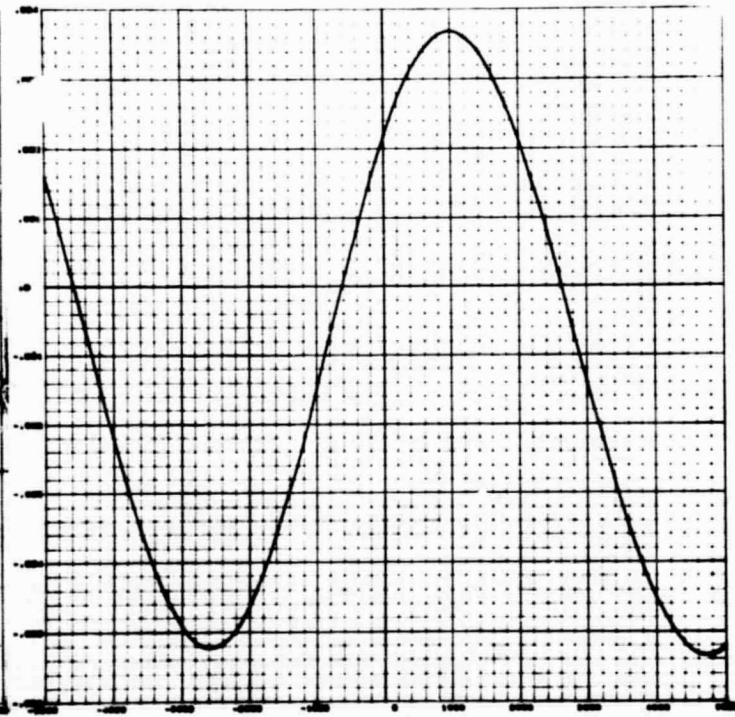
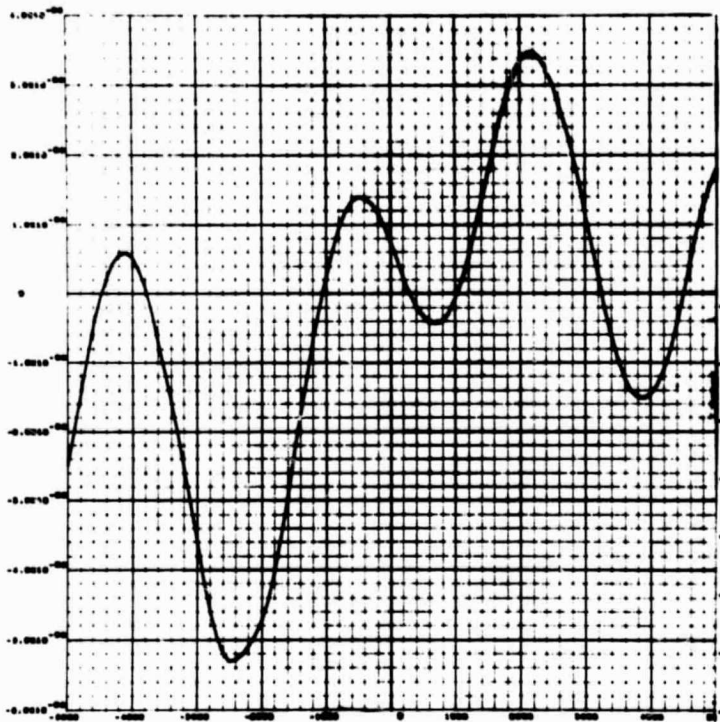


Fig. 3-31b - Cross-Correlation Functions of \dot{P} and Sunspot Number (using $+\text{SSN}$)

CROSS CORRELATION FUNCTION VS. TAU



CROSS CORRELATION FUNCTION VS. TAU

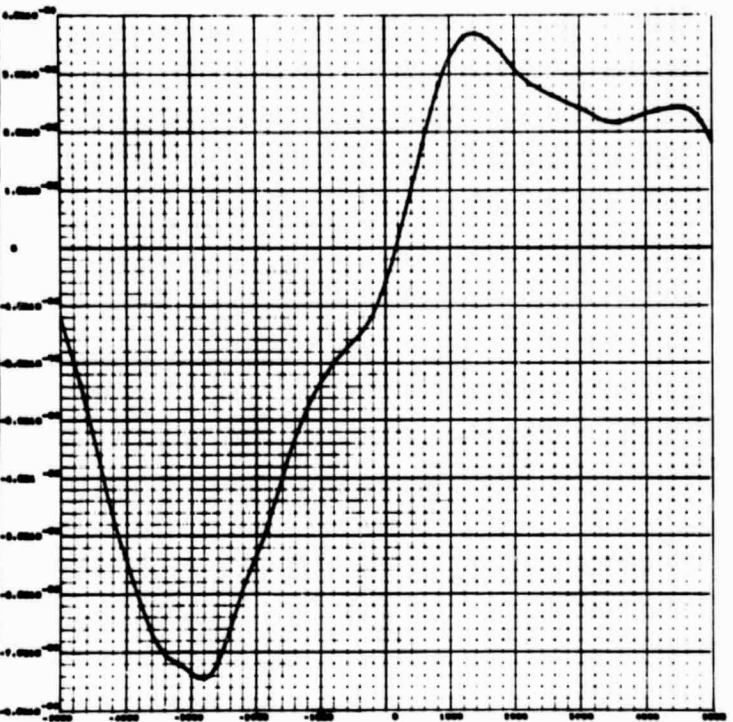
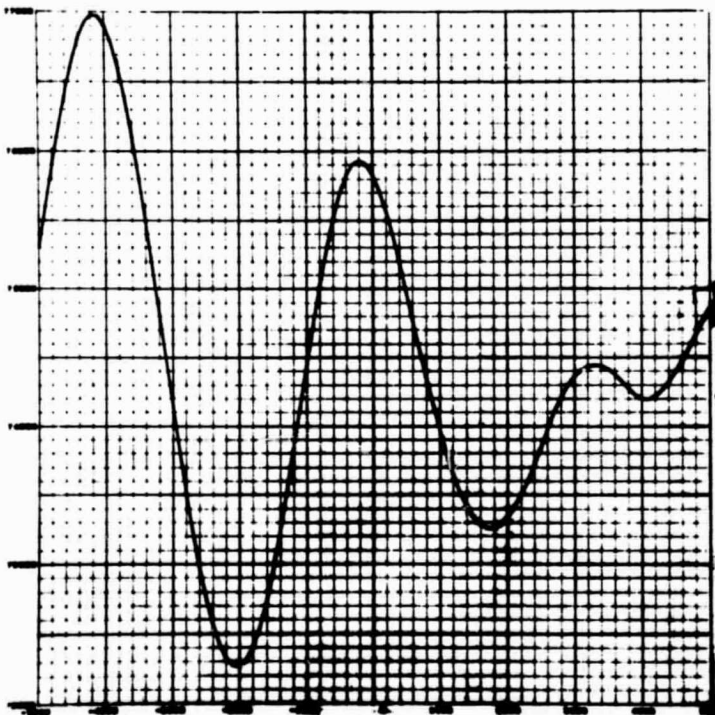


Fig. 3-32a - Cross-Correlation Functions of TAU and Sunspot Number (using |SSN|) Fig. 3-32b - Cross-Correlation Functions of Tau and Sunspot Number (using +SSN)

CROSS CORRELATION FUNCTION VS. TAU



CROSS CORRELATION FUNCTION VS. TAU

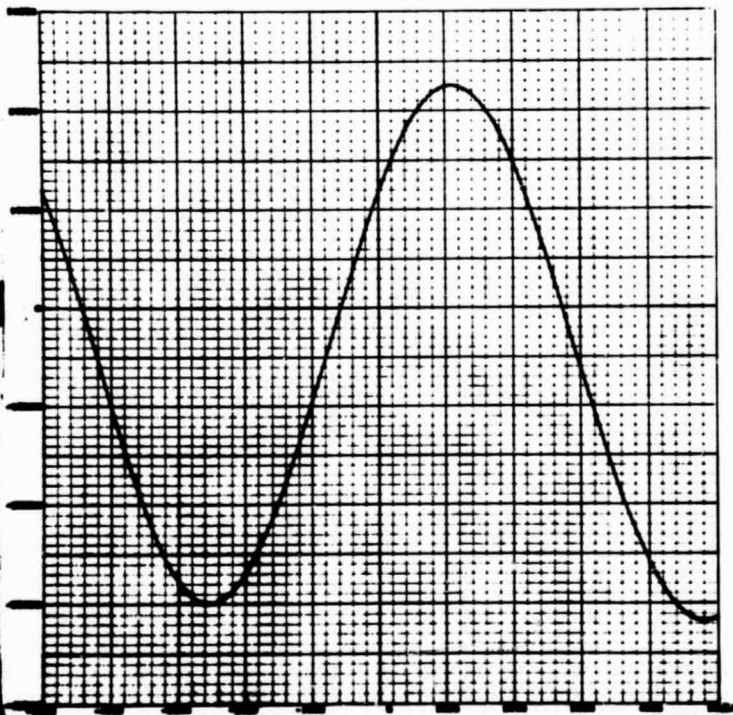
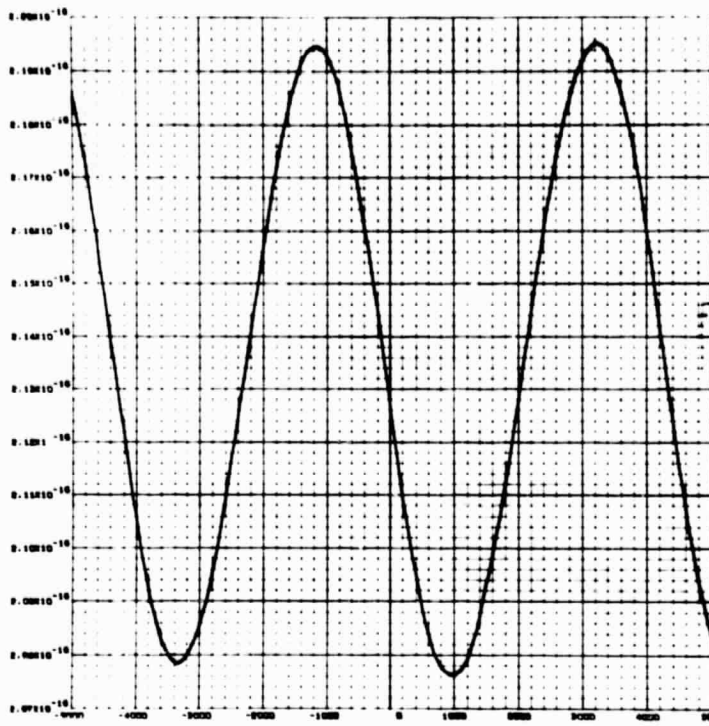


Fig. 3-33a - Cross-Correlation Functions of ROD and Sunspot Number (using |SSN|) Fig. 3-33b - Cross-Correlation Functions of ROD and Sunspot Number (using +SSN)

CROSS CORRELATION FUNCTION VS. TAU



CROSS CORRELATION FUNCTION VS. TAU

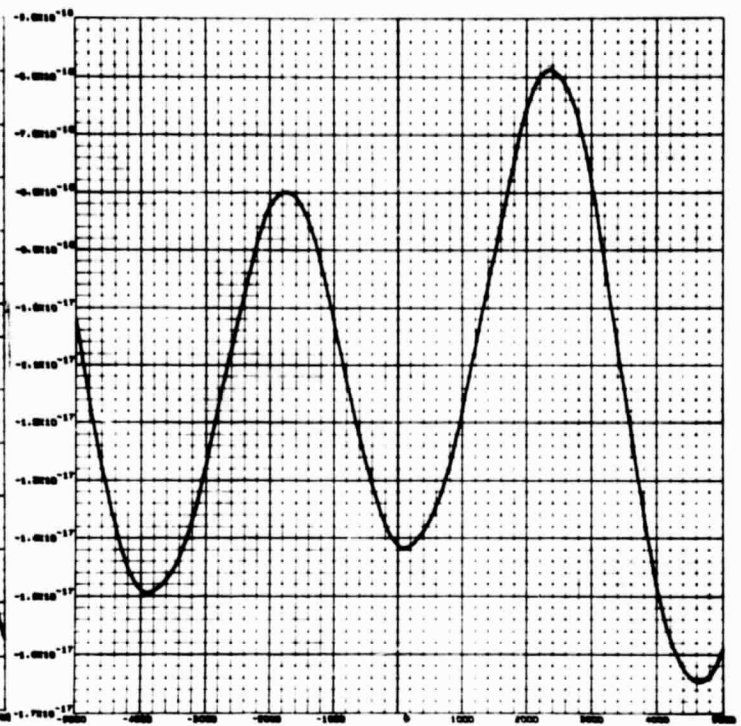
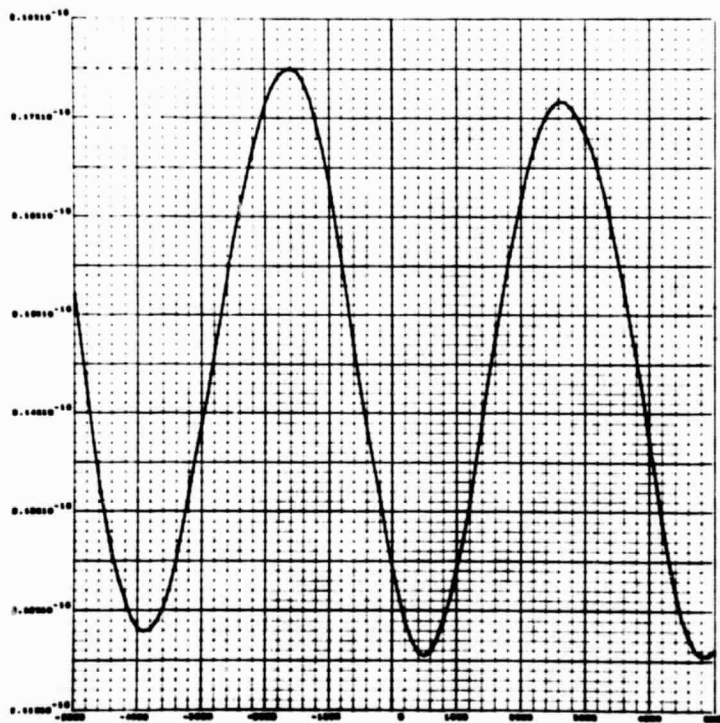


Fig. 3-34a - Cross-Correlation Functions of HF and Sunspot Number (using |SSN|) Fig. 3-34b - Cross-Correlation Functions of HF and Sunspot Number (using +SSN)

CROSS CORRELATION FUNCTION VS. TAU



CROSS CORRELATION FUNCTION VS. TAU

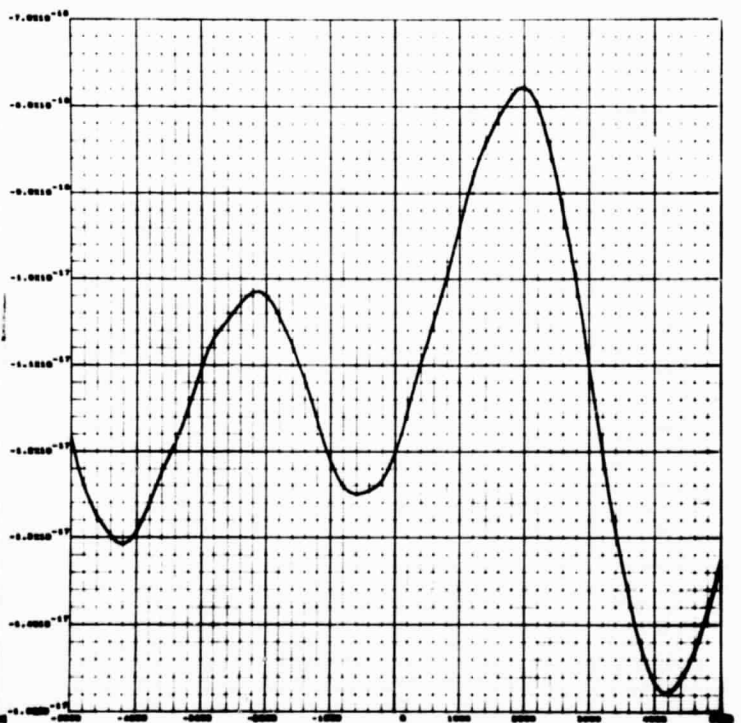


Fig. 3-35a - Cross-Correlation Functions of HF' and Sunspot Number (using |SSN|) Fig. 3-35b - Cross-Correlation Functions of HF' and Sunspot Number (using +SSN)

CROSS CORRELATION FUNCTION VS. TAU

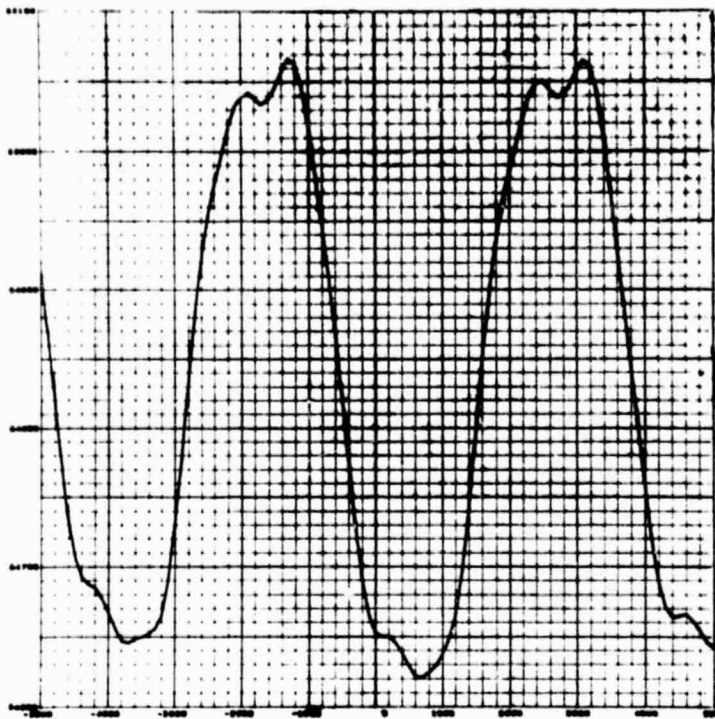


Fig. 3-36a - Cross-Correlation Functions of F3R and Sunspot Number (using |SSN|)

CROSS CORRELATION FUNCTION VS. TAU

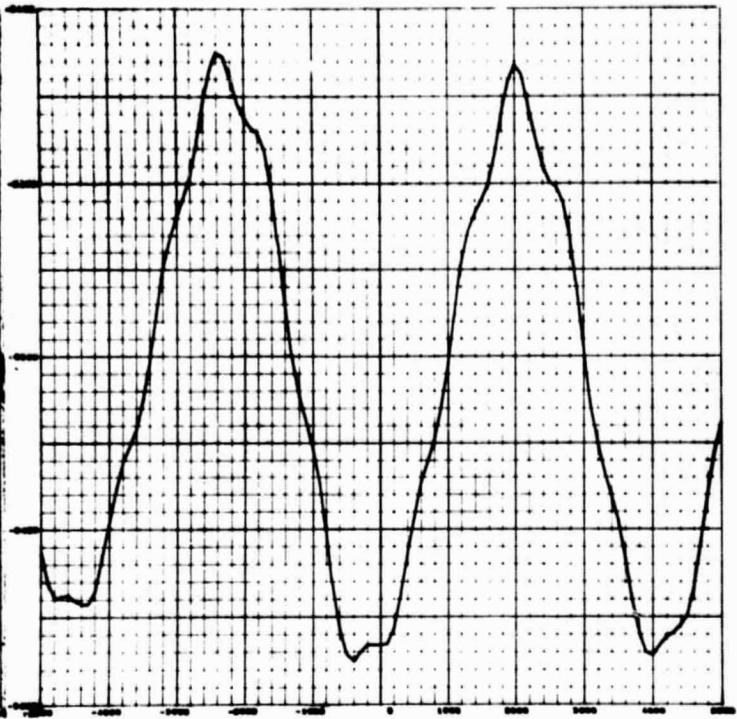


Fig. 3-36b - Cross-Correlation Functions of F3R and Sunspot Number (using +SSN)

CROSS CORRELATION FUNCTION VS. TAU

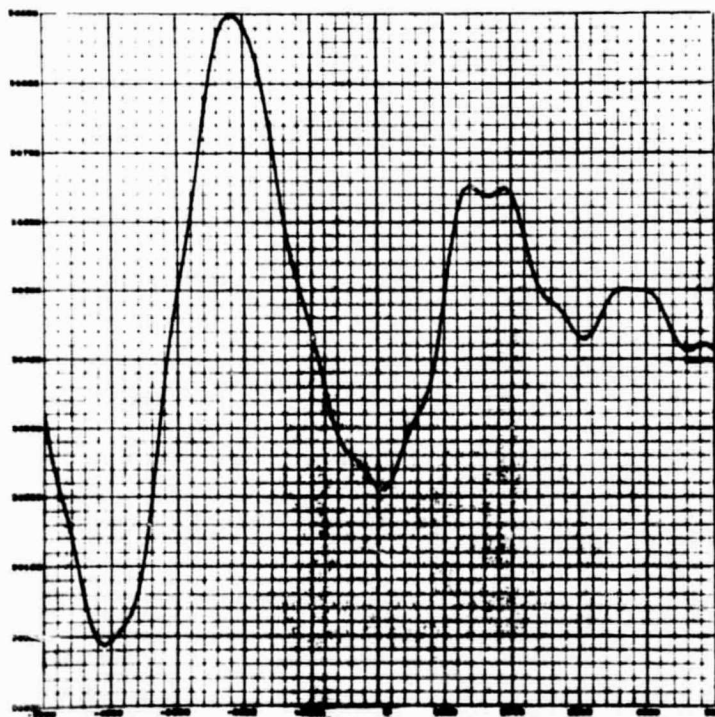


Fig. 3-37a - Cross-Correlation Functions of F3H and Sunspot Number (using |SSN|)

CROSS CORRELATION FUNCTION VS. TAU

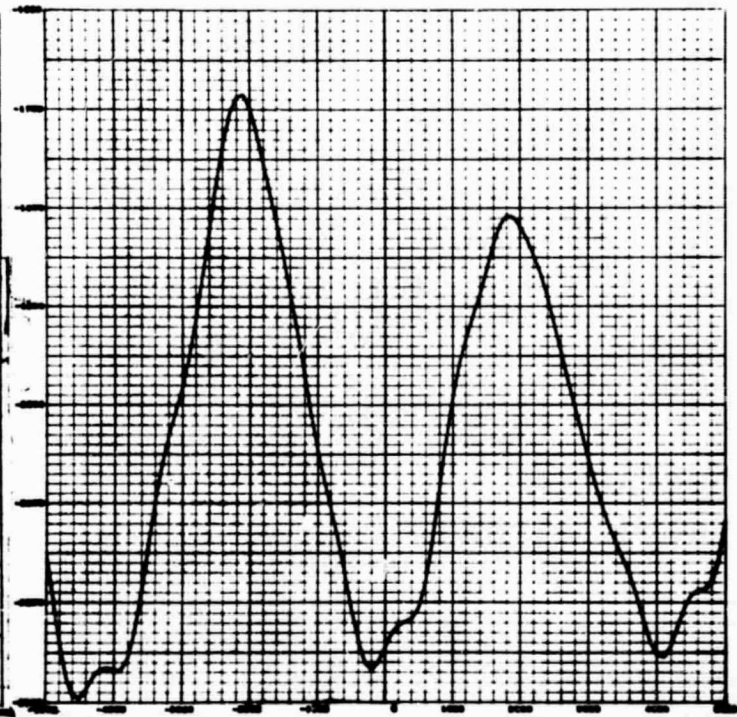
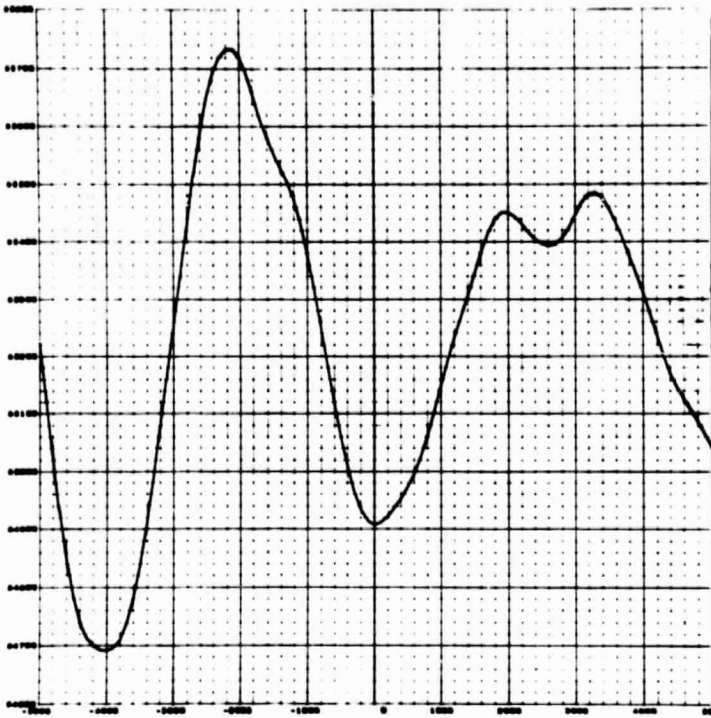


Fig. 3-37b - Cross-Correlation Functions of F3H and Sunspot Number (using +SSN)

CROSS CORRELATION FUNCTION VS. TAU



CROSS CORRELATION FUNCTION VS. TAU

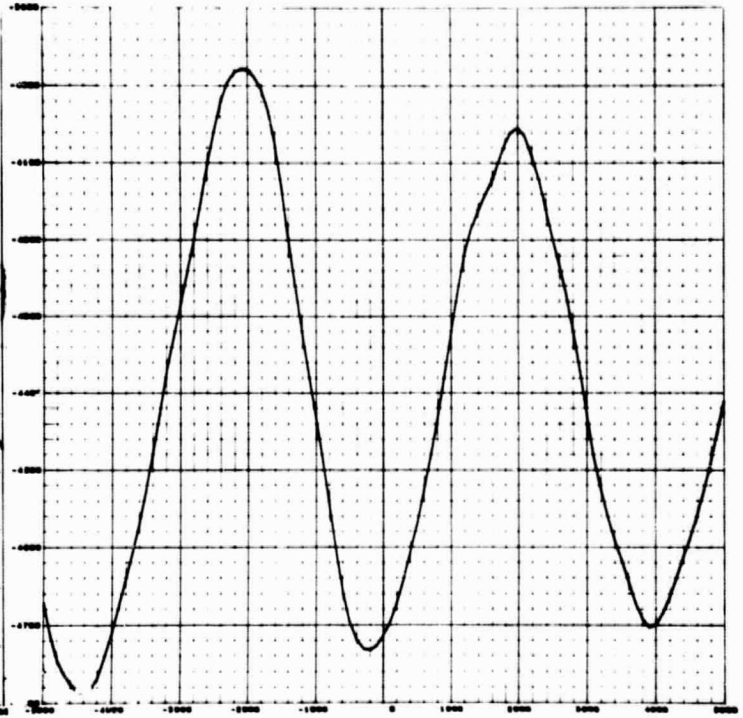
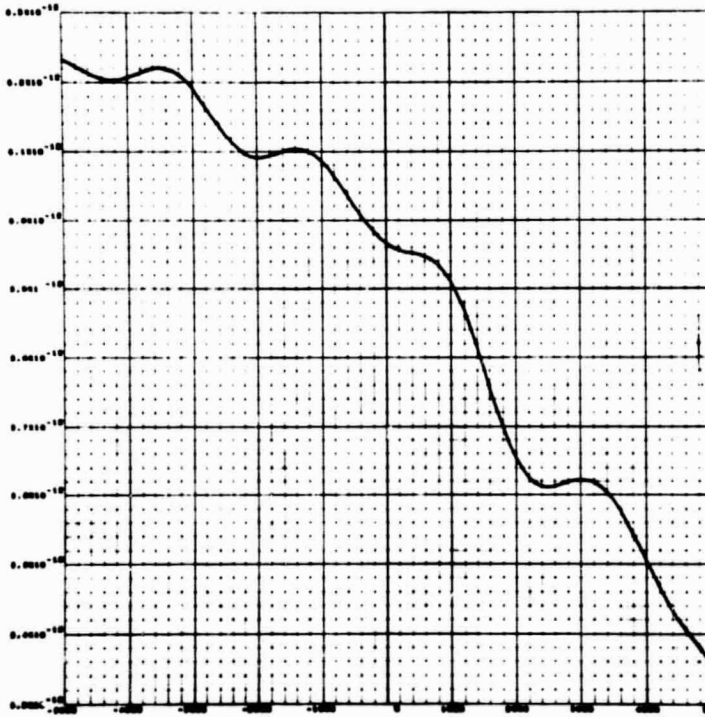


Fig. 3-38a - Cross-Correlation Functions of E_1 and Sunspot Number (using $|SSN|$)

Fig. 3-38b - Cross-Correlation Functions of E_1 and Sunspot Number (using $\pm SSN$)

CROSS CORRELATION FUNCTION VS. TAU



CROSS CORRELATION FUNCTION VS. TAU

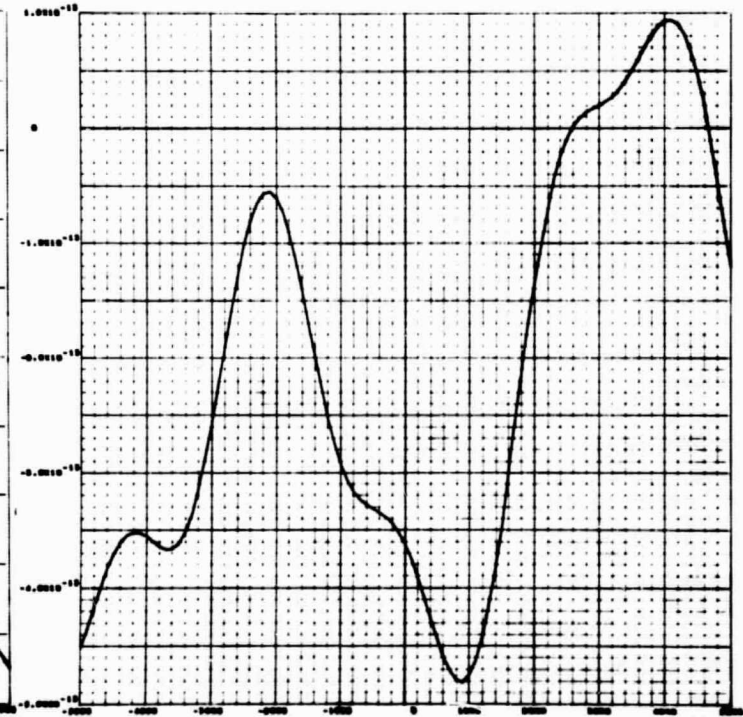
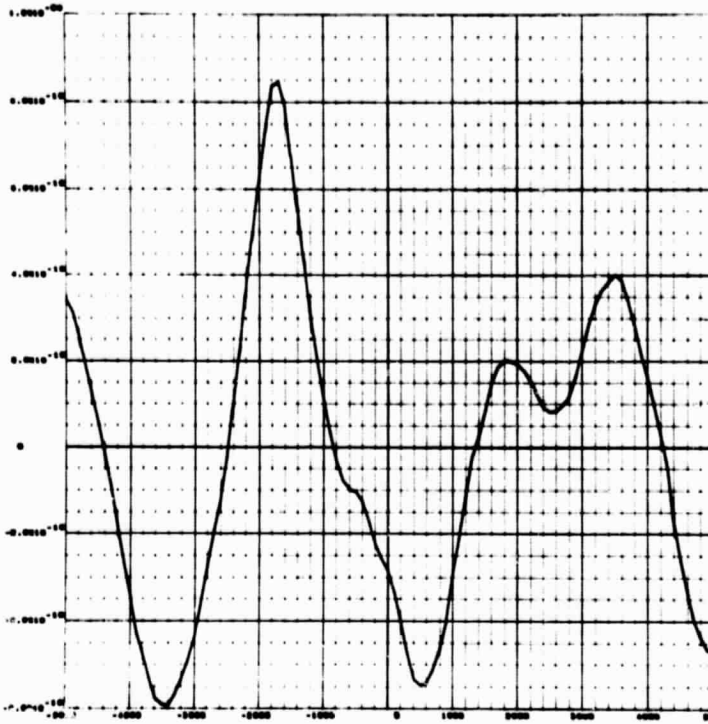


Fig. 3-39a - Cross-Correlation Functions of CUP and Sunspot Number (using $|SSN|$)

Fig. 3-39b - Cross-Correlation Functions of CUP and Sunspot Number (using $\pm SSN$)

CROSS CORRELATION FUNCTION VS. TAU



CROSS CORRELATION FUNCTION VS. TAU

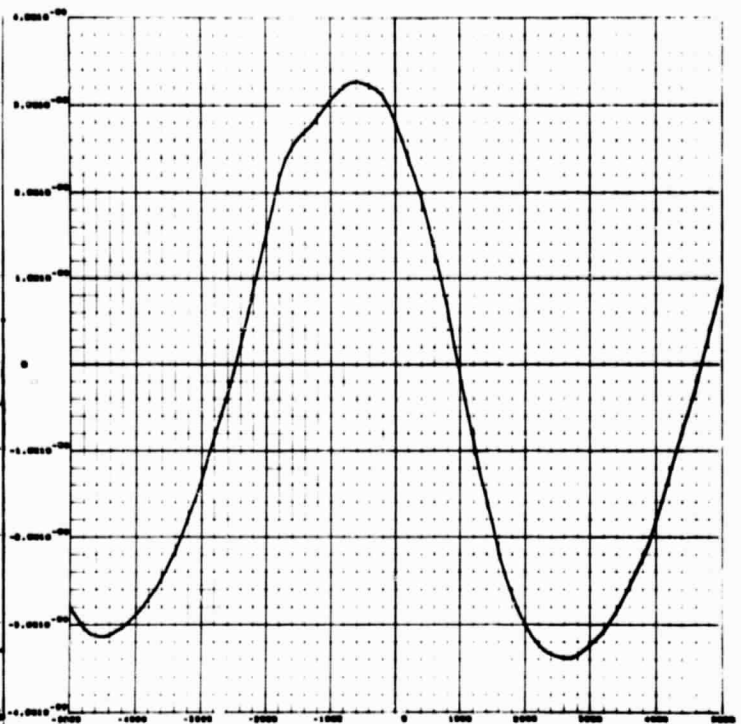
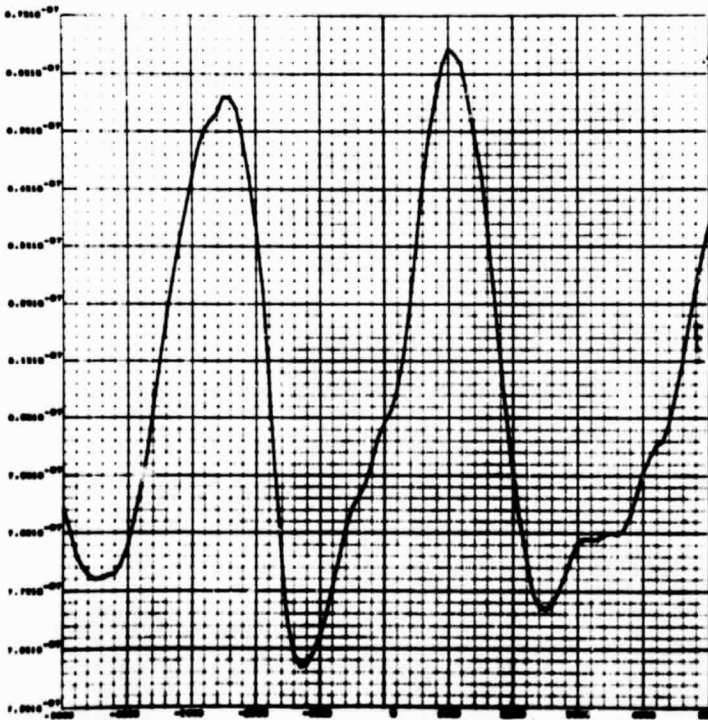


Fig. 3-40a - Cross-Correlation Functions of SCC and Sunspot Number (using $|SSN|$) Fig. 3-40b - Cross-Correlation Functions of SCC and Sunspot Number (using $\pm SSN$)

CROSS CORRELATION FUNCTION VS. TAU



CROSS CORRELATION FUNCTION VS. TAU

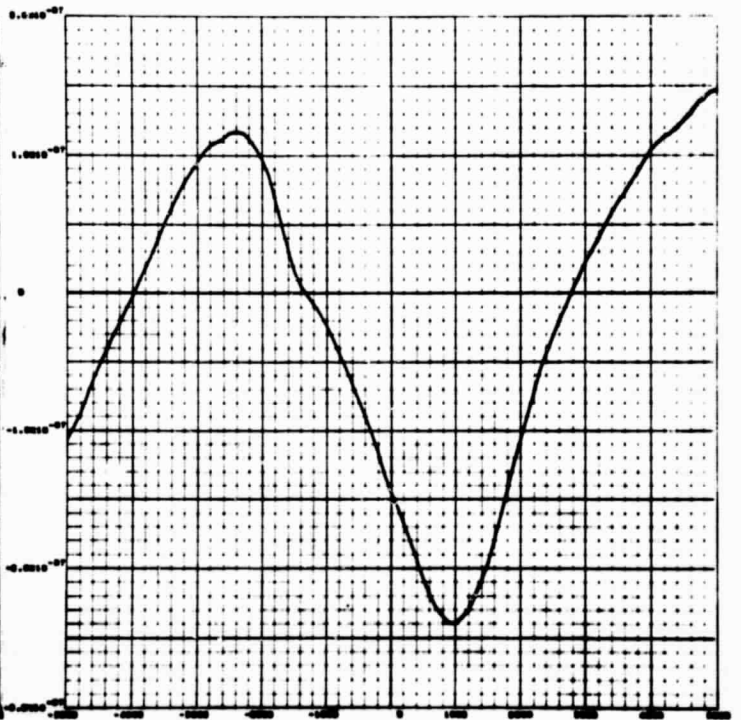
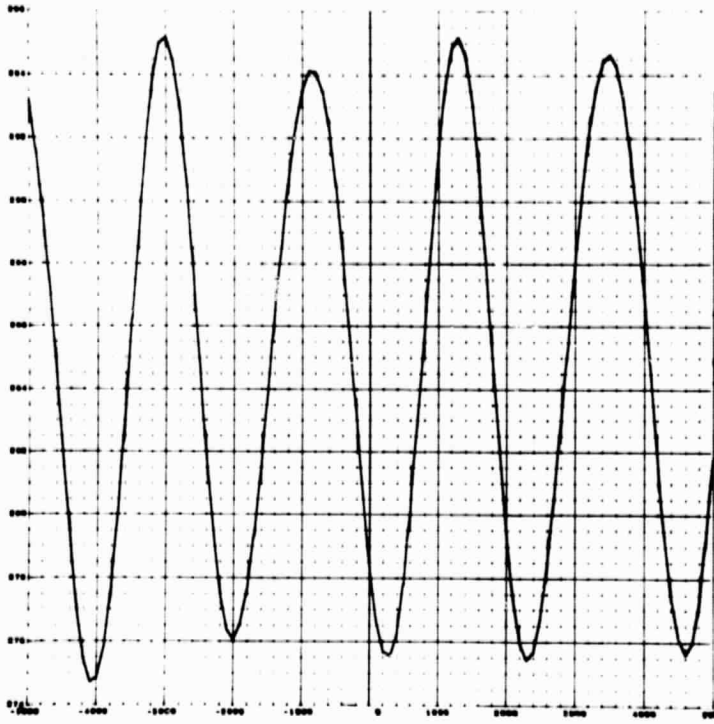


Fig. 3-41a - Cross-Correlation Functions of SSC and Sunspot Number (using $|SSN|$) Fig. 3-41b - Cross-Correlation Functions of SSC and Sunspot Number (using $\pm SSN$)

CROSS CORRELATION FUNCTION VS. TAU



CROSS CORRELATION FUNCTION VS. TAU

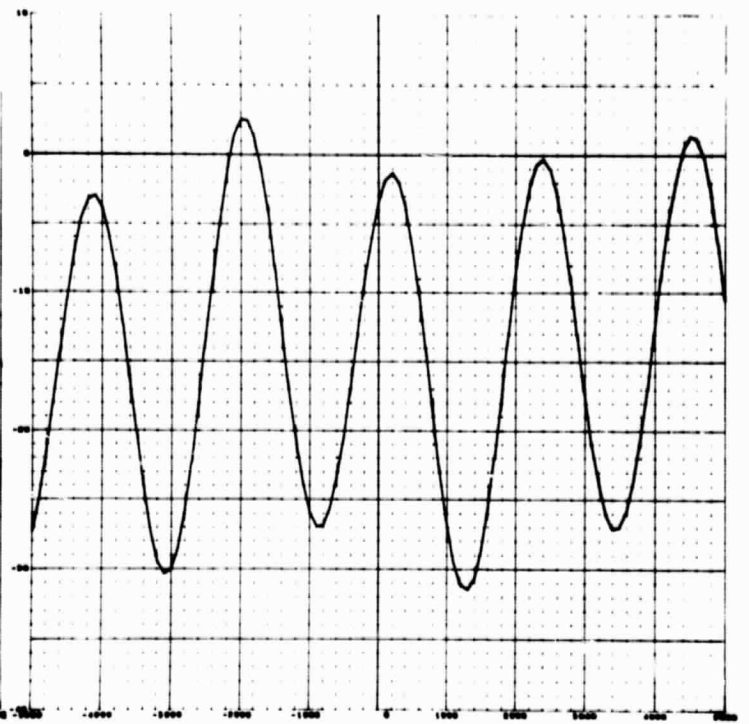


Fig. 3-42a - Cross-Correlation Functions of V_3 and Sunspot Number (using $|SSN|$) Fig. 3-42b - Cross-Correlation Functions of V_3 and Sunspot Number (using $\pm SSN$)

Section 4

NONLIN-ITLIN: THE TECHNIQUE USED TO
ESTIMATE SUNSPOT NUMBER

The NONLIN-ITLIN technique was developed recently by D. F. Specht (Ref. 16) for use with continuous predictor variables. In this study, the technique was used to estimate sunspot number using various predictor-variables associated with the planetary interactions with the sun. In the computer program NONLIN-ITLIN, NONLIN refers to an algorithm for a nonlinear regression performed on the data to combine individual predictors; and ITLIN refers to an iterative linear regression procedure, which is the final processor used for combining partial predictors from NONLIN.

NONLIN was programmed to provide the final processor (ITLIN) with many estimates of SSN. ITLIN simply combines these estimates into a final estimate with higher validity. Figure 4-1 shows the information flow through the NONLIN-ITLIN program. Variables X_1 and X_n are estimates of SSN based on NONLIN and \hat{SSN} is the final estimate of SSN using ITLIN.

4.1 NONLIN

NONLIN finds nonlinear transformations from the predictor space to an intermediate space (defined by the X variables). Since no statistical procedure can be invoked to find an unrestricted relationship between multiple predictor variables and a criterion variable without the danger of overfitting a finite sample of data points, NONLIN attempts to find a nonlinear relationship between only one, two, three or four raw measurements and SSN at a time. Even with this restriction in dimensionality of the problem, NONLIN imposes substantial smoothing to the resulting regression surface in order to avoid excessive overfitting. In this particular study the nonlinear relations between individual predictor parameters and SSN were found. The experiments were

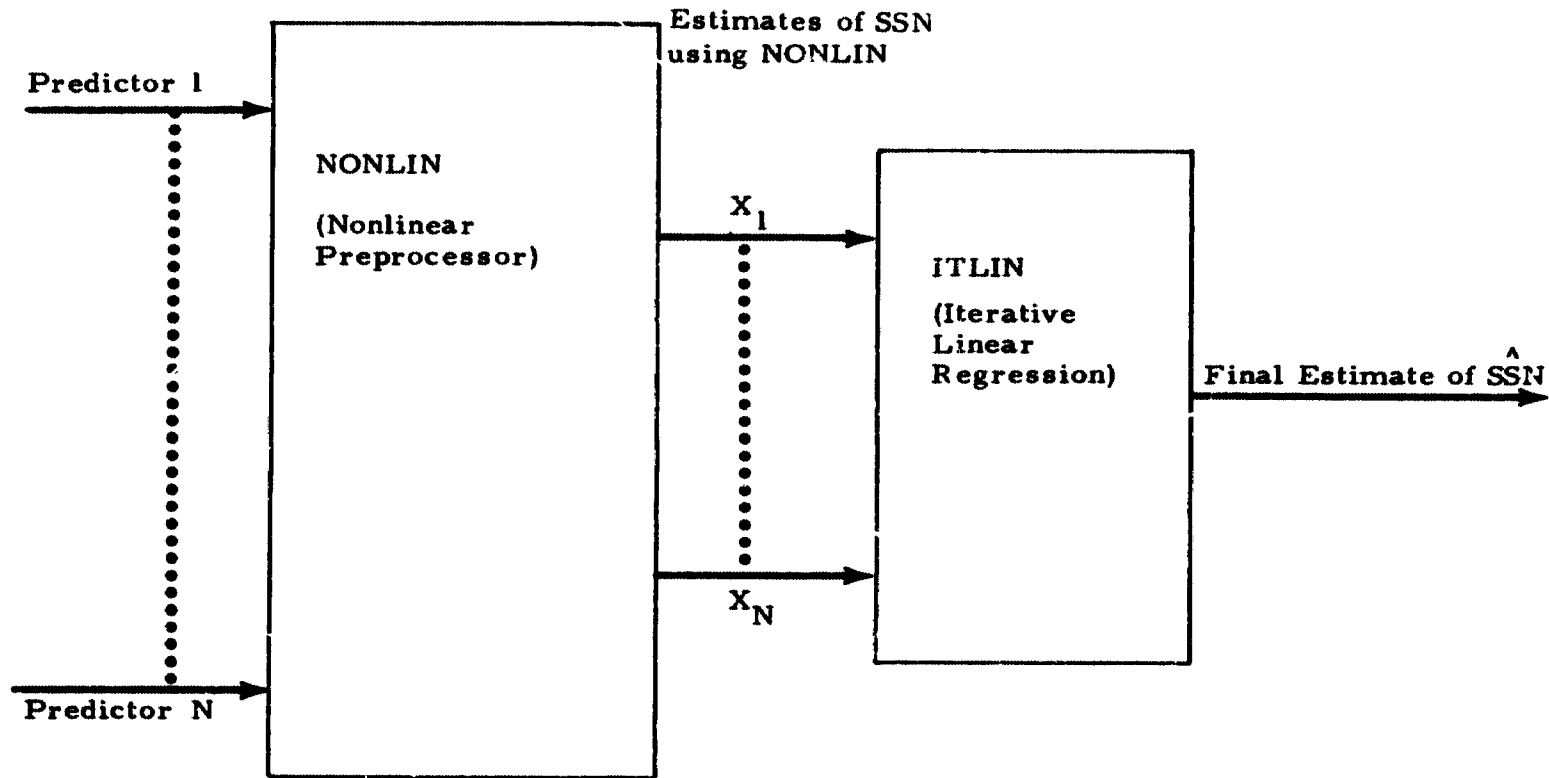


Fig. 4-1 - NONLIN/ITLIN Flow Diagram

not extended to combine two, three or four parameters at a time within the NONLIN portion of the analysis. Experiments of this type could be run in the future and there is a possibility that the estimates could be improved. However, the purpose of this study was to pick individual predictors and establish the applicability of NONLIN/ITLIN to the problem of estimating SSN, combining the parameters in the ITLIN program.

4.1.1 Formulation of NONLIN

A general description of NONLIN as provided by Specht in Ref. 16 is given below. See Ref. 16 for a more detailed description of the technique.

Let \underline{X} be a p component random vector variable with transpose $\underline{X}' \equiv [X_1, \dots, X_j, \dots, X_p]$ and Y be a one-dimensional random variable with a joint continuous distribution of density $f(\underline{x}, y)$. The regression of Y given $\underline{X} = \underline{x}$ is

$$E[Y|\underline{X} = \underline{x}] = \int_{-\infty}^{\infty} yf(\underline{x}, y) dy + \int_{-\infty}^{\infty} f(\underline{x}, y) dy \tag{4.1}$$

Using the consistent nonparametric estimators of the densities described later the regression can be estimated by the estimated regression

$$\hat{Y}(\underline{x}) \cong \frac{\sum_{i=1}^n Y_i \exp \left[-\frac{1}{2\sigma^2} \sum_{j=1}^p (X_{ji} - x_j)^2 \right]}{\sum_{i=1}^n \exp \left[-\frac{1}{2\sigma^2} \sum_{j=1}^p (X_{ji} - x_j)^2 \right]} \tag{4.2}$$

where

n = number of observations of \underline{X} and Y used in estimating the densities

\underline{X}_i and Y_i = the i^{th} observations of \underline{X} and Y, respectively

$\underline{X}'_i \equiv [X_{1i}, \dots, X_{ji}, \dots, X_{pi}]$

σ = a smoothing parameter

\underline{x}_1 in this study refers to the predictor parameters where p is the number of parameters used in each NONLIN pass. Y and \hat{Y} are the actual and estimated values of SSN.

It is further shown that the nonlinear regression Eq. (4.2) can be approximated to any desired accuracy by a polynomial-ratio regression estimate

$$Y^*(\underline{x}) = \frac{Q(\underline{x})}{P(\underline{x})} \quad (4.3)$$

where the coefficients of the polynomials are computed as a function of the observed sample. The advantage of the form Eq. (4.3) is that the observations are used only in the computation of the coefficients. Subsequent evaluation of $\hat{Y}(\underline{x})$ for a given vector \underline{x} is usually much faster using Eq. (4.3) rather than Eq. (4.2).

This same advantage is, of course, shared by classical polynomial regression equations, but the technique described has the following advantages compared with classical polynomial regression techniques utilizing a single polynomial:

- It provides a simple method of determining the coefficients. The calculation for the coefficient of a particular term amounts to little more than averaging the corresponding product of variables over the set of observations available.
- The computational and storage requirements increase only linearly with the number of coefficients used.
- The shape of the regression surface can be made as complex as necessary to closely approximate Eq. (4.1), or as simple as desired, by proper choice of the smoothing parameter σ . In spite of this flexibility, $Y^*(\underline{x})$ estimated from Eq. (4.3) is bounded by the minimum and maximum of the observations Y_i when $Q(\underline{x})$ and $P(\underline{x})$ are truncated at an even order.
- Because of the smoothing properties inherent in the density estimator, the number of coefficients used in the polynomials can approach or even exceed the number of observations in the sample with no danger of the regression surface overfitting the data when σ is suitably chosen.

Since the derivation of Eq. (4.3) from Eq. (4.2) is not dependent on \underline{X} being random, the computational advantages of the polynomial form can be utilized also when values of \underline{X} are specified in the design of an experiment and Y alone is a random variable. This property applies, of course, to ordinary polynomial regression as well.

In these experiments the polynomials $Q(\underline{x})$ and $P(\underline{x})$ of Eq. (4.3) were of sixth order and are in the form

$$Q(\underline{x}) = q_0 + q_1 x_i + q_2 x_i^2 + q_3 x_i^3 + q_4 x_i^4 + q_5 x_i^5 + q_6 x_i^6 \quad (4.4)$$

and

$$P(\underline{x}) = p_0 + p_1 x_i + p_2 x_i^2 + p_3 x_i^3 + p_4 x_i^4 + p_5 x_i^5 + p_6 x_i^6 \quad (4.5)$$

where the value i indicates which of the predictor parameters are being used. The values of these coefficients for each of the parameters used to estimate sunspot number are listed in Appendix B.

4.1.2 Normalization of $Y^*(\underline{x})$ to Decrease Error Due to Estimate of $f(x, y)$

The regression $E[Y|\underline{X} = \underline{x}]$ represents that function $h(\underline{x})$ which minimizes the mean-squared error, $E[Y - h(\underline{x})]^2$. However, even for large sample sizes, this objective is not realized by either $\hat{Y}(\underline{x})$ or $Y^*(\underline{x})$ because of systematic distortion of the estimated density which results when the smoothing parameter σ is greater than zero. Once this nonlinear relationship between Y and \underline{X} is found, however, the relationship between Y and \hat{Y} is essentially linear. Thus, the best linear conversion of \hat{Y} (in the least-squares sense) is obtained through simple linear regression of Y on \hat{Y} over the training portion of the data base. A corrected estimate of Y could be obtained by

$$\hat{\hat{Y}}(\underline{x}) = \alpha_0 + \alpha_1 Y(\underline{x}) \quad (4.6)$$

where

$$\alpha_0 = \frac{\left\{ \left[\sum Y_i \right] \left[\sum \hat{Y}(x_i)^2 \right] - \left[\hat{Y}(x_i) \right] \left[\sum Y_i \hat{Y}(x_i) \right] \right\}}{D} \quad (4.7)$$

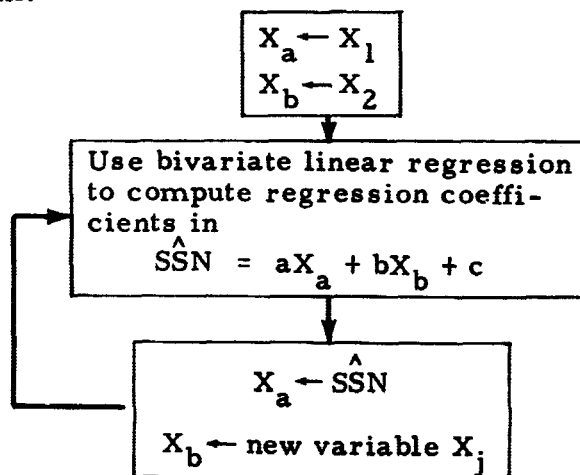
$$\alpha_1 = \frac{\left\{ n \left[\sum Y_i \hat{Y}(x_i) \right] - \left[\sum Y_i \right] \left[\sum \hat{Y}(x_i) \right] \right\}}{D} \quad (4.8)$$

$$D = n \sum \left[\hat{Y}(x_i) \right]^2 - \left[\sum \hat{Y}(x_i) \right]^2 \quad (4.9)$$

and the summations range from $i = 1$ to n where n is the total number of points involved. $N = 3200$ or 3923 for the experiments performed during this study. The values of α_0 and α_1 for the NOLIN estimates based on each of the prediction parameters are listed in Appendix B.

4.2 ITLIN

Since the X_i s generated by NONLIN are linearly related to SSN to a first order of approximation, no further nonlinear processing would appear to be necessary. In principle, the X_i s could be combined into a final estimation of SSN using multiple regression; however, computer time increased geometrically as a function of the number of variables. In recognition of the many raw variables that may be available to be combined, an iterative linear regression procedure was used. Using this procedure (designated ITLIN), the increase in computer running time increases only linearly with the number of predictor variables. The basic operations in the ITLIN program are illustrated below in a simplified form.



In the above simplified diagram, \hat{SSN} , X_a , X_b are arrays of numbers corresponding to cases in the training set. For each time, t_i of the training set, \hat{SSN}_i is the estimate sunspot number conditioned on X_{ai} and X_{bi} .

To start, the arrays of values corresponding to variables X_1 and X_2 are loaded into X_a and X_b , respectively. Using the standard linear regression procedure for two independent variables, \hat{SSN} results as the array of first estimates of the criterion variable. For the next iteration, this \hat{SSN} is loaded into the X_a array and a new variable (X_j) from NONLIN is loaded into the X_b array. The process is repeated until change in rms error reaches a point of diminishing returns. Program ITLIN keeps track of the cumulative effect of the coefficients a , b and c during all iterations so that the final \hat{SSN} can be calculated by a simple equivalent linear combination of the X_i s from NONLIN. These coefficients are given in Appendix C. After each iteration, ITLIN computes accuracy on both the training and testing sets. In addition to rms error over the entire history of the training set, and in the case of the first set of experiments the test set as well, rms error for various ranges of actual and estimated values are obtained. These error statistics were generated by searching through the actual values of SSN and finding all those values where $0 < |SSN| \leq 10$, $10 < |SSN| \leq 20$, etc. In each of these ranges the rms error was calculated. The same process was repeated for all the values of \hat{SSN} .

4.3 SCHEMATIC OF ENTIRE ESTIMATION PROCESS

Throughout the preceding sections the parameters used to estimated sunspot number have been exposed to a number of preprocessing procedures. In addition, the actual estimation procedure is complex and involves still more coefficients. Figure 4-2 provides a diagrammed, step-by-step description of the estimation process from beginning to end showing what is done and where in the report the pertinent information is located. The first three steps involve preprocessing: filtering to smooth the predictor parameters, cross-correlation with SSN to discover the appropriate time lag where correlation is best, and normalizing the predictors to make meaningful estimates of the probability density function. The normalizing coefficients were generated for

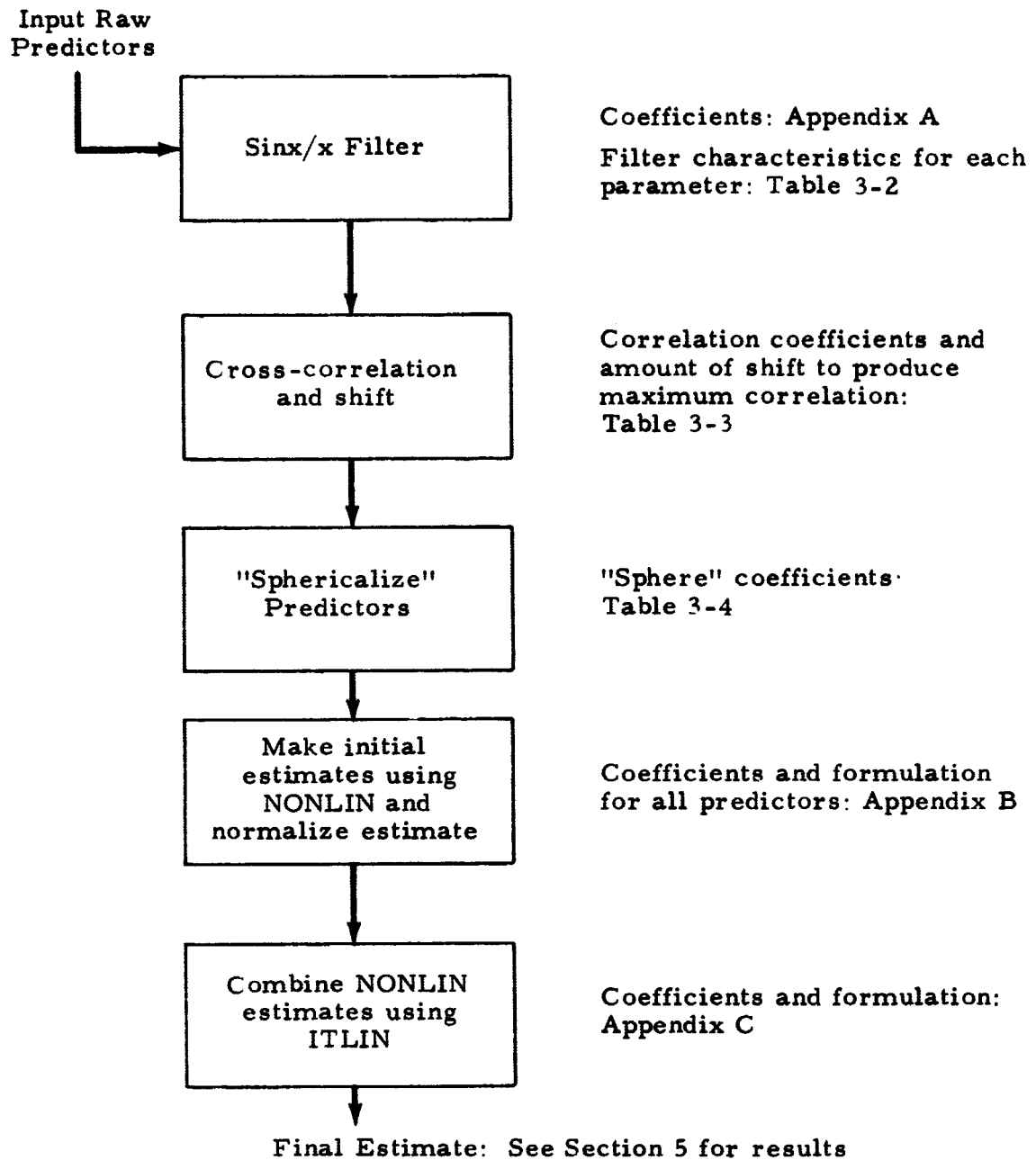


Fig. 4-2 - Flow Diagram of Entire Estimation Process

Phase 1 training case; i.e., the first 3200 training samples, and they were also used in the Phase 2 experiment (3923 training point) since the distributions of the parameters change only slightly with the increase in the number of samples. Thus, using one set of coefficients reduces the total number of coefficients involved in the experiments. Steps four and five involve NONLIN and include the polynomial-ratio regression estimate and the correlation of the estimate based on the training set information. In steps four and five (as well as step six) the coefficients are generated using only data in the training set. Then estimates are made over the entire ranges of the data training and testing set, and error statistics are generated. Step six combines the estimates made by NONLIN using ITLIN.

Section 5

RESULTS OF SUNSPOT ESTIMATION EXPERIMENTS

The results of this study are divided into two phases. Experiments of Phase I evaluated the NONLIN-ITLIN estimation technique using a training set (3200 data points), and a testing set (724 data points). These experiments were used to determine the best procedure to follow in making an actual prediction; specifically, whether the 11-year or 22-year sunspot cycle should be used, and which parameters should be used to make these estimates. In the Phase II experiment the information gained from Phase I was used to estimate sunspot number several years into the future using data since 1749 to generate the various coefficients.

5.1 PHASE I EXPERIMENT: EVALUATION OF THE NONLIN-ITLIN TECHNIQUE

In these experiments \pm SSN as well as $|\text{SSN}|$ were estimated and it was found that the magnitude of the rms error was smaller when $|\text{SSN}|$ were estimated compared to when \pm SSN were estimated. As a percentage of full-scale value, however, the estimates of \pm SSN are more accurate. Therefore, a decision was made to use the \pm SSN configuration to estimate sunspot into the future. It was suggested that efforts should be made to compensate for the fact that the regression analysis estimates the values of a waveform that tend toward the mean of the waveform. To attempt to compensate, a brief experiment was performed at the end of this study which estimated $\sqrt[3]{\text{SSN}}$ and SSN^3 , and then transformed these estimates to obtain the actual values of SSN.

5.1.1 Experiment Estimating \pm SSN

In these experiments accuracy (in rms error) was improved as more parameters were added, e.g., see Table 5-1. However, the addition of the

last few parameters caused little increase in accuracy because of the lack of correlation of these parameters with $\pm\text{SSN}$. The NONLIN coefficients used to obtain the transformation of each of the parameters along with the coefficients to make the first order correction of the estimate are given in Appendix B, Table B-1. The ITLIN coefficient used to combine these parameters into the final estimate of $\pm\text{SSN}$ are listed in Appendix C, Table C-1, for combinations of two through twenty-one NONLIN parameters. Since the increase in accuracy is slight after the parameter Tau is added, to conserve computer running time, the remaining experiments were run using the top fifteen parameters instead of all twenty-one.

A representative example of estimates of $\pm\text{SSN}$ is shown in Fig. 5-1. In this case 13 parameters were used. The symbol A represents the actual value of $\pm\text{SSN}$, the symbol E, the estimated values of $\pm\text{SSN}$. Figure 5-2 shows the errors between $\pm\text{SSN}$ and $\pm\hat{\text{SSN}}$. In both of these figures MJD -39920 to 24060 is the training set and MJD 24080 to 38540 is the test set. Table 5-1 lists the overall rms error for the estimates; however, it is known that the estimates will be more accurate near the mean of the waveform. Thus, the rms error was calculated over various intervals of data magnitude for both $\pm\text{SSN}$ and $\pm\hat{\text{SSN}}$. Table 5-2 lists these errors for the training set and testing set for the 13-parameter case. Figure 5-3 shows a plot of $\pm\text{SSN}$ banded by the appropriate rms error at each point and Fig. 5-4 is for $\pm\hat{\text{SSN}}$. These figures provide an estimate of confidence as to how well a given value of $\pm\text{SSN}$ can be estimated and how well a given value of $\pm\hat{\text{SSN}}$ approximates the value of $\pm\text{SSN}$.

5.1.2 Experiment Estimating $|\text{SSN}|$

Table 5-3 shows the change in accuracy of the $|\hat{\text{SSN}}|$ as parameters are added. The NONLIN coefficients are in Appendix B, Table B-2, and the ITLIN coefficients are in Appendix C, Table C-2.

The example to be discussed in detail is the experiment in which 14 parameters are used. Figure 5-5 shows $|\text{SSN}|$ and $|\hat{\text{SSN}}|$ as a function of time

and Fig. 5-6 is the error between actual and estimated values of $|\text{SSN}|$ for the training and testing sets. While the rms error magnitude is smaller than for the $\pm\text{SSN}$ estimates, the rms error as a percentage of full-scale (or maximum value) is greater than for the $\pm\text{SSN}$ case. Table 5-4 lists the rms error over various ranges of data magnitude for the 14-parameter case, and Figs. 5-7 and 5-8 show the plots with these error bands applied.

5.1.3 Experiment Estimating $\sqrt[3]{\pm\text{SSN}}$ and $\pm\text{SSN}^3$

Earlier it was shown that regression analysis tends to estimate toward the mean of a data set. The NONLIN attempts to correct for this characteristic (by performing a linear regression between the SSN and $\hat{\text{SSN}}$ over the training set) have not been completely successful. Another way to reduce this error is to estimate some transformation of the data and then perform the inverse transform to obtain the actual values. Such transforms could include SSN^x or log of the initial SSN. In this study, a brief experiment was run in which the $\sqrt[3]{\pm\text{SSN}}$ as well as $\pm\text{SSN}^3$ were used to note the change in error from the case in which $\pm\text{SSN}$ was estimated. In both cases only one parameter was used to estimate SSN, and in each case the error was obtained by taking the inverse transform of the $\hat{\text{SSN}}$ and comparing that to the actual values of $\pm\text{SSN}$.

When one parameter was used in estimating $\pm\text{SSN}$, the training and testing rms errors were 43.15 and 57.14, respectively, while the correlation coefficient between $\pm\text{SSN}$ and $\hat{\text{SSN}}$ was 0.6425. When $\sqrt[3]{\pm\text{SSN}}$ was estimated, the rms errors between $[\sqrt[3]{\pm\hat{\text{SSN}}}]^3$ and $\pm\text{SSN}$ were 48.14 and 55.14 and the correlation increased to 0.6476. When $\pm\text{SSN}^3$ was estimated, the rms errors between $\sqrt[3]{\pm\hat{\text{SSN}}^3}$ and $\pm\text{SSN}$ were 52.93 and 49.09, respectively, and the correlation coefficient fell to 0.4656. This indicates that these methods of transformation prior to processing do little to reduce the rms error; however, there are other methods that could be used in future experiments such as taking the log of SSN (since SSN goes negative it would be necessary to bias SSN a set amount in order to make use of the log concept). Although this simple transformation of SSN^x did not improve accuracy, there is hope that other transformations will.

5.1.4 Comparison of Experiments Used to Evaluate NONLIN/ITLIN

Of the three sets of experiments, the one producing the lowest rms error relative to the peak-to-peak values of SSN was the experiment using \pm SSN as the criterion. This configuration is also the one that correlates best with most of the predictor parameters (11 out of 21) and has the highest correlation coefficients ($\approx .70$). Because of these considerations as well as limited time during this study, the estimates of future sunspot numbers were obtained using only the \pm SSN configuration. Coefficients generated for the $|\text{SSN}|$ configuration during the evaluation phase of the study could be used, however, to estimate $|\text{SSN}|$ into the future.

5.2 PREDICTING SSN

To predict SSN into the future the \pm SSN configuration was used. A total of 3924 data points were used to train the regression technique and 250 values of $\pm\hat{\text{SSN}}$ were evaluated into the future. Two experiments were run in which this data base setup was used. In the first experiment, each of the 15 best predictors (best according to correlation coefficient) were used to find $\pm\hat{\text{SSN}}$ over the training portion of the data on an individual basis, i.e., ITLIN was not used. This was done to evaluate the conjecture by Ezekiel and Fox (Ref. 15) that correlation coefficient and error of estimate are not necessarily related. In the second experiment $\pm\hat{\text{SSN}}$ was found by combining the NONLIN estimates using ITLIN, and several years of future $\pm\hat{\text{SSN}}$ were evaluated.

5.2.1 Using Individual Parameters to find $\pm\hat{\text{SSN}}$

In this experiment the 15 best parameters according to correlation coefficient were used to estimate \pm SSN using NONLIN but not ITLIN. Thus, there were 15 individual estimates of \pm SSN rather than the usual 15 estimates which combine 1 through 15 predictors. Table 5-5 shows a listing of the 15 best predictors and the corresponding rms error over the training set for each. Note that rms error is almost always monotonically increasing as the correlation

coefficient is monotonically decreasing. This would indicate that the Ezekiel and Fox conjecture is not applicable in this case.

The experiment which follows shows the improvement when the NONLIN estimates are combined using ITLIN.

5.2.2 Combining NONLIN estimates to find $\hat{\pm}$ SSN into the Future

Accuracy is improved by combining estimates of $\hat{\pm}$ SSN as was shown in the Phase I experiments. Listed in Table 5-6 are the fifteen best parameters along with the rms error over the training set (of course it is impossible to know the error in the test set since these are predictions into the future).

The estimates of $\hat{\pm}$ SSN into the future are shown on Figs. 5-9 through 5-22 for cases where 2 through 15 predictors were used. The error band about each estimate was generated over the range of the training set and plotted about the estimated values to provide an estimate of the reliability of the estimates. The minimum rms error for the training set was 41.85, when all 15 parameters were used. Table 5-7 shows a breakdown of this rms error. These are the values of rms error used to generate the error bands on Fig. 5-22.

During the Phase I experiments the minimum rms error during training was 38.47 and this produced an rms error of 56.72 in the test set. If the same ratio were true in this Phase II experiment the rms error for the period into the future would be 61.70. While this is just an estimate of rms error for future predictions it is probably a reasonably good estimate. The addition of more and better parameters coupled with improvement in the NONLIN/ITLIN procedures would make closer estimates possible.

Table 5-1

ESTIMATIONS OF $\bar{+SSN}$ TO EVALUATE
NONLIN/ITLIN USING 21 PREDICTORS

Error Training	Error Testing	Parameter Added
43.15	57.41	Zeta
43.07	57.39	P
43.04	57.25	Vo
42.93	57.15	\dot{P}
42.50	56.96	\dot{P}
42.49	56.94	ROD
40.98	60.40	Ho
40.98	60.79	Ro
49.95	60.81	Ao
40.92	60.51	SCC
39.45	58.22	SSC
39.44	58.27	Tau
38.56	57.44	CUP
38.56	57.41	F3
38.47	56.72	F3H
38.41	*	HF'
38.34		HF
38.32		Jo
38.27		F3R
38.26		V3
38.20		Lo

Table 5-2
 RMS ERROR BETWEEN \pm SSN AND \pm SSN FOR
 DISCRETE RANGES OF DATA MAGNITUDE

Range of Values (Absolute Value)	Training Set				Testing Set			
	rms Error	No. Actual Points	rms Error	No. Est. Points	rms Error	No. Actual Points	rms Error	No. Est. Points
0 - 10	36	602	33	353	26	66	36	94
10 - 20	30	417	36	405	28	80	43	118
20 - 30	29	300	36	536	27	73	57	133
30 - 40	32	261	45	495	24	54	44	116
40 - 50	33	406	40	490	23	39	81	93
50 - 60	33	268	39	548	35	48	58	123
60 - 70	29	296	29	263	40	71	85	27
70 - 80	46	145	44	83	43	61	81	19
80 - 90	51	143	50	27	44	21		0
90 - 100	52	92		0	52	22		0
100 - 110	53	74		0	56	32		0
110 - 120	59	58		0	72	30		0
120 - 130	70	57		0	87	13		0
130 - 140	75	47		0	90	26		0
140 - 150	82	21		0	99	28		0
150 - 160	75	13		0	102	12		0
160 - 170	0	0		0	116	6		0
170 - 180	0	0		0	129	9		0
180 - 190	0	0		0	133	15		0
190 - 200	0	0		0	136	12		0
200 - 210	0	0		0	143	5		0

Overall rms error = 38.56 Training (10.7% of peak to peak)
 = 57.44 Testing (15.67% of peak to peak)

Table 5-3
 ESTIMATIONS OF |SSN| TO EVALUATE
 NONLIN/ITLIN USING 15 PREDICTORS

Error Training	Error Testing	Parameter Added
32.70	60.38	HF
32.60	61.01	HF'
32.50	61.41	F3R
32.49	61.07	F3
32.46	60.98	Ao
30.63	59.78	CUP
30.58	59.56	F3H
30.55	59.53	Jo
29.88	57.49	Tau
29.86	57.40	P
29.83	56.63	Lo
29.05	54.90	ROD
29.05	55.03	P
28.53	52.02	Vo
28.52	52.00	V3

Table 5-4
 RMS ERROR BETWEEN |SSN| AND |SSN|^A
 FOR DISCRETE RANGES OF DATA MAGNITUDE

Range of Values (Absolute Value)	Training Set				Testing Set			
	rms Error	No. Actual Points	rms Error	No. Est. Points	rms Error	No. Actual Points	rms Error	No. Est. Points
0 - 10	34	567	20	38	50	64	23	8
10 - 20	26	452	18	267	41	82	16	35
20 - 30	21	300	22	524	29	73	26	36
30 - 40	18	261	22	607	23	54	32	120
40 - 50	19	406	25	631	21	39	42	164
50 - 60	21	268	33	387	19	48	52	98
60 - 70	22	296	40	363	25	71	75	162
70 - 80	25	145	37	248	27	61	58	87
80 - 90	32	143	19	74	40	21	35	13
90 - 100	30	92	26	29	49	22		0
100 - 110	38	74	39	32	57	32		0
110 - 120	45	58		0	68	30		0
120 - 130	53	57		0	66	13		0
130 - 140	62	47		0	71	26		0
140 - 150	70	21		0	80	28		0
150 - 160	51	13		0	85	12		0
160 - 170	0	0		0	97	6		0
170 - 180	0	0		0	107	9		0
180 - 190	0	0		0	116	15		0
190 - 200	0	0		0	130	12		0
200 - 210	0	0		0	137	5		0

Overall rms error = 28.53 Training (14% of peak to peak)
 = 52.02 Testing (26% of peak to peak)

Table 5-5
 FINDING \pm SSN USING INDIVIDUAL PREDICTORS

Parameter	Correlation Coefficient	rms Error
Zeta	.70573	45.34
P	.69919	45.41
Vo	.68900	45.46
P'	.68502	45.84
P	.65830	47.02
ROD	.64322	46.44
Ho	.61610	49.29
Ro	.55459	52.47
AO	.43618	58.04
CC	.31237	55.60
SSC	.19178	60.03
Tau	.18118	58.80
CUP	.09417	62.36
F3	.09075	62.63
F3H	.08311	62.30

Table 5-6
RMS ERROR FOR TRAINING WHEN ESTIMATING
+SSN INTO THE FUTURE

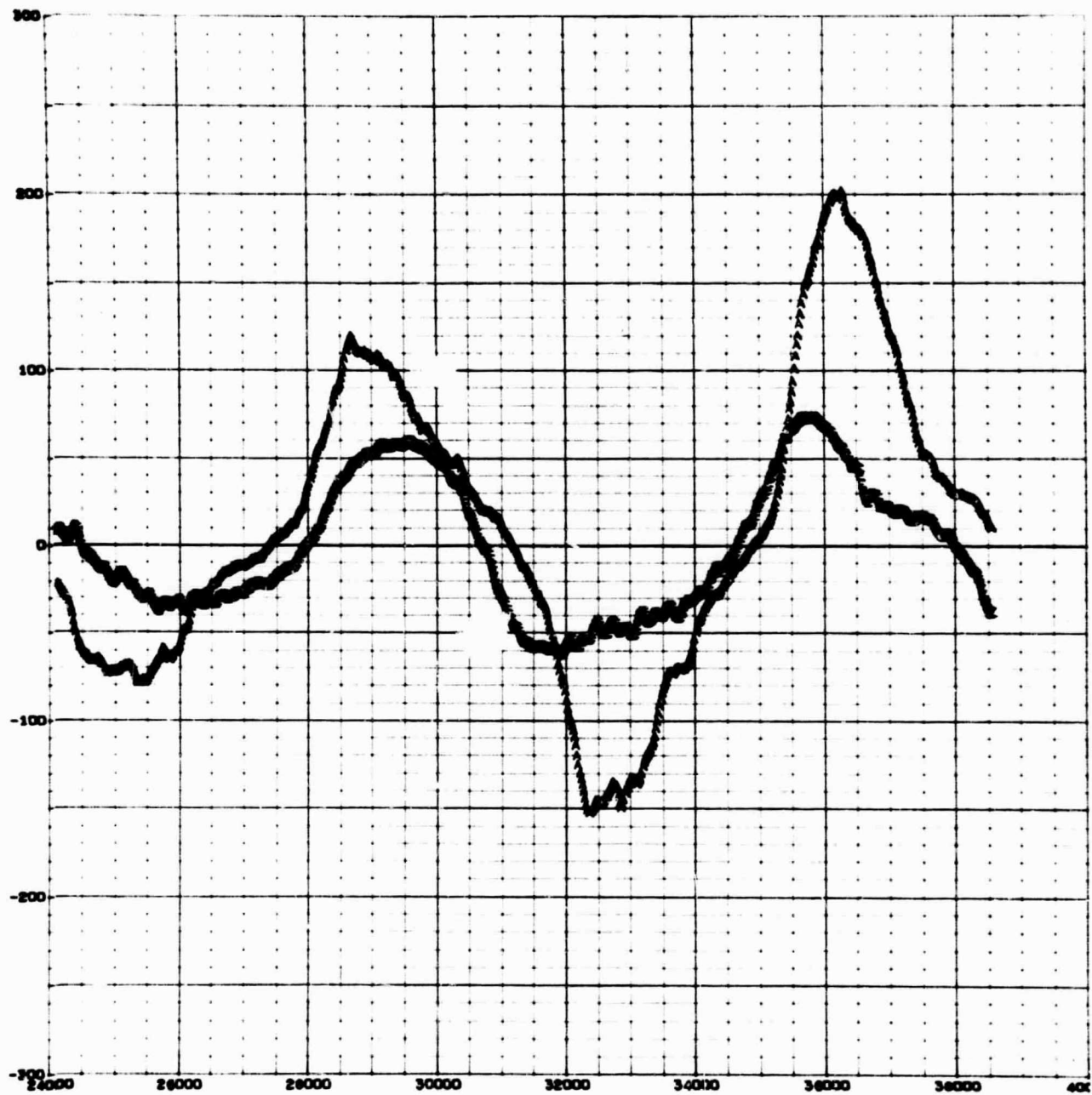
Parameter	rms Error
Zeta	45.34
P	45.29
Vo	45.21
\dot{P}'	45.11
\dot{P}	44.96
ROD	44.96
Ho	44.20
Ro	44.20
Ao	44.19
SCC	44.14
SSC	44.14
Tau	42.86
CUP	42.10
F3	42.00
F3H	41.85

Table 5-7
 RMS ERROR FOR VARIOUS RANGES OF $\pm \hat{SSN}$

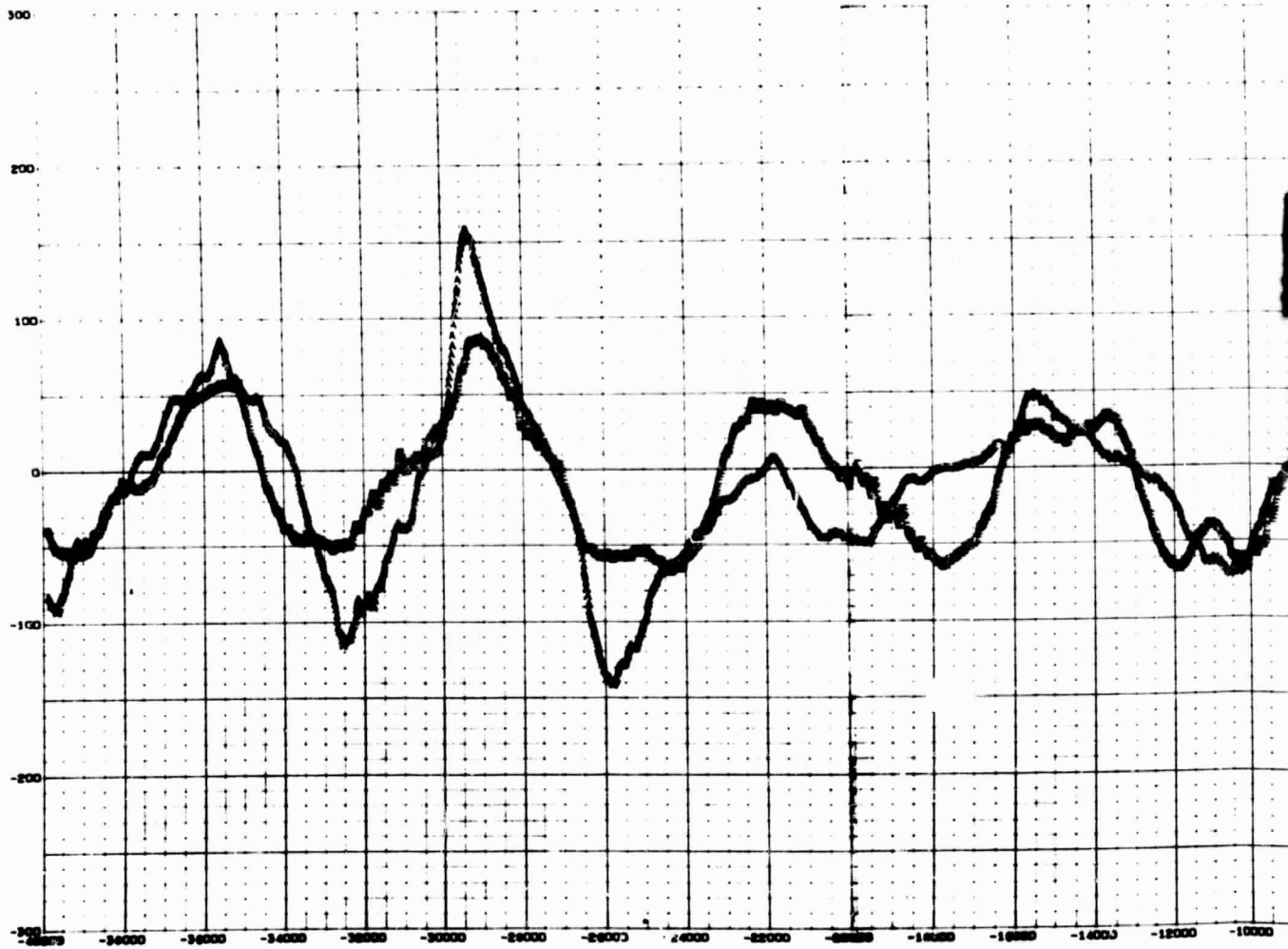
Range of $ \pm \hat{SSN} $	No. of Values in Given Range	rms Error
0 to 10	668	39
10 to 20	497	33
20 to 30	373	33
30 to 40	315	35
40 to 50	445	37
50 to 60	316	35
60 to 70	367	28
70 to 80	206	42
80 to 90	164	48
90 to 100	114	46
100 to 110	106	50
110 to 120	88	57
120 to 130	70	68
130 to 140	73	73
140 to 150	49	82
150 to 160	25	74
160 to 170	6	96
170 to 180	9	107
180 to 190	15	110
190 to 200	12	109
200 to 210	5	115

NOTE: Overall rms error training 41.85 (11.6% of peak-to-peak).

ESTIMATED AND ACTUAL SUNSPOT NUMBER

Fig. 5-1a - History of Actual and Estimated Values of \pm SSN (Testing Set)

ESTIMATED AND ACTUAL



FOLDOUT FRAME 14

ACTUAL SUNSPOT NUMBER

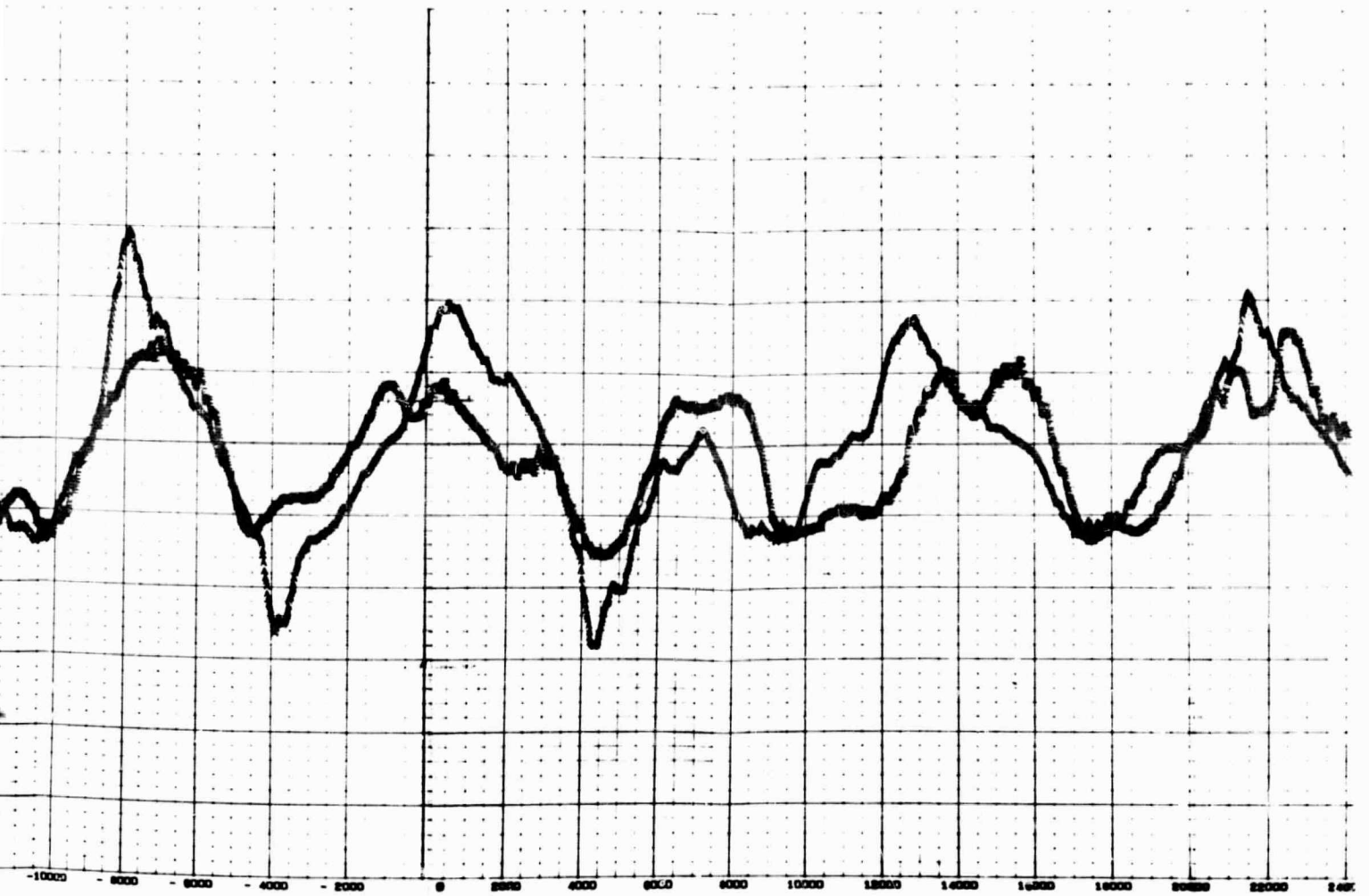


Fig. 5-1b - History of Actual and Estimated Values of \pm SSN (Training Set)

ESTIMATED AND ACTUAL SUNSPOT NUMBER

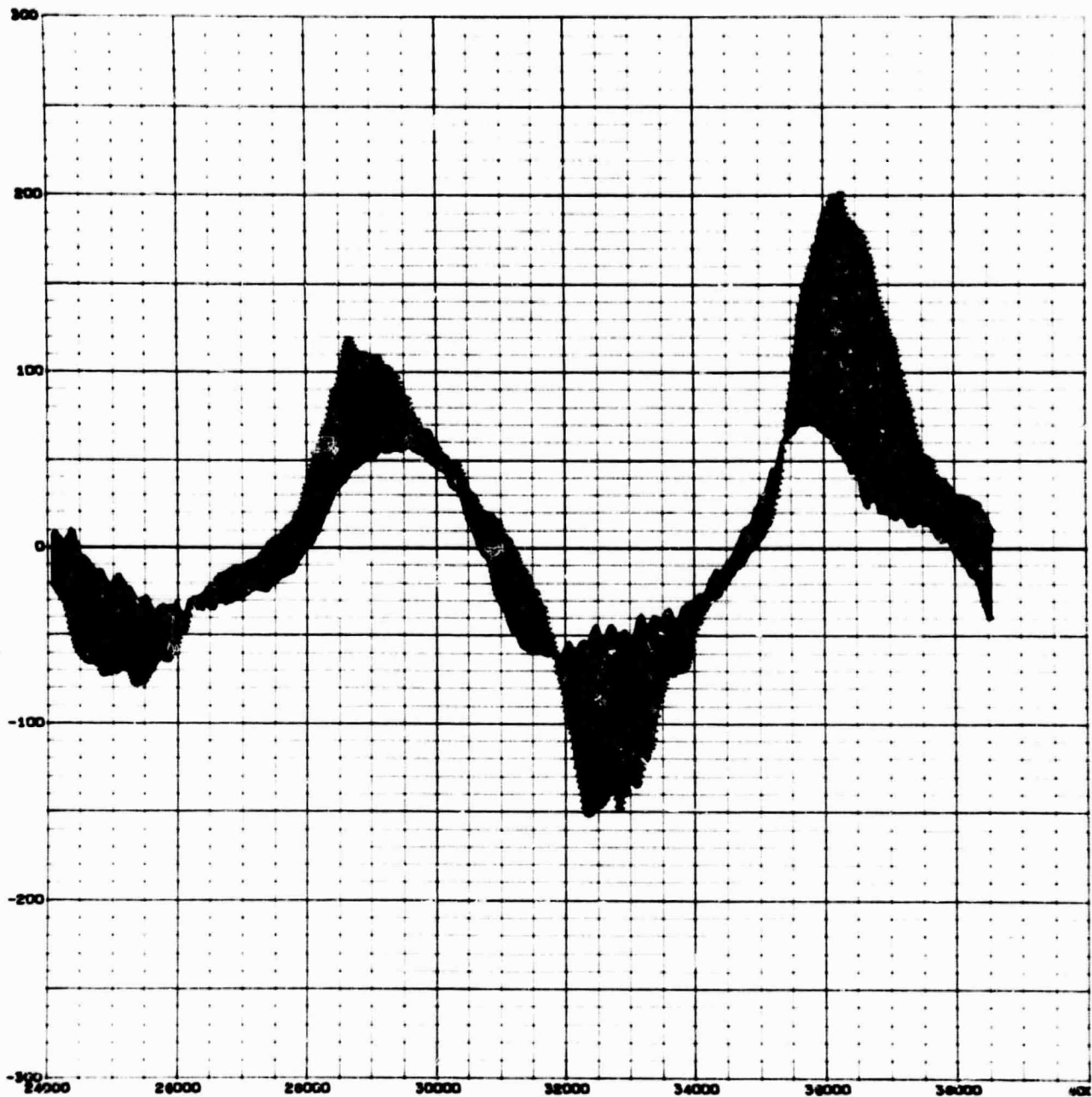
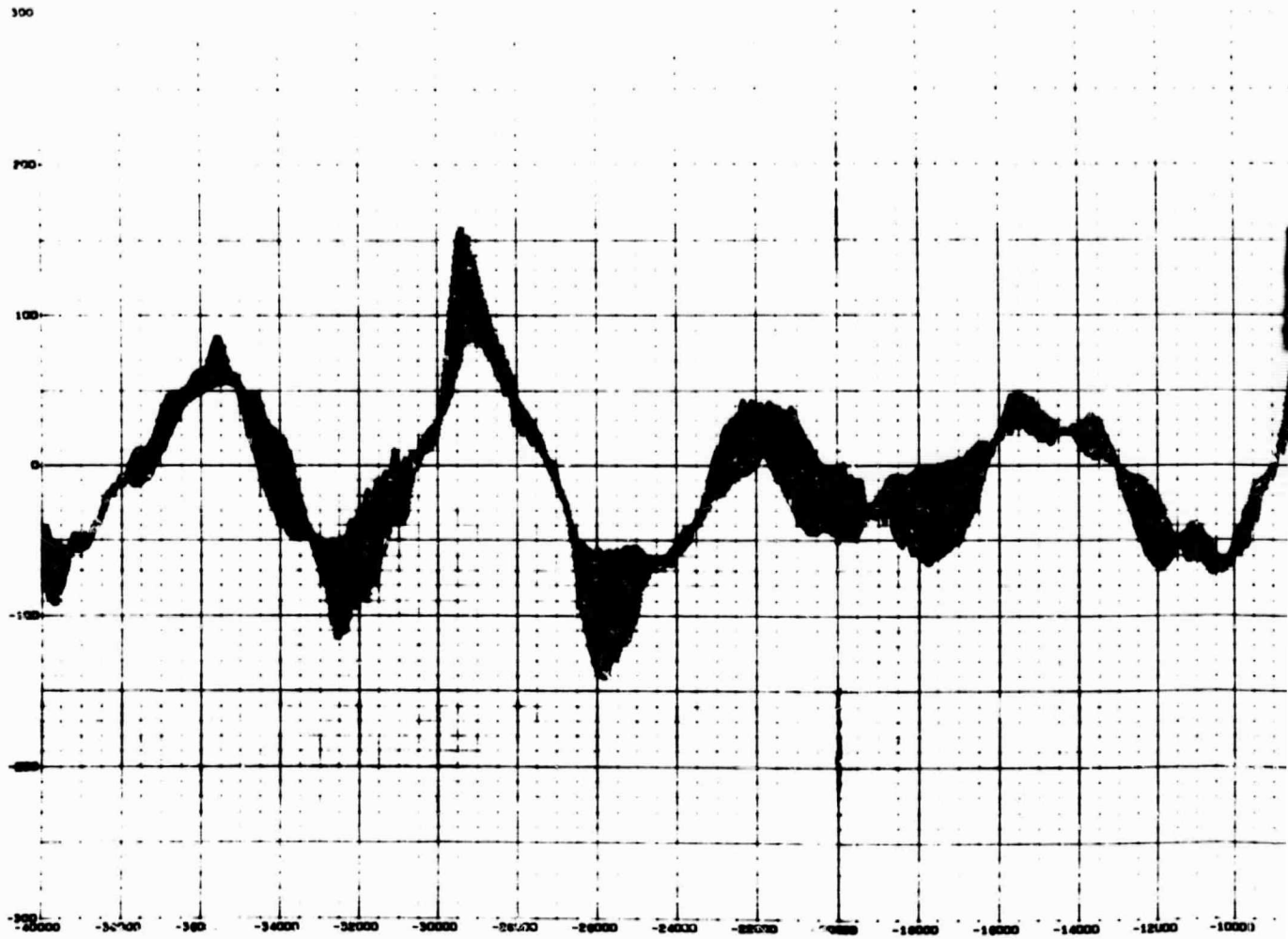


Fig. 5-2a - History of the Error Between the Actual and Estimated Values of \pm SSN (Testing Set)

ESTIMATED AND ACTUAL



FOLDOUT FRAME 1'8

ACTUAL SUNSPOT NUMBER

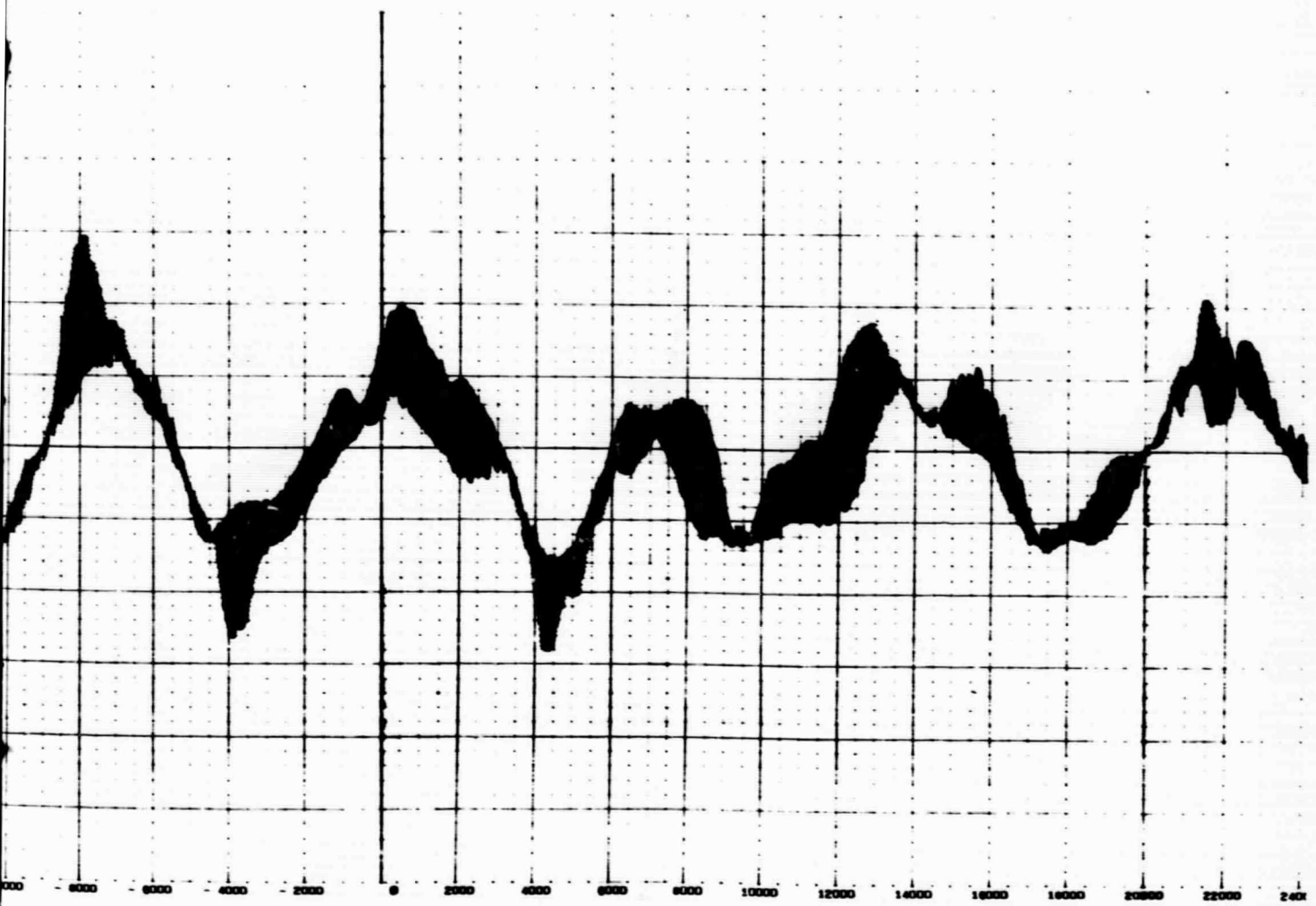


Fig. 5-2b - History of the Error Between the Actual and Estimated Values of +SSN (Training Set)

ESTIMATED AND ACTUAL SUNSPOT NUMBER

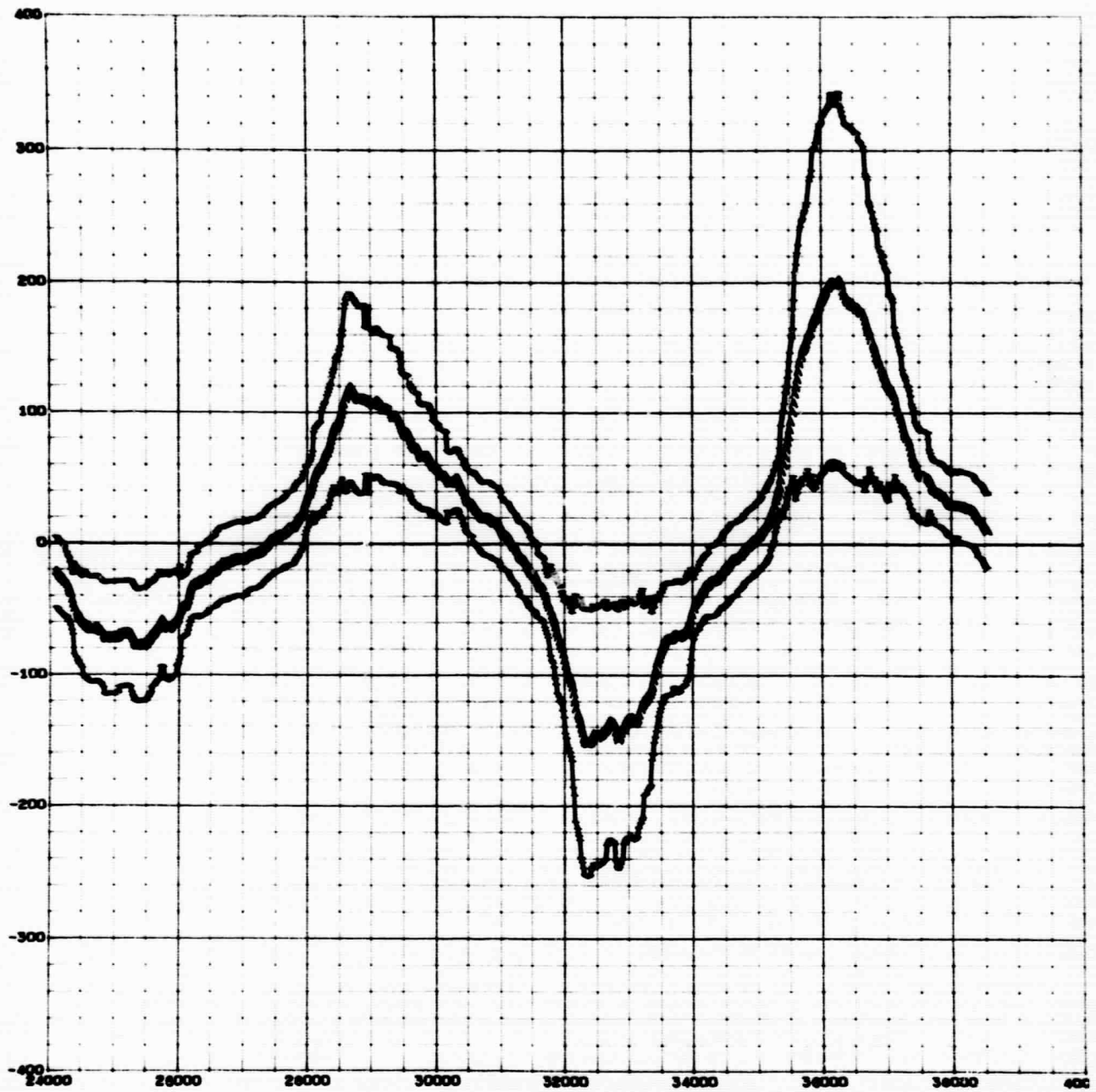
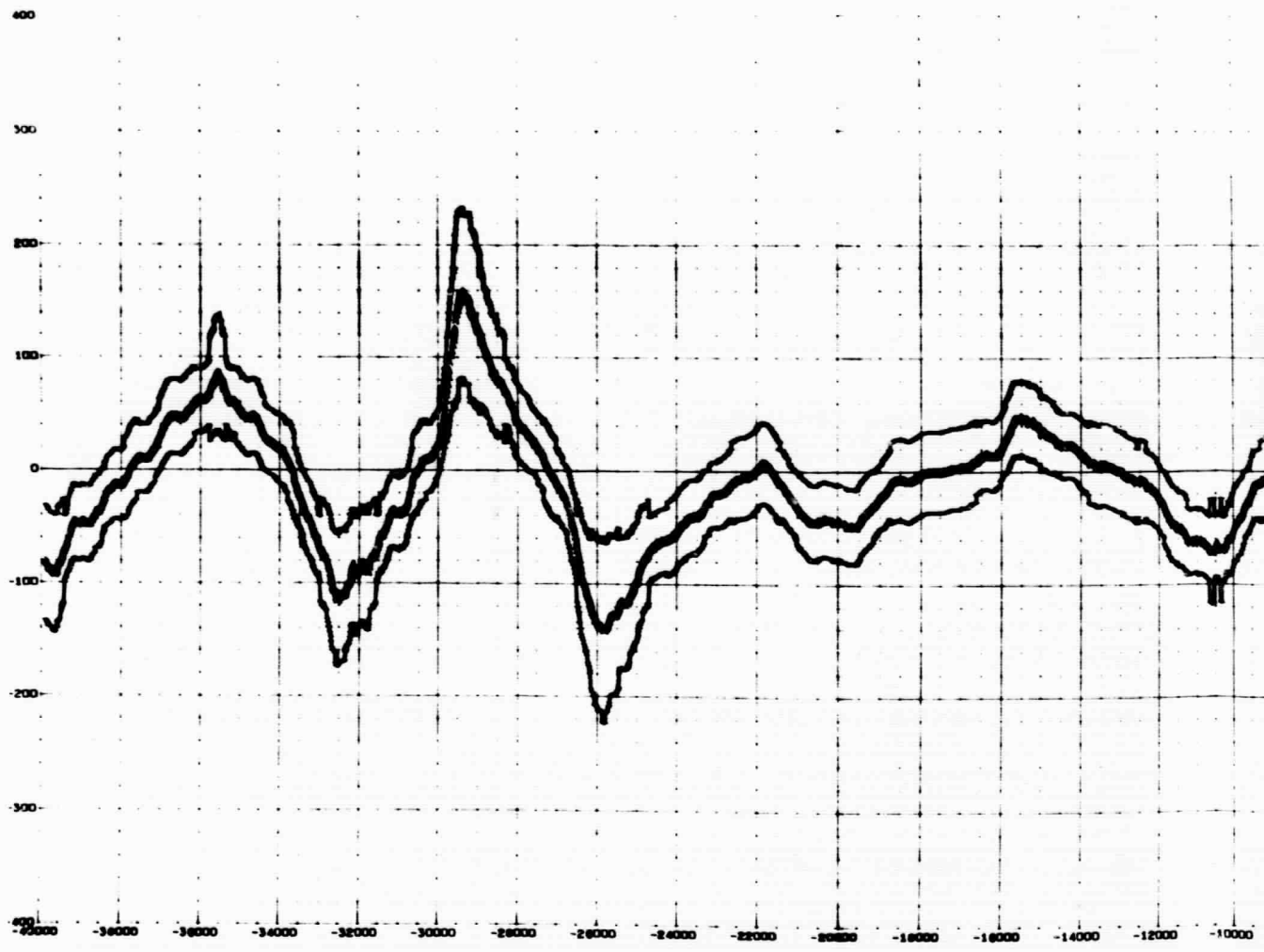


Fig. 5-3a - History of the Actual Values of \pm SSN with RMS Error Band (Testing Set)

ESTIMATED AND ACTUAL



ACTUAL SUNSPOT NUMBER

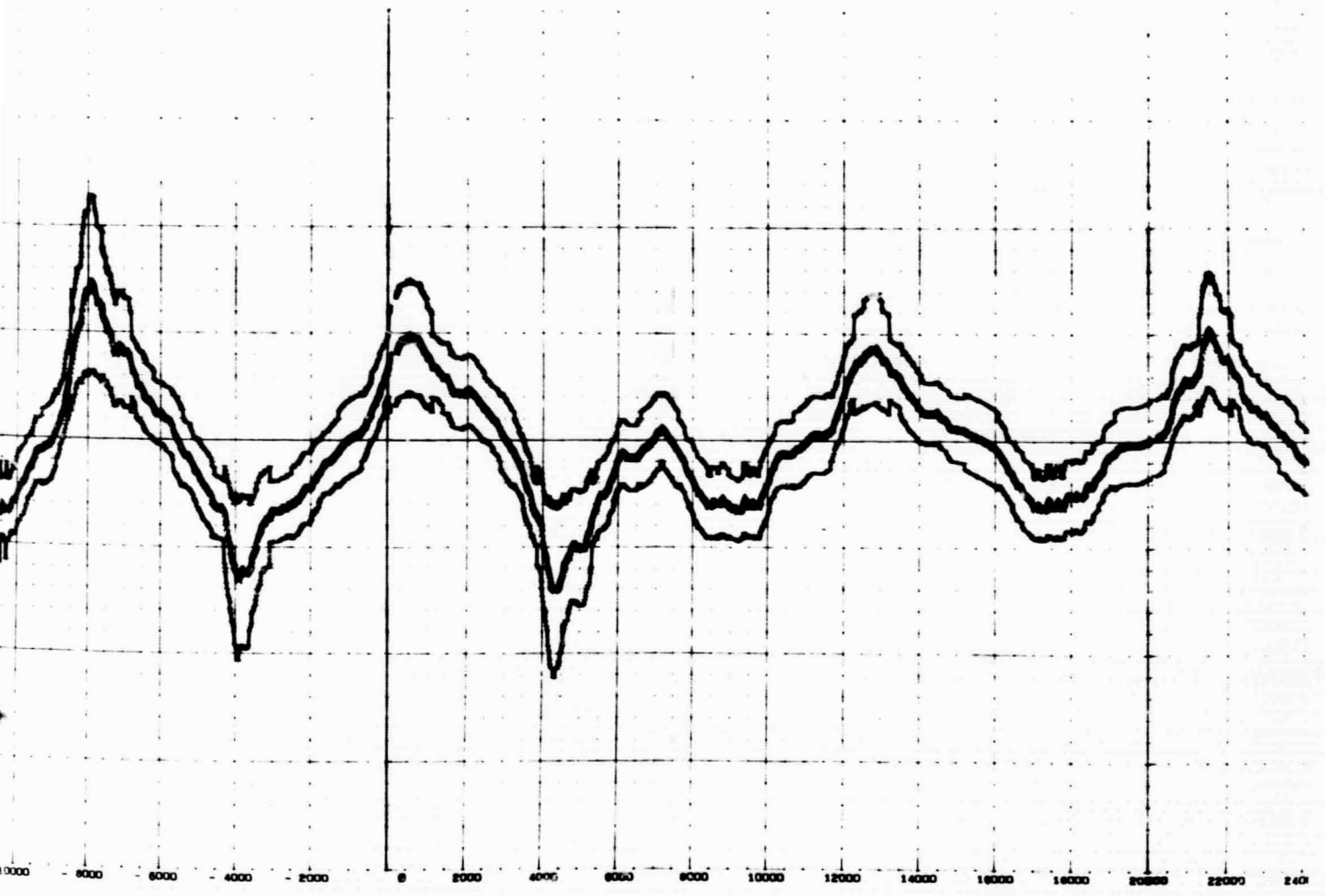


Fig. 5-3b - History of the Actual Values of +SSN with RMS Error Band (Training Set)

ESTIMATED AND ACTUAL SUNSPOT NUMBER

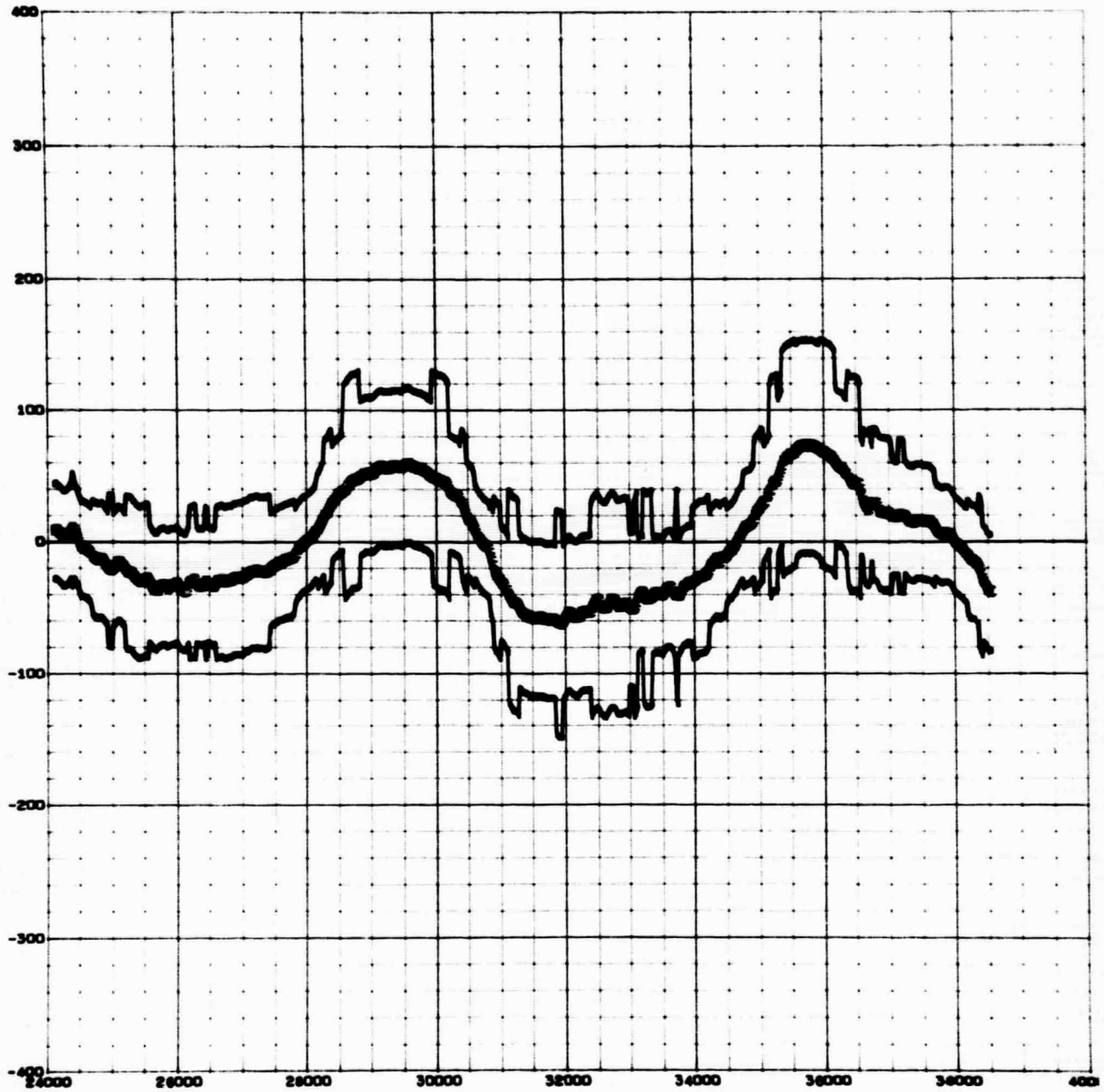
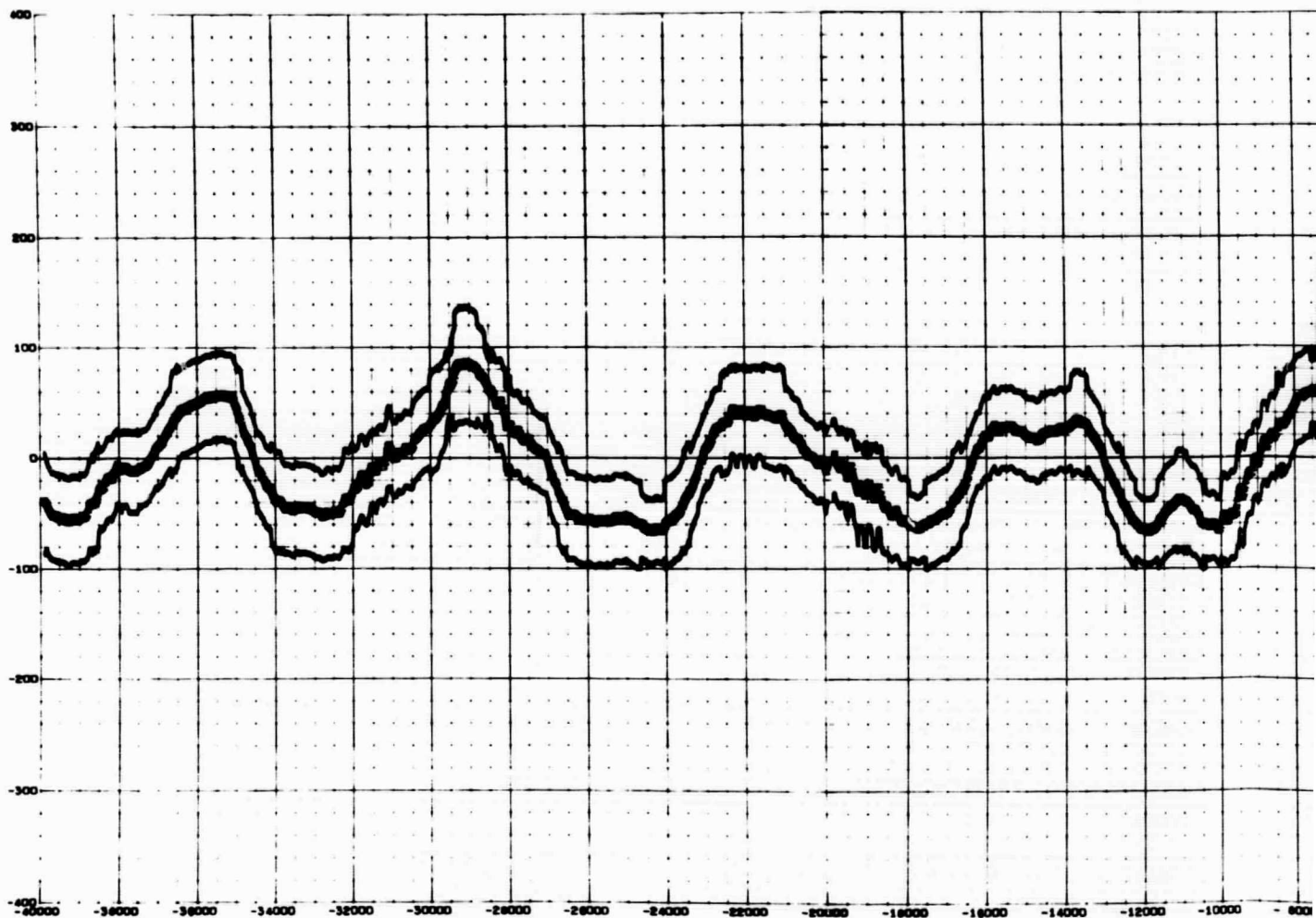


Fig. 5-4a - History of the Estimated Values of \pm SSN with RMS Error Band (Testing Set)

ESTIMATED AND ACTUAL SU



L SUNSPOT NUMBER

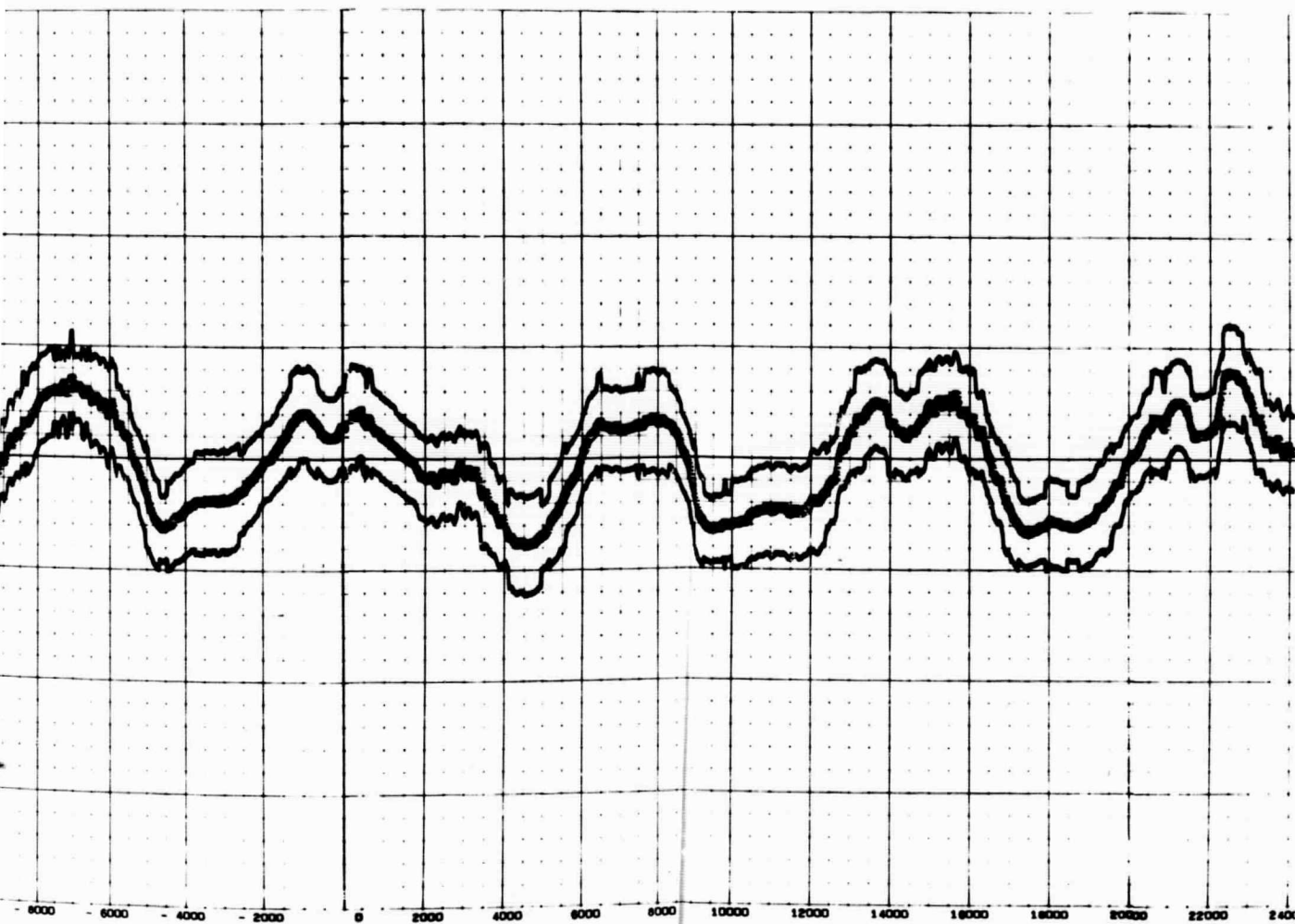


Fig. 5-4b - History of the Estimated Value of
+SSN with RMS Error Band
(Training Set)

ESTIMATED AND ACTUAL SUNSPOT NUMBER

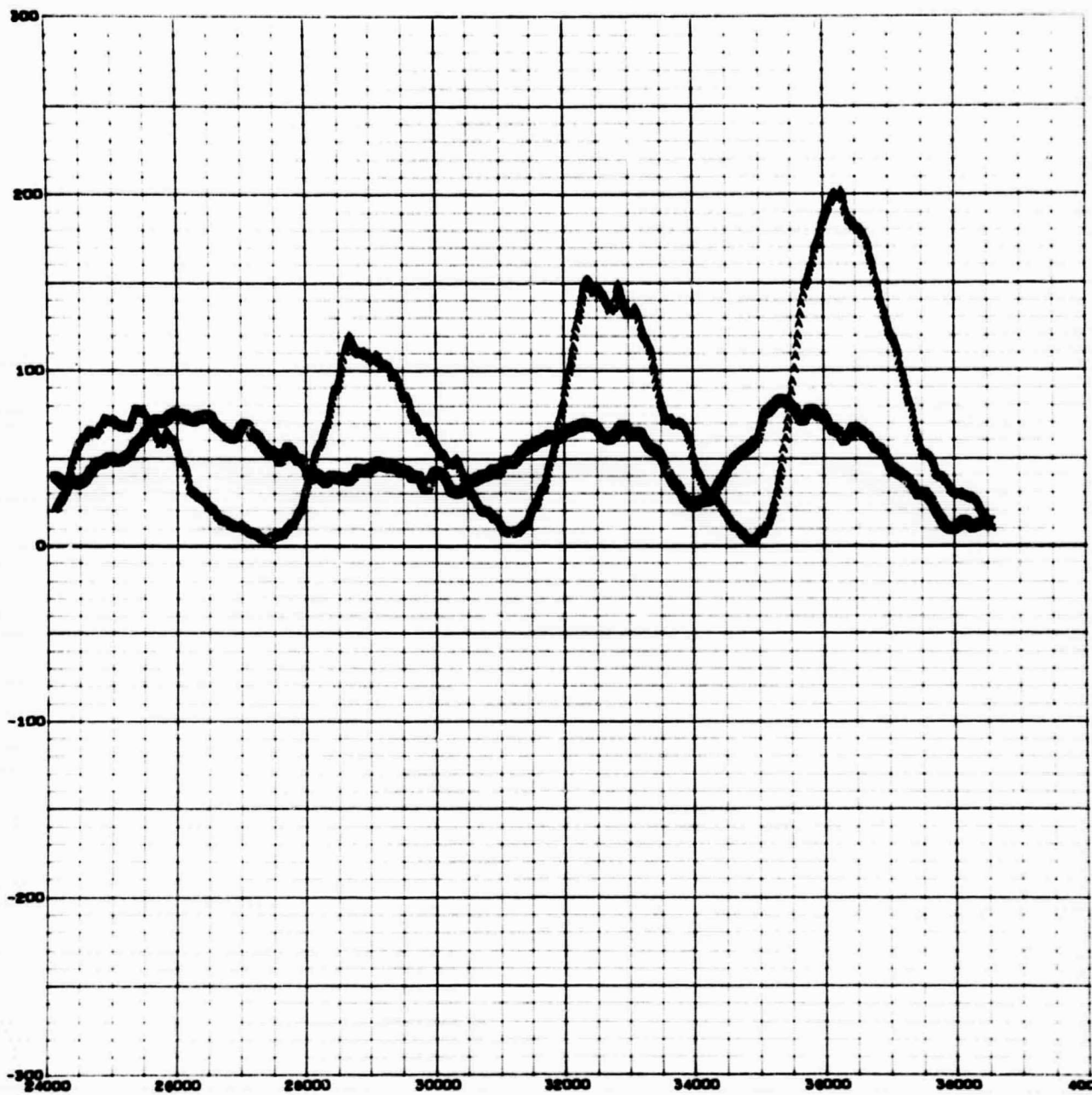
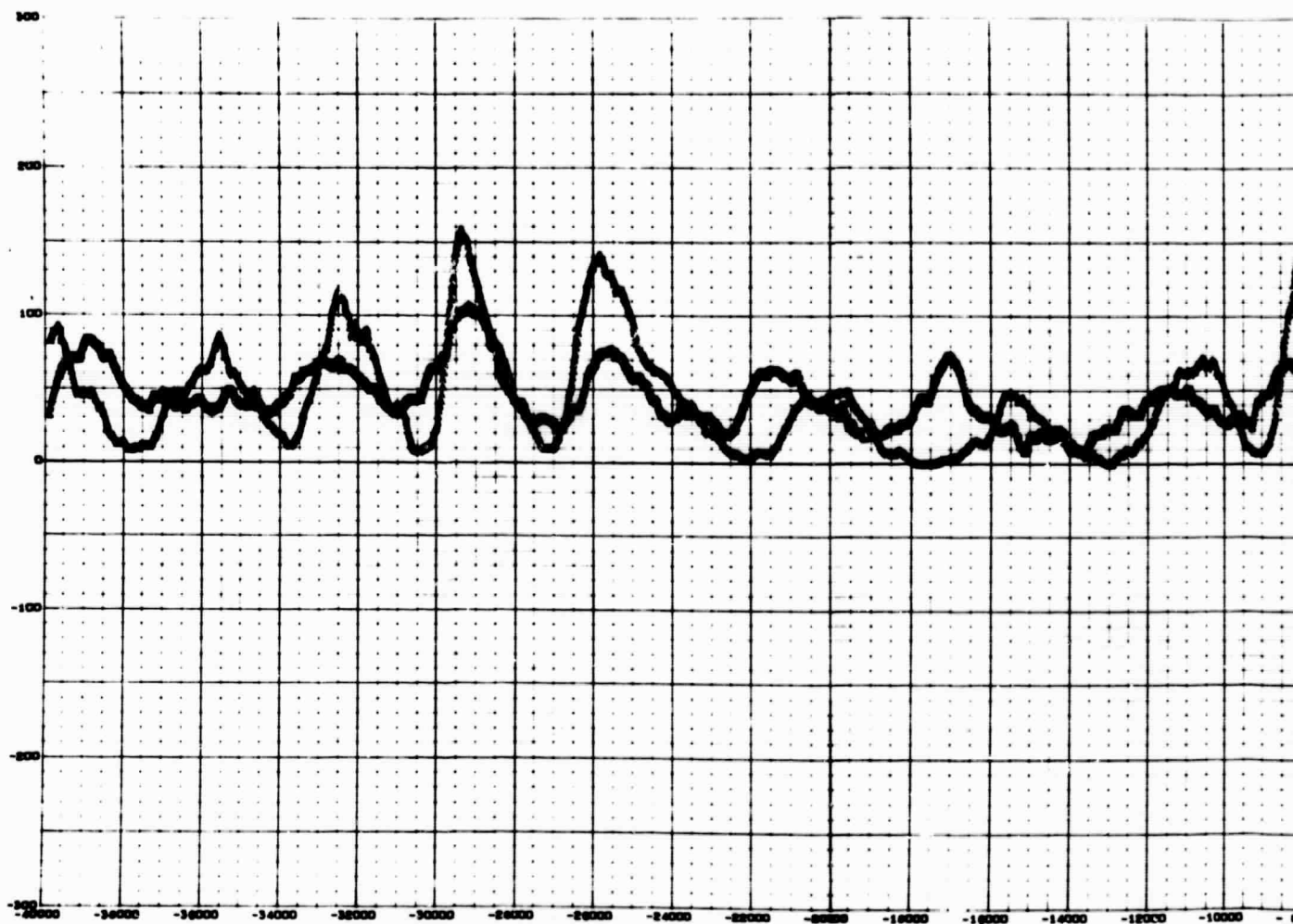


Fig. 5-5a - History of Actual and Estimated Values of |SSN| (Training Set)

ESTIMATED AND ACTUAL



TUAL SUNSPOT NUMBER

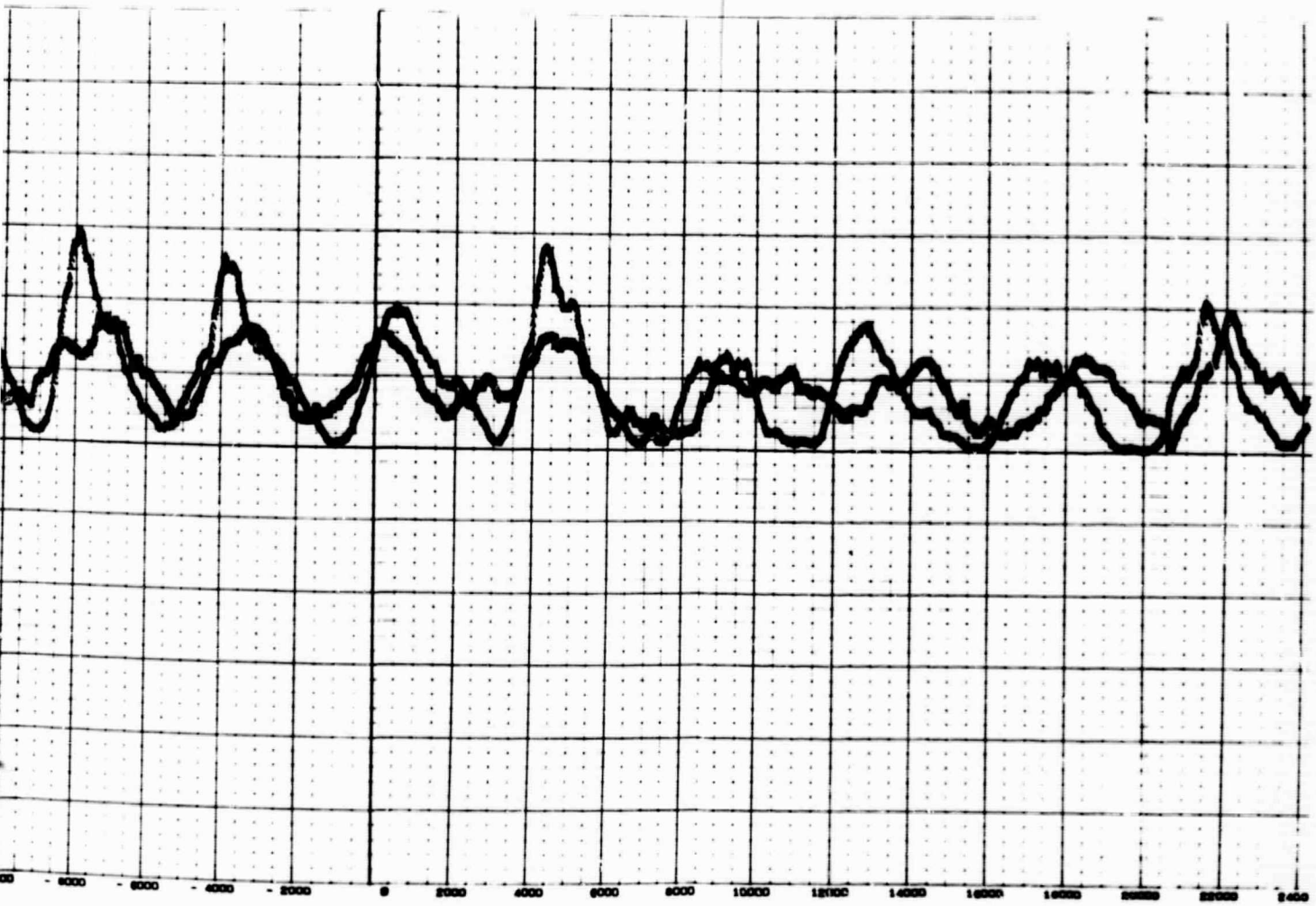


Fig. 5-5b - History of Actual and Estimated Values of |SSN| (Training Set)

ESTIMATED AND ACTUAL SUNSPOT NUMBER

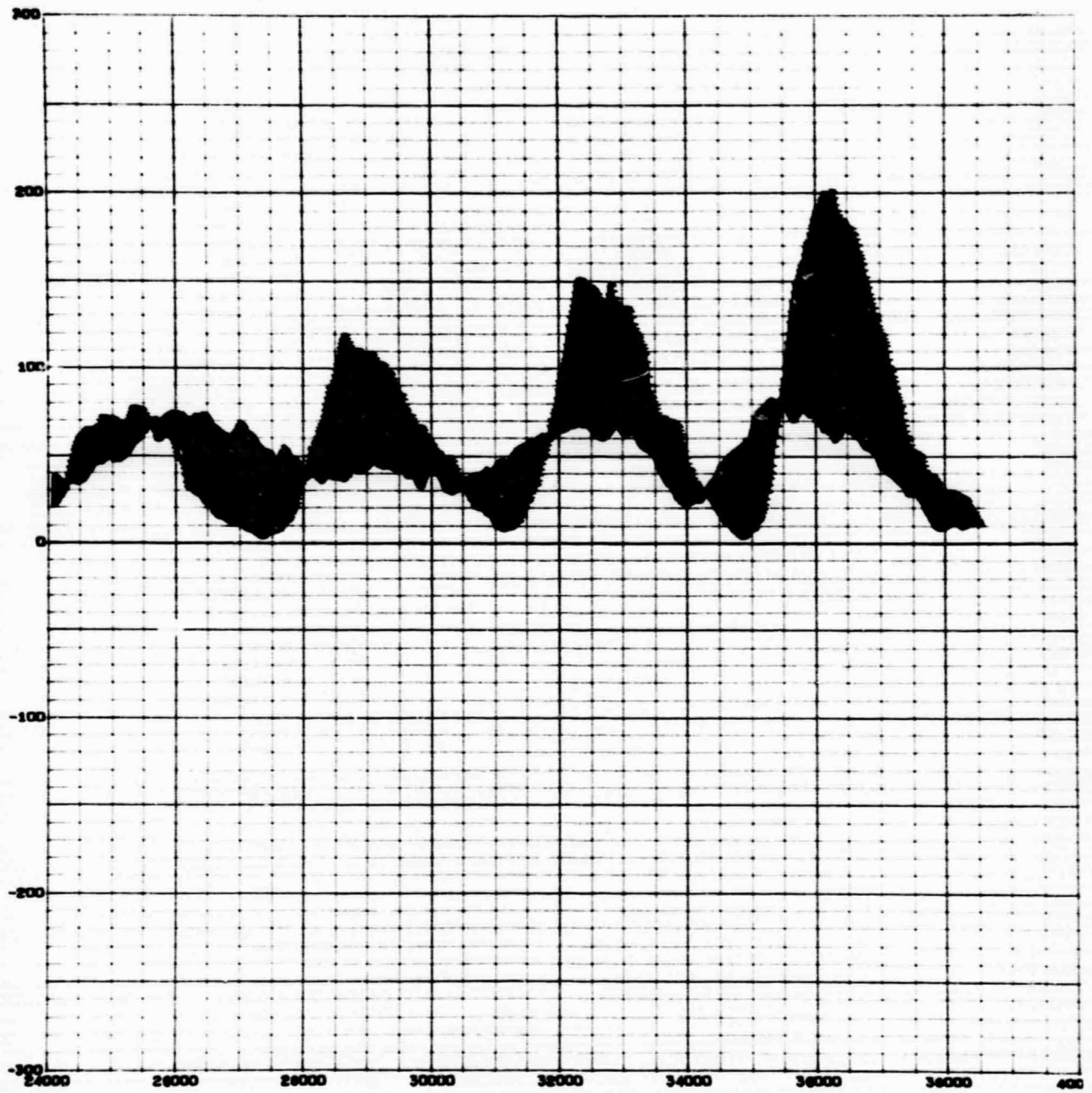
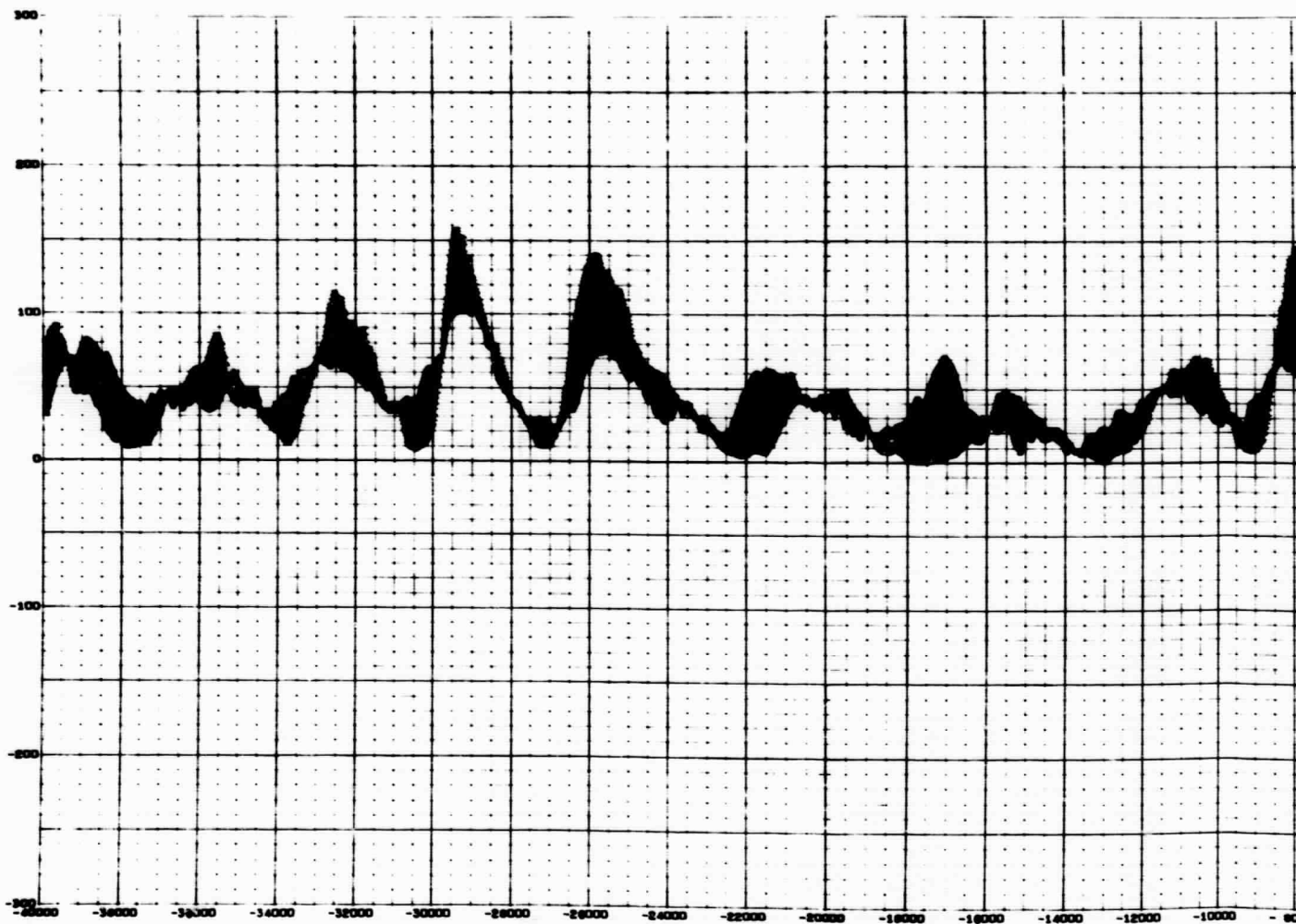


Fig. 5-6a - History of the Error Between the Actual and Estimated Values of |SSN| (Training Set)

ESTIMATED AND ACTUAL S



TUAL SUNSPOT NUMBER

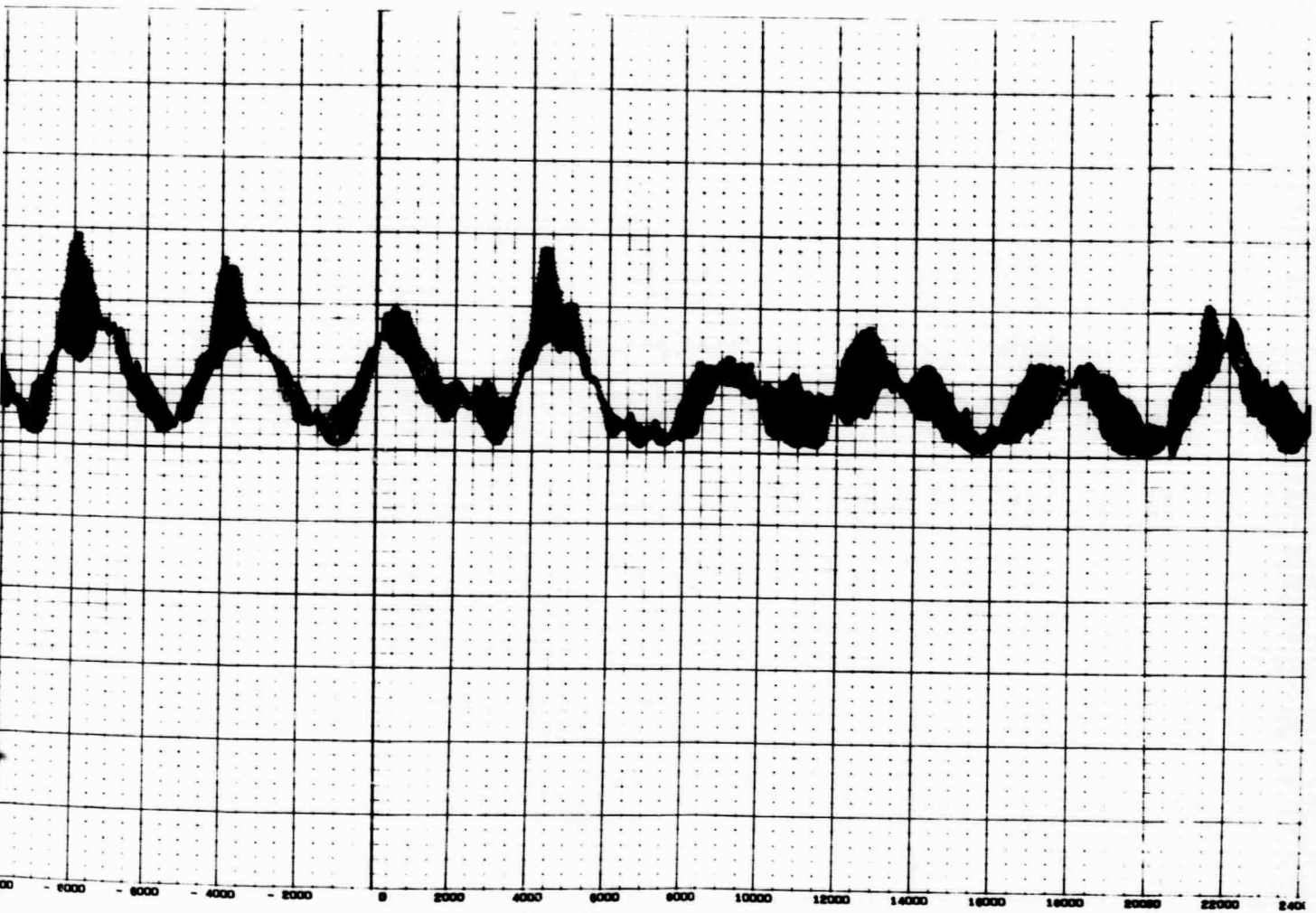


Fig. 5-6b - History of the Error Between the Actual and Estimated Values of |SSN| (Training Set)

PRECEDING PAGE BLANK NOT FILMED.

ESTIMATED AND ACTUAL SUNSPOT NUMBER

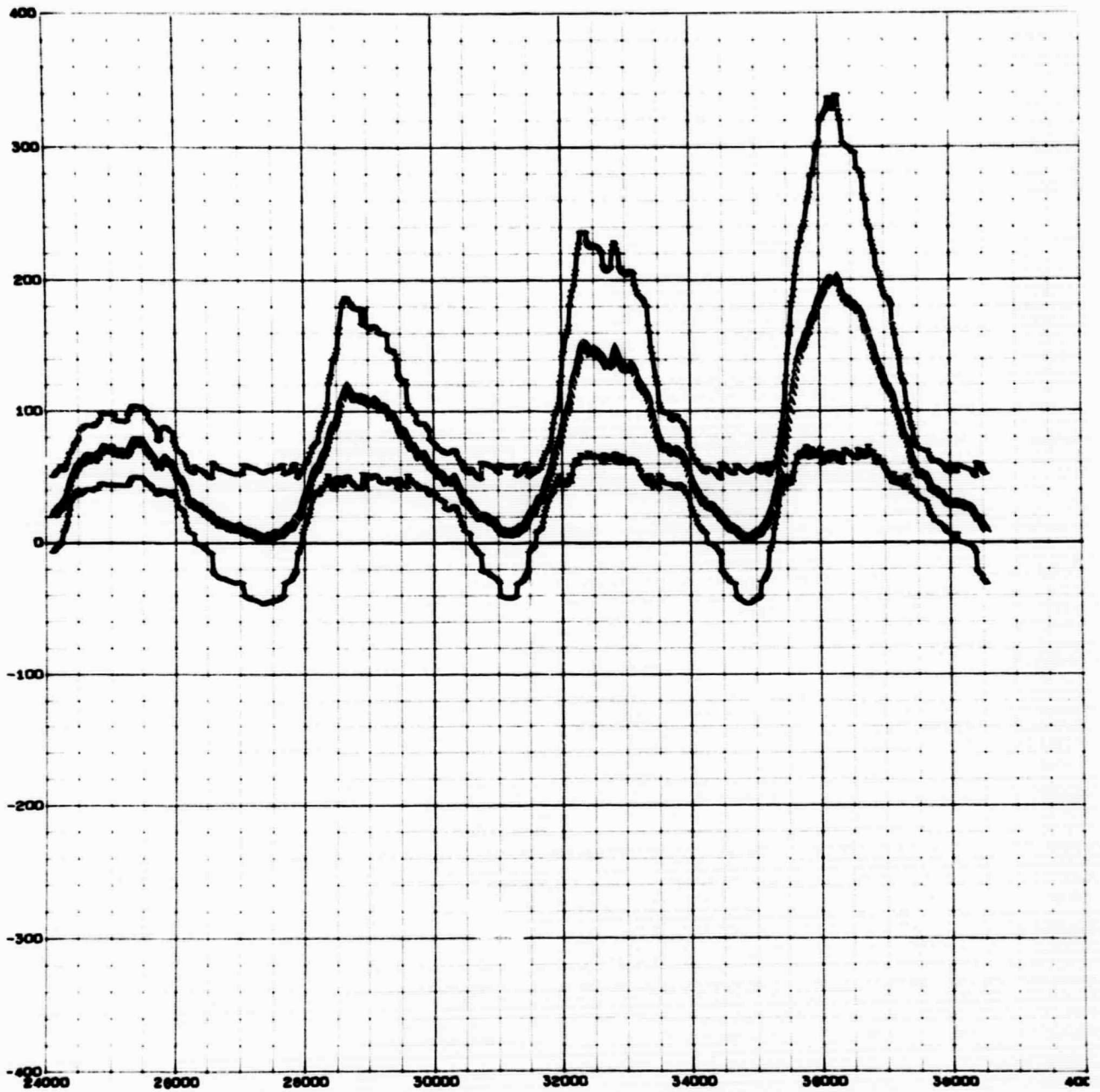
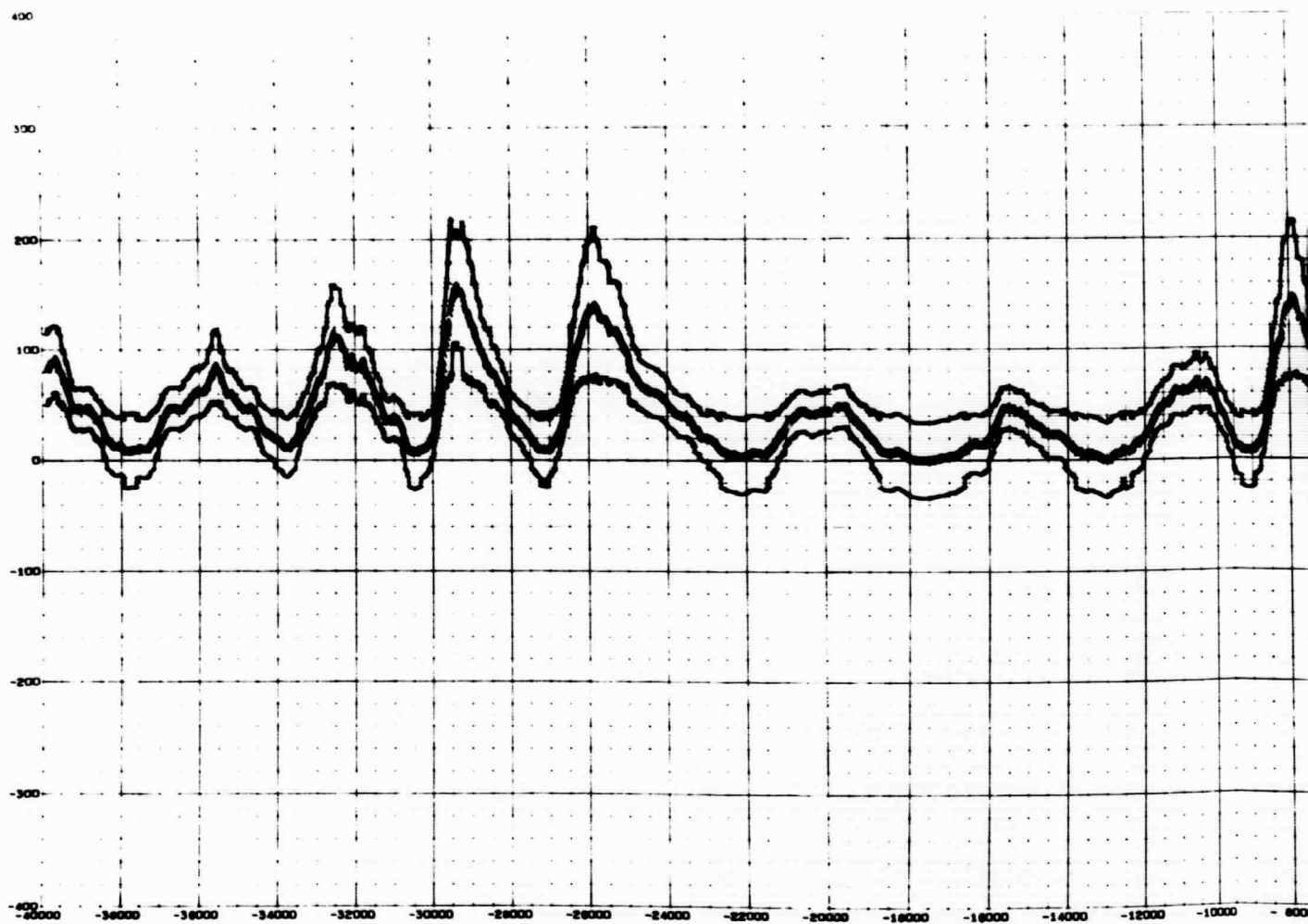


Fig. 5-7a - History of the Actual Values of |SSN| with RMS Error Band (Training Set)

ESTIMATED AND ACTUAL SU



ACTUAL SUNSPOT NUMBER

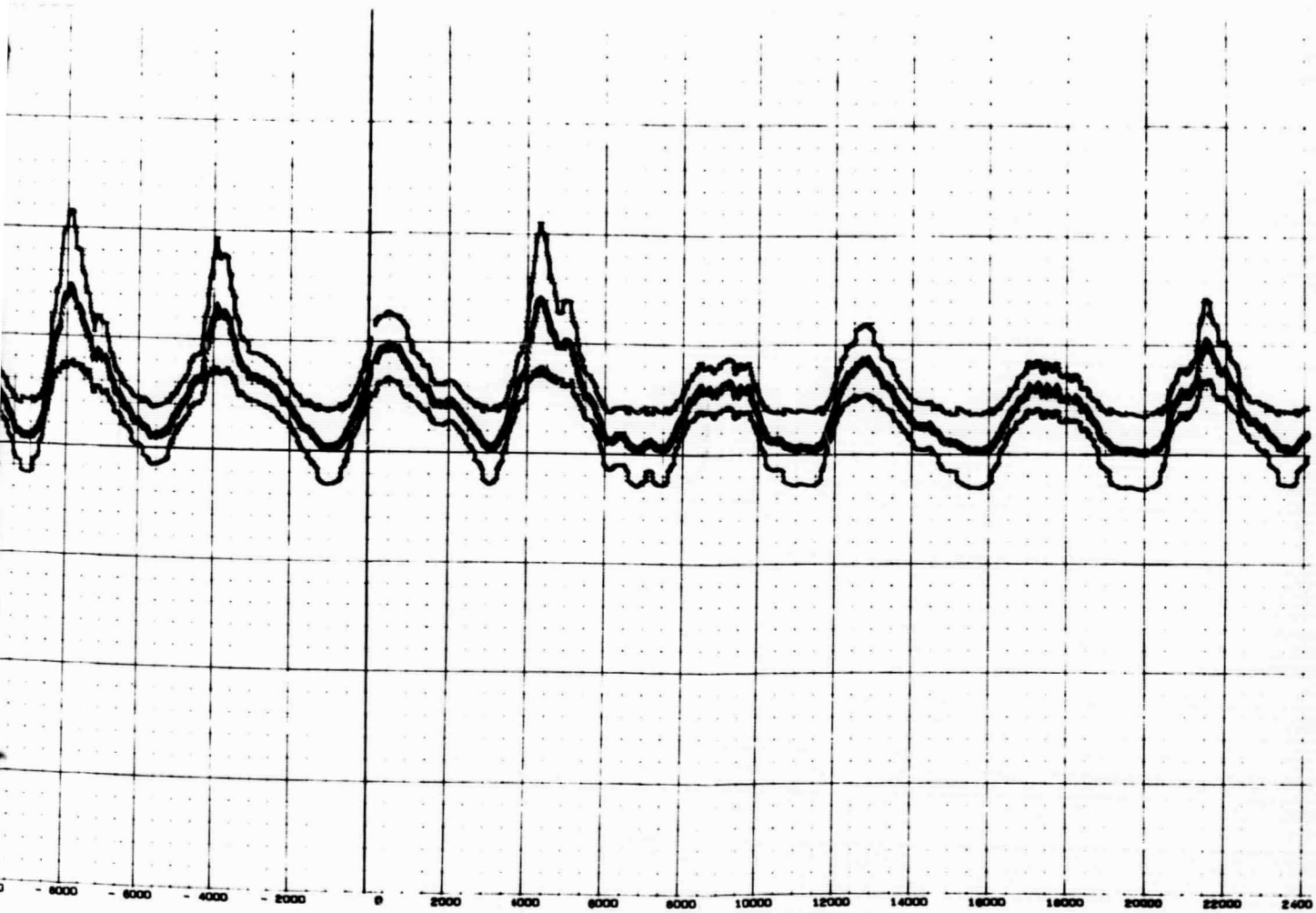


Fig. 5-7b - History of the Actual Values of
|SSN| with RMS Error Band
(Training Set)

ESTIMATED AND ACTUAL SUNSPOT NUMBER

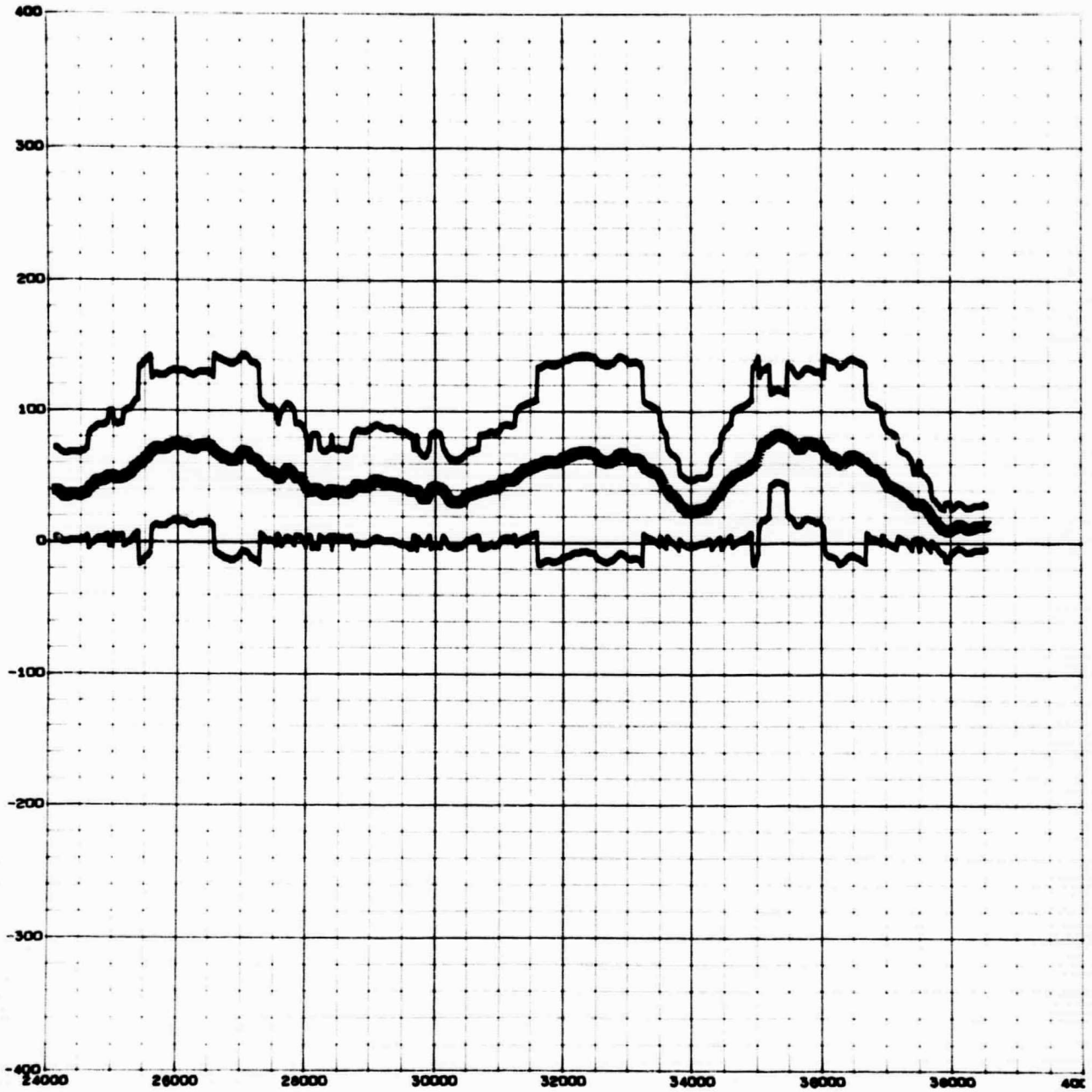
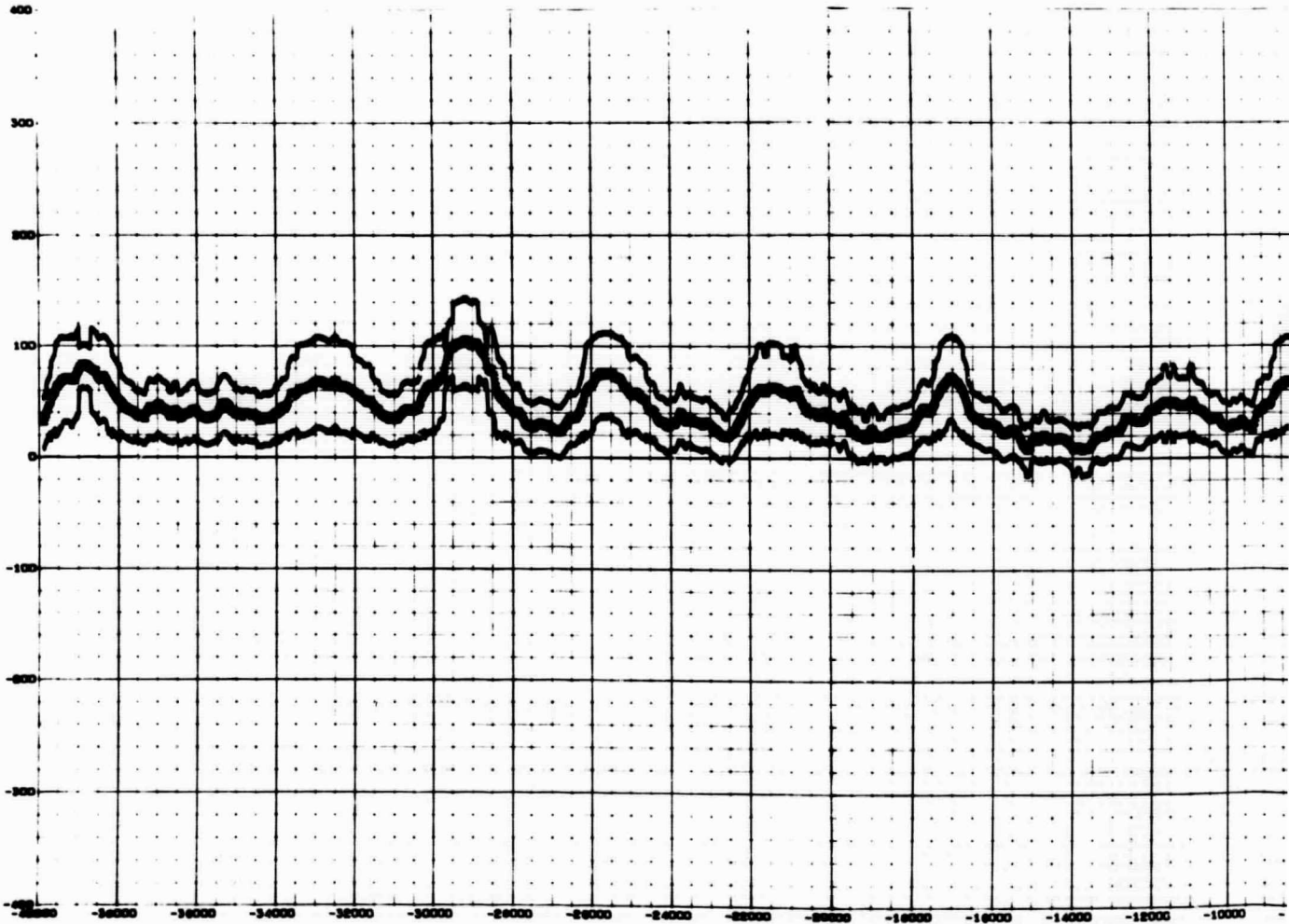


Fig. 5-8a - History of the Estimated Values of $|SSN|$ with RMS Error Band (Testing Set)

Page 40 Blank

ESTIMATED AND ACTUAL



FOLDOUT FRAME 42

ACTUAL SUNSPOT NUMBER

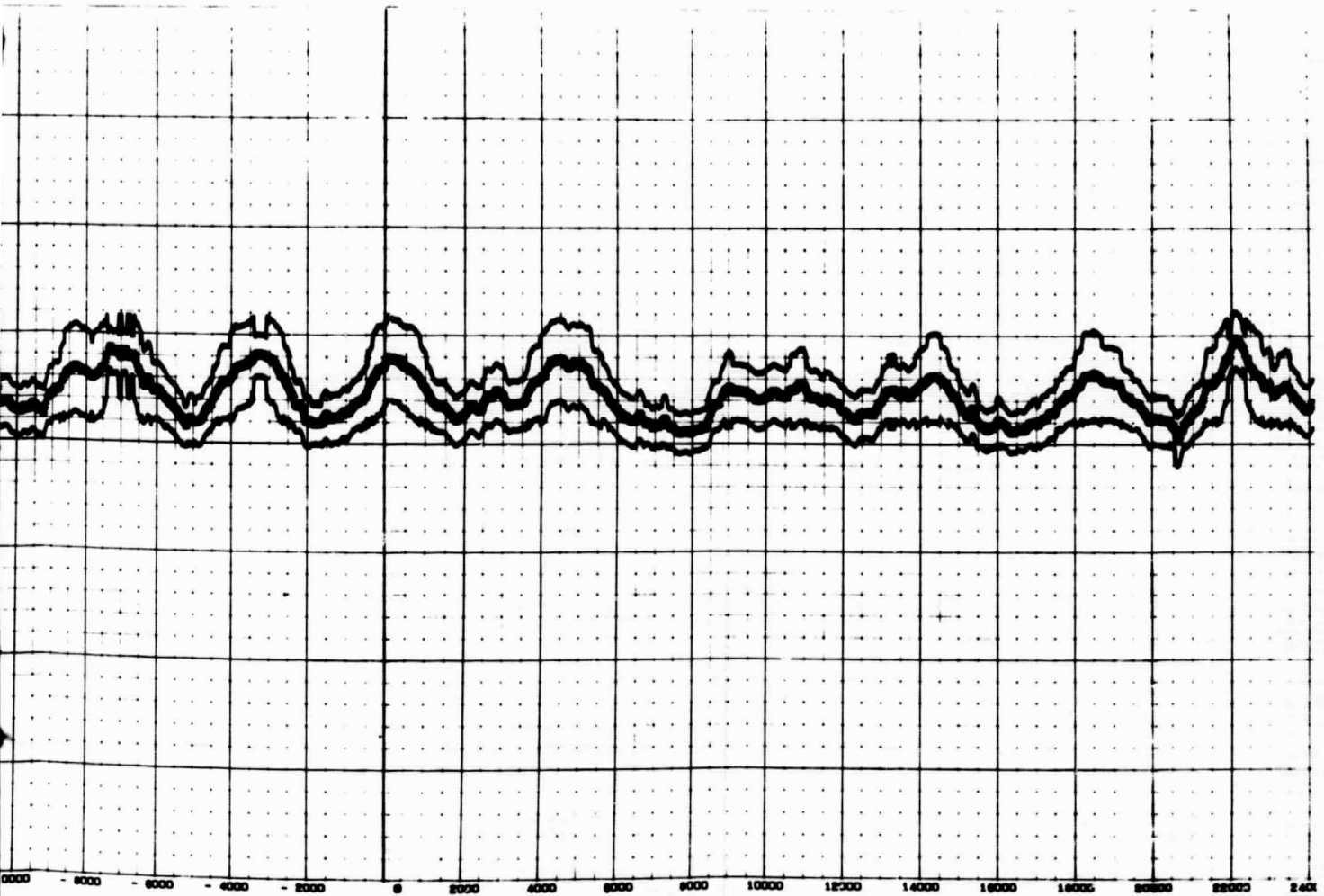


Fig. 5-8b - History of the Estimated Values
of $|SSN|$ with RMS Error Band
(Training Set)

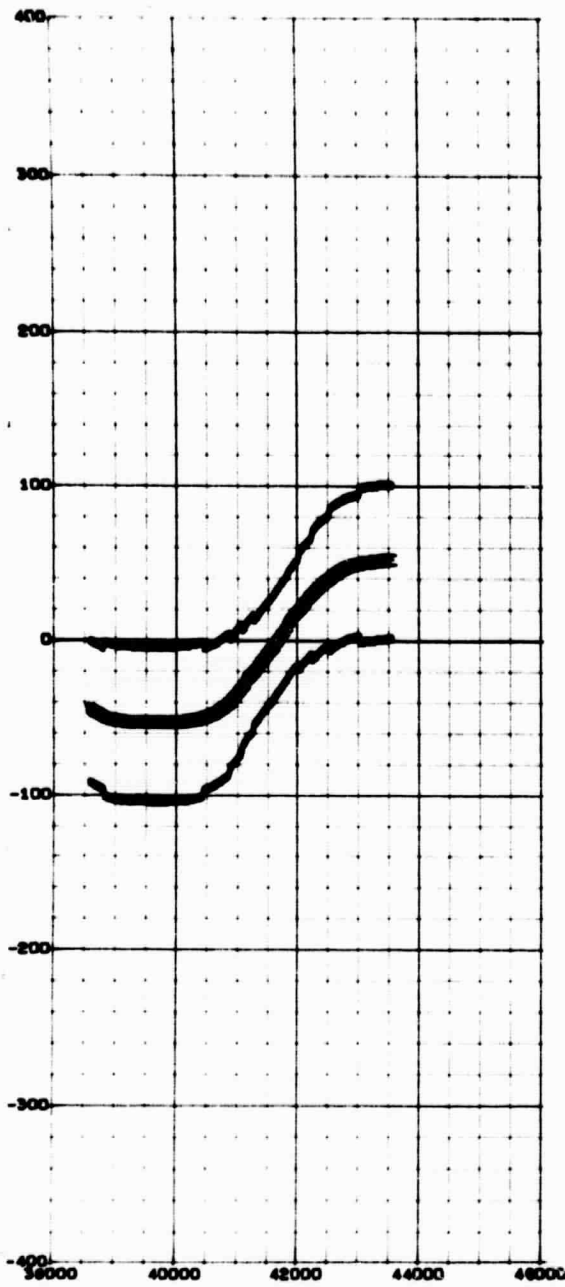


Fig. 5-9 - Future Estimates of +SSN Using Two Predictors

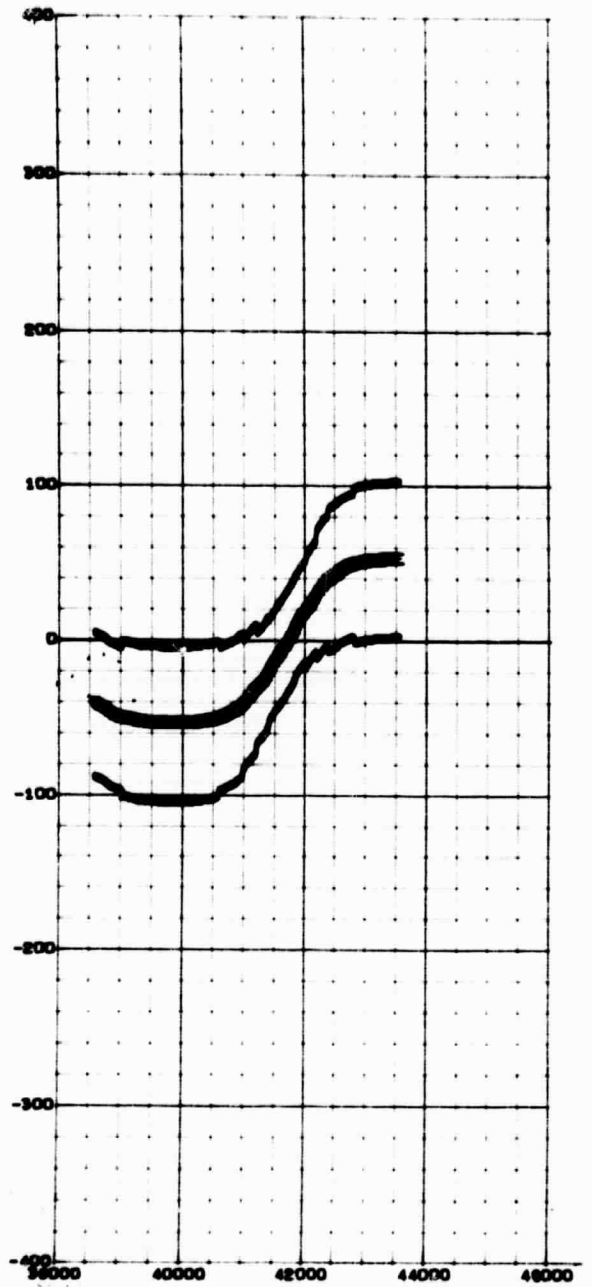


Fig. 5-10 - Future Estimates of +SSN Using Three Predictors

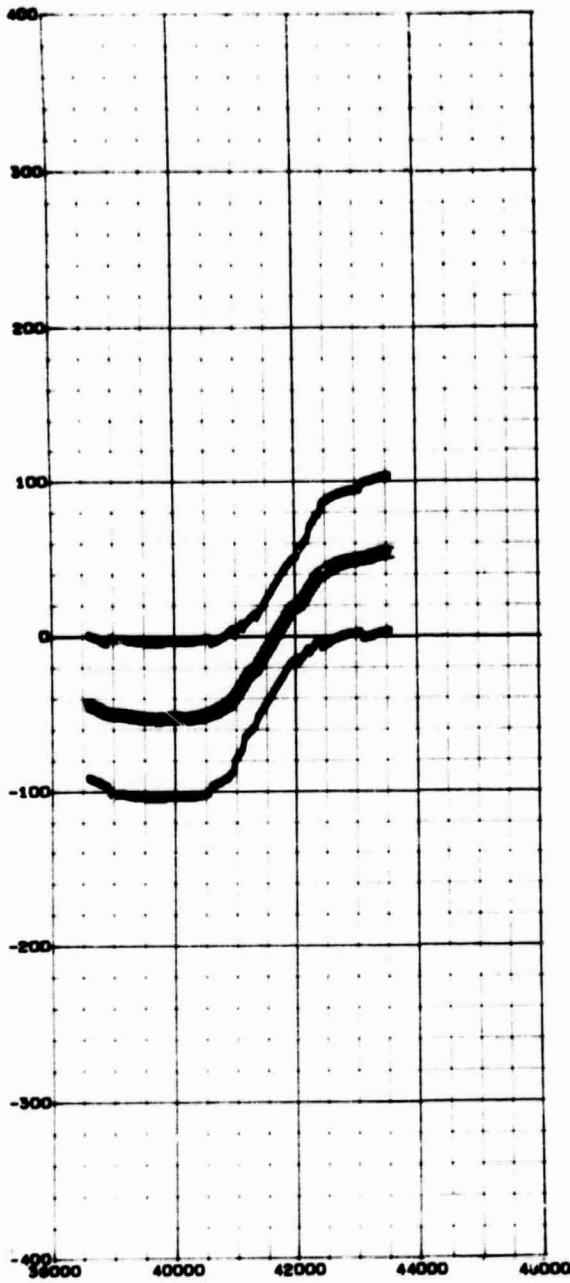


Fig. 5-11 - Future Estimates of +SSN Using Four Predictors

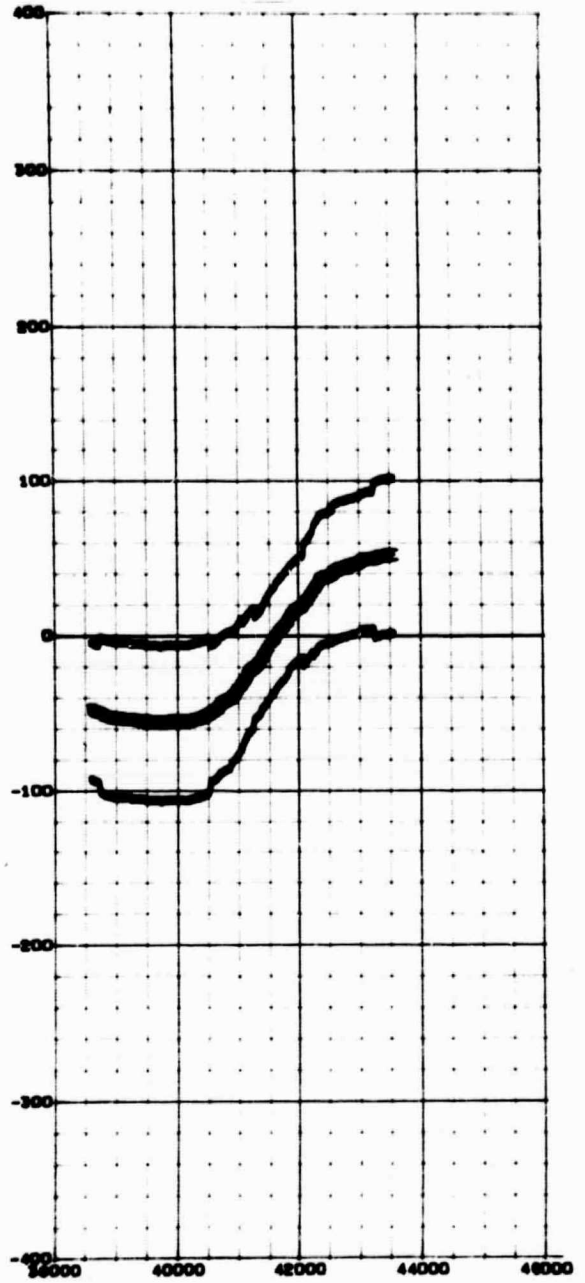


Fig. 5-12 - Future Estimates of +SSN Using Five Predictors

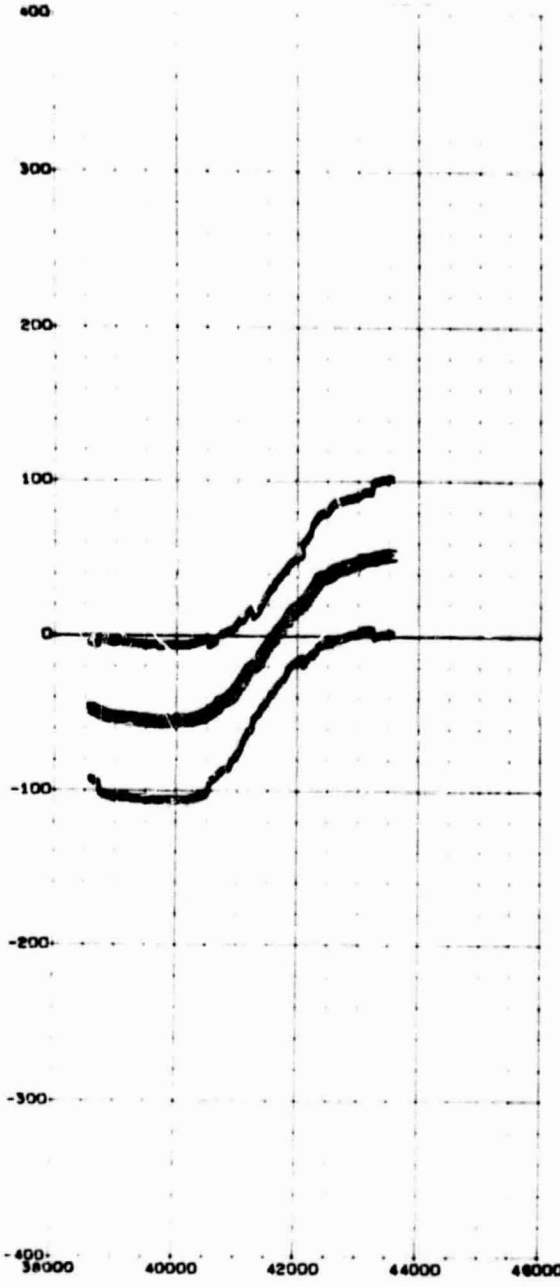


Fig. 5-13 - Future Estimates of +SSN Using Six Predictors

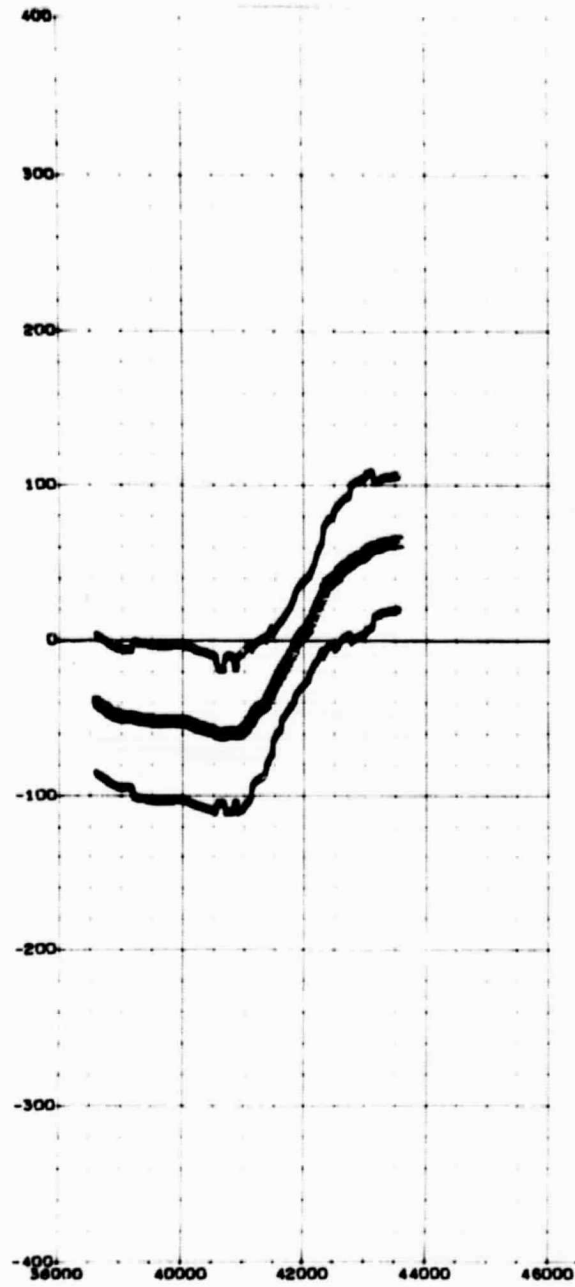


Fig. 5-14 - Future Estimates of +SSN Using Seven Predictors

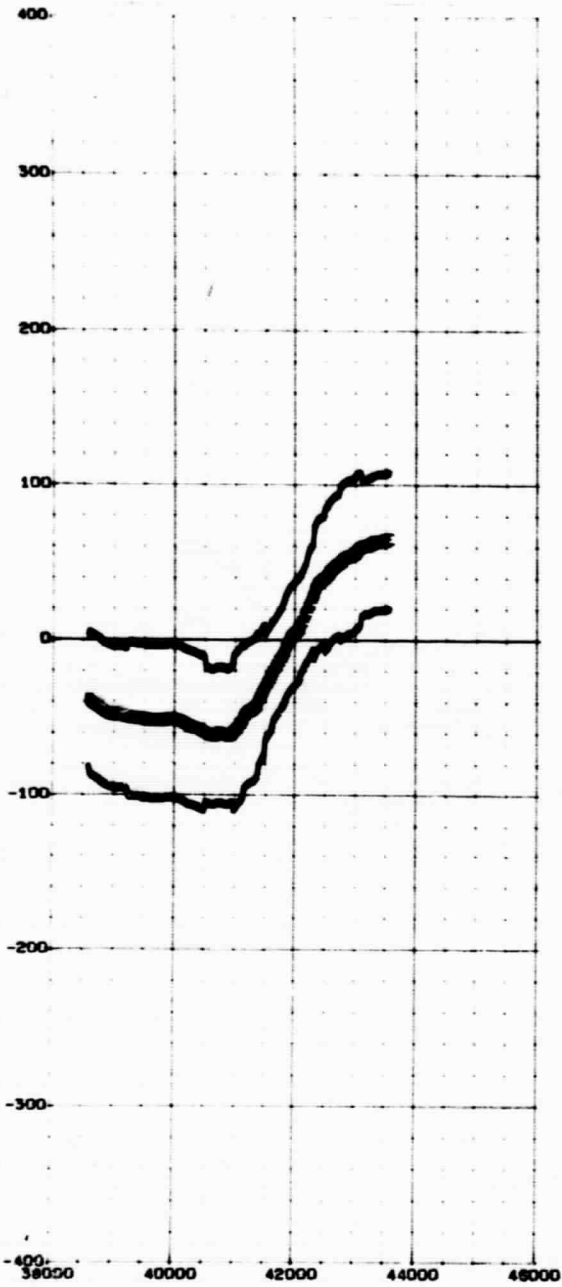


Fig. 5-15 - Future Estimates of +SSN Using Eight Predictors

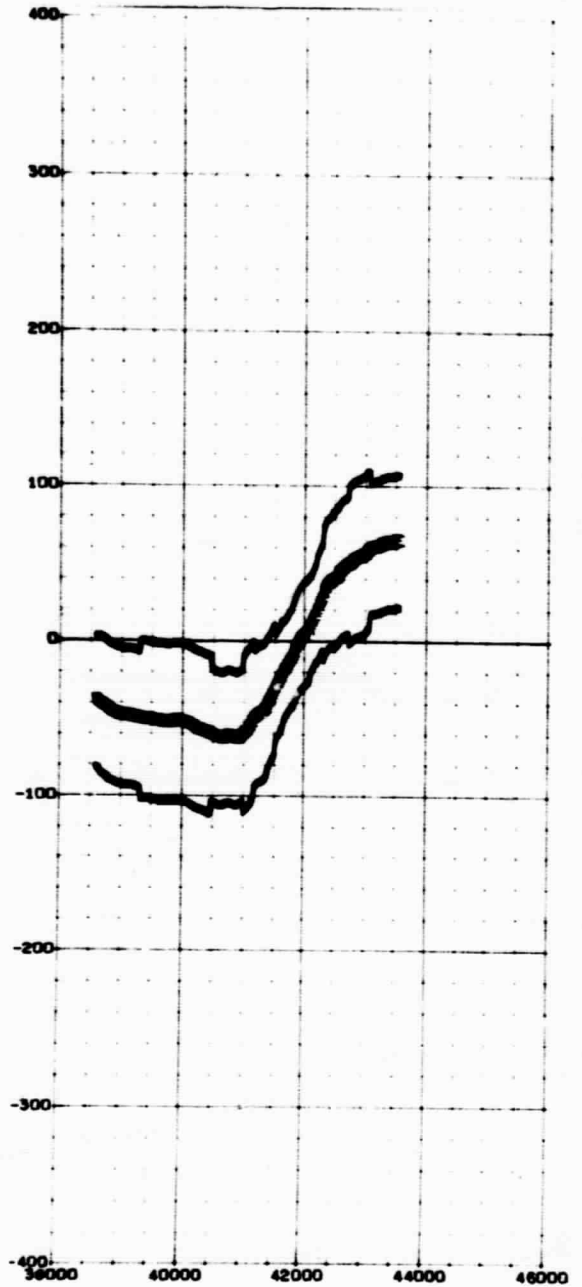


Fig. 5-16 - Future Estimates of +SSN Using Nine Predictors

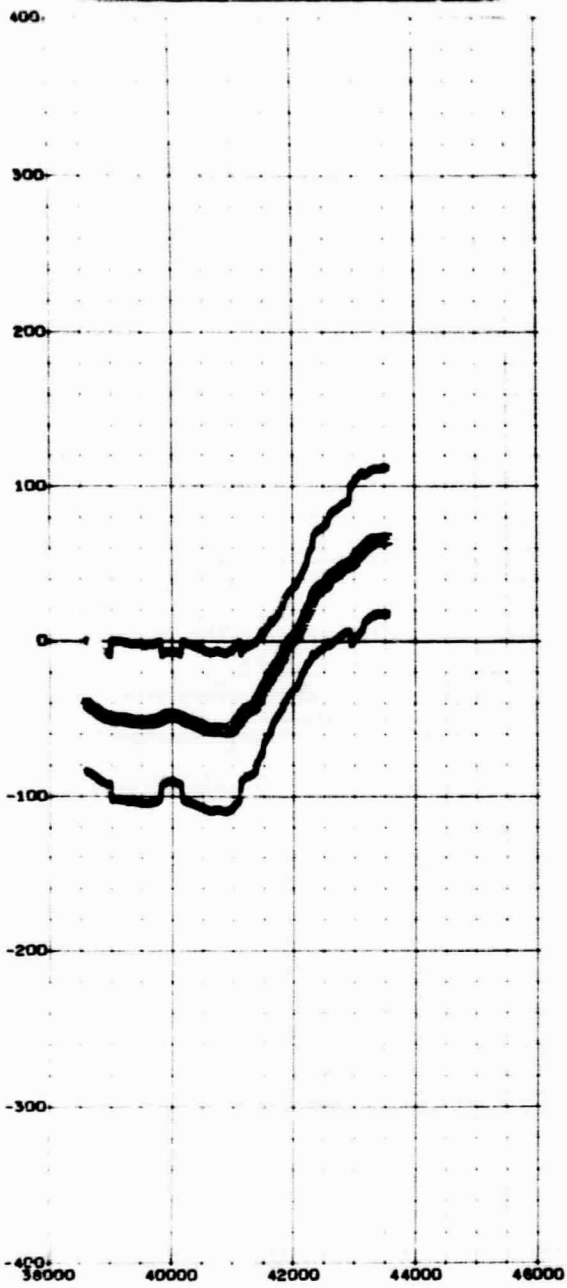


Fig. 5-17 - Future Estimates of +SSN Using 10 Predictors

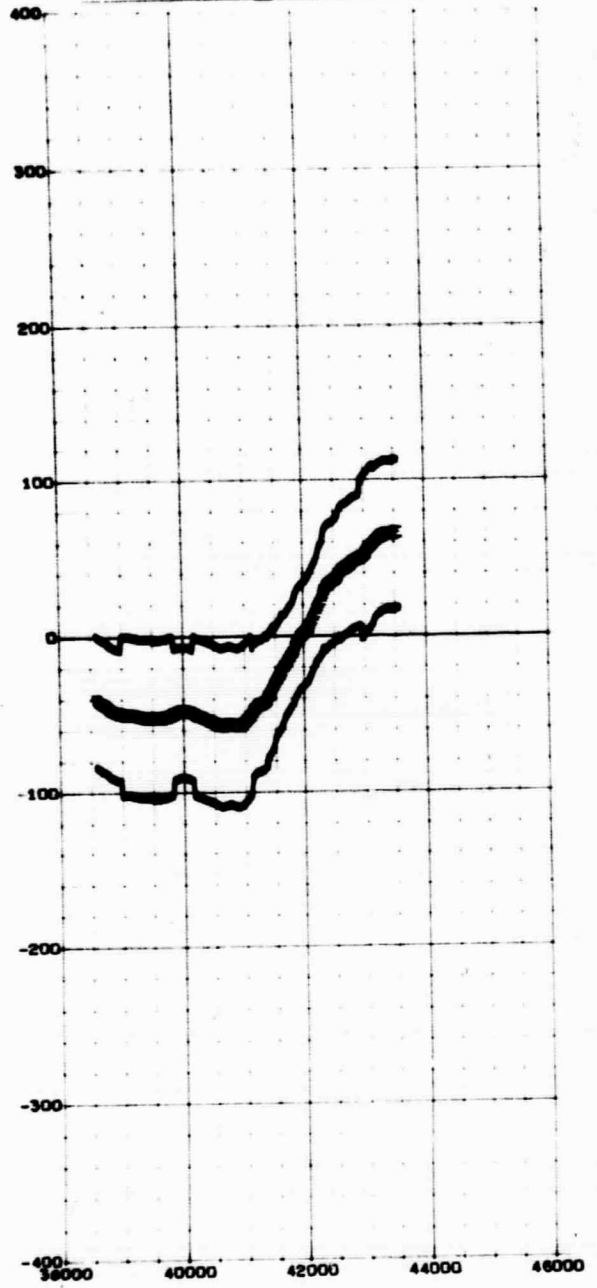


Fig. 5-18 - Future Estimates of +SSN Using 11 Predictors

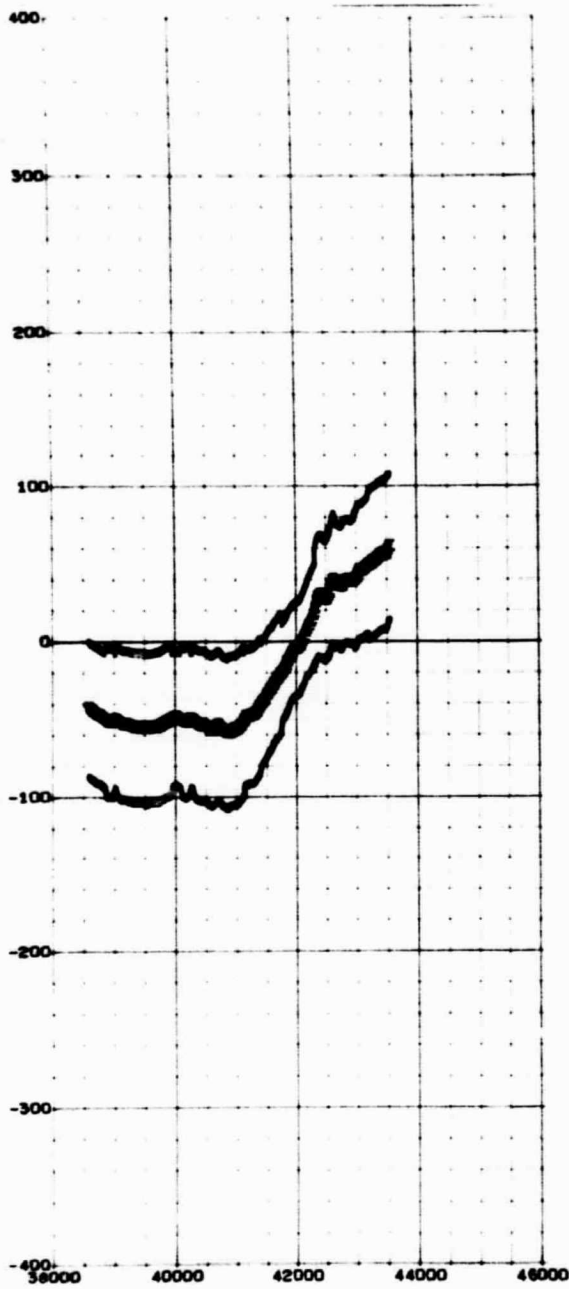


Fig. 5-19 - Future Estimates of +SSN Using 12 Predictors

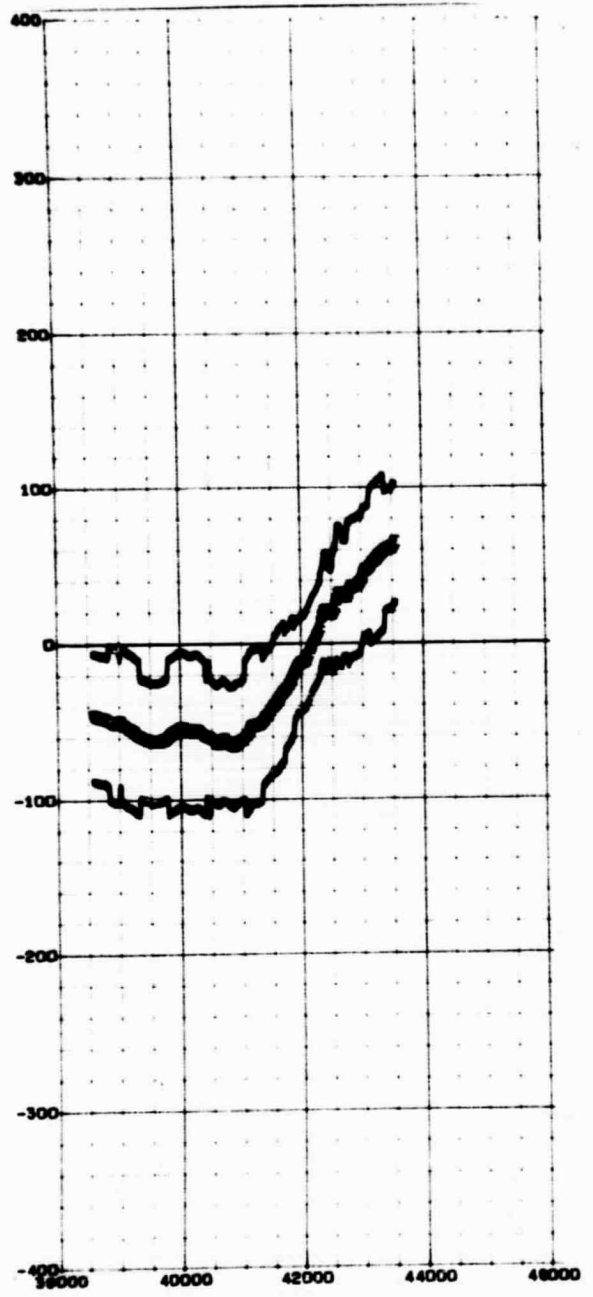


Fig. 5-20 - Future Estimates of +SSN Using 13 Predictors

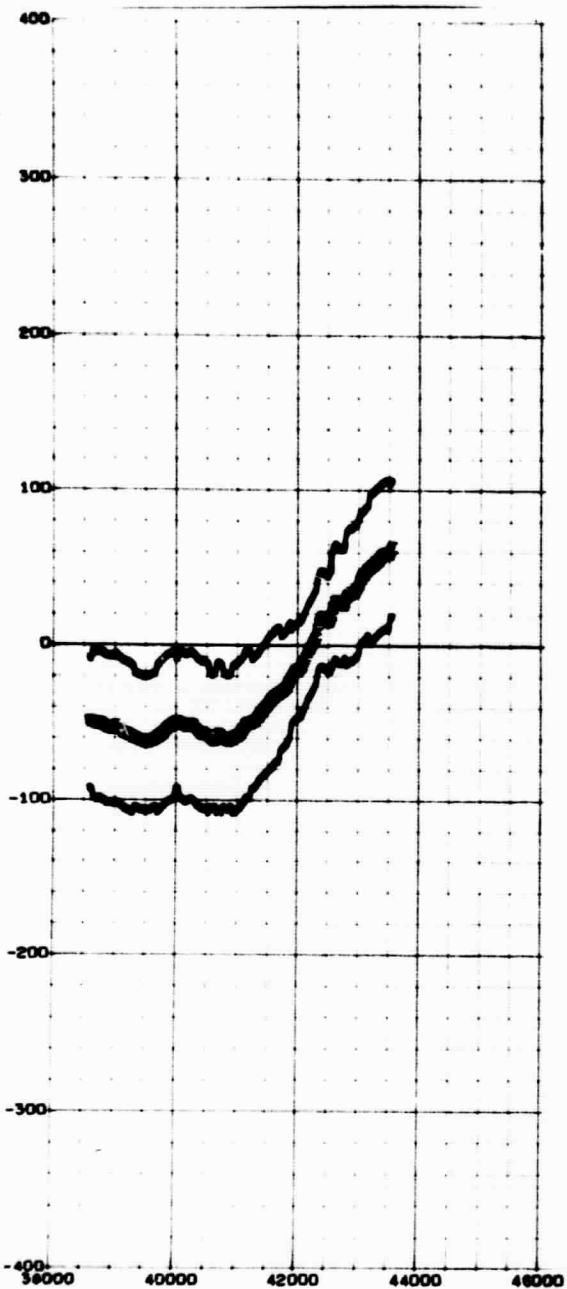


Fig. 5-21 - Future Estimates of +SSN Using 14 Predictors

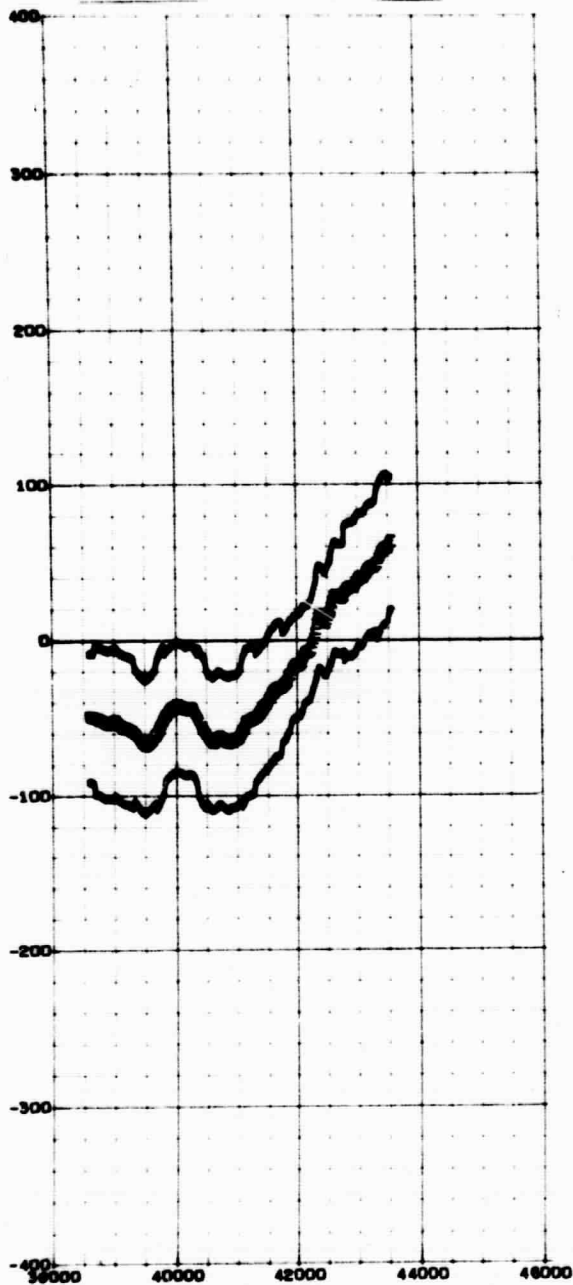


Fig. 5-22 - Future Estimates of +SSN Using 15 Predictors

Section 6 CONCLUSIONS

The basic goal of this study was to develop an improved method of forecasting solar activity. A number of eminent scientists have suggested that some relationship exists between solar activity and the interactions between the planets and sun. Neither the basic cause of solar activity nor its specific relationship to planetary interactions have yet been determined, although a number of proposed relationships have been provided. Objective of the Lockheed study was to use the available information in the best way possible to determine if a reliable forecast procedure is possible without having knowledge of the basic cause of the phenomenon. To accomplish the objective, the statistical techniques of nonlinear multiple regression were used to combine as many parameters as possible that might be descriptive of the unknown interaction. The result was a technique for predicting smoothed sunspot numbers that can be used as far into the future as the positions and velocities of the planets can be calculated. Planetary ephemeris data is the only information required to make a prediction.

The procedure was found to be feasible, but has not as yet demonstrated an acceptable accuracy. The best accuracies were achieved during Phase 1 of the experiment and were 10.7% of the peak-to-peak value during training and 16% of the peak-to-peak value for the open test set. This accuracy occurred when 13 parameters to estimate \pm SSN (22-year cycle) were used. When \pm SSN was predicted in the future, the minimum rms error during training was 11.6% of the peak-to-peak number.

In formidable investigations like this one, the most important gains are not always demonstrated in the formal results. However, much was learned during the study about the ways in which planetary influences can be used to

improve forecasting procedures; and firm recommendations can be made which, if followed, should yield significant improvements in the accuracy of the basic procedure. These recommendations are presented in Section 7.

Section 7 RECOMMENDATIONS

This study is an attempt to combine various parameters that describe planetary interactions with the sun into a forecast procedure for solar activity. Although the procedure does not yet demonstrate satisfactory accuracy, ideas arose during the investigation which could greatly improve the technique. The suggestions fall into two basic categories: (1) improvement of the basic data; and (2) improvement of the techniques used in the multiple nonlinear regression analysis. The first category encompasses such suggestions as predicting sunspot area instead of Wolf number, adding different predictors, etc. The second category is self-explanatory. Some of the more significant suggestions in each category are listed below.

- Improvement of Basic Data:
 - The basic approach thus far has been a direct estimate of sunspot number. It might be hypothesized that if planet influences are not the basic cause of solar activity, but serve to perturb some basic cycle, the planet influences should be used to predict the perturbations from the basic cycle rather than the cycle itself. One question which immediately arises is, "What is the basic cycle?" That question is, as yet, unanswered. If the average of the 19 known cycles were taken, a reasonable estimate could be expected. Other estimates, such as Fourier series, trigonometric expressions, etc. could also be tried. The predictors discussed in this study can then be combined statistically to produce estimates of the deviation of a future cycle from the base cycle.
 - Many of the problems thus far could well be attributed to the fact that the right parameter was not used as a predictor. A number of theories on the cause of sunspots could not be used because one of the requirements stipulated for predictors was that the parameter itself must be predictable. The only recourse to this problem is to include more predictors in the hope that the right one, or a parameter closely related to the

right one, will be found. This suggestion brings up the question, "Where may more predictors be found?" One answer is to wait for the results of further scientific investigations. Another solution which has been tried is to look at various components of the vector predictors. Most of the parameters used thus far have been the magnitudes of total vectors. Perhaps it is not the total vector which is important in relation to sunspots, but a component of it in a certain direction. Appendix D provides a preliminary look at components of vectors in two different coordinate systems. An example of how much a component might change from the total vector is shown in Fig. 7-1. Here the "T-N-B" components of the rate of change of radius of curvature (ROD) are shown. The total ROD is shown in Fig. 2-6. Notice how much clearer a waveform is given by the "T" component than the total.

- Finally, different measures of solar activity might be employed. In so doing, however, the relative scarcity of other measures would be a severe disadvantage. Figures 7-2 and 7-3 show a comparison between sunspot area and Wolf number.

- Improvement of the Regression Procedure:
 - Efforts should be made to optimize NONLIN to reduce the inherent error attributable to the estimation procedure. The optimization could be accomplished by changing the NONLIN estimation correction procedure and/or by transforming some of the values of SSN before the estimation is made. (The possibility of using a logarithmic transformation has been mentioned.)
 - Rather than change the NONLIN estimation correction procedure in general, a method should be found to correct SSN in particular to agree better with SSN.
 - A few predictors could be combined in the NONLIN portion of the experiment. Time permitted making combinations only in the ITLIN procedure.

49094G
500 50

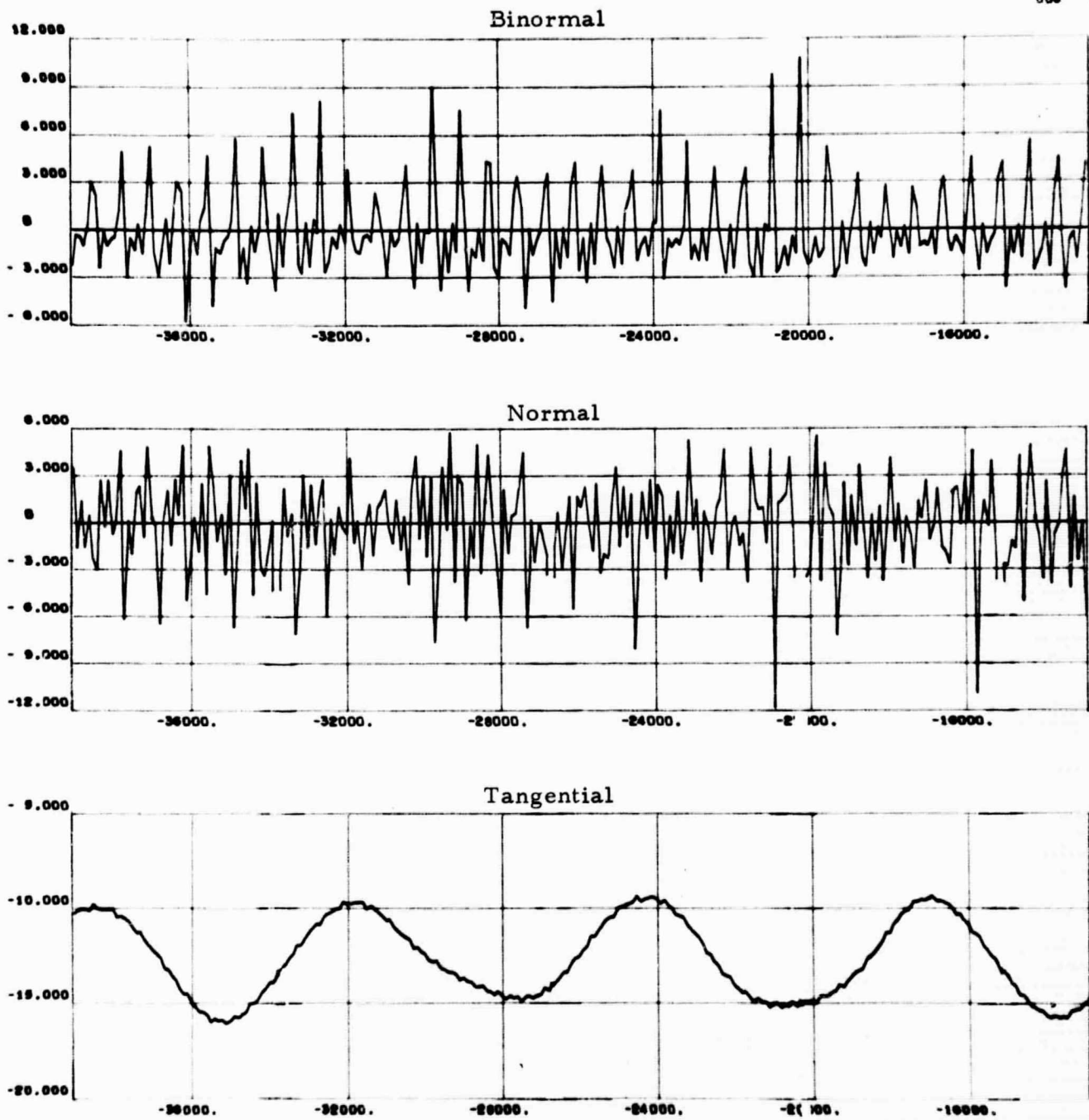
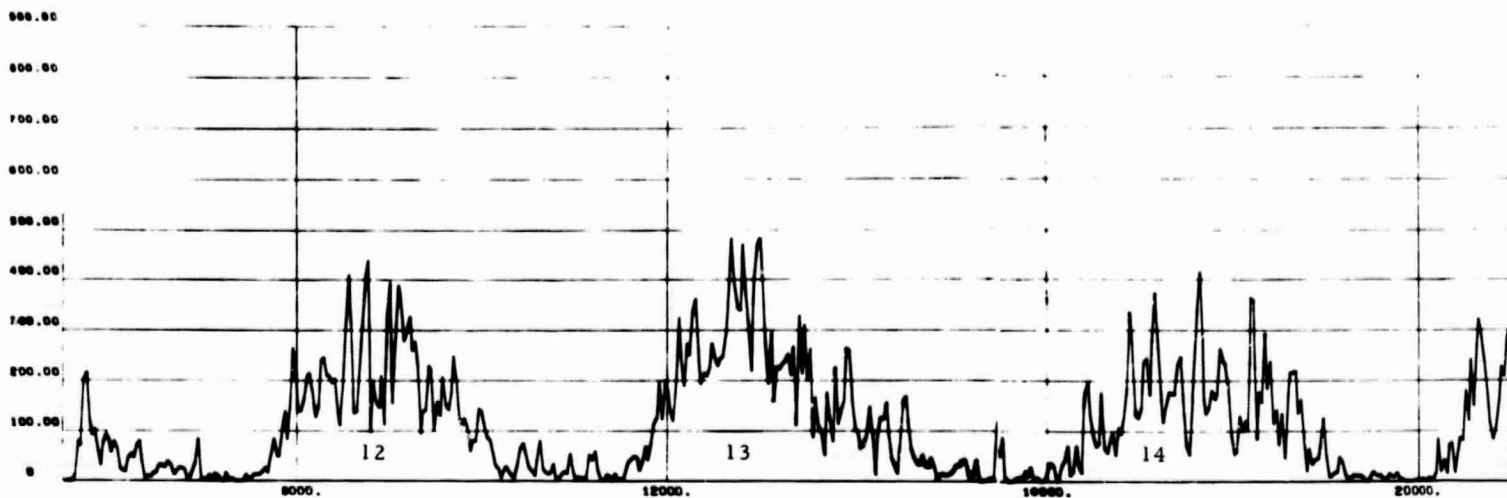


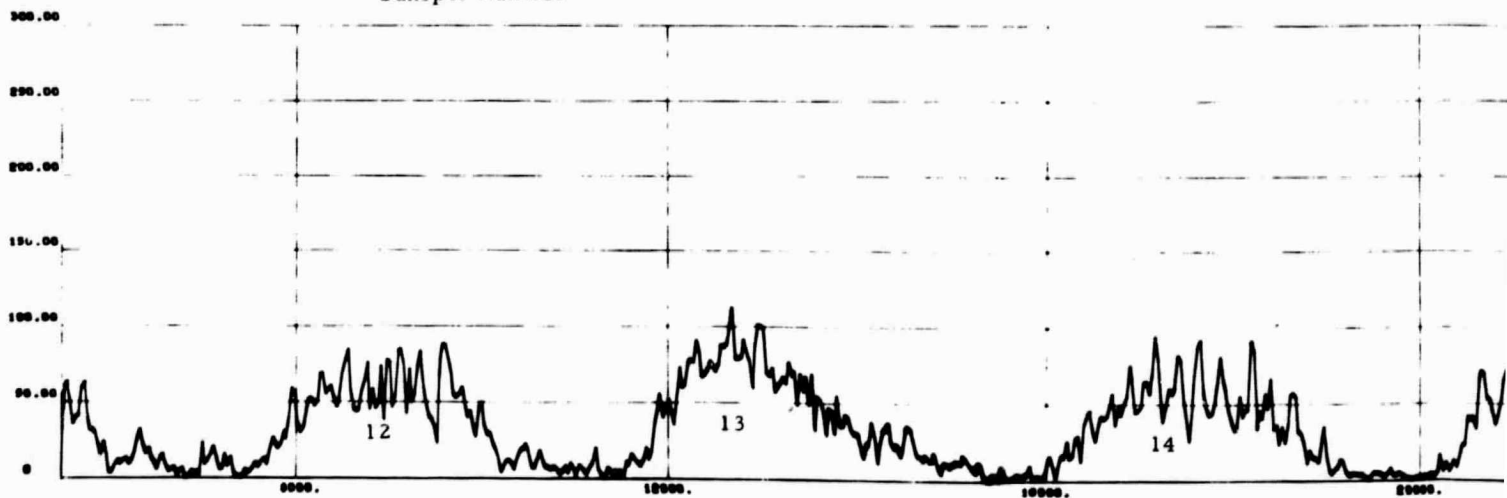
Fig. 7-1 - The Tangential-Normal-Binormal Components of $\dot{\bar{p}}$

Projected Area - Umbrae

40000
601



Sunspot Number



FOLDOUT FRAME of

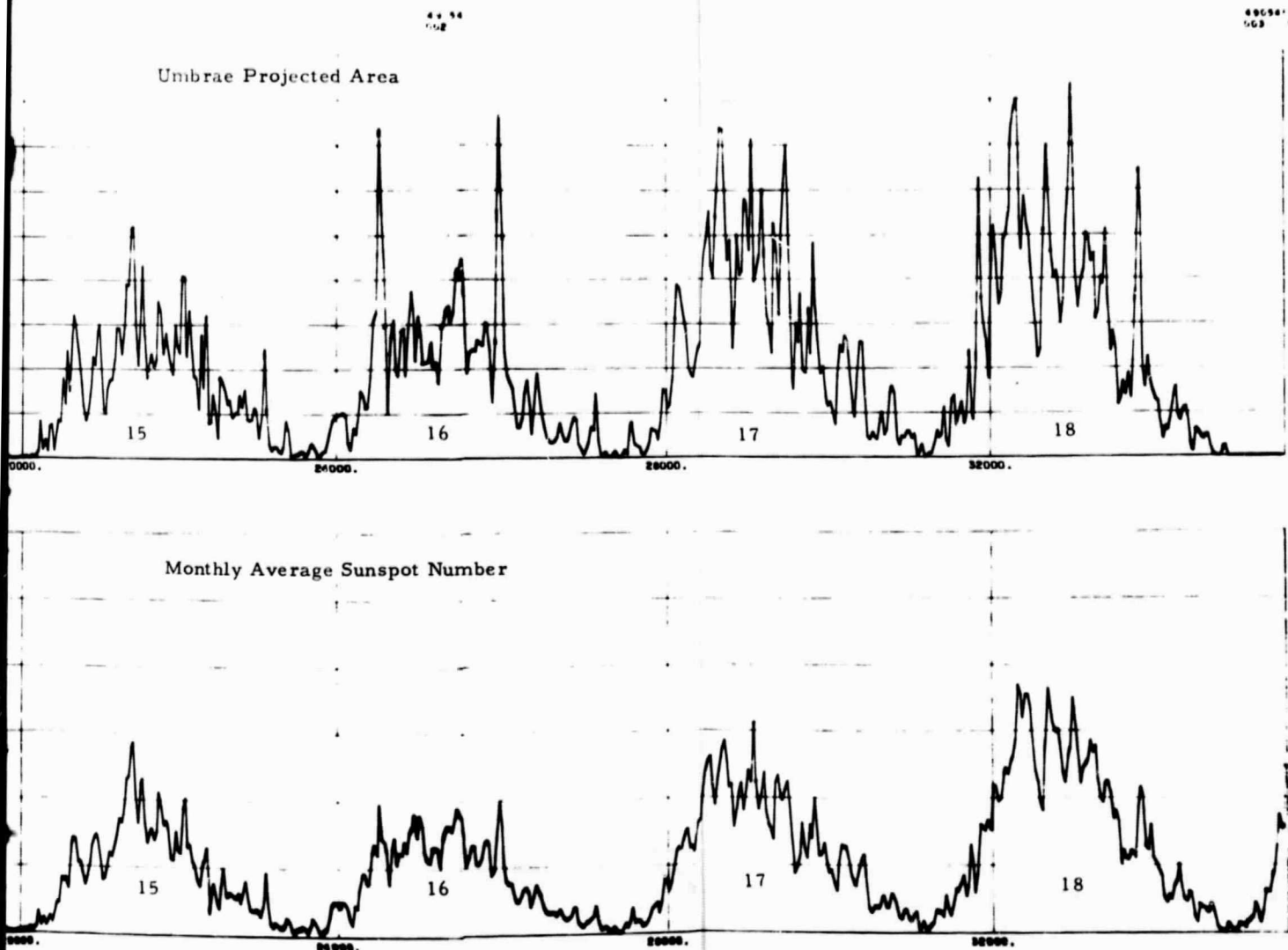
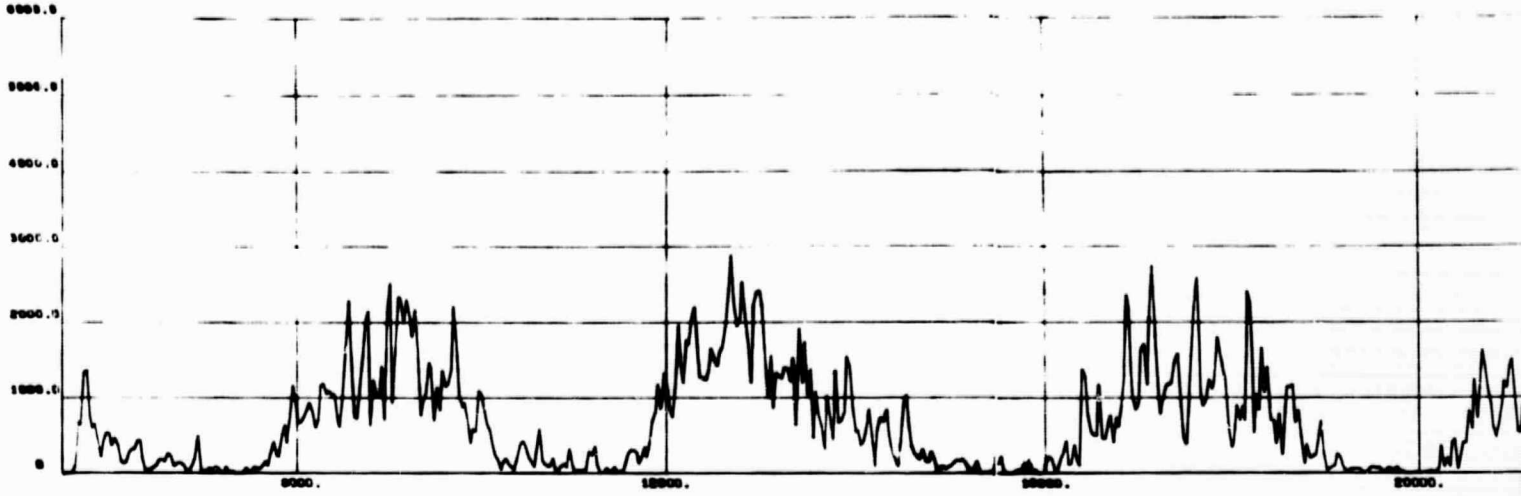


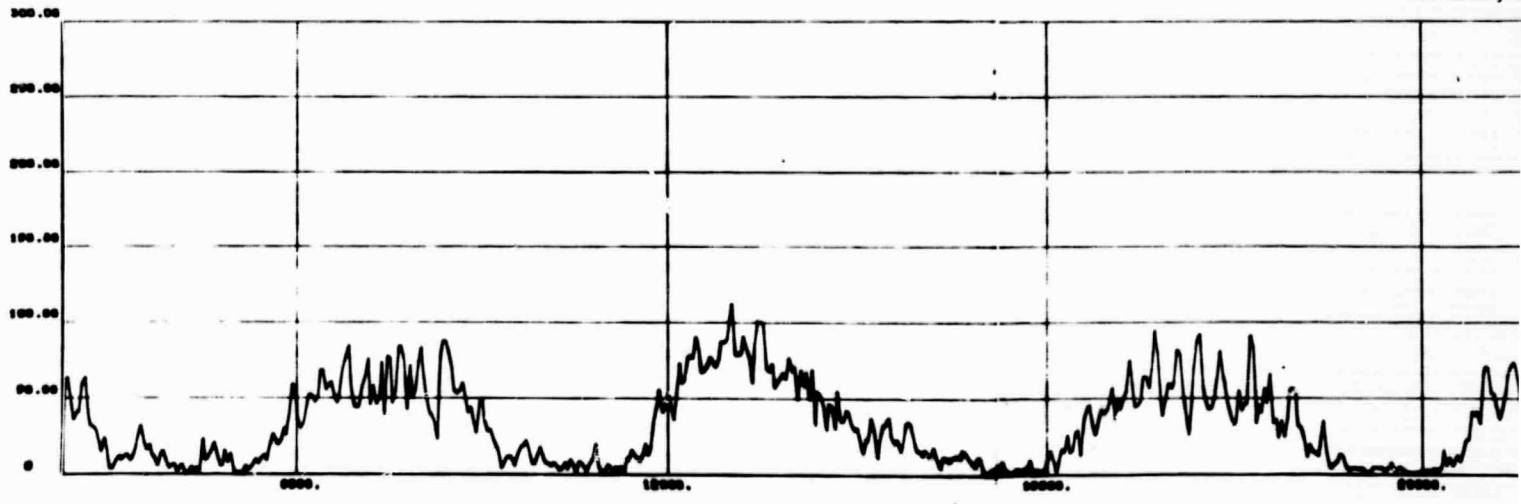
Fig. 7-2 - Different Measures of Solar Activity
- Umbrae Projected Area

4999
601

Whole Spots - Pro



Monthly



Foldout FRAME 6

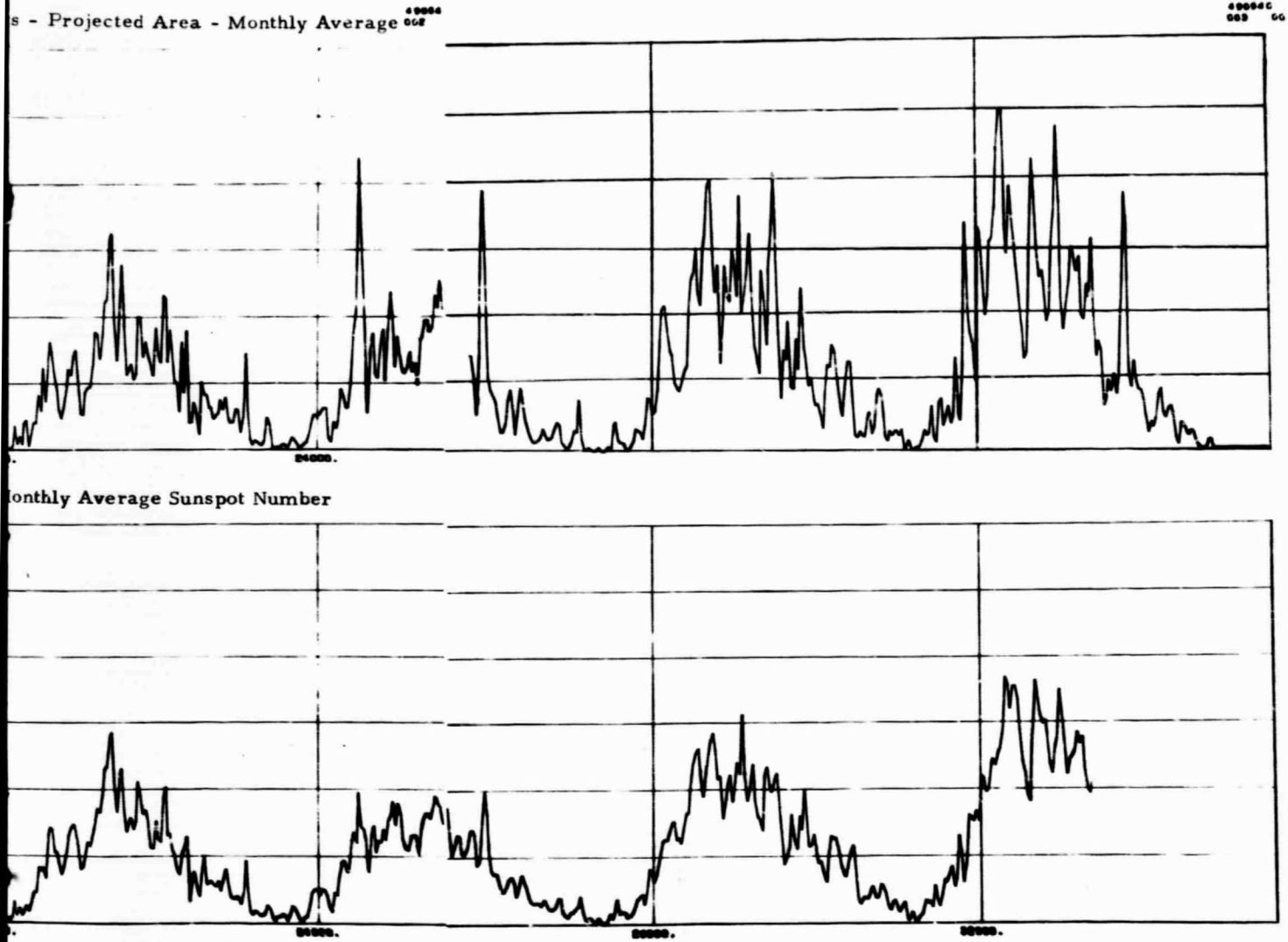


Fig. 7-3 - Different Measures of Solar Activity

Section 8
REFERENCES

1. Huntington, Ellsworth, Earth and Sun, an Hypothesis of Weather and Sunspots, Yale University Press, New Haven, Connecticut, 1923.
2. Jose, Paul D., "Sun's Motion and Sunspots," Astronomical Journal, Vol. 70, No. 3, April 1965.
3. Wood, R. M. and K. D. Wood, "Solar Motion and Sunspot Comparison," Nature, Vol. 208, October 1965, p. 129.
4. Arriaga, Nilo, "Relations Between Solar Activity and the Center of Gravity of the Planetary System," Journal of Geophysical Research, Vol. 60, 1965.
5. Bigg, E. K., "Influence of the Planet Mercury on Sunspots," Astronomical Journal, Vol. 72, No. 4, May 1967.
6. Suda, Takio, "Some Statistical Aspects of Solar-Activity Indices," Journal of the Meteorological Society of Japan, Vol. 40, No. 5, February 1962.
7. Nemeth, T., "An Attempt to the Explanation and to the Prediction of the Eleven-Year Cycle of Solar Activity," 1966. Pure & Applied Geophysics, Vol. 63, No. 1, pp.205 - 210.
8. Gold, L., "Gravitational-Magnetic Origin of Sunspots and Related Phenomena," 1959.
9. Takahashi, K., "On the Relation Between the Solar Activity Cycle and the Solar Tidal Force Induced by the Planets," Solar Physics, Vol. 3, 1968.
10. Schuster, A., "The Influence of Planets on the Formation of Sunspots," 1911. Royal Soc. of London, Proc., Series A, Vol. 85, pp. 309 - 323.
11. Dewey, E. R., "A Key to Sunspot-Planetary Relationship," Cycles, October 1968.
12. Michielsen, H. F. and M. A. Krop, "Development of a Computer Subroutine for Planetary and Lunar Positions," WADD Technical Report 60-118, August 1960.
13. Wood, K. D., "Long-Range Solar-Flare Prediction," Denver Research Institute, University of Denver, August 31, 1968.

14. Nicholson, S. B., Sky and Telescope 16 (1957), 272.
15. Ezekiel, M. and D. A. Fox, Methods of Correlation and Regression Analysis, John Wiley & Sons, Inc., New York, 1959.
16. Specht, D. F., "A Practical Technique for Estimating General Regression Surfaces," LMSC 6-79-68-6, Lockheed Missiles & Space Co., June 1968 (also available as DDC A672505).

Appendix A

SINX/X FILTER COEFFICIENTS FOR
THREE FILTER CONFIGURATIONS

Appendix A

SIN X/X FILTER COEFFICIENTS FOR THREE FILTER CONFIGURATIONS

1. $f_{co} = 1.0$ year Number of coefficients = 19

.1214092 .1190160 .1120319 .1009381 .0869062 .0697248 .0517179 .0334531 .0166444 .0016857 -.0104625 -.0192856
 -.0245634 -.0263680 -.0250413 -.0211484 -.0154151 -.0086536 -.0016841

2. $f_{co} = 0.5$ year Number of coefficients = 37

.1153946 .1131285 .1064898 .0959448 .0822268 .0662756 .0491594 .0319882 .0158248 .0016023 -.0099449 -.0183316
 -.0233482 -.0250637 -.0239025 -.0201022 -.0148525 -.0087255 -.0016009 .0045345 .0094971 .0129526 .0146429 .0145424
 .0128146 .0097812 .0058773 .0015984 -.0025558 -.0061339 -.0007770 -.0102537 -.0104717 -.0094848 -.0074755 -.0047287
 -.0015949

3. $f_{co} = 0.25$ years Number of coefficients = 73

.0576745 .0573900 .0565418 .0551449 .0532238 .0508126 .0479534 .0446961 .0410971 .0372181 .0331247 .0298858
 .0245700 .0202481 .0159878 .0118544 .0079093 .0042082 .0008008 -.0022703 -.0099705 -.0072736 -.0091422 -.0108274
 -.0116695 -.0122971 -.0125269 -.0123830 -.0119945 -.0111741 -.0100471 -.0087709 -.0073234 -.0057536 -.0041111 -.0024444
 -.0008001 .0007784 .0022514 .0035840 .0047467 .0057157 .0064737 .0070098 .0073186 .0074823 .0072683 .0069298
 .0064044 .0057157 .0048887 .0039524 .0029375 .0018757 .0007989 -.0002620 -.0012774 -.0022201 -.0030457 -.0037037
 -.0043877 -.0048334 -.0051248 -.0052579 -.0052338 -.0050581 -.0047405 -.0042944 -.0037361 -.0030855 -.0023634 -.0015928
 -.0007971

Sampling rate assumed to be one point every 20 days ($\frac{20}{365}$ years)

Appendix B
NONLIN COEFFICIENTS

Appendix B
NONLIN COEFFICIENTS

Each NONLIN transformation is

$$X'_i = \frac{Q(X)}{P(X)} = \frac{Q_0 + Q_1 X_i + Q_2 X_i^2 + Q_3 X_i^3 + Q_4 X_i^4 + Q_5 X_i^5 + Q_6 X_i^6}{P_0 + P_1 X_i + P_2 X_i^2 + P_3 X_i^3 + P_4 X_i^4 + P_5 X_i^5 + P_6 X_i^6}$$

where X_i is a given predictor parameter.

Then the correction of the estimate is made so that

$$X''_i = \alpha_0 + \alpha_1 X'_i$$

The values of these coefficients are tabulated for each of the applicable parameters for each of the experiments.

Table B-1
 COEFFICIENTS FOR EXPERIMENT EVALUATING NONLIN/ITLIN
 BY ESTIMATING \pm SSN

Parameter		Order of Coefficients						α_0	α_1	
		0	1	2	3	4	5			6
Zeta	Q	-1.274x4*	-6.075x4	-7.828x3	-4.823x4	-2.952x3	-1.876x4	5.519x3	-2.34	1.452
	P	1.729x3	6.328x1	1.276x3	5.735x1	1.312x3	-1.112x1	1.629x2		
P	Q	-1.175x4	-6.140x4	-4.273x3	-4.726x4	-3.915x3	-1.819x4	-6.749x2	-2.208	1.467
	P	1.730x3	-1.056x2	1.275x3	-2.499x1	1.308x3	1.991x1	1.631x2		
Vo	Q	-1.410x4	-5.920x4	-5.015x3	-4.541x4	-6.496x2	-1.836x4	2.701x2	-2.44	1.478
	P	1.760x3	1.334x1	1.237x3	-2.903x1	1.262x3	-1.211x1	1.605x2		
P'	Q	-1.373x4*	-6.266x4	-5.645x3	-4.367x4	-2.036x3	-1.702x4	2.047x2	-2.728	1.508
	P	1.765x3	5.787x2	1.228x3	1.230x1	1.249x3	-6.769x1	1.624x2		
P	Q	-3.544x3	-5.327x4	-5.838x2	-3.922x4	-8.949x3	-1.628x4	-2.232x3	-2.658	1.627
	P	1.857x3	-1.253x2	1.098x2	-5.502x1	1.138x3	3.534x0	1.598x2		
ROD	Q	-1.594x4	-5.895x4	-4.462x3	-4.263x4	2.323x3	-1.604x4	7.691x2	-2.572	1.523
	P	1.816x3	-7.642x1	1.189x3	-7.834x1	1.167x3	-1.582x1	1.480x2		
Ho	Q	-1.235x4	-4.842x4	-3.572x3	-3.557x4	-2.373x3	-1.511x4	-1.423x2	-2.658	1.583
	P	1.834x3	-1.913x2	1.140x3	-3.738x1	1.138x3	2.083x1	1.582x2		
Ro	Q	-1.30x4	-3.13x4	-7.33x3	-2.93x4	-3.48x4	-1.33x4	2.80x2	-3.722	1.655
	P	1.88x3	1.79x1	1.07x3	2.87x1	1.08x3	4.84x0	1.58x3		
Ao	Q	-1.40x4	-2.61x4	-1.84x2	-2.47x4	-2.26x4	-1.24x4	-8.63x3	-4.17	1.795
	P	1.93x3	-5.55x1	9.68x2	-2.45x1	1.05x4	5.32x0	1.66x2		
SCC	Q	-1.33x4	5.50x4	-2.02x4	5.15x3	-7.74x2	7.40x4	-4.75x3	-5.00	1.713
	P	1.55x3	-1.10x2	2.92x3	-1.15x1	1.21x2	-1.40x2	1.99x3		
SSC	Q	-2.48x4	-1.17x4	-3.08x3	-1.11x2	5.54x3	-5.76x3	1.97x3	-9.65	2.377
	P	2.14x3	-1.95x1	8.72x2	-3.59x1	7.44x2	-1.87x1	1.06x2		
Tau	Q	-2.32x4	2.67x4	-2.18x4	5.85x2	7.22x1	1.11x4	1.48x4	-16.18	2.861
	P	2.30x3	-1.35x3	3.05x3	-1.16x1	3.14x1	3.17x2	1.01x3		
CUP	Q	-1.91x0	1.00x4	-3.92x3	8.67x3	4.24x3	3.44x3	1.48x3	-5.73	2.025
	P	1.92x3	9.36x1	1.01x3	2.50x0	1.04x3	-6.86x0	1.58x2		
F3	Q	-9.57x3	4.50x3	-6.91x3	4.06x3	-6.70x3	1.66x3	-7.21x2	-2.57	1.482
	P	1.72x3	-3.44x1	1.28x3	-3.69x1	1.31x3	3.64x-1	1.62x2		
F3H	Q	-9.51x3	-1.49x3	-5.54x3	-4.10x3	-6.42x3	-1.98x3	-1.08x3	-1.12	1.791
	P	1.72x3	-1.15x2	1.31x3	-1.26x2	1.26x3	2.03x1	1.55x2		
HF'	Q	-7.08x3	-2.29x3	-1.42x4	-2.70x2	-3.53x2	-1.34x4	-2.12x4	-6.64	2.204
	P	1.05x3	5.81x1	3.26x3	5.94x0	7.41x1	2.80x2	4.18x3		
HF	Q	-9.31x3	-3.81x3	-1.81x4	1.65x2	-3.64x2	1.66x4	-1.86x4	-10.98	9.672
	P	1.04x3	-7.72x1	3.13x3	-5.06x0	7.28x1	-2.98x2	4.28x3		
Jo	Q	-9.01x3	3.43x3	-5.80x3	2.26x3	-6.27x4	1.06x3	-1.10x3	-3.01	1.670
	P	1.86x3	3.89x1	1.08x3	-4.48x1	1.10x3	-1.31x1	1.59x2		
F3R	Q	-4.97x3*	1.04x3	-2.71x4	-4.29x1	-5.18x2	-6.36x3	-2.47x4	-17.76	3.802
	P	8.14x2	-1.48x2	2.94x3	-1.45x1	7.89x1	-7.88x2	5.25x3		
V3	Q	-4.14x3	-6.54x3	-1.20x4	-1.17x1	-3.48x2	3.76x3	-2.51x4	-4.71	2.13
	P	7.71x2	-1.07x2	2.73x3	1.08x1	7.75x1	-5.27x3	5.50x3		

*xn indicates 10^n

Table B-2

NONLIN COEFFICIENTS FOR EVALUATING NONLIN/ITLIN
BY ESTIMATING |SSN|

Parameter		Order of Coefficients							Correction Coefficients	
		0	1	2	3	4	5	6	α_0	α_1
HF	Q	5.33x5*	9.95x3	9.71x4	4.16x3	1.83x4	2.69x4	6.47x5	19.5	1.435
	P	1.15x3	-9.22x1	2.19x3	-1.91x1	4.20x2	-3.68x1	1.48x3		
HF'	Q	8.00x4	-2.58x4	5.52x6	-1.57x4	5.48x4	-3.92x3	6.80x3	20.5	1.459
	P	1.75x3	-1.89x2	1.24x3	-4.76x1	1.26x3	3.24x1	1.61x2		
F3R	Q	8.52x4	1.92x4	4.71x4	9.22x3	4.76x4	3.96x3	6.94x3	27.2	1.619
	P	1.87x3	6.43x1	1.08x3	-4.31x1	1.09x3	-1.71x1	1.59x2		
F3	Q	3.03x4	-1.25x4	1.42x5	-1.43x3	4.10x3	-7.14x4	2.62x5	82.1	2.070
	P	7.22x2	-1.61x2	3.20x3	-1.20x1	8.98x1	-4.74x2	5.76x3		
Ao	Q	8.88x4	1.25x4	4.31x4	9.07x3	4.58x4	4.89x3	6.71x3	31.8	1.710
	P	1.92x3	-3.62x1	9.90x2	-1.65x1	1.06x3	3.74x0	1.66x2		
CUP	Q	4.96x4	4.05x4	1.43x5	1.58x3	3.11x3	4.68x4	1.72x5	24.4	1.54
	P	1.11x3	3.01x2	3.07x3	7.20x0	6.72x1	1.12x2	3.81x3		
F3H	Q	8.50x4	-1.25x4	4.60x4	-9.48x4	4.62x4	-3.91x4	6.82x3	37.0	1.83
	P	1.90x3	-8.78x1	1.06x3	-3.91x1	1.04x4	3.36x0	1.48x2		
Jo	Q	8.61x4	-5.28x3	4.56x4	-5.63x4	4.41x4	-3.59x3	6.58x3	34.9	1.78
	P	1.91x3	7.79x1	1.04x3	3.54x1	1.00x3	1.78x-1	1.47x2		
Tau	Q	9.43x4	-1.39x3	3.62x4	-4.29x3	3.22x4	-3.56x3	5.18x3	178.0	5.06
	P	2.14x3	-2.34x1	8.76x2	-3.60x1	7.44x2	-1.81x1	1.06x2		
P	Q	8.68x4	-6.86x2	4.63x4	-7.49x3	4.90x4	-3.95x3	6.77x3	90.00	3.02
	P	1.86x3	-5.48x1	1.07x3	-5.08x1	1.13x3	-8.56x0	1.61x2		
Lo	Q	8.65x4	-1.05x4	4.77x4	-1.73x3	4.39x4	2.29x3	5.68x3	31.6	1.71
	P	1.91x3	-4.05x2	1.10x3	-1.34x2	1.00x3	2.54x1	1.26x2		
ROD	Q	8.69x4	7.02x3	5.17x4	2.59x3	4.55x4	6.28x2	5.27x3	40.4	1.90
	P	1.81x3	-3.71x1	1.18x3	-6.87x1	1.16x3	-2.19x1	1.50x2		
P	Q	5.36x4	-1.14x4	1.03x5	-2.54x3	1.78x4	-9.31x3	6.28x4	23.5	1.47
	P	1.14x3	-8.61x1	2.24x3	-1.98x2	4.10x2	-5.84x2	1.49x3		
Vo	Q	8.63x4	1.94x3	5.15x4	4.03x3	4.79x4	2.00x3	5.73x3	74.3	2.51
	P	1.76x3	5.41x1	1.23x3	1.72x1	1.25x3	-5.82x0	1.62x2		
V3	Q	7.92x4	-1.94x3	5.73x4	-4.40x3	5.56x4	-2.00x3	6.44x3	60.4	2.35
	P	1.72x3	-2.70x1	1.28x3	-3.53x1	1.31x3	-1.41x0	1.62x2		

*xn indicates 10ⁿ

Table B-3

NONLIN COEFFICIENTS FOR FINDING \pm SSN INTO THE FUTURE

Parameters		Order of Coefficients						Correction Coefficients		
		0	1	2	3	4	5	6	α_0	α_1
Zeta	Q	-1.05×10^4	-8.68×10^4	-5.35×10^3	-7.22×10^4	2.04×10^3	-2.88×10^4	1.60×10^3	1.158	1.446
	P	2.11×10^1	9.44×10^1	1.57×10^3	2.21×10^1	1.61×10^3	-1.68×10^1	1.99×10^2		
P	Q	-7.71×10^3	-8.79×10^4	4.46×10^1	-7.13×10^4	-8.26×10^2	-2.81×10^2	-6.89×10^2	.868	1.456
	P	2.11×10^3	-1.18×10^2	15.6×10^3	-2.96×10^1	1.61×10^3	2.21×10^1	1.99×10^2		
Vo	Q	-9.68×10^3	-8.93×10^4	-1.61×10^3	-6.66×10^4	1.27×10^3	-2.64×10^4	2.49×10^2	1.178	1.492
	P	2.12×10^3	6.81×10^1	1.51×10^3	7.45×10^0	1.53×10^3	-9.62×10^0	1.99×10^2		
P'	Q	-1.27×10^4	-8.51×10^4	-2.19×10^3	-6.72×10^4	5.45×10^3	-2.75×10^4	1.51×10^3	1.036	1.487
	P	2.16×10^3	1.13×10^1	1.51×10^3	-2.64×10^1	1.54×10^3	-1.23×10^1	1.97×10^2		
P	Q	-4.85×10^3	-8.05×10^4	-1.36×10^3	-6.02×10^4	1.42×10^3	-2.43×10^4	-4.93×10^2	.775	1.593
	P	2.25×10^3	-7.36×10^1	1.38×10^3	-6.15×10^1	1.42×10^3	-9.96×10^0	1.95×10^2		
ROD	Q	-1.71×10^4	-8.40×10^4	-2.88×10^2	-6.30×10^4	1.17×10^4	-2.49×10^4	2.45×10^3	1.036	1.516
	P	2.21×10^3	-1.78×10^1	1.47×10^3	-8.11×10^1	1.44×10^3	-2.65×10^1	1.86×10^2		
Ho	Q	-9.61×10^3	-7.38×10^4	-1.32×10^3	-5.71×10^4	7.57×10^2	-2.44×10^4	4.80×10^2	1.191	1.565
	P	2.22×10^3	-1.99×10^2	1.42×10^3	-1.99×10^2	1.42×10^3	2.63×10^2	1.95×10^3		
Ro	Q	-1.17×10^4	-6.37×10^4	-6.56×10^3	-4.67×10^4	-3.36×10^2	02.04×10^4	1.60×10^3	2.170	1.645
	P	2.28×10^3	4.72×10^1	1.35×10^3	6.42×10^1	1.34×10^3	9.15×10^0	1.90×10^2		
Ao	Q	-2.75×10^3	-3.74×10^4	4.44×10^2	-3.40×10^4	-5.22×10^3	-1.76×10^4	2.01×10^2	1.640	1.797
	P	2.38×10^3	-8.84×10^1	1.17×10^3	-3.96×10^1	1.26×10^3	5.56×10^0	2.01×10^2		
SCC	Q	-3.82×10^3	9.77×10^4	-1.49×10^4	5.03×10^3	-5.31×10^2	-1.66×10^5	-2.61×10^4	2.170	1.707
	P	1.80×10^3	4.53×10^1	4.69×10^3	-7.96×10^0	8.96×10^1	-4.27×10^2	4.39×10^3		
SSC	Q	-2.20×10^4	4.84×10^4	-1.31×10^4	9.94×10^2	2.98×10^2	-2.02×10^4	2.37×10^4	11.100	2.757
	P	2.88×10^3	-1.77×10^3	3.77×10^3	-1.60×10^1	3.60×10^1	3.41×10^2	1.06×10^3		
Tau	Q	-2.64×10^4	-1.73×10^3	-2.07×10^3	-1.19×10^4	1.15×10^4	-7.81×10^3	3.80×10^3	7.980	2.728
	P	2.64×10^3	-4.57×10^1	1.04×10^3	-2.20×10^1	8.92×10^2	-8.81×10^0	1.32×10^2		
CUP	Q	-1.64×10^4	1.38×10^4	4.67×10^2	1.03×10^4	7.43×10^3	3.97×10^3	1.72×10^3	2.34	1.892
	P	2.37×10^4	9.76×10^1	1.22×10^3	7.51×10^0	1.24×10^3	-7.50×10^0	1.89×10^2		
F3	Q	-6.95×10^3	-8.96×10^3	-2.28×10^3	-8.99×10^3	-1.77×10^3	-3.96×10^3	-3.79×10^2	1.223	1.532
	P	2.11×10^3	-1.09×10^2	1.61×10^3	-1.88×10^1	1.55×10^3	2.01×10^1	1.91×10^2		
F3H	Q	-8.95×10^3	-8.35×10^3	-1.96×10^4	1.38×10^2	-2.91×10^2	-2.46×10^4	-9.82×10^3	11.78	3.543
	P	1.28×10^3	-1.11×10^2	3.84×10^3	-1.08×10^1	8.87×10^1	-5.38×10^2	5.12×10^3		

Appendix C
ITLIN COEFFICIENTS

Appendix C
ITLIN COEFFICIENTS

The final estimate of SSN is in the following form:

$$\hat{SSN} = \beta_0 + \sum_{i=1}^N \beta_i X_i''$$

where i refers to an individual predictor parameter and N is the total number of predictors. To use ITLIN at all $N > 1$. The following tables provide the β coefficients as predictor parameters are added.

Table C-1
ITLIN COEFFICIENTS FOR EXPERIMENT EVALUATING NONLIN/ITLIN
BY ESTIMATING ±SSN

Parameters Added	Coefficient Numbers (Coefficient 1 is for Parameter 1, etc)																				
	0	1	2	3	4	5	6	7	8	9	10	11	12	13	14	15	16	17	18	19	20
1 Zeta																					
2 P	-.257	.3920	.6109																		
3 Vo	-.2067	.3071	.4787	.2251																	
4 P'	-.0516	.1762	.2746	.1291	.4356																
5 P	-.1413	.1204	.1877	.0883	.2978	.3713															
6 ROD	-.1325	.1144	.1783	.0838	.2829	.3532	.0541														
7 Ho	-.8329	.2103	.3277	.1541	.5199	.6489	.0999	-1.0699													
8 Ro	-.9605	.2141	.3336	.1569	.5292	.6606	.1017	-1.0891	-.0365												
9 Ao	-.6634	.2083	.3246	.1527	.5150	.6428	.0989	-1.0540	-.0356	.0790											
10 SCC	-.2862	.2021	.3150	.1481	.4996	.6237	.0960	-1.0235	-.0345	.0766	.0735										
11 SSC	3.255	.1874	.2920	.1374	.9633	.5783	.0890	-.9490	-.0320	.0710	.0681	.5568									
12 Tau	3.062	.1881	.2931	.1378	.4650	.5809	.0893	-.9525	-.0321	.0713	.0684	.5588	-.0258								
13 CUP	6.536	.1837	.2863	.1346	.4542	.5670	.0873	-.9305	-.0314	.0696	.0668	.5459	-.0252	.6569							
14 F3	7.542	.1836	.2861	.1345	.4539	.5665	.0872	-.9297	-.0313	.0696	.0668	.5455	-.0252	.6564	.1897						
15 F3H	11.869	.1834	.2859	.1344	.4535	.5661	.0871	-.9290	-.0313	.0695	.0667	.5450	-.0252	.6559	.1896	.8312					
16 HF'	16.034	.1833	.2856	.1343	.4531	.5655	.0870	-.9281	-.0313	.0675	.0666	.5445	-.0251	.6552	.1894	.8304	.7589				
17 HF	18.649	.1825	.2844	.1380	.4512	.5632	.0867	-.9243	-.0312	.0692	.0664	.5423	-.0250	.6525	.1886	.9270	.7558	.4135			
18 Jo	15.755	.1831	.2853	.1342	.4526	.5649	.0869	-.9271	-.0312	.0894	.0666	.5439	-.0251	.6545	.1892	.8295	.7580	.4148	-.5615		
19 F3R	18.533	.1825	.2845	.1338	.4513	.5633	.0867	-.9244	-.0312	.0692	.0664	.5423	-.0250	.6526	.1886	.8271	.7558	.4136	-.5599	.4476	
20 V3	17.757	.1827	.2847	.1339	.4516	.5637	.0868	-.9251	-.0312	.0692	.0664	.5422	-.2051	.6531	.1888	.8277	.7564	.4139	-.5603	.4480	-.1682

Table C-2
ITLIN COEFFICIENT FOR EXPERIMENT EVALUATING NONLIN/ITLIN
BY ESTIMATING (SSN)

Parameters Added	Coefficient Numbers (Coefficient 1 is for Parameter 1, etc)															
	0	1	2	3	4	5	6	7	8	9	10	11	12	13	14	15
1 HF																
2 HF'	5.007	1.750	-.8665													
3 F3R	- 2.298	1.369	-.6777	.3567												
4 F3	- 4.142	1.262	-.6248	.3289	.1243											
5 Ao	- 7.496	1.118	-.5534	.2913	.1101	.1985										
6 CUP	- 52.92	1.119	-.5538	.2915	.1102	.1987	1.001									
7 F3H	- 60.00	1.070	-.5296	.2788	.1054	.1900	.9572	.2597								
8 Jo	- 54.92	1.125	-.5570	.2932	.1109	.1998	1.006	.2601	-.2359							
9 Tau	- 80.26	1.054	-.5220	.2748	.1039	.1872	.9435	.2513	-.2211	.7201						
10 P	- 84.828	1.028	-.5089	.2679	.1013	.1825	.9198	.2441	-.2155	.7019	.1714					
11 Lo	- 97.76	1.014	-.5019	.2642	.0999	.1800	.9071	.2416	-.2126	.6923	.1690	.3306				
12 ROD	-134.65	.995	-.4925	.2592	.0980	.1766	.8901	.2370	-.2086	.6793	.1658	.3244	.8869			
13 P	-139.12	.9895	-.4897	.2578	.0974	.1756	.8850	.2357	-.2074	.6754	.1649	.3226	.8819	.1218		
14 Vo	-156.77	.9353	-.4629	.2436	.0921	.1660	.8366	.2228	-.1960	.6335	.1559	.3049	.8336	.1151	.6251	
15 V ₃	-153.32	.9395	-.4649	.2447	.0325	.1667	.8403	.2238	-.1969	.6413	.1565	.3063	.8373	.1157	.6279	-.0974

C-3

Table C-3
ITLIN COEFFICIENTS FOR PREDICTING \pm SSN INTO THE FUTURE

Parameter Added	Coefficient Numbers (Coefficient 1 is for Parameter 1, etc)															
	0	1	2	3	4	5	6	7	8	9	10	11	12	13	14	15
1 Zeta																
2 P	-.1314	.6193	.3842													
3 Vo	-.0956	.3943	.2446	.3701												
4 P'	-.1059	.2904	.1802	.2726	.2763											
5 P	-.2789	.2331	.1446	.2188	.2217	.2251										
6 ROD	-.2791	.2315	.1436	.2173	.2202	.2235	.0072									
7 Ho	-.4582	.3603	.2235	.3382	.3427	.3478	.0112	-.6603								
8 Ro	-.5293	.3677	.2281	.3452	.3498	.3550	.0114	-.6739	-.0334							
9 Ao	-.4841	.3634	.2255	.3411	.3457	.3509	.0113	-.6660	-.0330	.0329						
10 SCC	-.2862	.3492	.2166	.3278	.3322	.3371	.0108	-.6399	-.0317	.0316	.0896					
11 SSC	-.2602	.3489	.2165	.3275	.3319	.3369	.0108	-.6394	-.0316	.0316	.0895	.0043				
12 Tau	1.6880	.3210	.1991	.3013	.3054	.3099	.0100	-.5882	-.0291	.0291	.0824	.0040	.4577			
13 CUP	3.5165	.3170	.1967	.2975	.3016	.3060	.0098	-.5809	-.0287	.0287	.0813	.0039	.4520	.7153		
14 F3	4.6504	.3158	.1959	.2965	.3005	.3049	.0098	-.5788	-.0286	.0286	.0811	.0039	.4504	.7127	.5024	
15 F3H	6.5343	.3132	.1943	.2941	.2980	.3024	.0097	-.5741	-.0284	.0284	.0804	.0039	.4496	.7068	.4982	.4177

C-4

Appendix D

COMPONENTS OF VECTOR PREDICTORS

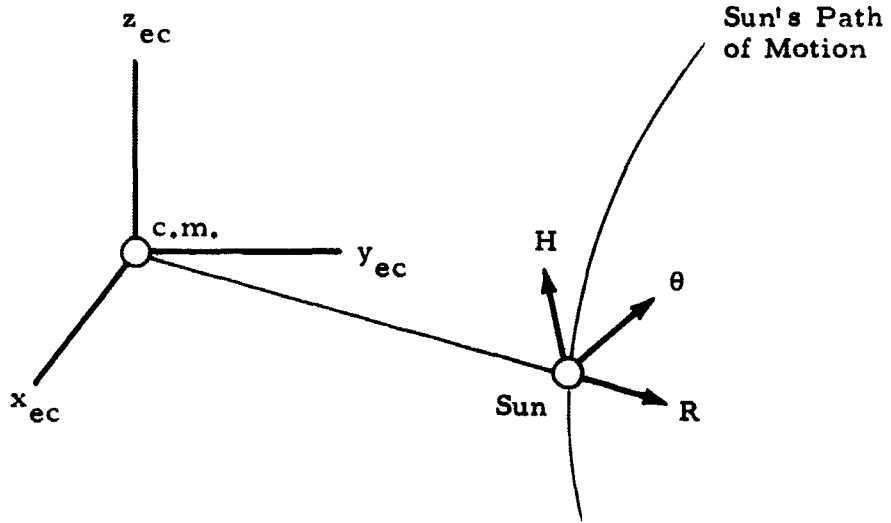
Appendix D

COMPONENTS OF VECTOR PREDICTORS

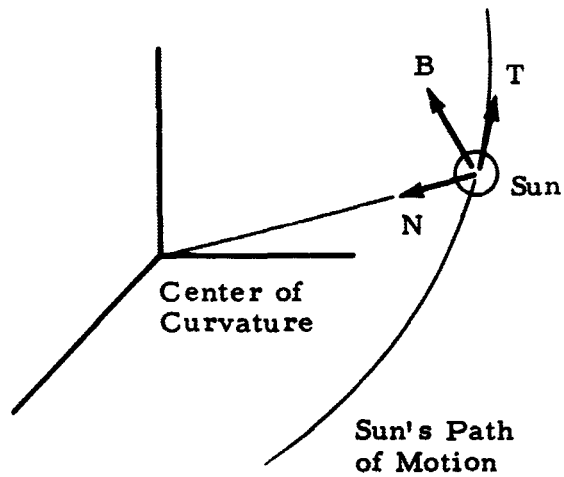
D.1 GENERAL

Several of the predictors generated for this study are vector quantities. To investigate the manner in which these vectors change with time, the first approach was to compute the magnitude of the vector. The vector also changes direction with time, which may be important in correlation studies. To represent the change in direction of the vector as a function of time in a meaningful manner, there are several possibilities. Direction might be represented in terms of angles, or direction cosines relative to a wide variety of coordinate systems, fixed or rotating; and the history of these angles then studied. Also, components of the vector might be chosen in a meaningful coordinate system. The approach chosen was to compute the three orthogonal components of the vector in two coordinate systems. The two systems used are the "Tangential-Normal-Binormal (TNB)" and the "Radial-Transverse Binormal (R θ H)" systems. In the choice of these systems, it was anticipated that the results of physical forces would be more closely related to systems which are expressive of the motions described. For instance, in the TNB system, velocity is directed along the tangential unit vector and acceleration along the tangential and normal unit vectors; whereas, if an arbitrary rectangular system fixed in space were chosen, no component would have any particular meaning.

The orientations of these systems are illustrated in the following diagrams.



RθH Coordinate System



TNB Coordinate System

In the RθH system, R is directed along the radius vector from the c.m. to the Sun's position; θ is perpendicular to R, in the plane of motion, and in the same sense as the velocity; H completes the right-handed system. In the TNB system, T is tangential to the path of motion in the direction of the velocity; N is in the plane of motion, normal to the velocity; and B completes the right-handed system. These unit vectors can be defined in terms of the known ecliptic system as follows.

• RθH System. The radial unit vector is easily obtained from the previously calculated position.

$$\bar{R} = \frac{\bar{R}_o}{R_o}$$

The binormal unit vector \bar{H} is defined from the angular momentum vector about the c.m.,

$$\bar{H} = \frac{\bar{H}_o}{H_o} = \frac{m_s \bar{R}_o \times \bar{V}_o}{H_o}$$

Finally, the transverse unit vector can be obtained as

$$\bar{\theta} = \bar{H} \times \bar{R}.$$

• The TNB System. Unit vectors in the TNB system can be computed in terms of parameters which define the path of motion. The tangential unit vector is obtained from the velocity

$$\bar{T} = \frac{\bar{V}_o}{V_o} .$$

The normal unit vector can be obtained from the acceleration vector,

$$\bar{a}_o = \ddot{S}\bar{T} + \frac{v_o^2}{\rho} \bar{N}$$

$$\bar{N} = \frac{\rho}{v_o^2} (\bar{a}_o - \ddot{S}\bar{T}) .$$

The binormal unit vector is then easily computed from the other two.

$$\bar{B} = \bar{T} \times \bar{N} .$$

D.2 COMPONENTS OF VECTORS IN THE TNB SYSTEM

The vectors can be resolved by taking the dot product of the vector with the unit vectors defined above; for example, the components of acceleration could be computed as

$$a_T = \bar{a}_o \cdot \bar{T} = a_x T_x + a_y T_y + a_z T_z$$

$$a_N = \bar{a}_o \cdot \bar{N} = a_x N_x + a_y N_y + a_z N_z$$

$$a_B = \bar{a}_o \cdot \bar{B} = a_x B_x + a_y B_y + a_z B_z .$$

In some cases, however, the calculations can be simplified and at the same time more insight into the nature of the predictors can be gained. For instance, again considering acceleration it is known that

$$\bar{a}_o = \ddot{S}\bar{T} + \frac{v_o^2}{\rho} \bar{N} .$$

Thus,

$$a_T = \ddot{S} = \frac{\bar{a}_o \cdot \bar{v}_o}{v_o}$$

$$a_N = \frac{v_o^2}{\rho}$$

$$a_B = 0$$

Other predictors whose components in the TNB system might possibly be of interest are discussed below.

D.2.1 Distance from the Center of Mass to the Sun

The displacement vector from the c.m. to the Sun is known in terms of the ecliptic coordinates $(\bar{i}, \bar{j}, \bar{k})$,

$$\bar{R}_o = x_o \bar{i} + y_o \bar{j} + z_o \bar{k}.$$

The T component is

$$R_T = \bar{R}_o \cdot \bar{T} = \frac{\bar{R}_o \cdot \bar{V}_o}{V_o}$$

$$R_T = \frac{1}{V_o} (x_o V_x + y_o V_y + z_o V_z).$$

The N component is

$$R_N = \bar{R}_o \cdot \bar{N}$$

$$R_N = x_o N_x + y_o N_y + z_o N_z.$$

The B component is

$$R_B = \bar{R}_o \cdot \bar{B}$$

$$R_B = x_o B_x + y_o B_y + z_o B_z.$$

D.2.2 Jerk Vector

The TNB components of the rate of change of acceleration are determined as follows. Acceleration is

$$\bar{a}_o = \ddot{S}\bar{T} + \frac{v_o^2}{\rho} \bar{N}.$$

Taking the derivative,

$$\bar{J}_o = \frac{d\bar{a}_o}{dt} = \ddot{S}\bar{T} + \dot{S}\dot{\bar{T}} + \frac{2\rho v_o \dot{v}_o - v_o^2 \dot{\rho}}{\rho^2} \bar{N} + \frac{v_o^2}{\rho} \dot{\bar{N}},$$

repeating the expressions for the rates of change of the unit vectors,

$$\dot{\bar{T}} = \frac{\dot{S}}{\rho} \bar{N}$$

$$\dot{\bar{N}} = v_o r\bar{B} - \frac{v_o}{\rho} \bar{T},$$

and evaluating \ddot{S}

$$\ddot{S} = \frac{d}{dt} \left(\frac{\bar{a}_o \cdot \bar{v}_o}{v_o} \right)$$

$$\ddot{S} = \frac{v_o (\dot{\bar{a}}_o \cdot \bar{v}_o + \bar{a}_o \cdot \dot{\bar{v}}_o) - (\bar{a}_o \cdot \bar{v}_o) \dot{v}_o}{v_o^2}$$

$$\ddot{S} = \frac{1}{v_o} (\bar{J}_o \cdot \bar{v}_o + a_o^2) - \frac{\dot{v}_o}{v_o^2} (\bar{a}_o \cdot \bar{v}_o).$$

The jerk vector becomes

$$\begin{aligned} \bar{J}_o &= \left[\frac{1}{V_o} (\bar{J}_o \cdot \bar{V}_o) + a_o^2 - \frac{\dot{V}_o (\bar{a}_o \cdot \bar{V}_o)}{V_o^2} - \frac{V_o^3}{\rho^2} \right] \bar{T} \\ &+ \left[\frac{2\rho V_o \dot{V}_o}{\rho^2} - \frac{V_o^2 \dot{\rho}}{\rho^2} + \frac{V_o \dot{V}_o}{\rho} \right] \bar{N} \\ &+ \frac{V_o^3}{\rho} \bar{B} . \end{aligned}$$

Since

$$\frac{a_o^2}{V_o} = \frac{\dot{V}_o (\bar{a}_o \cdot \bar{V}_o)}{V_o^2} - \frac{V_o^3}{\rho^2} ,$$

the components are

$$J_T = \frac{\bar{J}_o \cdot \bar{V}_o}{V_o} = \frac{1}{V_o} (J_x V_x + J_y V_y + J_z V_z)$$

$$J_N = \frac{3V_o \dot{V}_o}{\rho} - \frac{V_o^2 \dot{\rho}}{\rho^2}$$

$$J_B = \frac{V_o^3}{\rho} .$$

D.2.3 Angular Momentum about the Center of Mass

The TNB components of \bar{H}_o may be obtained by manipulating the definition of \bar{H}_o .

$$\bar{H}_o = m_s \bar{R}_o \times \bar{V}_o$$

$$\bar{H}_o = m_s (R_T \bar{T} + R_N \bar{N} + R_B \bar{B}) \times (V_o \bar{T})$$

$$\bar{H}_o = m_s (R_B V_o \bar{N} - R_N V_o \bar{B}) .$$

Assuming a knowledge of R_B and R_N from the previous paragraph, the components of \bar{H}_O are

$$H_T = 0$$

$$H_N = m_s R_B V_o$$

$$H_B = m_s R_N V_o .$$

D.2.4 Rate of Change of Angular Momentum about the Center of Mass

The rate of change of \bar{H}_O in component form is likewise determined from its definition.

$$\begin{aligned}\bar{L}_O &= \dot{\bar{H}}_O = m_s \bar{R}_O \times \bar{a}_O \\ \bar{L}_O &= m_s (R_T \bar{T} + R_N \bar{N} + R_B \bar{B}) \times \left(\dot{\bar{S}} \bar{T} + \frac{V_o^2}{\rho} \bar{N} \right) \\ \bar{L}_O &= m_s \left(R_T \frac{V_o^2}{\rho} \bar{B} - R_N \dot{\bar{S}} \bar{B} + R_B \dot{\bar{S}} \bar{N} - \frac{R_B V_o^2}{\rho} \bar{T} \right) .\end{aligned}$$

Thus,

$$L_T = -m_s \frac{R_B V_o^2}{\rho}$$

$$L_N = m_s R_B \dot{\bar{S}}$$

$$L_B = m_s \left(\frac{R_T V_o^2}{\rho} - R_N \dot{\bar{S}} \right) .$$

D.2.5 Angular Momentum about the Center of Curvature and Rate of Change of Angular Momentum about the Center of Curvature

The angular momentum about the center of curvature from its very nature is easily expressed in TNB components.

$$\bar{P} = m_s \rho V_o \bar{B} .$$

So that

$$P_T = 0$$

$$P_N = 0$$

$$P_B = m_s \rho V_o .$$

Likewise, the rate of change of angular momentum about the center of curvature is easily obtained from the previous analysis.

$$\dot{P} = m_s \left[\rho v_o^2 \tau \bar{N} - (\dot{\rho} v_o + \dot{v}_o \rho) \bar{B} \right]$$

$$\dot{P}'_T = 0$$

$$\dot{P}'_N = m_s \rho v_o^2 \tau$$

$$\dot{P}'_B = -m_s \dot{\rho} v_o - m_s \rho \dot{v}_o .$$

D.2.6 Rate of Change of the Radius of Curvature

The rate of change of the radius of curvature was derived in the previous section as

$$\dot{\bar{\rho}} = \dot{\rho} \bar{N} + \rho \dot{\bar{N}}$$

$$\dot{\bar{\rho}} = \dot{\rho} \bar{N} + \rho \left(v_o \tau \bar{B} - \frac{v_o}{\rho} \bar{T} \right)$$

$$\dot{\bar{\rho}} = \dot{\rho} \bar{N} + \rho v_o \tau \bar{B} - v_o \bar{T} .$$

Thus,

$$\dot{\rho}_T = -v_o$$

$$\dot{\rho}_N = \dot{\rho}$$

$$\dot{\rho}_B = \rho v_o \tau .$$

D.3 COMPONENTS OF VECTORS IN THE $R\theta H$ SYSTEM

The components of the vector predictors in the radial-transverse-binormal system are most easily computed from the scalar product approach. Since this technique is rather general, no particular examples will be discussed.